Naturally Derived Chemical Additives as Renewable Alternatives in Polyvinylchloride Formulations for Application in Decorative Coatings.

Ellana Ruth Beard

Submitted in accordance with the requirements for the degree of

Doctor of Philosophy

The University of Leeds

School of Chemistry

May, 2018

The candidate confirms that the work submitted is her own, except where work which has formed part of jointly authored publications has been included. The contribution of the candidate and the other authors to this work has been explicitly indicated below. The candidate confirms that appropriate credit has been given within the thesis where reference has been made to the work of others.

In Chapter 3.7 – Ellana Beard carried out the synthesis and analysis of the citric acid derivatives, under the guidance and supervision of Natalia Sergeeva and Michelle Ledward. Ellana provided overall project direction to the work carried out.

E. Beard, M. Ledward and N. Sergeeva, Bio-based additives as renewable alternatives for polyvinylchloride formulations and application in paper coatings, ***RSC Adv*.,** 2017, **7**, 31428-31432.

Acknowledgements

I would like to formally acknowledge the Sergeeva research group for their dedication and support throughout the completion of my PhD. In particular, Dr Natalia Sergeeva, for her ongoing advice, support, expertise and friendship.

I would like to thank Graham & Brown, without whom the project would be impossible, for the funding, opportunities and experience they have provided me throughout the years. Special thanks are also due Dr Michelle Ledward for her provision and guidance, as well as Dr Yu Yao, Ms Chloe Parrington and Ms Tahira Bush for ongoing assistance with manufacturing processes, plastisol formulations and L*a*b* analysis while on site at Graham & Brown.

Special acknowledgements are due to Mr Algy Kazlauciunas for his contribution of TGA, DSC and SEM analysis throughout the project, as well as Mr Martin Huscroft who aided the HPLC development and methodology.

I would like to thank industrial partners who have provided access to equipment for this project, including Perkin Elmer, Waters, and Speciality Coatings.

Further thanks are tremendously due to my wonderful partner and family, whose unwavering support and confidence have helped me no end throughout my studies.

I would finally wish to thank the University of Leeds for the opportunity and facilities to carry out this work.

Abstract

Chemical additives are important materials in the plastics and polymers industries, utilised widely to manipulate the chemistry and resultant physical properties of polymeric products. One group of such additives are chemical blowing agents. Blowing agents are materials commonly used to produce a low density, cellular structure within a polymeric matrix through the generation of gas via thermal decomposition. No chemical blowing agents does this more efficiently than azodicarbonamide. Azodicarbonamide is used across a multitude of applications, and is a high gas yielding, cost-effective, adjustable blowing agent. All commercially used chemical additives are subject to strict, stringent regulatory protocols and azodicarbonamide is no exception. In 2012 the European Chemicals Agency, registered azodicarbonamide as a Substance of Very High Concern due to evidence of respiratory sensitisation. This classification has resulted in a commercial need for suitable replacements for azodicarbonamide for a number of applications. One of these applications is the decorative coatings industry.

This study outlines the potential of many materials within an existing decorative coating formulation under standard manufacturing conditions and compares the results to those of the currently used azodicarbonamide. Recommended known alternatives have been studied both independently and in a co-blowing agent system with azodicarbonamide, showing mixed results. Furthermore, a range of bio-based and naturally arrived fragments such as citric acid and urea, have been utilised to synthesise a library of sustainable chemical additives as potential alternatives to azodicarbonamide. The additives were implemented into formulation and analysed for properties such as colour, gloss, expansion, surface structure and internal cellular structure, in comparison with the control azodicarbonamide formulation.

Furthermore, the classification of azodicarbonamide as a Substance of Very High Concern, limits its use to a restriction of 0.1% w/w in products. A quantitative analytical technique has been investigated in attempt to accurately identify residual amounts of azodicarbonamide within decorative coating products.

Abbreviations

Abbreviation	Term
ADCA	Azodicarbonamide
D2TG	2nd derivative of the TGA
DEAD	Diethyl azodicarboxylate
DMF	Dimethylformamide
DMSO	Dimethyl sulfoxide
DPT	N-N-dinitrosopentamethylene tetramine
DSC	Differential scanning calorimetry
DTG	1st derivative of the TGA
ECHA	European Chemicals Agency
EU	European Union
GU	Gloss units
HPLC	High performance liquid chromatography
HRMS	High resolution mass spectrometry
HSE	Health and Safety Executive
IR	Infrared
Mag.	Magnification
NMR	Nuclear magnetic resonance
OBSC	4,4'-oxybis(benzenesulfonyl semicarbazide)
OBSH	4,4'-oxybis(benzenesulfonyl hydrazide)
PVC	Polyvinylchloride
REACH	Regulatory, Evaluation, Analysis of Chemicals
SEM	Scanning electron microscopy
SVHC	Substances of very high concern
TGA	Thermo gravimetric analysis
THF	Tetrahydrofuran
TSH	Toluenesulfonyl hydrazide
TSSC	Toluenesulfonyl semicarbazide
UPC^2	Ultra-performance convergence chromatography
UV-Vis	Ultraviolet-Visible Spectroscopy
ΔE	Delta E (colour change)

Glossary of Terms

Term	Definition
Annex XIV	Authorisation list
Annex XV	Candidate list
Blowing Agent	An additive which releases gas upon thermal decomposition
Curing	Drying by the evaporation process of solvents
Gloss	The shine or lustre on a smooth surface
Kicker	An additive complex that activates the thermal decomposition of the blowing agent
Plastisol	A liquid substance that can be converted to solid plastic by heating, consisting of particles of synthetic resin dispersed in a non-volatile liquid

Table of Contents

List of Figures

List of Tables

List of Schemes

Chapter 1 Introduction

1.1 Sustainability of the Polymer Coatings Industry

Within the chemical industry, the need for naturally derived chemical materials is rapidly developing. As the world becomes more environmentally conscious, the commercial chemicals market must keep up, and the polymers and plastics industries are no exception. Renewable polymeric materials and bioplastics are constantly being developed [1, 2] with the aim to fulfil the goal of providing a greener and more sustainable plastics industry. [3] Bioplastics produce biomass by recycling the carbon dioxide (CO_2) emitted during production and disposal. [4] This makes them carbon-neutral materials and contributes to lowering overall CO_2 emissions, [4] an essential requirement for environmental protection. [5, 6] Bioplastics are polymers obtained from bio-sources. [4] A bioplastic can be produced by the modification of the polymer repeat unit and/or the introduction of copolymers. [4, 7, 8] These advances in bioplastics are essential for maintaining the sustainability of the plastics industry, and developments are increasing rapidly. That said, many applications do not have suitable bioplastic alternatives as the physical property limitations of bioplastics confine their application in many areas. Over the last few decades, the emissions associated with polyvinylchloride (PVC) products have been significantly reduced by almost half. [9] However, PVC is still required in such vast quantities, that there is no suitable bioplastic substitution for all applications.

Polyvinylchloride (PVC) has been a commonly used material since its introduction to commercial production in 1933. [10, 11] PVC is the third most abundantly used plastic, behind polyethylene and polypropylene, [12] accounting for a total of up to 20% of all plastics manufactured world-wide. [10] Approximately 6 million tonnes of PVC are manufactured within Europe per annum. [13] PVC coatings are an essential component in a number of applications, the most predominant of which are the packaging [14, 15] and construction [16] industries; however, others include healthcare, [17] floorings, [18] optical devices [19] and wall coverings and furniture. [20]

1.1.1 The Importance of Naturally Derived Chemical Additives for PVC Formulations

The multitude of industries utilising PVC products means that numerous varying properties are required from the materials. For example, flexible PVC material for cables and wrapping, [21] as well as rigid PVC for items such as window frames and packaging. [22] This means that plentiful additives and formulations must be developed to fulfil these varying physical properties. It is essential to ensure that all additives and components within PVC formulations do not contribute to the toxicity or emissions of the overall process and maintain the products sustainability. [9, 23, 24] Despite the developments in the overall reduction of PVC emissions, [9] it is still essential to continue to reduce emissions by ensuring chemical additives within formulations do not contribute to the toxicity. This will further advance the sustainability of the products and industries associated with heavy PVC usage. [25, 26]

In the decorative coatings industry, the use of chemical additives is vital. Chemical additives are used to manipulate the physical properties of PVC coatings. Common chemical additives in PVC formulations can include activators, stabilizers, [27] pigments, [28] blowing agents, [29] levelling agents and more. It is essential that additives within formulations for coatings minimize the surface defects that can form on the coatings during the heating and curing stages of production. [30] These additives are referred to as levelling agents. [31] Levelling agents stabilize against defects by breaking down high surface tension gradients and spontaneously creating a lower surface tension film to create a smooth, glossy surface. [31-33]

Common defects that can be eliminated through the use of levelling agents include orange peel effects, craters, fish-eyes and ghosting. The orange peel effect is a common result of the coating application method. These leave a wavy surface with a high surface area. [32] Levelling agents lower the surface tension to create better flow, by reducing the localised attraction forces; resulting in a flat surface with a lower surface area. Craters are formed when there is incompatible contamination such as filler compounds or solvents. [32] Fish-eye defects are when a crater reaches a depth that reveals the substrate. These are generally formed through high levels of contamination or severe internal incompatibility.

Rectification of these defects requires a levelling agent with a lower surface tension than that of the contamination material. Ghosting is a defect that can occur during the curing process, particularly for high viscosity coatings, and results in an unevenness of the thickness of the coating. To overcome this problem wetting is required. Wetting uses a levelling agent to displace air from the surface ensuring that the surface tension of the coating is lower than that of the substrate material, [31] thus allowing even spreading of the coating.

When modifying formulations for coatings, it is essential to consider these potential defects since alternative and naturally derived chemical additives may not result in the same physical appearance of the modified coating. Furthermore, when multiple additives are required it is advantageous to minimise components within a formulation by utilising materials with dual properties, for example in a foamed coating, the use of a blowing agent that also aids dispersion by acting as a levelling agent, can potentially reduce the associated toxicity of the final product.

1.2 Polymeric Foams and Blowing Agents

Blowing agents, sometimes referred to as foaming agents, [34] are additives used to produce a cellular structure within a polymeric composition [35] through the generation of gas within the solid mass. [36] A blowing agent is categorised as either physical or chemical, dependant on how the gas is generated. [37] A physical blowing agent produces gas by a physical state change. This state change can arise by controlling or changing various experimental conditions, such as heating, cooling or a change in pressure. [38]

Chemical blowing agents; however, release gas as the result of a chemical reaction such as thermal decomposition. [36] The reaction carried out by chemical blowing agents produces a more effective foam structure [39] in high-density materials [40] than that of physical blowing agents. Chemical blowing agents allow for greater control over the structure of the final foam produced and the reaction conditions of the process. [37] This is useful in industry as it provides versatility of application. This said, chemical agents can be more costly than their physical counterparts [40] which may not be advantageous for commercial use, particularly for smaller applications.

Chemical blowing agents are used in a variety of applications across a range of industries, one of which is the production of polymer foams. [37] Polymer foams are extremely common and can be found in many everyday items, including disposable food containers, insulation materials and soft furnishings. [41] The cellular structure of the foam, introduced by the blowing agent, provides the polymer with a reduced density [38] and increased tensile strength and impact resistance [34]. These properties, among others, make polymer foams very desirable in many commercial markets.

The uniformity and size of the pores that create the foam can be controlled by the composition, grade, concentration and particle size of the powdered blowing agent used. [34] Research on the particle size and composition of chemical blowing agents shows the influence these variables have on the quality, structure and uniformity of the foam produced. Work by Petchwattana and Covavisaruch in 2011 [34] shows that the overall cell size within the foam becomes smaller as the concentration of blowing agent is increased in the formulation. Furthermore, it is shown that as the particle size increases, as does the foam cell size. These findings are supported by the earlier work of Riley *et al.* [42] in 1967 which also states that control of the particle size can improve control of the decomposition temperature when using activating agents such as barium, cadmium, zinc and tin. This is advantageous as a more uniform cellular structure produces more closed cells and subsequently results in a higher expansion ratio. This high ratio is a result of excess gas that would normally be lost from the system, being contained within the newly closed cells. [43]

The quality of the foam structure is vital in the manufacture of safety critical items such as insulation for cables and shock resistant items to ensure they are consumer safe. Cellular uniformity is not required for the safety of items in various decorative applications. Furthermore, a highly uniform foam structure can result in excessive foam thickness which is not always desirable. As cellular uniformity is controllable, chemical blowing agents provide the option for a variety of different foam arrangements as required. It is essential to consider the cellular uniformity produced by various different blowing agents as a poor structure can result in collapsing of the foam.

1.2.1 The Use of Azodicarbonamide as a Blowing Agent

Azodicarbonamide (ADCA) **1**, is the most commonly used chemical blowing agent in the production of polymer foams [36].

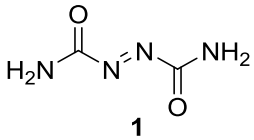

1

ADCA is a yellow powder also used as a blowing agent in the food industry. [44] It was developed in Germany during the Second World War after the toxicity of the formerly used compound, azobis(isobutyronitrile), made it redundant. [37, 38] ADCA has been used commercially since the 1950's and has a wide versatility due to its high gas yield [45] and modifiability. [38] Some applications include the production of heat-insulating coatings, [46] waterproof materials, [47] sealants [48] and wallpapers. [49] The decomposition temperature of untreated ADCA is 210 °C, at which point gases such as nitrogen and carbon monoxide, are given off and white sublimates and residues are formed. [50] There are numerous suggested thermal decomposition pathways of ADCA quoted in the literature. [51, 52] These pathways lead to decomposition products such as urea **2**, urazole **3**, cyanuric acid **4**, biurea **5** and isocyanic acid **6** [45] shown in Figure 1.1.

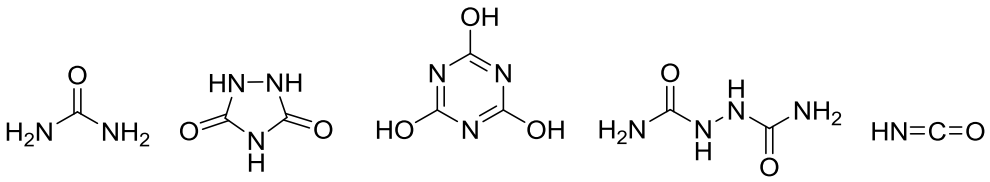

2 **3** **4** **5** **6**

Figure 1.1 Chemical structures of ADCA thermal decomposition compounds. Urea **2**, urazole **3**, cyanuric acid **4**, biurea **5** and isocyanic acid **6** (Left to Right)

The decomposition products, in particular solid residues, are an important consideration when selecting a blowing agent as they can remain within a formulation and can be present in the final product. For this reason, it is important that the mechanism of breakdown is known so that the products can be most accurately assessed.

In 1975, Prakash *et al*. [50] challenged the previously accepted pathways by suggesting that two simultaneous decomposition mechanisms occur. This

mechanism was later confirmed by the work of Robledo-Ortiz *et al.* [53] in 2008. This mechanism was not previously known as urazole was unidentified in the IR spectrum due to the overlap of all urazole **3** absorptions with the biurea **5** and cyanuric acid **4** signals. Decomposition reaction 1 (Figure 1.2) shows the breakdown of ADCA **1** into biurea **5**, nitrogen and isocyanic acid **6**. The second decomposition reaction (Figure 1.3) forms urazole **3**, nitrogen, isocyanic acid **6** and urea **2** [50].

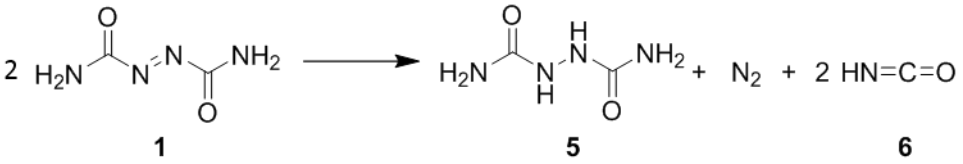

Figure 1.2 Decomposition reaction 1. The breakdown of azodicarbonamide **1** into biurea **5**, nitrogen and 2 units of isocyanic acid **6**.

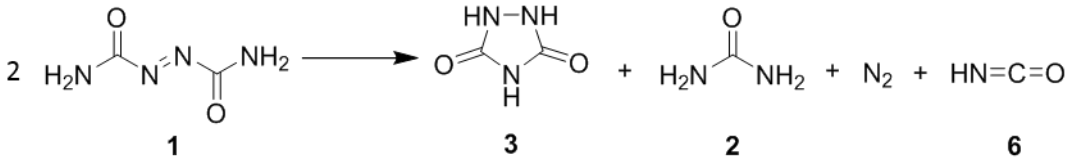

Figure 1.3 Decomposition reaction 2. The breakdown of azodicarbonamide **1** into urazole **3**, urea **2**, nitrogen and isocyanic acid **6**.

Prolonged exposure to temperatures higher than 180 °C results in the decomposition of biurea **5**, to yield additional amounts of urazole **3** and ammonia. Furthermore, the urea formed in decomposition reaction 2 is unstable and dissociates to ammonia and isocyanic acid **6**, thus making urea **2** a difficult component to detect in the sublimates. [53] The excess isocyanic acid **6** can undergo polymerisation to yield cyanuric acid **4** which is also found in the decomposition residue. The secondary break down pathways and reactions of the decomposition products themselves led to the misunderstanding of the overall mechanism in early research; [52] however, the presence of urazole **3** below 180 °C confirms its formation from azodicarbonamide **1** itself and therefore the second decomposition reaction (Figure 1.3). [50]

The two simultaneous decomposition reactions are aided by the self-assembly of the ADCA molecules into highly favourable monoclinic sheets, as shown in Figure 1.4. The arrangement is stable through the formation of non-covalent interactions between each molecule and the 4 adjacent molecules. During thermal decomposition the non-covalent bonds are broken, but the

proximity of each molecule results in the formation of the decomposition products by the cleavage of various covalent bonds and protonation.

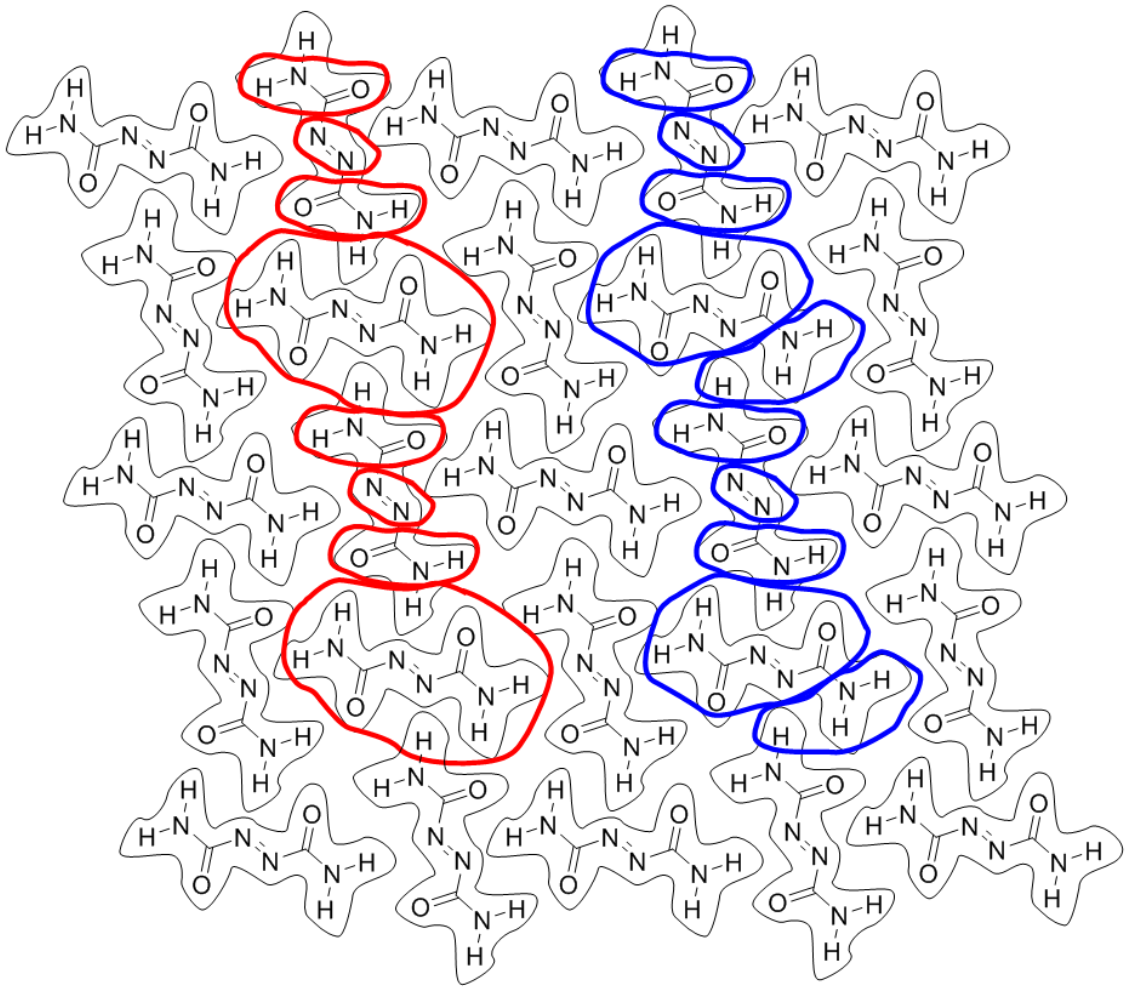

Figure 1.4 Azodicarbonamide molecules arranged in one-dimensional monoclinic sheets highlighting how the structural pattern aids the formation of the decomposition products of reaction 1 (red) and reaction 2 (blue), adapted from Prakash *et al.* [50]

The composition of the residues, gases and sublimates formed through thermal decomposition at a set temperature is constant. This consistency confirms the one-dimensional arrangement where a more rigid structure is held, as opposed to random interactions between colliding molecules.

As previously stated, full decomposition of ADCA occurs at 210 °C; however, activating compounds such as ZnO, CdO and PbO result in the decomposition temperature being reduced to anywhere between 160-190 °C. [54] Furthermore, the addition of aliphatic hydroxyl amine compounds and their salts combined with heavy metal oxides can further reduce the decomposition temperature to as low as 110 °C if required. [55] This variable temperature range

provides versatility, thus allowing ADCA to be used in many different processes. In addition to these properties, ADCA is stable, easily handled [56] and readily available for low cost. [57] The coloured nature of the powdered compound can result in a yellow stain, which is detrimental in colour sensitive applications. However, this can be avoided using systems above 150 °C. The use of activating agents does have some drawbacks due to the restriction of heavy metals in commercial products. It is important to consider the British Standard: BS EN 15102:2007 +A1:2011 industrial EU standard [58] when using techniques of this nature.

Despite its numerous advantages, the Austrian Competent Authority submitted a dossier [59] highlighting azodicarbonamide as a potentially toxic compound in 2012. This dossier categorises ADCA on the candidate list as a compound having equivalent concern as a carcinogen and could result in the restriction of its use in the EU. Although not considered in the classification act, the degradation of ADCA yields the by-product semicarbazide **7**.

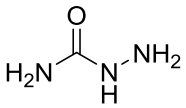

7

Semicarbazide **7** is a potentially toxic compound and therefore traces within a product are not desirable [60]. The research of Nestmann *et al.* [61], into the levels of semicarbazide **7** present in baby food jars that use ADCA as a sealant, suggests that the amount present once the product reaches consumers, presents limited toxic threat. However, industrial workers are exposed to high levels of the compound and are consequently at a higher risk of developing associated health problems. [62]

1.2.2 Specific Applications in Decorative Coatings

Design and colour are the two most important factors when it comes to customer selection of wall coverings[i]. One essential component of design within this industry is the use of foam to create embossed effects, thus making the use of blowing agents essential. ADCA is the most commonly used chemical foaming agent for expanded decorative coatings. Since the inclusion of ADCA on the

[i] Information from Graham and Brown sales data and customer feedback

candidate list alternative blowing agents have be sought. There are some specific industrial processes such as food conditioning, where alternatives have been found that result in little to no effect on the products produced [61]. That said, there is currently no suitable alternative to ADCA as a blowing agent for PVC foams, in particular for decorative coatings manufacture. This is due partly to the variable decomposition temperature and very advantageous gas yield ADCA provides, [45] which is not replicated in other classes of blowing agent. The complete restriction of ADCA would have a global impact due to the vast number of polymer foam applications in which it is essential.

In decorative applications qualities such as odour, colour, foam structure and cost are major factors and must be considered as well as toxicity and efficiency of gas yield when selecting an alternative to ADCA. [37] The absence of a suitable alternative within this industry would ultimately lead to a significant reduction in the number of available products. Currently in the manufacture of expanded decorative coatings, ADCA is added to the plastisol formulation before application to the substrate by coating or printing processes. The treated substrate is heated during the manufacturing process which initiates the thermal decomposition of ADCA within the plastisol mixture. This process creates a low density, foamed texture which is a highly desirable design aspect. Textured patterns are also produced through use of blowing agents. ADCA is either applied to a specific area of the design causing foam here alone, this is done by printing, or more commonly, the blowing agent is evenly coated across the entire unit followed by the compression of certain areas by embossing, to leave a pattern[ii]. These effects are currently unachievable without the use of ADCA. If ADCA were to be fully authorised and restricted for use in the EU a replacement compound would be critical. That said, the initial classification of ADCA puts certain pressures upon industry to develop methodologies to a safer and less toxic alternative.

To be successful the new blowing agent not only needs to successfully create sufficient foam within the polymer formulation, it also needs to have the appropriate properties to fulfil the specific commercial needs and fit into the existing industrial process. A suitable replacement would need to be non-toxic

[ii] Information provided by Graham & Brown: general manufacturing process

and non-harmful to humans, animals and the environment. Furthermore, it must be easy to handle and dispose of. Any replacement additive must also be colourless and odourless as to not affect the physical properties of the resultant coating.

1.2.3 Current Alternatives to Azodicarbonamide

There are numerous alternate blowing agents available on the market. The original dossier submitting ADCA for classification lists potentially suitable known alternatives. [59] Most of these are physical blowing agents and not applicable to PVC formulations. Five chemical alternatives were submitted, some of which are used widely throughout industry, whereas others are limited to specific applications. [59] A literature review was carried out, focused on the properties, uses and hazards of existing blowing agents. Blowing agents are characterised into classes of similar structure and often exhibit similar chemical and physical properties within the class. Key data including; appearance, molecular weight, density, decomposition temperature, amount of gas produced, solubility, hazards, incompatibility and applications were collected for each compound, these were then compared and contrasted to ADCA to identify any potentially suitable, existing alternative.

ADCA belongs to the azo class. The second well known blowing agent in this class is Azobis(isobutyronitrile); [37] however, this compound is not a suitable alternative as it was classified as toxic previous to the wide spread use of ADCA. For this reason it is listed as ‘not recommended’ for commercial use in the USA [63] and can be ruled out without further investigation.

1.2.3.1 Carbonate Compounds

Other commonly used compounds include those of the carbonate class, in particular sodium hydrogen carbonate (better known as bicarbonate of soda or $NaHCO_3$) which was suggested in the original dossier. [59] Bicarbonate of soda is commonly used in the food and medicinal industries. One common application of $NaHCO_3$ is as a dough conditioner and it is a readily available alternative in foods that previously used ADCA. It is also suited for use in the medicinal industry. [64, 65] There are many advantages to bicarbonate of soda; it is very cost effective, [66] has low parent and by product toxicity [64] and is highly water

soluble creating ease of handling and disposal. [45] These beneficial qualities make it fit for purpose in the food and medicinal industries.

That said, literature findings suggest that bicarbonate of soda is not practical for use in polymers as it is not sufficiently dispersible within the resin to create an even foaming structure [37]. Furthermore, it has a lower than desired decomposition temperature of 150 °C. This is outside the melt viscosity range of PVC plastisol formulations, which occurs at 180-210 °C. [37] Bicarbonate of soda is also limited to certain experimental conditions, for example; it cannot be used in high pressure environments, [64] which limits its use in some industrial processes. It also has a very low gas yield in comparison to ADCA, which could result in an unsatisfactory foam and potential collapsing in polymer mixtures. [45] this data suggests that $NaHCO_3$ would not provide a suitable direct replacement of ADCA in the current formulation. However, limited research has been published on the effects of endothermic blowing agents such as $NaHCO_3$ within flexible polymer coatings, therefore the efficiency of the material within the application is widely unknown.

1.2.3.2 Tetrazole Compounds

The tetrazole compound, 5-phenyltetrazole **8** was also listed in the Austrian dossier and can be considered as a direct alternative to ADCA in some applications due to the comparable decomposition temperature of 215 °C [45].

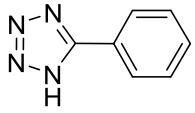

8

Compound **8** yields 1.22 moles of gas per mole of reactant which is advantageous against ADCA's 0.97 moles per mole [37]. However, despite these advantages, tetrazole compounds are very difficult to handle and present an explosive risk during the heating process [67]. For this reason, they are not practical for a large scale industrial production and therefore would be impractical within this project.

1.2.3.3 Hydrazine Compounds

The compounds, 4,4'-oxybis(benzenesulfonyl hydrazide) **9** and toluenesulfonyl hydrazide **10** were submitted by the Austrian dossier as alternatives for PVC and rubber applications. [59]

The first of these, 4,4'-oxybis(benzenesulfonyl hydrazide) (OBSH) **9**, is currently the second most commonly used blowing agent in the plastics and polymer industries after ADCA, mainly due to its high gas yield. [68] Therefore, it is a popular choice for many industrial processes as an alternative to ADCA.

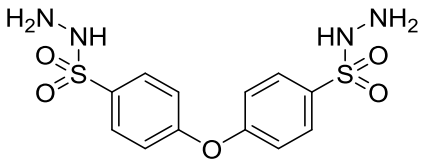

9

The compound OBSH **9** has a high gas yield, [45] is odourless [37] and has very little known toxicity associated with it or its by-products. [69] These properties, among others, make it a commonly used blowing agent in natural and synthetic rubber foaming as well as in the formation of various thermoplastic foamed products. [70] For these reasons OBSH **9** was suggested by many industries, including the dossier, as a potential alternative to ADCA.

Despite its many advantages, the decomposition temperature of 160 °C [45] is too low to be compatible with current plastisol formulation. This means that in order for OBSH **9** to be most effective, new plastisol formulations may be required to ensure that the mixture has a suitable melt viscosity to accommodate the blowing agent. [37] The development of these plastisol formulations is both time consuming and costly, and therefore would not be the most beneficial pathway. That said, the high gas yield of OBSH is advantageous and if suitable within the formulation, could lead to overall cost efficiency. The study of OBSH within flexible PVC coatings is limited; however, the success in areas such as flexible rubbers suggests that there may be some scope for the use of OBSH within the decorative coatings industry. [64]

Toluenesulfonyl hydrazide (TSH) **10**, is also a hydrazine class blowing agent. It is a highly water soluble molecule [71] that produces an evenly distributed foam. [37]

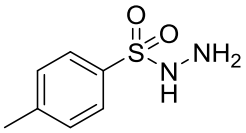

10

The decomposition temperature of **10** is lower than OBSH **9** [72] and the compound produces a strong, unpleasant smell. [37] Additionally TSH **10** is classified as toxic, under the toxic substances control act, [73] as there is evidence of exposure causing dermatitis. [74] Therefore, is not a useful blowing agent in many industrial practises and can be ruled out from investigation.

The hydrazine class also contains the blowing agent hydrazo dicarbonamide (also known as biurea **6**). This compound has a very similar chemical structure to ADCA where the azo bond has been reduced to the hydrazo, single N-N bond. Biurea **6** is one of the main solid by-products of the thermal decomposition of ADCA (Figure 1.2), accounting for 37% of the by-products produced by ADCA, [50] as well as being a blowing agent in its own right.

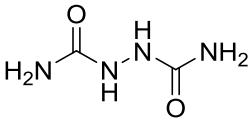

6

The high decomposition temperature, of 245°C, [45] means that it may not be practical at current manufacturing temperatures. However, there is evidence that decomposition can start at temperatures as low as 180 °C, resulting in the production of urazole **3** and ammonia. [50] Similarly to ADCA, biurea is also a known respiratory sensitizer and shows evidence of toxic effects in humans. [38, 75] Biurea **6** is not currently classified under the control substances act but it is possible that it could be presented for consideration in the future. That said, the gas yield is 0.86 moles per mole and it is highly soluble in water, making it easily disposable. [45] These properties are beneficial; however, they are not compensation for the risks associated with the undesirable toxicity profile. For this reason, biurea can be excluded from the study.

1.2.3.4 Carbazide Compounds

Carbazide compounds have the same structural backbone as OBSH **9** and BSH **10**, where the terminal hydrazine (H_2N-NH_2) group is replaced with a carbazide (H_2N-NH-CO-NH_2) group. This class of compounds have higher decomposition temperatures than both the hydrazine compounds and ADCA. With full decomposition occurring around 230 °C, [76] the current manufacturing process would require more efficient, yet more costly, ovens as there are no known activating substances to lower the temperature quoted in the literature. That said, the structural similarities between the carbazide group and ADCA, could lead to a similar activation by compound such as ZnO, resulting in lowering the decomposition temperature.

Toluenesulfonyl semicarbazide (TSSC) **11** has a high gas yield allowing for 1.36 moles of gas per mole [68] and was the final compound suggested in the dossier [59].

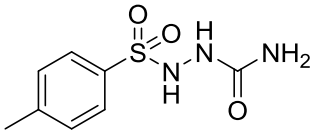

11

This is advantageous as less starting compound is required to achieve comparative results. Furthermore the compound is odourless, [76] non-toxic [77] and soluble in a variety of organic and aqueous solvents including methanol, THF and water. [78] These qualities, along with its decomposition temperature, make it very useful in the production of hard PVC foams. That said, there is no evidence of this success being replicated in the existing process for soft polymer foaming without significant changes to the industrial process. Furthermore, there is indication of skin and respiratory sensitisation through prolonged expose to TSSC **11**. [78] There are limited studies supporting this toxicity; however, it is still an important consideration when associating compounds to large scale industrial processes.

The compound 4,4'-oxybis(benzenesulfonyl semicarbazide) (OBSC) **12** shows the highest gas yield per mole of the compounds investigated. [76] OBSC **12** is a costly material; [79] however, the yield of 2.68 moles per mole makes the compound more cost effective than it would otherwise be. This said, over

foaming must be considered. A high gas yield could produce too much foam or a poorly structured foam with larger, uneven pore sizes. This could be considered a disadvantage as it would increase the thickness of the coating and could lead to collapsing of foamed areas, which is not desirable.

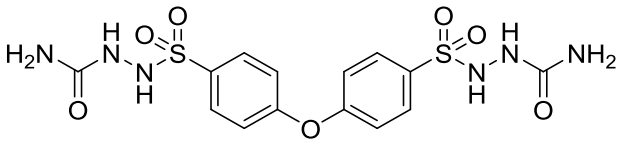

12

The compound OBSC **12** fully decomposes at 220 °C, [76] similar to ADCA. [45] This makes OBSC **12** more suited to elevated temperature processes. One example of this is 'foam-in-place' technology [80] where moulds are treated at high temperatures to create low density parts for the aerospace and automotive industries. Further disadvantages for the use in the manufacture of decorative coatings are that it is not soluble in aqueous media and that it has a distinct odour. [45] Considering these properties, OBSC **12** and TSSC **11** can be ruled out as direct replacements for ADCA within the decorative and wallpaper industries.

1.2.3.5 Nitroso Compounds

The final class of compounds investigated as potential alternatives to ADCA is the nitroso compounds. The most widely used blowing agent in this category is *N,N'*-dinitrosopentamethylene tetramine (DPT) **13**.

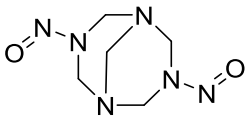

13

DPT **13** has a suitable thermal decomposition temperature and gas yield to be used in the existing plastisol coating formulations. [45] The decomposition temperature of 210 °C can be further lowered with activating agents to give a range of 130-190 °C, [37] as in ADCA. Moreover, DPT **13** is already used in commercial PVC foaming and shows little evidence of toxicity in the parent or decomposition products. [81] Further advantages applicable to the decorative applications are DPT's non-colouring and non-staining qualities [37] preventing any interference with design. However, DPT **13** has a strong fishy odour as a

result of the amine compounds released upon thermal decomposition, whilst this can be supressed with the addition of urea and melamine, this smell makes DPT **13** inappropriate for use in the decorative industry. [37] DPT was ruled out from further investigation.

1.2.3.6 Patented Compounds and Methods

There are currently a vast number of compounds patented as chemical blowing agents worldwide. It is important to consider compounds with active patents to ensure that repetition does not occur. A total of approx. 220 patents were investigated for the purpose of this study. Many of the identified patents concern the previously mentioned common blowing agents; however, others reference structures that could potentially provide an alternative to ADCA. Many of the compounds quoted in the patents are derivatives containing the hydrazo or azo structure, where various functional groups are added or removed from commonly used compounds. For example, the 2011 patent issued to Hebei Jiameile Plastic Products Co, Ltd, Peop, Rep, China [82] shows the use of ADCA **1**, TSH **10** and DPT **13** alongside an azo compound, diazoaminobenzene **14**.

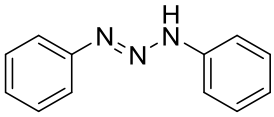

14

The above patented method focuses on the use of modified blowing agents for the successful foaming of yoga mat materials. Diazoaminobenzene **14** is used in a mixture with ADCA in this case. Due to its low melting point of 98 °C it is unlikely that it would be a viable blowing agent when used independently. [37]

Other azo compounds, include the diethyl ester derivative of ADCA **1**, known as diethyl azodicarboxylate or DEAD **15**, used in the production of decorative sheets. [83]

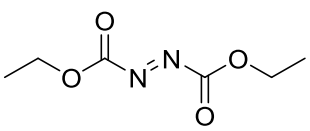

15

This work, carried out in 1986, uses a wide range of known blowing agents in various ratios and combinations to achieve the desired level of foaming. These include the previously mentioned diazoaminobenzene **14**, ADCA **1**, TSH **10**,

OBSH **9** and DPT **13**. [83] As well as being used as a blowing agent, DEAD **15** is primarily known as a widely used reagent in important reactions such as the Mitsunobu reaction of alcohols. [84] DEAD **15** has a melting point of 120 °C [83] which is too low for consideration as a replacement for ADCA, furthermore the compound is highly toxic and light sensitive. [85] Undiluted, the compound can produce a powerful explosion when heated above 100 °C. [86] Without further research it is unknown what explosive risks the compound may present when diluted within a plastisol.

The use of sulfonyl hydrazides appears in multiple patents, many of which include phenol groups and have similar structures the compounds in the hydrazide and semicarbazide classes. Variation of the diphenyl bridge, shown in Figure 1.5, in the OBSH **9** structure is referenced in two active patents. [83, 87]

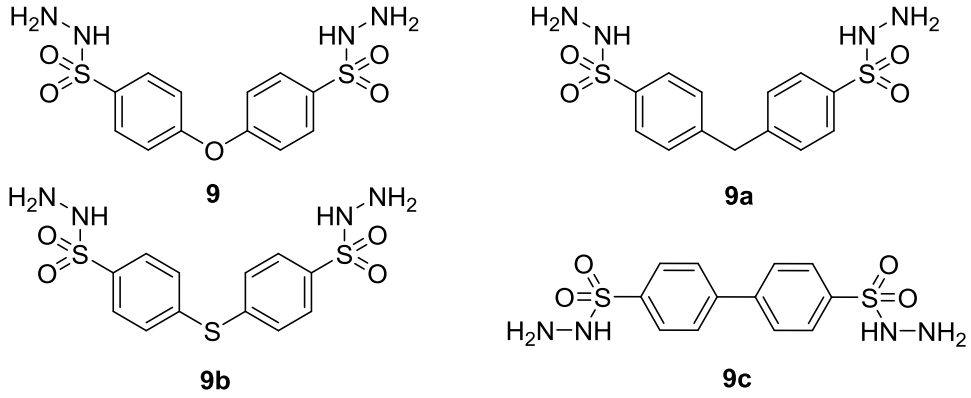

Figure 1.5 Derivatives of OBSH **9** used as blowing agents in the production of decorative sheets (**9a** and **9b)** and thermoplastic synthetic materials (**9c**)

While these compounds prove to be successful for their desired applications, it is predicted that each of these compounds will possess similar disadvantages as those discussed in paragraph 1.2.3.3 for OBSH **9**. Primarily low-quality foam production leading to the collapsing of foamed areas in PVC plastisol's for decorative coverings.

The patents also show compounds containing both sulfonyl groups and sulfide bridges. Compounds such as *p*-toluenesulfonyl disulfide **16** and benzenesulfonyl tetrasulfide **17** are used in conjunction with ADCA for the formation of various foamed plastics and shown in Figure 1.6

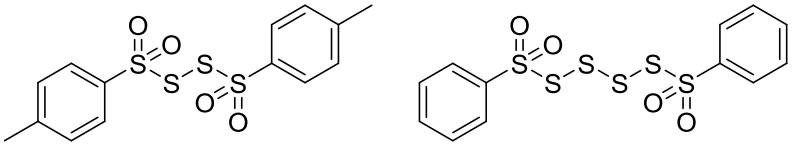

16 **17**

Figure 1.6 Sulfide compounds used with ADCA, *p*-toluenesulfonyl disulfide **16** and benzenesulfonyl tetrasulfide **17**

These sulfonyl sulphide compounds have a dual purpose in their use with ADCA. As well as increasing the efficiency of ADCA as a blowing agent they also act as activators. The compounds are used alongside zinc oxide to lower the decomposition temperature of ADCA and create a more economic system. [88] That said it is predicted that the number of sulfur atoms present in compounds of this type may produce a strong, unpleasant smell [89] which is undesirable in the target application. [90]

Many compounds identified by the literature and patent searches proved to be incompatible with the current experimental conditions of the decorative coating production process; mainly due to toxicity and unsuitable decomposition temperatures. However, some structures did provide a useful backbone which could be modified to contain functional groups that would potentially make them more suitable. The 2012 study by Sanita *et al.* shows the use of citric acid alongside ADCA and sodium bicarbonate for the foaming of plastic beads in household electronics [91]. Citric acid is a non-toxic compound that allows for both electrophilic and nucleophilic attack. This versatility of functional groups allows for numerous potential modifications, which could lead to a more suitable blowing agent in the target application.

The literature study of compounds such as OBSH and TSSC proved inconclusive in the target application. Little information is available about their efficiency in plastisol formulations, further investigation could identify suitability.

Many of the patents studied, made use of co-blowing agent systems. This technique could prove advantageous in the application of decorative coatings if no direct alternative for ADCA is identified. Co-blowing agent systems could allow for modification of physical properties by blowing agents that otherwise would be unsuitable. As seen in the case of diazoaminobenzene, which successfully utilised in conjunction with ADCA despite its decomposition temperature outside the suitable range. [82]

Chapter 2 REACH Regulations

2.1 What is REACH?

REACH is a governmental enforcement division of the European Chemicals Agency (ECHA) responsible for the “Regulation, Authorisation and Restriction of Chemicals” within the EU. [92] REACH came into force in 2007 and since this time every chemical manufactured in, or exported into the EU, in quantities of 1 tonne or more, must be approved and comply with the strict regulations set in place by the organisation. Some specific exclusions do exist, such as medicines and foodstuff additives, which have separate legislations with specific provisions relating to the products end uses. More chemicals excluded from the REACH regulations are substances such as radioactive substances and non-isolated intermediates. That said the majority of chemicals used in industry are included in this system in an attempt to protect both human health and the environment from the use of toxic chemicals. The system also aims to enhance innovation, competitiveness and free movement within the EU market and promote alternative methods of assessment. [93]

2.1.1 Registration and Authorisation of Chemicals

It is the responsibility of manufacturers and importers to register all chemicals with ECHA along with a required data set. Without this data it is illegal to manufacture or supply these substances. [94] Currently the organisation is in a ‘pre-registration’ stage, which was put in force to prevent an unmanageable influx of registrations upon commencement in 2007. Pre-registration allowed for existing compounds to become part of a staggered three-phase registration program over the first 11 years of REACH statute, whereas new substances required immediate registration. In 2018, the deadline for registration under the three-phase system will have ended and all substances will be registered in the same way. [95]

Once registered, the substance is subject to both risk and hazard assessments based on the data set provided. [96] The results of which are submitted to the ECHA, at this stage each member state can evaluate the substance considering risks to human health and can submit a dossier for authorisation to REACH if it is deemed necessary. [97] Once a dossier is

submitted and accepted by REACH, the compounds are added to the Candidate List for Authorisation (Annex XV) while they are investigated for potential hazardous and harmful properties. Evaluation can identify if a substance requires prioritisation for authorisation, if a proposal to change the classification is necessary and if labelling of a product is required. However, once listed, there is currently no process to remove compounds from the candidate list. [96]

If a compound is found to have serious health consequences, or is persistent within the environment resulting in the bioaccumulation in animals, it can be listed as a substance of very high concern (SVHC). [98] Substances presenting 'equivalent concern' are also characterised as SVHC's and undergo the same examination. It is a legal requirement to communicate information of SVHC's present in articles and mixtures. SVHC's are also subject to authorisation and restrictions if a public consultation of interested parties present the necessary information to the ECHA. [99] Restrictions can include a total ban on supply to the general public, a limitation of imports or quantitative restrictions. Industries can apply for authorisation to use restricted substances by providing adequate evidence that the substances can be controlled or that the socio-economic benefits outweigh the risks associated. [96]

2.1.2 Enforcement of REACH

The member states within the EU are required to have an enforcement regime. In the UK this is managed by the Health and Safety Executive (HSE). [100] They must monitor inspections of substances to an acceptable standard and report all findings to REACH in five year intervals. [101] The co-operation and exchange of information between the member states is fundamental in the success of REACH. Member states must facilitate each other in the evaluation of SVHC's and power is given to agree on arrangements within the member states so that the most suitable authority can carry out the evaluation. Failure to comply with the legal requirements of the REACH legislation can result in an unlimited fine and/or up to 2 years imprisonment for the persons involved. [100] Despite the UK's decision to remove itself from the EU, it currently remains a member state within ECHA[iii] and therefore the policies of REACH must still be enforced within the UK. Regulations may change as the exit deal moves forward;

[iii] Accurate as of December 2017.

however, it is important to consider REACH regulations as they apply to any material imported or exported in the EU, in quantities of 1 tonne and above.

2.2 Importance of REACH within the Project

When developing a new substance for industrial processes it is essential to ensure that it conforms to any toxicity, health and safety and/or environmental restrictions to ensure safe work practise. Due to the registration process, controlled by REACH, if a substance exhibits potential hazard to health, it is exposed to authorisation and potential bans. When developing a novel compound, it is important to gain as much information as possible to present during the registration process. The substance must undergo toxicity and animal testing to identify any hazards to human health or the environment. This testing would be carried out further down the timeline, when a substance is identified as viable, as part of the implementation into industry before commercial launch. [102] However, during the development stage, proposed decomposition mechanisms can give an initial indication of toxicity or potential hazards that may arise during the breakdown of the materials. When considering decomposition, modification with various functional groups can potentially minimise toxic by-products and lower the risks associated. Furthermore, by looking at the classification of chemically similar substances some knowledge can be gained, and predictions made into how the substance may be classified.

2.2.1 REACH and Azodicarbonamide

First reports of ADCA toxicity were as early as 1984, when Bonsall published a short communication summarising ADCA as a cause of dermatitis. [103] In 1994 the ‘EC working group on Classification and Labelling of Dangerous Substances’ concluded that previously exposed individuals showed sensitivity to ADCA. [59] A few years later, in 1996, the EU classified ADCA as a respiratory sensitiser. [104]

In September 2012, the Environment Agency Austria, on behalf of the Austrian Competent Authority proposed ADCA as a substance of very high concern (SVHC). [59] The proposal summarised that “there is scientific evidence of probably serious effects to human health or the environment which give rise to an equivalent level of concern.” In December 2012, the proposal was approved

and ADCA was included on the ‘Candidate List of Substances of Very High Concern for Authorisation’, due to an “Equivalent level of concern having probable serious effects to human health”. [98]

This classification, was due to evidence of asthmatic reactions and increasing cases of respiratory sensitization. [62] This makes the use of azodicarbonamide less desirable within commercial industries. Under REACH regulations it is required that ADCA must form less than 0.1% by weight of any final product exposed to the public. [105] It is still relatively unknown what chronic effects trace levels of the substance may hold as the mechanism for respiratory sensitisation by ADCA is unknown [106] and initially little research was published on the case since its addition to the candidate list in December 2012. [105]

The recommendation for the inclusion of ADCA on the authorisation list (Annex XIV) was opposed by ten-member states of the EU REACH commission. Much work has been carried out over the last 5 years to challenge the classification of ADCA. An independent task force has carried out studies in attempt to disprove the respiratory sensitisation classification of ADCA. [104] A review published in 2017 by Arts *et al*. concluded that ‘ADCA has the potential to cause allergic sensitisation of the respiratory tract, and on that basis should not be classified as a respiratory allergen’, stressing that negative responses in skin sensitisation tests, should eliminate the consideration of ADCA as a respiratory sensitiser. [106]

In December 2016 the REACH committee ruled to postpone the classification of ADCA as it was identified that there was limited experience in the authorisation of broad use chemicals. Therefore, it was decided that due to the high volume of ADCA used across numerous industries, authorisation would be unmanageable without a standard methodology for quantitative testing. Although this decision is in place there is no indication from the ECHA committee as to when or if ADCA will be moved to authorisation level (Annex XIV).

The fluid nature of REACH status and ongoing developments concerning ADCA must be considered while undertaking such a project and aims and objectives must be modified to accurately represent the current socioeconomic status and imminent industrial need.

Chapter 3 Results and Discussion

3.1 Quantitative Analysis of Residual Azodicarbonamide in Final Articles

All compounds on Annex XV, including ADCA, are subject to certain restrictions. These restrictions mean that any product made using ADCA must contain less than 0.1% w/w residual compound, or the SVHC must be declared to the customer. [98] With this in mind it is important to develop an easy analytical technique that can accurately measure the amount of residual ADCA in the finished goods.

The current method for ADCA detection recognised by the HSE is soxhlet extraction.[iv] That said, this method is costly, time consuming and requires THF, which is highly flammable and difficult to store in some industrial environments. [107] Furthermore, the control ADCA samples analysed by soxhlet extraction show a 10% discrepancy from the known concentration which is a large margin of error for an analytical study.

Developments into alternative quantitative techniques have been made over recent years. Successful high performance liquid chromatography (HPLC) methodologies are available for the detection of azodicarbonamide in flour. [108, 109] Furthermore, the HSE has issued a standardized HPLC method for the detection of inhalable azodicarbonamide from air filters. [110]

Despite these developments for other applications, the quantitative analysis of the azodicarbonamide encapsulated within polymer matrixes has not been widely published. This is most likely due to the difficulties surrounding sample preparation and the extraction of the azodicarbonamide from the product.

[iv] Standard Industrial test method – reports issued by John Ashworth ltd

3.1.1 Choosing a Quantitative Technique

A viable technique for the quantitative detection of ADCA within polymer matrixes must be quick, simple and cost effective, to best suit the needs of industry.

Many analytical techniques are available for quantitative analysis. For example, UV-Vis spectroscopy can be used to quantitatively analyse UV active materials within mixtures. This technique is routinely utilised in the biochemical industry, including for the quantitative analysis of tissues. [111] Environmental studies also include applications such as the qualitative and quantitative study of waste water by UV-Vis. [112] A previous study was carried out to establish a viable quantitative analysis technique for ADCA within polymer coating samples using UV-Vis. The UV-Vis calibration for raw ADCA powder confirmed quantitative analysis with reliable results. However, the coating samples containing known concentrations showed no corresponding peak to ADCA in the spectra. This could be due to the concentration of ADCA being too low, or interference from the plastisol absorption. This data suggests that UV-Vis is not a viable method for the quantitative analysis of ADCA in wallpaper samples and no further investigation was carried out for this technique.[v]

High performance liquid chromatography (HPLC) is a routinely used technique for quantitative analysis in many applications. HPLC is a highly selective technique as the analyte has affinity for both the stationary and mobile phases, thus creating competition between the two phases. [113] Quantitative HPLC is used in applications such as, polymers for medical applications, [114] analysis of substances such as aspirin and caffeine in pharmaceuticals [115] and quantitative detection of low concentrations, such as identification of mycotoxins. [116] When comparing the methods of soxhlet extraction and HPLC, the initial start-up costs for HPLC can prove more expensive; however, for routine evaluation, the running costs are relatively low and very rapid.[vi]

[v] Private Communication – Graham & Brown UV-Vis Study
[vi] Private Communication – Costing Analysis from Perkin Elmer

Ultra-performance convergence chromatography (UPC^2) is a relatively new technique developed by Waters™. [113] Convergence chromatography is a technique that harnesses the benefits of both gas and liquid chromatography in one streamlined system. Separation is achieved by manipulating the density of the supercritical fluid-based mobile phase, typically CO_2. The diversity of the stationary phase allows for a large selectivity of separation. [117] The use of the supercritical CO_2 mobile phase, eliminates the need for harmful solvents, furthermore analysis times are significantly reduced compared to traditional liquid chromatography techniques. These properties make UPC^2 a viable technique for industrial analysis as long term running costs would be reduced. [113] UPC^2 methodologies have be utilised in many industries including applications in food science, [118-120] cosmetics [121] and pharmaceuticals. [122, 123] That said, few methodologies have been developed in terms of materials chemistry, despite the large remit of potential applications.[vii]

3.1.2 HPLC Development

As previously mentioned, the detection of ADCA in products such as flours, is already a well-established technique, therefore the use of a HPLC method for the quantitative analysis of ADCA within wallpaper is a potential alternative.

To investigate this theory, initially a calibration curve was created for raw powder ADCA. The powder was dissolved in DMSO and diluted to create a range of known concentration samples. These samples were run in a mobile phase of 95% ethyl acetate and 5% DMSO with an experimental time of 10 minutes. The calibration was plotted using the average area of the ADCA peak in the chromatogram of 3 repetitions of 5 known concentrations of ADCA. The concentrations started at a minimum 0.04 µg/mL and ranged to a maximum 0.20 µg/mL, increasing in steps of 0.04 µg. The average data of the three repetitions gave a linear fit. To confirm the accuracy of the technique, a separate set of prepared known concentrations were tested on a second HPLC machine of a similar specification. The results showed a linear fit graph where R^2 equals 0.9999 and 0.9986, for the two repeats, confirming the reliability and reproducibility of the technique. (Figure 3.1)

[vii] Private Communication – Collaboration with Waters™

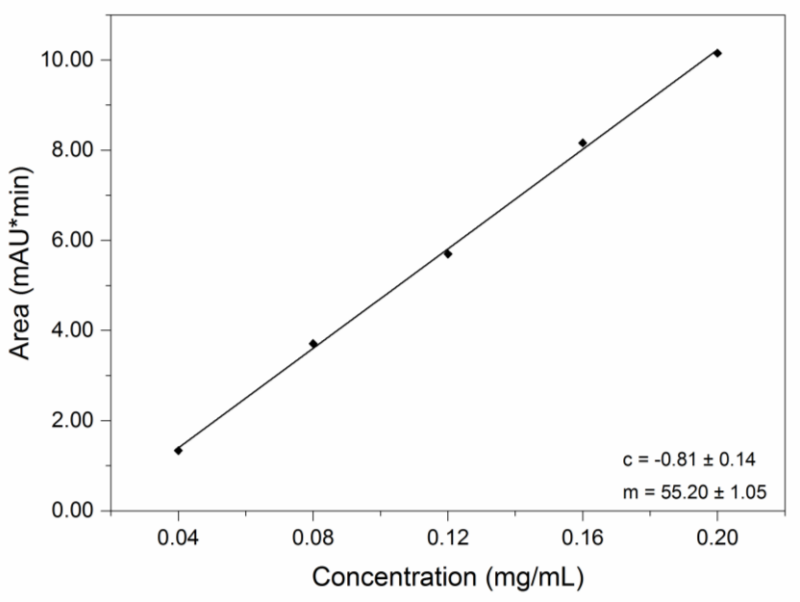

Figure 3.1 Standardisation curve of the average concentrations of known samples of azodicarbonamide in mg/mL

A second calibration curve was generated using plastisol samples containing known concentrations of ADCA. Samples were prepared to contain 0.5%, 1.0%, 2.0% and 3.0% ADCA. To ensure an accurate ADCA concentration the formulations were cured at 120 °C for 24 seconds. The utilisation of a lower temperature ensures that decomposition of ADCA does not occur, thus maintaining the concentration. The plastisol samples were prepared using DMSO and ethyl acetate as in the published method for the determination of ADCA from the HSE. [110] The plastisol samples were ran under the same HPLC method as the ADCA raw powder calibration to maintain comparability. Due to the numerous components in the plastisol composition, significantly more peaks were observed in the chromatogram of these samples. However initial tests carried out with Perkin Elmer, based on the HSE recommended HPLC methodology for detection of ADCA within air filters, [110] suggested that the 95% ethyl acetate and 5% DMSO mobile phase solvent system allowed for complete separation of the peaks. The ADCA generally appeared as a strong, sharp peak at around 6 minutes in isolation from the plastisol peaks.

The plastisol samples were tested and repeated 3 times; however, the results obtained were not repeatable (Table 3.1).

Table 3.1 HPLC peak areas of the ADCA known concentration 0.5-3.0% plastisol samples repeated 3 times.

Sample Concentration w/w (%)	**Peak Area (mAU*min)**			**Average**	**Error (±)**
	Repeat 1	**Repeat 2**	**Repeat 3**		
0.5	2.48	No Peak	No Peak	2.48	n/a
1.0	8.83	10.72	16.46	15.34	5.95
2.0	21.57	40.09	31.03	30.90	9.26
3.0	49.20	76.80	No Peak	63.00	13.81

The table shows that the range of peak area for each concentration is significantly large. The initial results were not reliable. As well as large discrepancies in peak area, the retention time varied hugely between samples, ranging from 0.50 to 4.32 minutes. These variations suggest that this is not a reliable method for ADCA within a plastisol sample.

It was hypothesised that the low solubility of ADCA in ethyl acetate [124] caused the material to precipitate in the mobile phase, therefore altering retention time and the peak area observed due to the difference in ADCA concentration. When using DMSO as a co-solvent, it is unadvisable to lower the concentration of EtOAc in the mobile phase below 95% as pressure build up occurs within the capillaries of the HPLC system.[viii]

Azodicarbonamide has good solubility in DMF, therefore a range of DMF and DMSO mobile phases were analysed. The use of DMF resulted in an overlap between multiple peaks in the chromatogram and therefore did not allow for reliable quantitative analysis of ADCA. The ratio, and gradient, of the two solvents was modified to analyse the effect on the peak separation (Table 3.2).

[viii] Private Communication – Method Development with HPLC Technicians

Table 3.2 DMF: DMSO HPLC mobile phase concentrations

Sample	DMF %	DMSO %	Gradient
1	98	2	No
2	95	5	No
3	95	5	Gradient from 5-0% DMSO over 10 minutes
4	100	0	Gradient from 0-5% DMSO over 10 minutes

The modification of the mobile phase concentration was unsuccessful in separating the plastisol and ADCA peaks in the chromatogram. The gradients ranging from 0-5% DMSO, were repeated over a 15 and 20 minute period; however, this caused a shift in the retention time of both the plastisol and the ADCA peaks with no separation. As previously mentioned, due to the viscosity of DMSO, concentrations cannot exceed 5%. To enable larger concentration variations of DMF, the DMSO was exchanged for ethyl acetate and more concentrations were tested (Table 3.3).

Table 3.3 DMF: EtOAc HPLC mobile phase concentrations

Sample	DMF %	EtOAc %	Gradient
1	98	2	No
2	95	5	No
3	90	10	No
4	85	15	No
5	80	20	No
6	30	70	Gradient from 70-5% EtOAc over 10 minutes
7	95	5	Gradient from 5-70% EtOAc over 10 minutes

The use of ethyl acetate allowed the concentration of DMF to be lowered to 30%. It was found that decreasing the concentration below 30% could cause insolubility of the compound resulting in a precipitation within the mobile phase and blockage of the HPLC column. The ratios of solvent stated in the table above did not allow separation of the two peaks in the chromatogram. Gradients were ran ranging from 70% to 5% EtOAc, over a 10-minute period and repeated for a

20 minute run time. These gradients did not allow separation of the plastisol and ADCA peaks, as shown below for sample 6 (Figure 3.2).

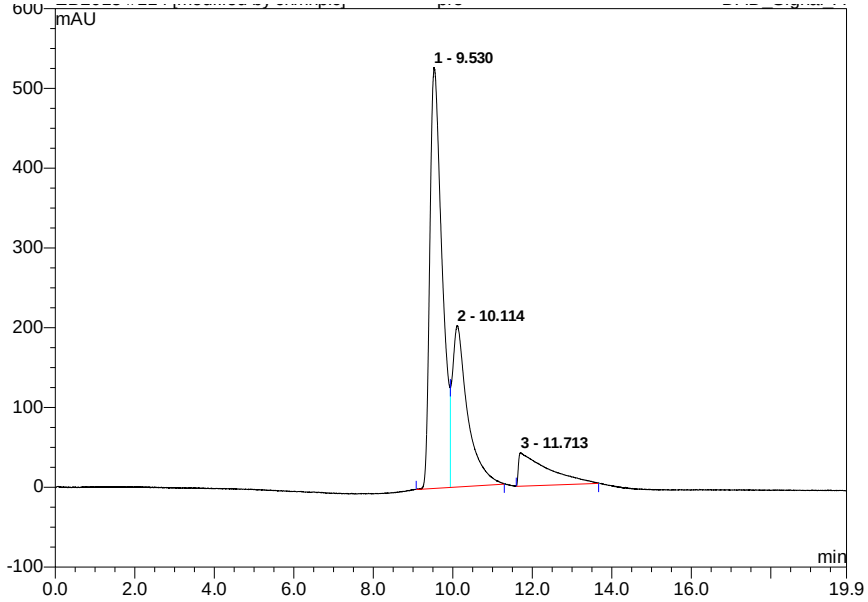

Figure 3.2 HPLC Chromatogram of sample 6 – mobile phase gradient of 70-5% EtOH in DMF over 20 minutes, showing overlap of peaks.

These mobile phase tests concluded that DMF was not an appropriate mobile phase solvent for this application. Furthermore, the irreproducibility of the chromatograms using the ethyl acetate: DMSO (95:5) mobile phase means that the technique is not reliable and that ADCA concentration cannot be determined with complete confidence. For this reason, alternative quantitative analytical techniques were investigated.

3.1.3 UPC^2 Development

UPC^2 is an alternative chromatography technique to HPLC, recently developed by Waters^{TM}. [113] The method utilises liquid CO_2 as the mobile phase which could be used to eliminate the problems observed in the traditional HPLC technique, where the low solubility of ADCA in organic solvents resulted in precipitation in the mobile phase and pressure build up within the HPLC system at some concentrations. The sample preparation was kept consistent with the standard HPLC method so that a direct comparison could be made.

Using the UPC^2 system, the overall run time was significantly reduced from 20 minutes, in HPLC, to 5 minutes. The ADCA peak appeared in isolation at approx. 2.5 minutes. The peaks corresponding to the plastisol appeared at 0.5

minutes. This showed a significant separation and ensured that there would be no interference between the plastisol and the ADCA peaks.

To test the initial parameters, 4 known concentration samples were tested using the UPC^2 method. These consisted of a 1% and 2% ADCA plastisol sample on a paper backing (paper samples) and a 1% and 2% ADCA plastisol sample that had been removed from its backing (film samples). The screening test identified a suitable column and methanol as the co-solvent. 6 repeats were ran of the 2% film sample and the results were reproducible within an error margin of ± 0.0295%. A calibration was run by varying the injection volume of the 2% film sample. This calibration curve was used to back calculate the percentage concentrations for all samples. The concentrations are shown in Table 3.4.

Table 3.4 Experimental UPC^2 concentrations for the known plastisol and film samples.

Sample	Concentration	Corrected Concentration[a]
1% Film Sample	1.108	n/a
2% Film Sample	1.926	n/a
1% Paper Sample	0.725	1.089
2% Paper Sample	1.233	1.853

a Corrected to account for weight of the paper backing

The initial screening tests of the wallpaper samples provided evidence that the materials could be analysed using UPC^2. Therefore, further tests were carried out in order to validate the method. A 4-point calibration was carried out and repeated 3 times for the ADCA raw powder.

Table 3.5 Calibration data for the raw powder ADCA repeats.

Concentration (mg/mL)	Peak Area (mAU*min)			+/-	% Error
	Repeat 1	Repeat 2	Repeat 3		
0.20	0.524	0.551	0.522	0.01453	2.73
0.25	0.724	0.697	0.820	0.06165	8.25
0.50	1.669	1.701	1.737	0.03423	2.01
1.00	3.686	3.736	3.695	0.02471	0.67

The initial calibration showed a high level of accuracy; however, all repeats were ran on one sample. All results in the repeated raw powder calibration show lower margin of error when compared to the average soxhlet error of 10%. Of all the samples analysed a higher error margin was observed in the case of the 0.25 mg/mL sample, this could be due to human error during sample preparation. However, the value was still below those observed in the current method. The calibration had a linear fit with $R^2 = 0.99995$. (Figure 3.3)

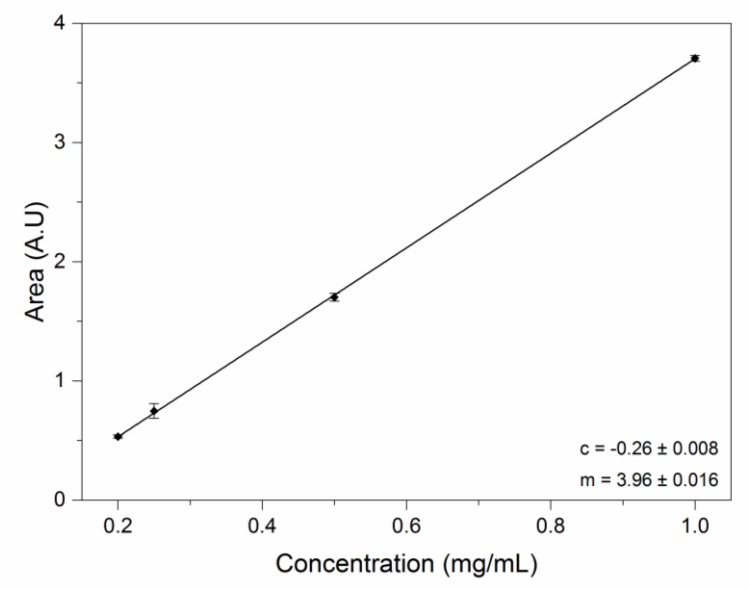

Figure 3.3 Standardisation curve of the average concentrations of known samples of azodicarbonamide in mg/mL

Repeat calibrations were ran for both the paper and film samples. Error margins in this case proved significantly higher with errors as high as 75% observed in the paper samples. This result suggested no correlation between the known concentrations and the observed values.

It was determined that the sample preparation was the underlying factor in the accuracy of the samples. The high reproducibility of the raw powder calibration confirmed this theory. The use of DMSO dissolved the plastisol while leaving the cellulose matter of the paper intact. For future improvement, a study can be carried out to identify a more suitable solvent to dissolve the wallpaper sample in its entirety. Various resins can then be screened as a filtration system before subsequent 0.22 µm analytical filtration. The novel UPC^2 technique shows potential as an effective industrial test method; however, sample preparation and methodology would need to be defined and specific to product type and chemistry.

3.2 Novel Formulation Developments Utilising Known Foaming Agents

Due to its inclusion on the REACH Annex XV, ADCA is restricted to a maximum concentration of 0.1% w/w in final articles, before declaration. [98] The postponement imposed on the classification of ADCA in 2016 suggests that ADCA will stay on the Candidate List (Annex XV) for some time. [104] Therefore, for the time being a complete removal of ADCA from commercial products is not required. That said, the low residual percentage restriction would still be in place.

Formulations using lower concentrations of ADCA have been investigated. Simply reducing the concentration of ADCA within the standard formulation, decreases the expansion of the plastisol coating as less gas will be generated.[ix] [45] To counteract this lower expansion, a range of co-blowing agent formulations were created using ADCA and the known alternatives listed in the original REACH dossier. [59] Of the known alternatives cited in the dossier, some were eliminated prior to this screening due to known health and safety, toxicological or process risk associated with the materials. Success of the co-blowing agents could eliminate the need for a novel compound if ADCA remains on Annex XV indefinitely, and subsequently reduce the cost and time required to implement a new industrial process.

The following novel formulations were tested under standard manufacturing conditions and cured at 210 °C.[x] The resulting plastisol coatings were analysed by SEM for surface texture, cell size, distribution, structure and overall expansion level. Gloss data was also analysed for a full comparison of the resultant physical properties.

3.2.1 Control ADCA Expanded Formulation

The standard formulation contains 1.92% w/w blowing agent before heating.[x] This equates to a molar concentration of 0.161 mmol per gram of plastisol. A control sample of the standard ADCA expanded plastisol (**P_{ADCA}**) was manufactured under standard conditions and analysed for comparative study. (Figure 3.4)

[ix] Graham and Brown – Formulation Study
[x] Graham and Brown – Standard Manufacturing Procedure

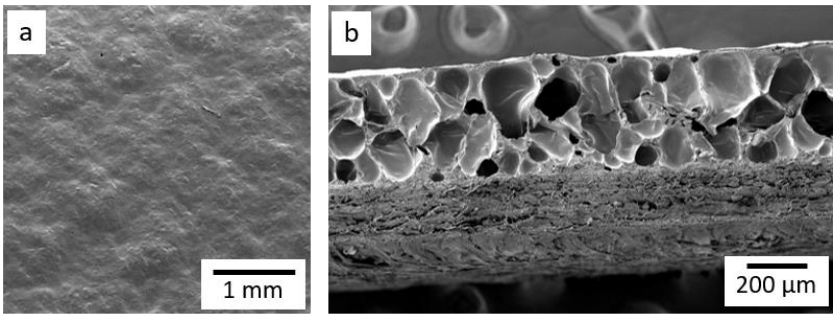

Figure 3.4 SEM micrographs of the control sample **P_{ADCA}** (a) surface at x18 Mag and (b) cross-section at x75 Mag.

The foamed layer in the control sample, **P_{ADCA}**, shows an overall expansion of 400 µm. (b, Figure 3.4) This expansion range is the most commonly used foam depth at Graham & Brown; however, one of the major advantages to using ADCA is that the expansion can be easily controlled by changing the concentration of blowing agent.[xi] This allows different formulations to give varying expansion ratios and create a range of design effects. For the purpose of this study, replication of the expansion depth of 40 µm was desired.

The internal cells in the **P_{ADCA}** sample are evenly dispersed and show a fairly regular cell size, ranging from approx. 45-300 µm. This dispersion gives a homogeneous matt appearance to the plastisol surface with minimal surface defects. (a, Figure 3.4) The desired surface properties are a smooth, white, matt finish. The average surface gloss value for the sample **P_{ADCA}** was 1.3 GU. This value is within the desired matt region of ≤10 GU.

3.2.2 OBSH Co-Blowing Agent Formulations

In the first instance 4,4'-oxybis(benzenesulfonyl hydrazide) (OBSH) **9** was investigated. OBSH is the second most commonly used blowing agent in the plastics and polymer industries after ADCA. [37] It is a popular choice for many industrial processes as an alternative to ADCA and is therefore listed on the original dossier document as a recognised alternative.

One advantage to OBSH is high gas production, with a gas yield of 125 mL/g, [68] The decomposition point of OBSH is 160 °C, [37] suggesting that it is not suitable for implementation in the current PVC plastisol without adjustment of the standard formulation.

[xi] Graham & Brown – Formulation Study

A formulation containing molar equivalent of OBSH **9** was prepared (**P9**) under standard manufacturing conditions for comparative study. (Figure 3.5)

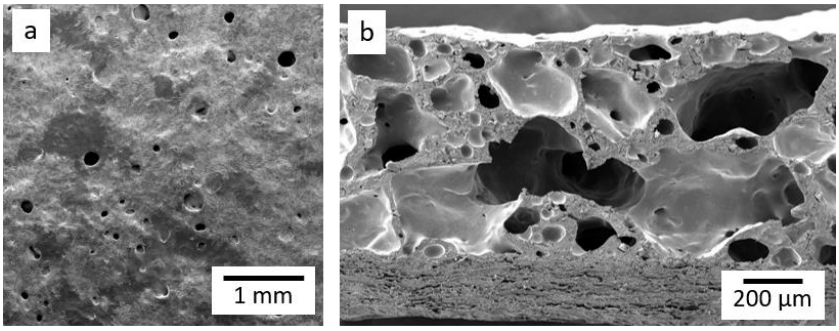

Figure 3.5 SEM micrographs of sample **P9** (a) surface at x18 Mag and (b) cross-section at x75 Mag.

The decomposition of OBSH results in surface defects on the formulation surface, including large craters and an irregular texture. (a, Figure 3.5) The observed surface texture attributed to a gloss reading of 1.0 GU, comparable to that of $\mathbf{P_{ADCA}}$. However, the cross-section micrograph of sample **P9**, confirmed that the surface defects are largely due to a highly irregular cellular structure, with cell sizes ranging from approx. 25-700 µm. (b, Figure 3.5) As well as an irregular cell size, the foam possesses an open cell structure where individual cells have connected with one another to create large cells and channels. This open cell structure also means that the foam has the potential collapse creating further visible surface defects. OBSH produces an expansion level of approx. 760 µm, almost double to that observed in the control sample $\mathbf{P_{ADCA}}$ (Figure 3.4). Despite the significant increase in expansion, the quality of the foam produced is significantly reduced.

A co-blowing agent of ADCA and OBSH in a 1:1 molar ratio ($\mathbf{P9_{1:1}}$) was created in attempt to reduce the irregular and open cell structure created by 100% OBSH. The co-blowing agent should theoretically reduce the volume of overall concentration of ADCA required for sufficient expansion levels as the high gas yield of OBSH has proved to increase expansion significantly. Furthermore, **P9** showed minimal colouration, observed yellowing saturation (b*) was significantly lower with a value of 2.7, compared to 4.96 in the case of $\mathbf{P_{ADCA}}$. To analyse these advantageous properties further, the co-blowing agent sample was formulated to the same molar concentration as the control sample $\mathbf{P_{ADCA}}$.

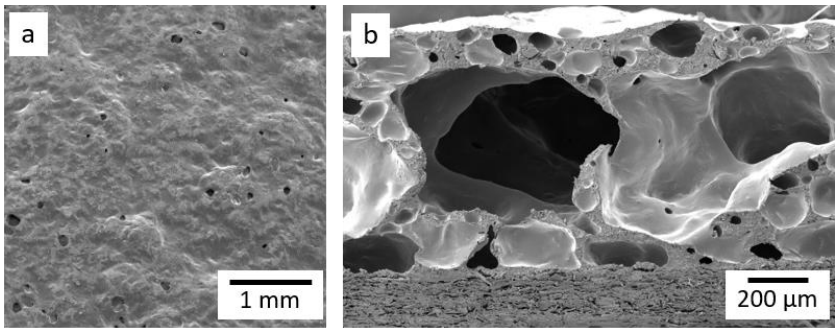

Figure 3.6 SEM micrographs of sample **P9$_{1:1}$** (a) surface at x18 Mag and (b) cross-section at x75 Mag.

The co-blowing agent system (**P9$_{1:1}$**) showed a smoother surface when compared to the sample **P9**, with significantly fewer surface defects observed in the SEM micrograph. (a, Figure 3.6) This suggests that the addition of ADCA within the formulation aids the distribution of the blowing agents to create a more homogeneous surface effect. This homogeneous texture attributed to a low gloss value of 0.3 GU.

That said, the cross-section analysis of sample **P9$_{1:1}$** (b, Figure 3.6) showed an increase in both expansion and cell size range when compared to the OBSH sample **P9**. (Figure 3.5) Cells ranging from approx. 30 µm up to approx. 830 µm in diameter were observed. These very large gas pockets create a mostly open cell structure and make the foam more susceptible to collapse and craters. The irregular structure of this foam suggests that the two blowing agents do not mix sufficiently and are not evenly dispersed, further suggesting that they are incompatible materials in a co-blowing agent system.

This study concluded that the colour and gloss properties shown by OBSH were advantageous to the desired application. However, highly irregular expansion levels and internal cellular structures render OBSH not suitable as a direct alternative to ADCA within the current formulation, both independently and as part of a co-blowing agent system. However, due to the lower decomposition temperature of OBSH, further investigation could identify a more optimal manufacturing temperature for the desired physical properties within this application.

3.2.3 TSS Co-Blowing Agent Formulations

Toluenesulfonyl semicarbazide (TSSC) **11** is a commonly used blowing agent in the production of hard PVC foams due to its high decomposition temperature and gas yield. [76] TSSC decomposes at 235 °C, [68, 77] which is above the melt viscosity temperature of soft PVC. [37] However, it is hypothesised that, the decomposition temperature could potentially be decreased by combination with ADCA in a co-blowing agent system. In the first instance the effects of TSSC independently within the current formulation (**P11**) were analysed.

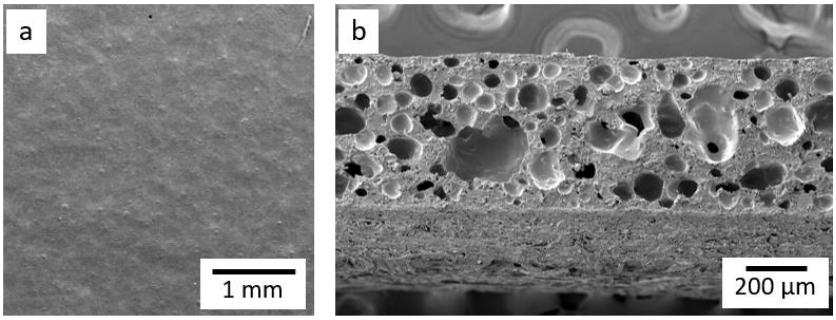

Figure 3.7 SEM micrographs of sample **P11** (a) surface at x18 Mag and (b) cross-section at x75 Mag.

When added to the current formulation at equivalent molar concentration, the observed surface of **P11**, is smooth and defect free. (a, Figure 3.7) This smooth topography, attributed to a high gloss level of 20.1 GU. This reading is well outside the desired matt region of GU ≤10. The sample **P11** was within the suitable colouration range for decorative applications.

Sample **P11** shows an overall expansion level of 540 µm. (b, Figure 3.7) This is approx. 1.35 x the expansion observed in the control sample $\mathbf{P_{ADCA}}$. Despite the high expansion, **P11** produced a densely packed foam with a small average cell size of approx. 100 µm. The densely packed foamed cells could be the result of slow, or incomplete, decomposition of TSSC as the decomposition temperature is not met under standard operating conditions. The current formulation is optimised to the decomposition of ADCA. Kicker complexes within the formulation lower the observed decomposition temperature of ADCA and promote gas production within the system. Further investigation could potentially identify a suitable additive optimised to TSSC.

As with OBSH, a co-blowing agent formulation was produced containing ADCA and TSSC in a 1:1 molar ratio (**P11$_{1:1}$**). The resulting formulation included the same overall concentration of co-blowing agent as the control **P$_{ADCA}$**.

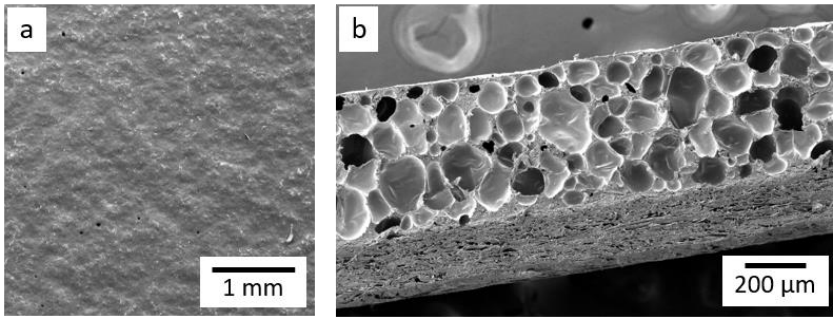

Figure 3.8 SEM micrographs of sample **P11$_{1:1}$** (a) surface at x18 Mag and (b) cross-section at x75 Mag.

The observed surface of sample **P11$_{1:1}$**, (a, Figure 3.8) showed more texture than the corresponding sample **P11**. (b, Figure 3.7) Furthermore, small pinhole defects had formed upon the surface, suggesting more disorder within the formulation **P11$_{1:1}$** during curing. This disorder attributed to the significantly lowered gloss value of 6.9 GU. This value is within the desired matt region and indicates that ADCA is the more contributing additive in terms of surface texture.

The cross-section analysis of sample **P11$_{1:1}$**, (b, Figure 3.8) showed an overall expansion of 510 µm, comparable to that of **P11** (540 µm, Figure 3.7) The cellular structure of sample **P11$_{1:1}$** was far less dense and the foam was more evenly dispersed than observed in sample **P11**. The cell size ranged from approx. 35-180 µm and was more comparable to that of the control sample **P$_{ADCA}$**. (Figure 3.4) The increase of approx. 100 µm when compared to the expansion of **P$_{ADCA}$** suggests that TSSC compliments the blowing capability of ADCA creating greater expansion at lower concentrations. This result is advantageous as the residual concentration of ADCA retained in final article could be reduced.

Further investigation would be required to identify optimal concentration ratios of TSSC and ADCA and to determine if expansion level can be controlled through formulation adaptations. Despite the advantages observed in the preliminary screening of the co-blowing agent formulation, **P11$_{1:1}$**, commerciality must be considered. TSSC is a costly raw material, [45] furthermore, recent studies provide indication of skin and respiratory sensitisation as a result of

prolonged exposure. [78] These negative properties could impact the efficiency of TSSC as a direct commercial alternative to ADCA

3.2.4 Citric Acid Co-Blowing Agent Formulations

Citric acid **18** is a naturally derived polycarboxylic acid which acts as an endothermic blowing agent by the production of carbon dioxide upon thermal decomposition. [68]

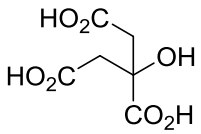

18

Citric acid is a practical blowing agent used in the production of many products such as low-density films [125] and polyethylene foams. [126] The practicality of citric acid as a blowing agent is partly due to its low parent and residual toxicity. The decomposition of citric acid occurs from 160 °C, [37] which is concurrent with the melt viscosity range of the PVC plastisol. [127]

Citric acid **18** was implemented into the standard manufacturing formulation in place of ADCA (**P18**) and the resultant physical properties of the samples were analysed for surface defects, expansion, internal cell formation, colour index and gloss readings.

The SEM micrographs of the sample **P18** showed a high level of incompatibility within the system. This is evident from the large craters across the coating surface, (a, Figure 3.9) with an average size of 0.12 mm.

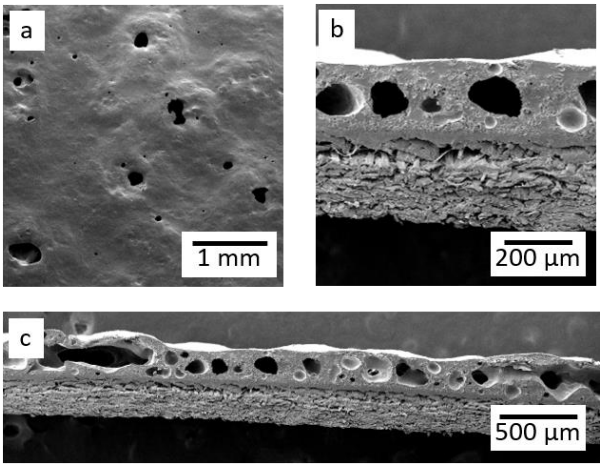

Figure 3.9 SEM micrographs of sample **P18** (a) surface at x18 Mag, (b) cross-section at x75 Mag and (c) cross-section at x33 Mag.

The cross-section micrographs of sample **P18** (b, c, Figure 3.9) provide evidence that these surface defects are a direct result of the formation of large internal gas pockets. The irregularity observed within the plastisol matrix of the sample **P18** suggested that the citric acid was not evenly distributed across the coating, resulting in areas of high cell concentration. The gas formed in the case of **P18** did not significantly contribute to the overall expansion with an observed level of 244 µm.

The low distribution observed in the micrographs could be due to the large particle size and low solubility of citric acid within the formulation. The raw material was milled to standard specification[xii] to reduce particle size before implementation into the formulation mixture. However, the irregularity observed in the cross-section micrographs suggested that more extensive mixing is required in the case of citric acid.

The sample **P18**, also exhibited strong coloration as decomposition occurred. (Figure 3.10) As the temperature was increased the colour of the coating increased significantly a ΔE of 36.00 observed at 210 °C.

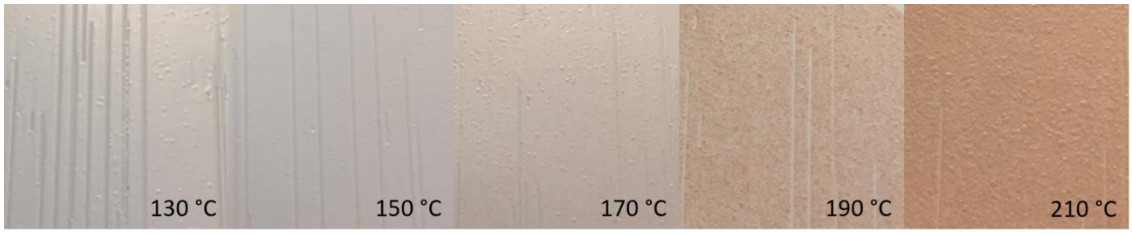

Figure 3.10 Photographic images of sample **P18** at 130-210 °C.

The observed colour change from 170 °C is in agreement with the decomposition range of citric acid which initiates at 160 °C. Furthermore, the photographic images show the surface disruption caused by citric acid particles blocking the automatic k-bar during sample manufacture, and subsequently exposing the substrate surface. This is particularly apparent in the 130 °C coating sample. (Figure 3.10)

Despite the reported efficiency of citric acid in other applications, the initial analysis suggests that citric acid is not a viable blowing agent in the production

[xii] Graham & Brown – Standard Manufacturing Process

of foamed decorative coatings. A co-blowing formulation containing citric acid and ADCA in a 1:1 ratio (**P18$_{1:1}$**) was prepared for further analysis.

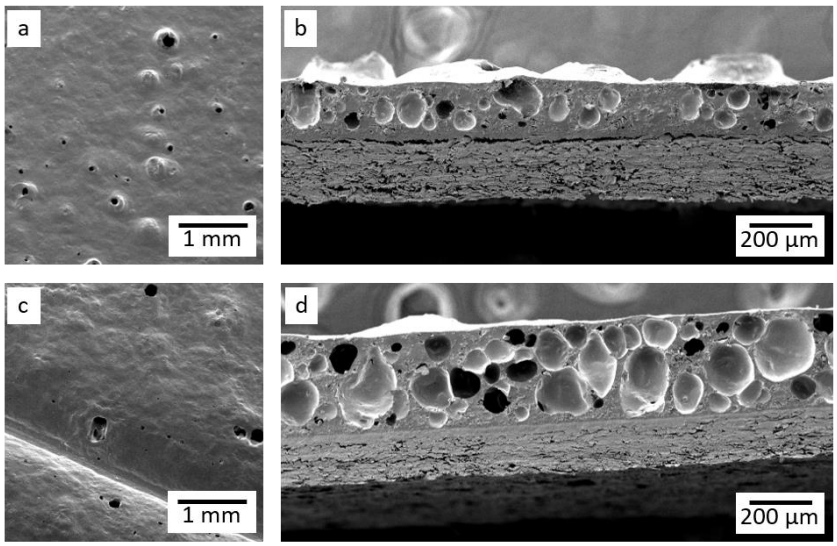

Figure 3.11 SEM micrographs of the sample **P18$_{1:1}$**, (a) surface cured at 190 °C at x18 Mag (b) cross-section cured at 190 °C at x75 Mag (c) surface cured at 210 °C at x18 Mag and (d) cross-section cured at 210 °C at x75 Mag.

Surface defects were observed in the co-blowing formulation **P18$_{1:1}$** at both 190 °C and 210 °C. (a, c, Figure 3.11) However, a reduction in crater size was observed when compared to sample **P18**. The average crater size in sample **P18$_{1:1}$** was 0.07 mm, approx. 0.05 mm less than observed in **P18**. This suggests that ADCA does contribute to the surface topography; however, citric acid is the most contributing factor. The large particle size caused ridges in the plastisol coating, exposing the substrate. This was caused by the k-bar drawdown and can be clearly seen in the 210 °C sample of **P18$_{1:1}$**. (c, Figure 3.11).

The cross-section micrographs of sample **P18$_{1:1}$**, provided evidence of incompatibility at 190 °C. (b, Figure 3.11) The cross-section showed an uneven cellular structure within the plastisol. Furthermore, large craters can be seen on the upper surface of the cross-section, confirming that the surface defects are resultant of the gas produced. Irregular distribution of undissolved particles can cause an uneven pressure build-up within the system as decomposition occurs. This can lead to a disruption of the surface tension and the formation of large craters on the coating surface.

At 210 °C, the ADCA within the formulation contributed to an overall expansion of 300 µm. The increase of 100 µm from the applied coating is 50% lower than the level observed in the control sample **P$_{ADCA}$**. This is concurrent with

P18$_{1:1}$ containing 50% less ADCA and suggests that the citric acid within the formulation has no influence on the overall expansion.

Furthermore, as observed in the sample **P18**, the coloration of the co-blowing agent formulation **P18$_{1:1}$** increased as the temperature increased, (Figure 3.12) although not as significantly as shown in sample **P18**.

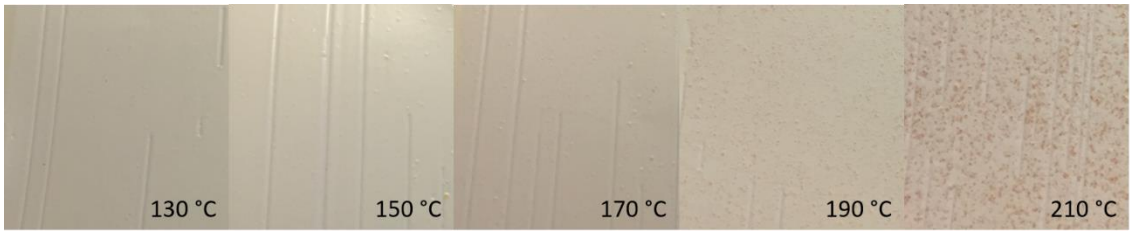

Figure 3.12 Photographic images of sample **P18$_{1:1}$** at 130-210 °C.

The colouration caused by the citric acid within the formulation can be seen in the photographic images. (Figure 3.12) At 210 °C a ΔE of 6.93 was observed. Despite this colour change, if solubility issues surrounding citric acid were resolved, this colouration could likely be corrected by optimisation of optical brighteners and bleaching agents within the formulation.

The initial study suggested that citric acid was not a suitable direct alternative to ADCA for application in foamed decorative coatings. This unsuitability was largely due to strong colouration effects observed in the samples **P18**. That said, at 210 °C some expansion was observed in the case of **P18** providing evidence that the carboxylic acid functional group contributes to the formation of carbon dioxide gas. Further study can identify if increased concentrations of citric acid increased the observed expansion.

3.2.5 Sodium Hydrogen Carbonate Co-Blowing Agent Formulations

Sodium hydrogen carbonate ($NaHCO_3$) **19**, also known as bicarbonate of soda, is an endothermic blowing agent commonly used in the food and baking industries. [64] $NaHCO_3$ has a low decomposition temperature [37] and relatively low gas yield [45] when compared to ADCA which suggests that use of $NaHCO_3$ independently may produce a low quality foam. However, $NaHCO_3$ is cost effective [66] and nontoxic [37] and limited study has been carried out on its efficiency within poly- formulations. The combination of $NaHCO_3$ with ADCA could provide a viable formulation to reduce the residual ADCA retained in the

product whilst maintaining foam efficiency. A formulation containing molar equivalent levels of $NaHCO_3$ (**P19**) was prepared and analysed.

Minor pinhole defects were observed on the surface of sample **P19**. (a, Figure 3.13) The generally smooth surface attributed to a relatively glossy surface with a gloss value of 16.0 GU. However, the L*a*b* data for **P19** showed a strong yellow saturation with a b* value of 12.96, which is detrimental to decorative applications.

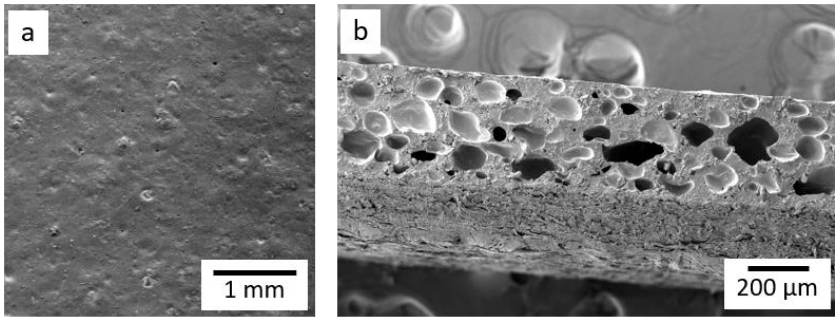

Figure 3.13 SEM micrographs of sample **P19** (a) surface at x18 Mag and (b) cross-section at x75 Mag.

The cross-section micrograph of **P19**, (b, Figure 3.13) showed that the cellular structure produced was relatively dense with fewer gas pockets observed than in the exothermic blowing agents (**P9** and **P11**). The gas cells produced accounted for an overall expansion of 370 µm, approx. 94% of the expansion seen in the control sample $\mathbf{P_{ADCA}}$. (Figure 3.4) On average the cells observed in **P19** were irregular and relatively small compared to $\mathbf{P_{ADCA}}$. This result can be attributed to the low decomposition temperature of $NaHCO_3$. At temperatures below the melt viscosity temperature of PVC, the plastisol is too viscous to allow permeation by gas molecules. Although the cell structure is unfavourable, the even distribution of the cells suggests that the $NaHCO_3$ particles are evenly dispersed within the formulation matrix.

As with the previously analysed known alternatives, a co-blowing agent formulation was made to contain $NaHCO_3$ and ADCA in a 1:1 ratio, ($\mathbf{P19_{1:1}}$) whilst the overall concentration of blowing agent remained constant.

The surface micrograph of the co-blowing agent system $\mathbf{P19_{1:1}}$, (a, Figure 3.14) showed a more homogeneous surface than compared to the sample **P19**.

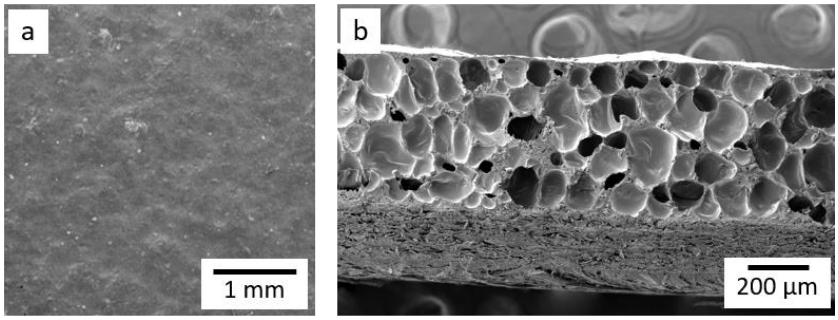

Figure 3.14 SEM micrographs of sample **P19$_{1:1}$** (a) surface at x18 Mag and (b) cross-section at x75 Mag.

The absence of minor pinhole defects suggests that the formulation system is more favourable, and distribution has increased. The texture of the coating surface resulted in a decreased gloss value of 7.3 GU compared to 16.0 GU observed for **P19**. This reduction in GU suggests that addition of ADCA to the formulation creates more disorder and disruption to the coating surface. Furthermore, the addition of ADCA contributed to a reduction in the colouration of the coating compared to sample **P19** with a b* value of 8.48.

The co-blowing agent sample **P19$_{1:1}$** showed an increased expansion level compared to the $NaHCO_3$ sample **P19** and the control sample **P$_{ADCA}$**. The cross-section micrograph (b, Figure 3.14) showed an expansion level of 0.53 mm a total increase of 0.16 mm and 0.13 mm compared to **P19** and **P$_{ADCA}$** respectively. This higher expansion suggests that $NaHCO_3$ encourages the generation of gases when combined with ADCA.

As well as an increased overall expansion, the co-blowing agent formulation **P19$_{1:1}$**, showed an evenly distributed cellular structure. The observed cell size range was approx. 45-200 µm, comparable to that of **P$_{ADCA}$**. (45-300 µm) These results suggest that $NaHCO_3$ is readily dispersed within the plastisol mixture and contrasts the data presented in the Plastics Engineering Handbook [37] which states that $NaHCO_3$ is not dispersible enough in plastisol resins to create even foam structures.

The sample **P19$_{1:1}$** gives the most positive result compared to the other known alternatives in this study. The resultant foamed plastisol **P19$_{1:1}$** exhibits many of the desired physical properties whilst reducing levels of ADCA by half. This, coupled with the low cost and toxicity of $NaHCO_3$, suggests that the

formulation **P19$_{1:1}$** is a viable alternative to the use of ADCA in foamed decorative coatings.

Due to the success of this system, further $NaHCO_3$/ADCA co-blowing agent ratios were investigated in order to analyse the controllability of the foam produced. Samples containing 2:1 (**P19$_{2:1}$**), 3:1 (**P19$_{3:1}$**) and 4:1 (**P19$_{4:1}$**) ratios of $NaHCO_3$ to ADCA were prepared whilst maintaining the overall concentration of 0.161 mmol per gram in the formulation. Across the concentrations of $NaHCO_3$ the observed coating surfaces remained consistently smooth. (Figure 3.15)

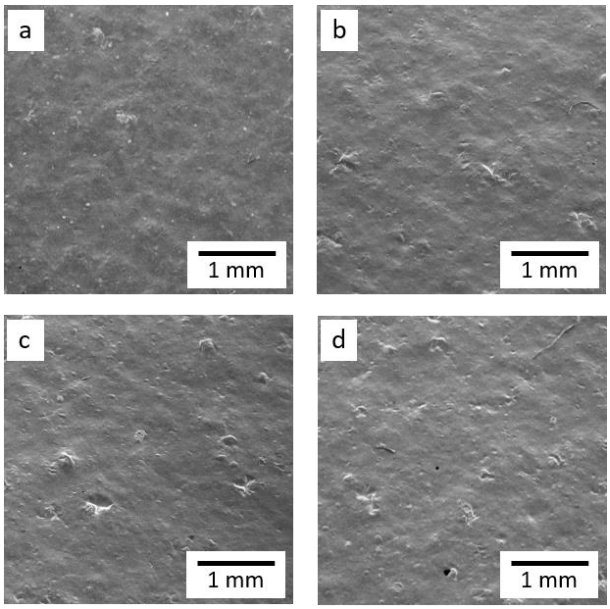

Figure 3.15 SEM surface micrographs of (a) sample **P19$_{2:1}$** (b) sample **P19$_{2:1}$** (c) sample **P19$_{3:1}$** and (d) sample **P19$_{4:1}$** at x18 Mag.

However, minor defects were observed in the surface micrographs of samples **P19$_{3:1}$** and **P19$_{4:1}$** (c, d, Figure 3.15) suggesting that lower levels of ADCA attributed to decreased distribution within the formulation.

Furthermore, decreasing levels of ADCA resulted in increased gloss levels. The glossmeter readings confirm that all samples are considered within the matt region. The increase in GU is minimal as the concentration of ADCA decreases; however, it does show that concentrations of less than 20% ADCA would give a ‘semi-gloss’ finish, (semi-gloss surfaces are those with GU values of 10-70) which is undesirable.

The table below (Table 3.6) shows the glossmeter results for each sample.

Table 3.6 Gloss reading values of plastisol samples containing ADCA and $NaHCO_3$, in ratios 1:1, 1:2, 1:3 and 1:4.

ADCA: $NaHCO_3$ Ratio	**85° beam angle reading (GU)**
1:1	7.3
1:2	8.3
1:3	8.9
1:4	9.6

As the concentration of $NaHCO_3$ increases the resulting foam structure becomes more irregular and the range in cell size increases due to the formation of larger gas pockets. (Figure 3.16)

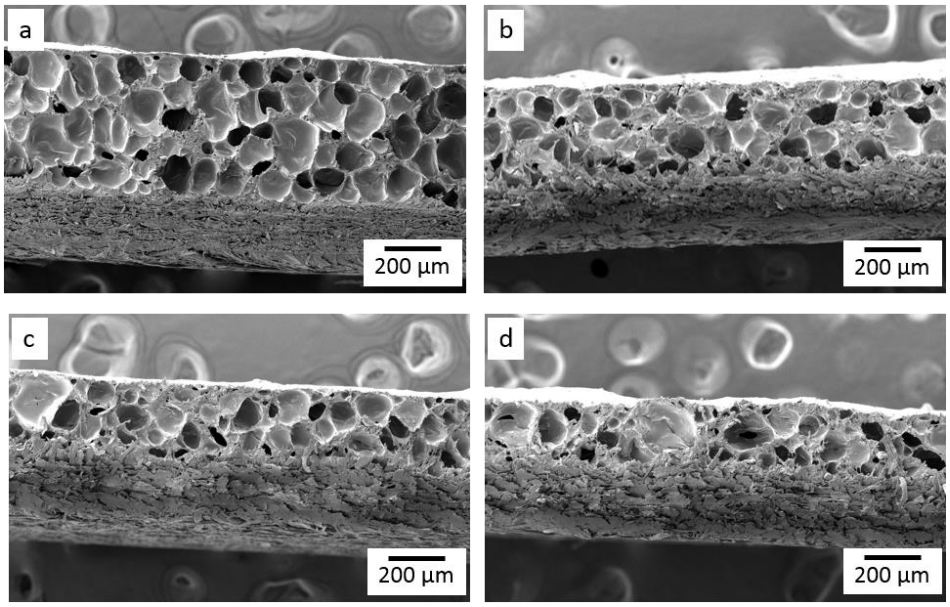

Figure 3.16 SEM cross-section micrographs of (a) sample **P19$_{1:1}$** (b) sample **P19$_{2:1}$** (c) sample **P19$_{3:1}$** and (d) sample **P19$_{4:1}$** at x75 Mag.

This irregularity suggests that ADCA is the controlling blowing agent and aids the dispersion of the particles within the plastisol. This hypothesis was further supported as the distribution in the 4:1 sample (**P19$_{4:1}$**) was less dense than observed in the 100% $NaHCO_3$ sample **P19**. This suggested that even low levels of ADCA can aid the formation of larger gas cells within the formulation. (**P19$_{4:1}$** range of 27-240 µm vs **P19** range of 13-130 µm)

Despite the evidence of gas pockets within the matrix of sample **P19$_{4:1}$** (d, Figure 3.16) no significant expansion was observed as the plastisol layer exhibited a depth of 210 µm. This suggests that 20% ADCA is the lowest acceptable level of ADCA within the analysed formulation. The expansion levels of the concentration ratio samples were compared. As the concentration of ADCA decreases the overall expansion decreases, as expected. The expansion levels for samples **P19$_{1:1}$** (50% ADCA), **P19$_{2:1}$** (33% ADCA), **P19$_{3:1}$** (25% ADCA) and **P19$_{4:1}$** (20% ADCA) are shown in the graph below. (Figure 3.17)

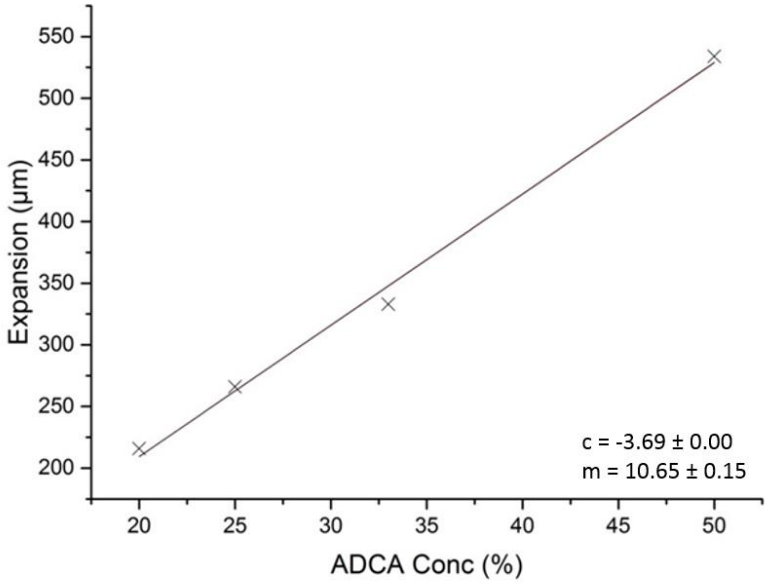

Figure 3.17 Graph depicting expansion in micrometres Vs the concentration of ADCA in percentage

This analysis confirmed that the level of expansion can be controlled through variation of the concentration of the two blowing agents within the system. The large expansion range of 210-530 µm as ADCA concentration is increased from 20-50% shows the high level of controllability obtained by this system. To replicate the expansion of 400 µm obtained by the current control formulation **P$_{ADCA}$**, the graph indicates that a 38% ADCA to 62% $NaHCO_3$ mixture is required. This correlates to an ADCA concentration within the overall formulation of just 0.73% as opposed to the current level of 1.92%. This data suggests that the co-blowing agent system can be used to provide the desired expansion whilst decreasing the amount of ADCA used in the formulation.

Furthermore, as the level of ADCA was decreased the colouration of the coating decreased with b* values reducing from 8.48 (**P19$_{1:1}$**) to 4.69 (**P19$_{4:1}$**) across the concentration range

The co-blowing agent formulation containing $NaHCO_3$ and ADCA shows potential as a technique to decrease the quantity of residual ADCA in the final product whilst maintaining the efficient foaming capabilities. To fully analyse the practicality of this formulation it is important to test the co-blowing agent in modified formulations to analyse the effect other components within the formulation have on the system. Tests must also be done on a large scale 'replica factory' production line, if the formulation is to be considered for wider manufacture. The formulation must also be tested for compatibility with the subsequent coating and embossing stages of decorative coating manufacture and costings must be analysed in comparison to the current procedure.

3.2.6 Conclusions of the Novel Formulation Developments Utilising Known Foaming Agents

The study of the known alternatives gave insight into the practicality of these materials in the desired application.

In the case of OBSH, the data obtained confirmed that it was not a suitable alternative to ADCA when implemented into the current formulation. Further temperature studies could identify a more suitable working temperature; however, the incompatibility observed as large open cellular structures, in the cross-section micrographs, allowed OBSH and its derivatives to be ruled out this study.

The analysis of TSSC, showed a suitable level of expansion; however, the density of the foam within the 100% TSSC sample (**P11**) was impractical. That said, TSSC was compatible in the co-blowing agent system with ADCA resulting in a more regular cellular structure and expansion level comparable to that of **P$_{ADCA}$**. Modification of the TSSC structure could potentially emulate these results whilst eliminating the toxicological downsides to the use of TSSC.

The endothermic blowing agents citric acid and sodium hydrogen carbonate are cost effective and nontoxic, making them beneficial to this application. In terms of citric acid, the sample **P18**, showed high colouration effects due to decomposition of the material. This is detrimental to decorative

applications. That said, expansion levels of approx. 250 µm showed the potential of the carboxylic acid groups to produce a cellular structure within the PVC plastisol matrix. This suggests that carboxylic acid containing compounds could be well utilised in the polymer foams industry.

Sample **P19**, showed suitable expansion levels; however, the densely packed cellular structure resulting in a highly smooth, glossy surface. The co-blowing agents containing $NaHCO_3$ and ADCA showed promise as a direct replacement to ADCA in the desired application. $NaHCO_3$ and ADCA proved compatible within the formulation and the resultant physical properties of the coatings was advantageous.

The co-blowing agent coating **P19$_{1:1}$** showed a regular, evenly dispersed cellular structure. Furthermore, the surface topography was smooth and gloss readings were within the desired matt range. The expansion level of 530 µm observed in sample **P19$_{1:1}$** proved controllable dependant on the percentage of $NaHCO_3$: ADCA within the formulation. This study showed that the expansion could be controlled between 200 µm and 530 µm by varying the concentration of ADCA from 20-50% whilst maintaining the overall percentage of blowing agent within the formulation at 1.92%. It further confirmed that the control expansion (**P$_{ADCA}$**) of 400 µm can be achieved using 72% less ADCA.

This study provided evidence that levels of ADCA in the current formulation can be reduced without significantly affecting the physical properties of the coatings. However, removal of ADCA from the formulation resulted in detrimental foam quality.

Further study can identify the properties of the co-blowing agents in various blown coating formulations. A further study can also be undertaken to identify the compatibility of the new formulations with various dyes, pigments and flame-retardant coatings used within the decorative industry. These studies would be required before commerciality of the formulations.

3.3 Synthetic Requirements of the Project

A suitable alternative to ADCA not only needs to successfully create sufficient foam within the plastisol formulation, it also needs to fulfil the specific commercial needs and, ideally, fit into the existing industrial process, whilst being compatible with REACH regulations.

To ensure the new compound is a suitable alternative, it must hold certain idealistic properties. The blowing agent, and its by-products, must be non-toxic and non-harmful to humans, animals and the environment. This would reduce the risk of future classification or authorisation under REACH. Furthermore, it must be disposable in a green, environmentally friendly yet cost effective manner, this makes water soluble molecules most favourable as they are both easy to handle and dispose of.

Currently, the plastisol formulation is heated to 210 °C during the manufacturing process. Therefore, full thermal decomposition of the new blowing agent must occur at or below this temperature as it is too costly and impractical for the current industrial process to exceed this limit. That said, lower decomposition temperatures are more advantageous from an economic perspective since lower temperatures are more energy and cost efficient. Typical PVC polymer formulations have a melt viscosity of approximately 150-210 °C. [37] This is the temperature at which the polymer has a suitable viscosity to undergo foaming and therefore, it would be most beneficial if the decomposition temperature of the new compound coincides with this range. It is possible to adjust the melt viscosity of a plastisol with various formulation modifications; however, in the first instance it is paramount to identify and test additives within the existing melt viscosity range to limit the number of variables. The identification of a successful additive within this range would keep costs low as the overall formulation would not need to be altered.

Due to the colour sensitive nature of the desired end use, coloured compounds should be avoided, or should be correctable with common optical and whitening agents. Further to this, the blowing agent must be odourless to prevent any unpleasant smell being present in the final consumer product.

As well as the physical restrictions of each specific novel additive, the industrial nature of this project also imposes time and cost restraints. The cost of

the starting materials and reagents must be considered as well as the experimental time scale, yield and purity levels. The schematic below (Figure 3.18) shows the extent of the synthetic and analytical work required for such a commercial project. Whilst multiple compounds may be routinely synthesised on the small scale (Left hand side scatter) this number significantly reduces by the limitations surrounding scale up. The materials must then be tested within the formulation before final analytical study and characterisation can take place.

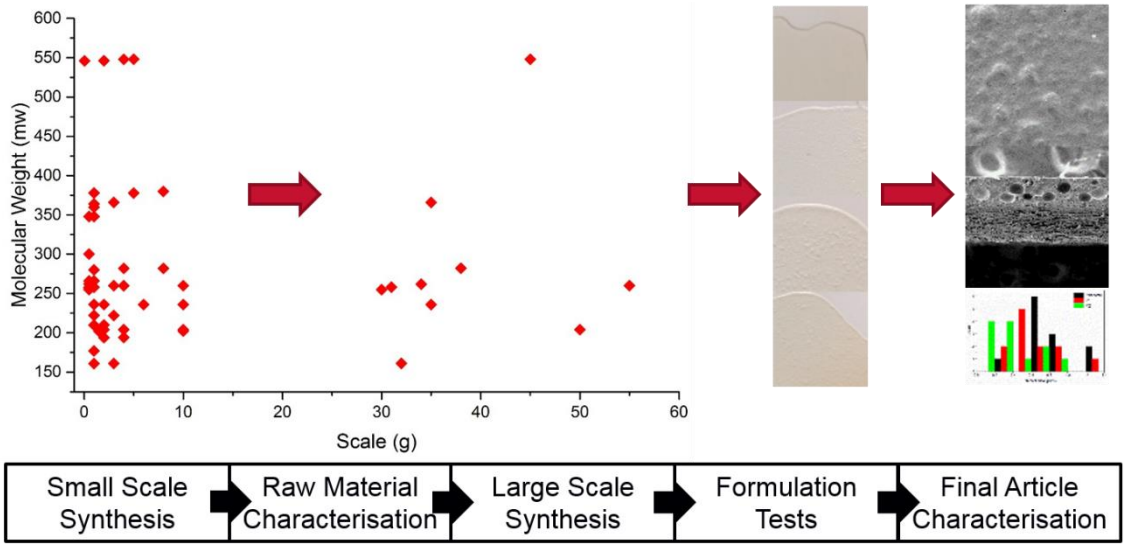

Figure 3.18 Schematic showing synthetic strategy from small scale synthesis to final article characterisation.

To ensure the synthetic work is carried out efficiently the following experimental guidelines (Table 3.7) were agreed on:

Table 3.7 Experimental guidelines for commercial synthesis and economic efficiency.

1. All starting materials and reagents must sum a maximum of £100 per 100 g
2. Synthesis on the small scale (<5g) must be completed within a 1-week time scale
3. Purity must exceed 90% (excluding residual solvent)
4. The small-scale reaction yield must be over 50% for scale up
5. Synthesis on the large scale (>100 g) must be completed within a 3-week time scale
6. Purity must still exceed 90%

Each novel chemical additive must satisfy each of the above limitations to be tested for blowing agent efficiency within the plastisol formulation.

3.3.1 Synthetic Strategy to Achieve Commerciality

As per the industrial requirements the following guidelines were created (Figure 3.19).

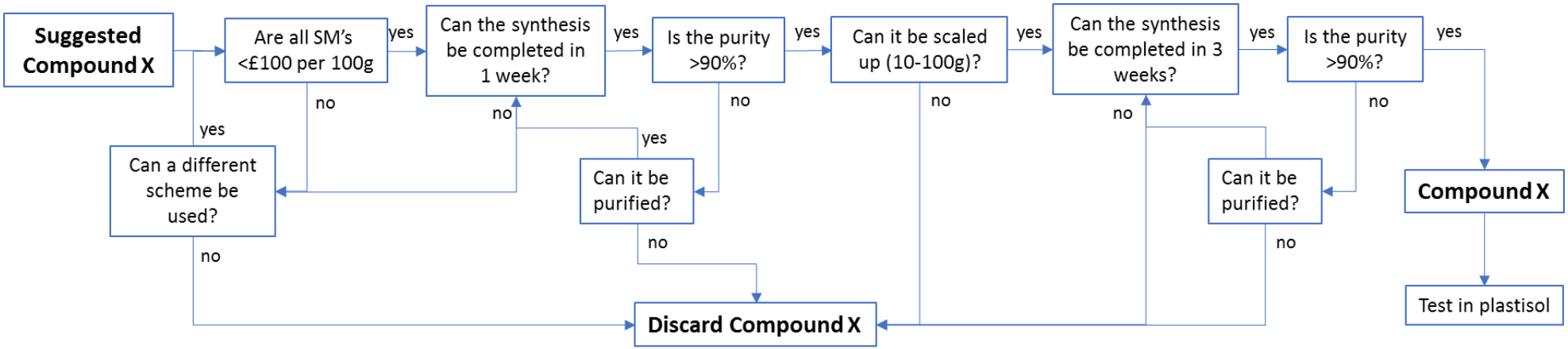

Figure 3.19 Flow chart depicting the synthetic approach to each desired compound, ensuring commercial time and costing efficiencies were met

3.4 Semicarbazide Derivatives

Semicarbazide **7** is a known, white solid decomposition product of azodicarbonamide. [128] The small molecule compound has a decomposition point typically occurring between 175-185 °C. [129] which is within the melt viscosity range of the PVC plastisol. [127]

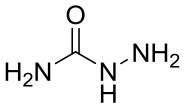

7

Semicarbazide is a derivative of the natural compound urea and can be naturally isolated from foods, such as honey and shellfish. [130-132]

The structural similarities between semicarbazide and azodicarbonamide allow for a series of derivatives with potentially similar physical properties to ADCA. Furthermore, the chemical structure of semicarbazide allows for the stable formation of chelates. [133] This could be advantageous within the formulation as chelation with the kicker metal ions (K and Zn)[xiii] could encourage decomposition of the semicarbazide derivatives. [134] The proposed chelation of a semicarbazide with kicker complexes is shown below (Figure 3.20).

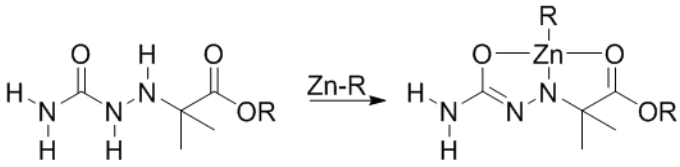

Figure 3.20 Potential chelation of a semicarbazide derivative to form a Zn complex

Semicarbazide was modified using carboxylic acids in an attempt to boost the gas yield through the formation of carbon dioxide during thermal decomposition. Tartronic acid and 2-hydroxyisobutyric acid were used to compare the subsequent gas yield from the di- and mono- carboxylic acid derivatives. Due to the high commercial availability, semicarbazide hydrochloride was purchased for the purpose of this project. High levels of residual semicarbazide can prove toxic, [61] this must be considered during the modification of the semicarbazide molecule.

[xiii] Graham and Brown standard formulation additives

3.4.1 Synthesis and Characterisation of the Semicarbazide Derivatives

In attempt to maximize the gas production of the semicarbazide derivatives, aliphatic hydroxy-carboxylic acid compounds were selected for reaction with semicarbazide hydrochloride. The hydrazo function of the semicarbazide molecule replaces the OH-group in the corresponding hydroxycarboxylic acid reagent to yield various asymmetric compounds with structural similarities to azodicarbonamide.

Tartronic acid **20**, 2-hydroxyisobutyric acid **21** and 2-aminoisobutyric acid **22** were reacted with semicarbazide hydrochloride **7**. (Scheme 3.1)

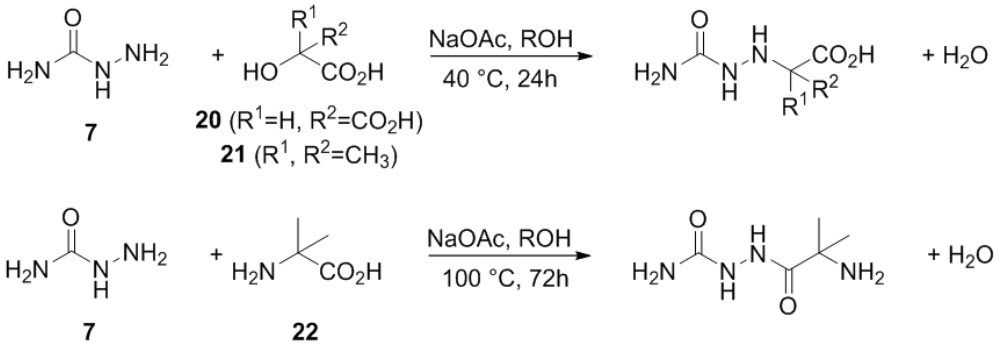

Scheme 3.1 Generic schemes of the synthesis of the semicarbazide series.

The following target compounds **23-25** were synthesised (Figure 3.21).

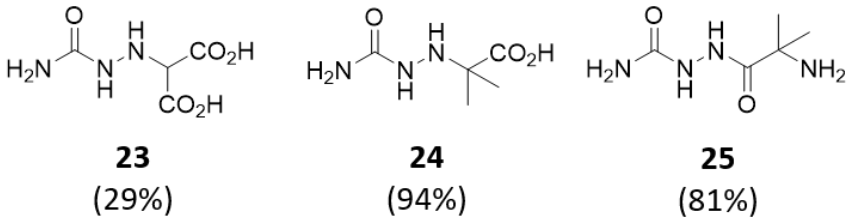

Figure 3.21 Chemical structure of the semicarbazide compounds **23-25**.

Significant peaks in the IR spectrum for the characterisation of hydrazo molecules account for a contemporaneous presence of the C-N, N-H and N-N stretching vibrations. All compounds **23-25** exhibit a strong peak in the region of 1000-1300 cm^{-1} (C-N), the N-N stretching vibration (1600 cm^{-1}) and N-H stretches (3300 cm^{-1} and 3500 cm^{-1}) and bends (1580-1650 cm^{-1}) [135] confirming the presence of the hydrazo group. Furthermore the absence of the sharp peak between 3590 cm^{-1} and 3650 cm^{-1} [136] in the spectra of the compounds confirmed that the reaction had occurred and the hydroxy function

had been replaced as expected, and that no starting material remained in the reaction mixture. The essential IR peaks for the characterisation of the novel compounds are listed in Table 3.8.

Table 3.8 IR data for compounds **23-25**.

Compound	C-N[a]	N-H[b] (bend)	N-H[c] (stretch)	C=O[d]
23	1119	1623	3348	1717
24	1168	1588	3367	1666
25	1112	1584	3446	1670

a Typical region 1000-1300 cm^{-1}
b Typical region 1490-1650 cm^{-1}
c Typical region 3300-3500 cm^{-1}
d Typical region 1600-1750 cm^{-1}

The NMR data confirmed the characterisation of the materials **23-24**. In the case of compound **25**, the ^{1}H NMR spectrum identified the presence of multiple tautomeric forms, through the contemporaneous presence of several CH_3 environments. A high number of functional groups within **25** capable of tautomerisation and H-bonding allows for numerous forms to co-exist, resulting in the complex ^{1}H NMR spectrum. (Figure 3.22)

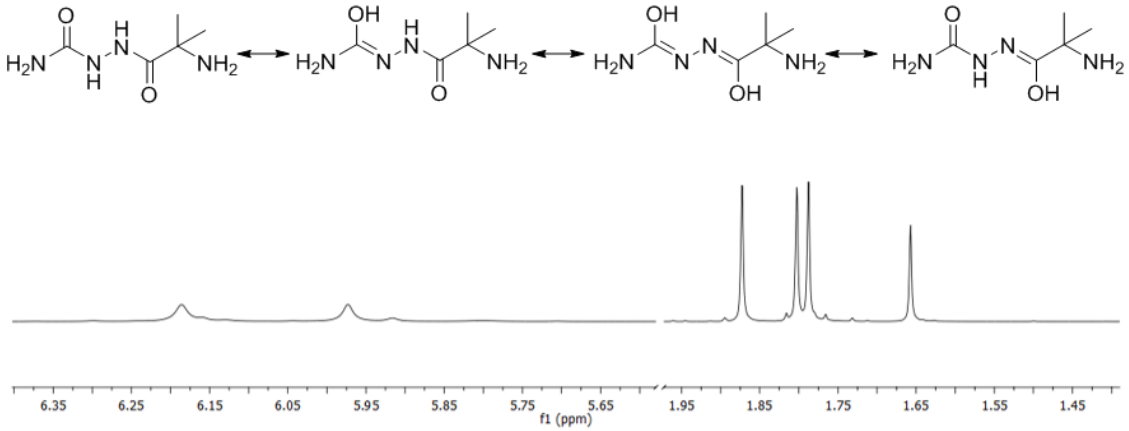

Figure 3.22 ^{1}H NMR spectrum of **25**, showing potential tautomeric forms and multiple CH_3 signals in the region of 1.7-1.9 ppm and NH signals in the region of 5.85-6.2 ppm.

The longer run time required for the ^{13}C NMR analysis, identified that the compound **25**, was unstable in solution as a colour change of colourless to purple was observed after a prolonged storage in both chloroform and DMSO. This circumstance, prevented analysis of the pure material by ^{13}C NMR spectroscopy.

3.4.2 Thermal Behaviour, Stability and Decomposition Pathway of Compounds 23-25

Thermal gravimetric analysis (TGA) and differential scanning calorimetry (DSC) were used to evaluate the thermal properties of compounds **23-25** as these techniques can be used to predict the behaviour of the additives within the coating formulation at various cure temperatures. Due to the open vessel TGA, the mass loss observed in the TGA thermogram cannot be conclusively characterised as decomposition due to the chance of evaporation. However, the TGA data can give valuable information as to the thermal range and phase transitions of the synthesised materials prior to large scale industrial testing.

Typical temperatures including the temperature at 10% mass loss in the TGA ($T_{-10\%}$), the maximum thermal degradation temperature (T_{max}) from the 1st derivative of the TGA (DTG), and the phase transition temperature in the DSC (T_{DSC}) are summarized in Table 3.9.

Table 3.9 TGA and DSC data for compounds **23-25**.

Compound	TGA		DSC
	$T_{-10\%}$[a]	T_{max}[b]	T_{DSC}[c]
23	140	155, 223	123
24	123	222	138
25	159	197	170

a Temperature at 10% mass loss in the TGA
b Maximum thermal degradation temperature from the 1st derivative of the TGA
c Phase transition temperature in the DSC

All the additives in the semicarbazide series (**23-25**) show pyrolysis processes, characterised by T_{max} and T_{DSC}, within the suitable melt viscosity range of the PVC plastisol.

Of the compounds in the semicarbazide series, additive **23** was the only material to display a two-step pyrolysis process, with T_{max} observed at 155 °C and 223 °C (a, Figure 3.23). This is supportive with the theory that multi decarboxylation steps occurred in the polycarboxylic acid materials.

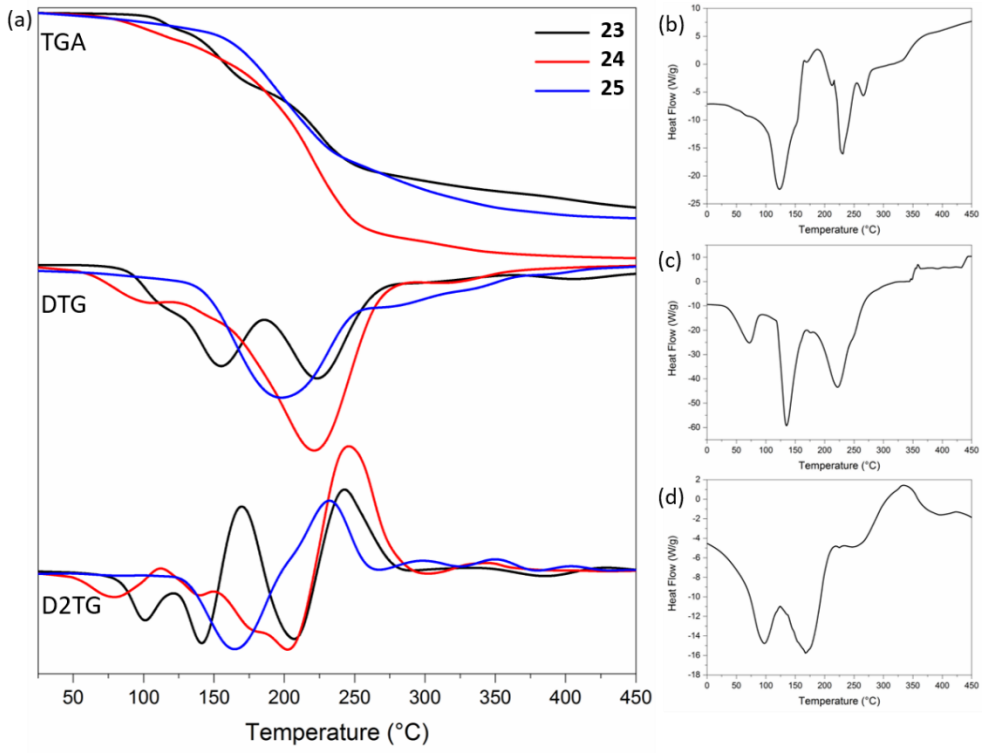

Figure 3.23 (a) TGA, DTG and D2TG analysis for compounds **23-25**. (b) DSC of compound **23**, (c) DSC of compound **24** and (d) DSC of compound **25**.

Compound **24** was characterised as a one-step decomposition process with an onset of pyrolysis, T_{max} of 222 °C, accounting for around 58% mass loss. The start of pyrolysis identified in the D2TG thermogram at 120 °C is conducive with the DSC data which shows a phase transition in the same temperature region (a, c, Figure 3.23). This data suggests that the thermal decomposition of additive **24** occurs across the range of approx. 130 – 230 °C.

Compound **25** also showed a one-step decomposition process with T_{max} of 197 °C and T_{DSC} of 170 °C. The TGA data confirms that the compound **25**, is thermally stable, suggesting that pH/ solvent can lead to the uncertain results observed during the NMR analysis. Due to these factors and the observed colour change when exposed to solution it was decided not to carry compound **25** forward for formulation testing.

The observed decomposition ranges for compound **23** and **24**, correlate to the melt viscosity range of the PVC plastisol suggesting that additives **23-24** are compatible with the formulation system.

3.4.3 PVC Coating Formulations, Temperature Dependency and Colour Correlation of the Semicarbazide Series

To study derivatives **23** and **24** within polymer matrix, plastisols **P23** and **P24,** were formulated to the standard specification of 16.1 mmol of blowing agent per 100g, manufactured and analysed to determine the effect on coating efficiency, surface wetting and coating coverage. The formulations have been cured at 130 °C, 150 °C, 170 °C, 190 °C, 210 °C and 230 °C to correspond with the melt viscosity range of the PVC plastisol. This allowed temperature dependency studies to be carried out for each of the materials. The samples cured at 130 °C were set as control samples, with ΔE for each sample from 150 – 210 °C (Table 3.10).

Table 3.10 L*a*b* data and ΔE values for samples **P23**, **P24** and $\mathbf{P_{ADCA}}$.

	130 °C			ΔE			
Entry	**L***	**a***	**b***	**150 °C**	**170 °C**	**190 °C**	**210 °C**
P23	93.72	-0.07	-0.19	0.25	0.46	0.90	2.65
P24	93.07	0.53	2.65	0.88	0.95	0.64	0.79
P_{ADCA}	92.55	-0.96	11.55	0.51	0.53	1.18	6.81

Compound **23**, showed minimal colour change between 150 °C and 190 °C, with ΔE <1. The observed increase in ΔE for samples $\mathbf{P23_{210}}$ (Table 3.10) was conducive with the thermal decomposition data which showed an onset of the second pyrolysis at T_{max} of 223 °C. It was predicted that the colouration observed in coating sample $\mathbf{P23_{210}}$ would be correctable using optical brighteners and/or bleaching agents. Concentrations of these materials, already present in the formulation, could potentially be increased in order to counteract the colouration caused by the by-products of thermal decomposition of additive **23**.

Compound **24** in $\mathbf{P24_{130\text{-}210}}$, showed very little colour change (Figure 3.24) across the temperature range with ΔE <1 observed in all cases. This is advantageous in colour sensitive applications, such as wallpapers, as the additives within the formulation appear not to contribute to the overall colouration of the plastisol coating surface.

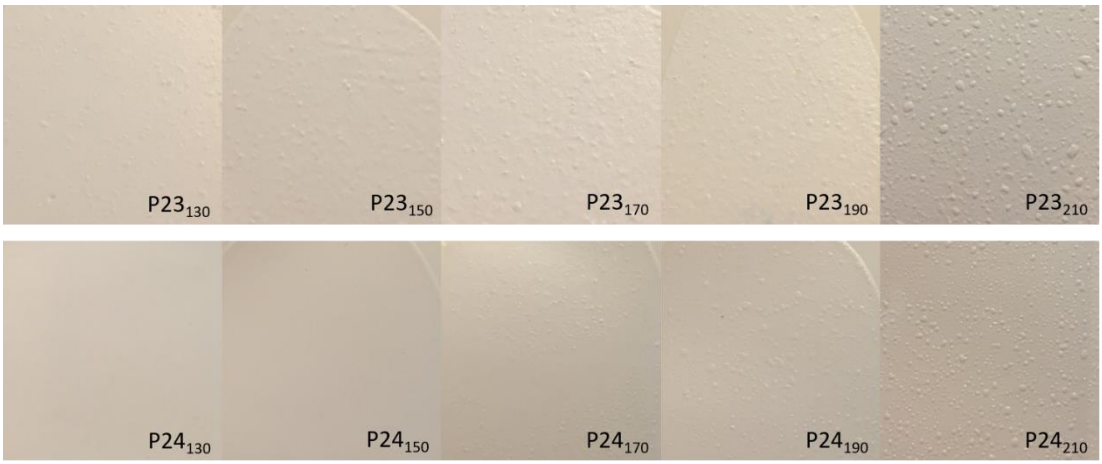

Figure 3.24 Photographic images of samples **P23$_{150}$ – P23$_{210}$** and **P24$_{150}$ – P24$_{210}$**.

The L*a*b* data for both the analysed materials in the semicarbazide series was promising in terms of decorative applications. (Figure 3.25)

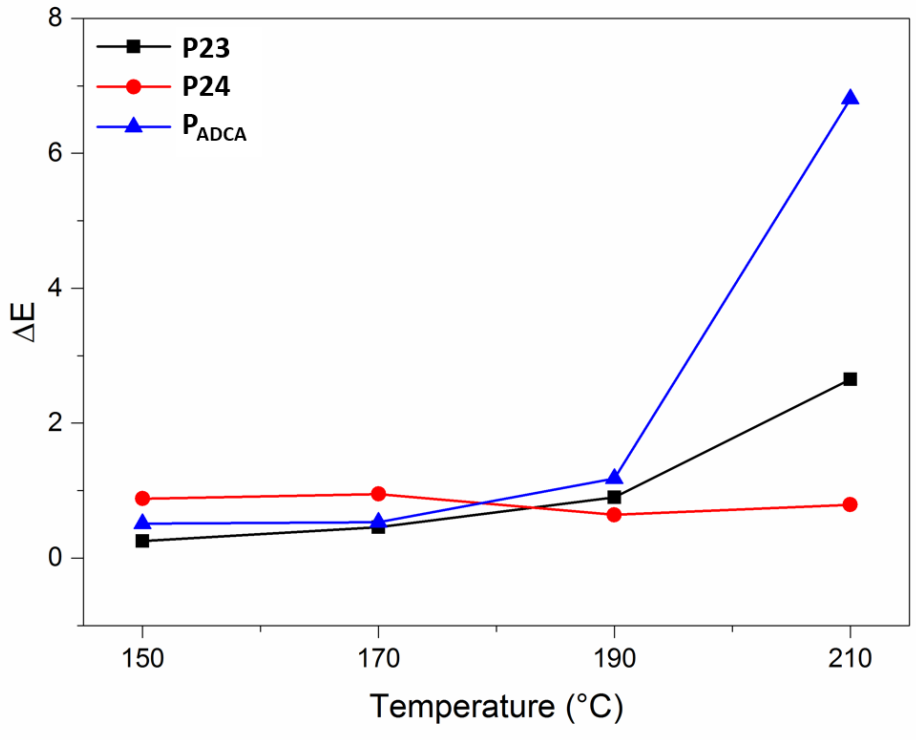

Figure 3.25 Graph depicting ΔE for samples **P23$_{150}$ – P23$_{210}$**, **P24$_{150}$ – P24$_{210}$** and **P$_{ADCA}$**.

The observed colour changes across the temperature range were negligible in comparison with the control expanded sample **P$_{ADCA}$**. That said the graph clearly shows the increased colour change (ΔE) observed for sample **P23$_{210}$**. (Figure 3.25)

3.4.4 Surface Texture and Microstructure of the Semicarbazide Series

3.4.4.1 Surface Texture Analysis of the Semicarbazide Series

The external and the internal cellular structure of the paper samples **P23** and **P24**, formulated with compounds **23** and **24**, were analysed with scanning electron microscopy (SEM). The plastisol coatings were compared to that standard expanded control sample $\mathbf{P_{ADCA}}$ which shows a regular internal cell structure and evenly distributed smooth, matt surface. A standard 'blank' formulation $\mathbf{P_{blank}}$ was also prepared by the same method and contained no chemical blowing additives. Sample $\mathbf{P_{blank}}$ presents an uneven surface, which is the result of irregularly sized gas pockets throughout the sample. The defects are observed across the sample surface ranging from 0.31-1.46 mm with the average defect size ca. 0.80 mm. (Figure 3.26)

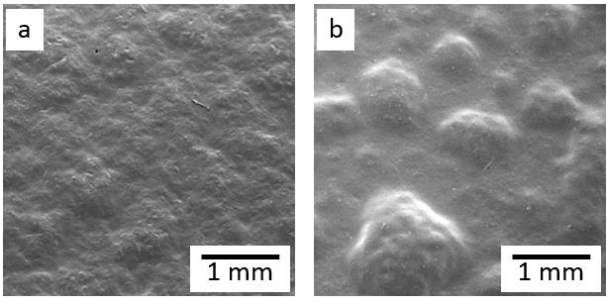

Figure 3.26 SEM surface micrographs of the control plastisol's (a) $\mathbf{P_{ADCA}}$ and (b) $\mathbf{P_{blank}}$ at x18 Mag.

The decomposition of additive **23**, was evident by the surface effects observed in the SEM images of **P23**. Sample $\mathbf{P23_{170}}$ (a, Figure 3.27) showed large holes upon the coating surface, conducive with the breakage of large gas bubbles created by thermal decomposition. Smaller pinholes were also evident on the surface of the $\mathbf{P23_{170}}$ sample. This is conducive with the TGA results which characterised the first pyrolysis step at 155 °C (a, Figure 3.23).

As the temperature was increased to 190 °C, the larger crater-like surface defects are no longer observed. Pinhole defects are still visible across the surface, but the absence of larger defects gives an overall smoother appearance. At 210 °C, $\mathbf{P23_{210}}$ showed large gas bubbles across the surface, comparable to those observed in $\mathbf{P_{blank}}$. The defects shown in $\mathbf{P23_{210}}$ were likely due to the

second pyrolysis step at T_{max} of 223 °C. In the case of **P23$_{210}$** the surface defects are also visible by the naked eye (Figure 3.24).

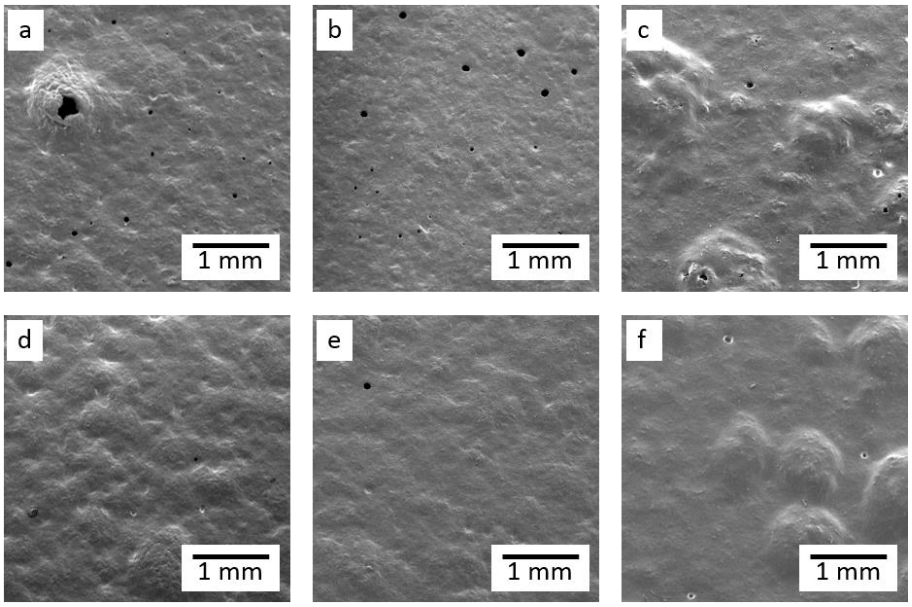

Figure 3.27 SEM surface micrographs of samples (a) **P23$_{170}$**, (b) **P23$_{190}$**, (c) **P23$_{210}$**, (d) **P24$_{170}$**, (e) **P24$_{190}$** and (f) **P24$_{210}$** at x75 Mag.

The graph (Figure 3.28) shows that significantly less pinhole defects were observed at 210 °C in **P23**. This result supports the TGA data which shows T_{max} around 220 °C and suggests that decomposition aids dispersion. In the case of samples **P24**, less defects were observed across the whole temperature range, which suggests that the system was more favourable.

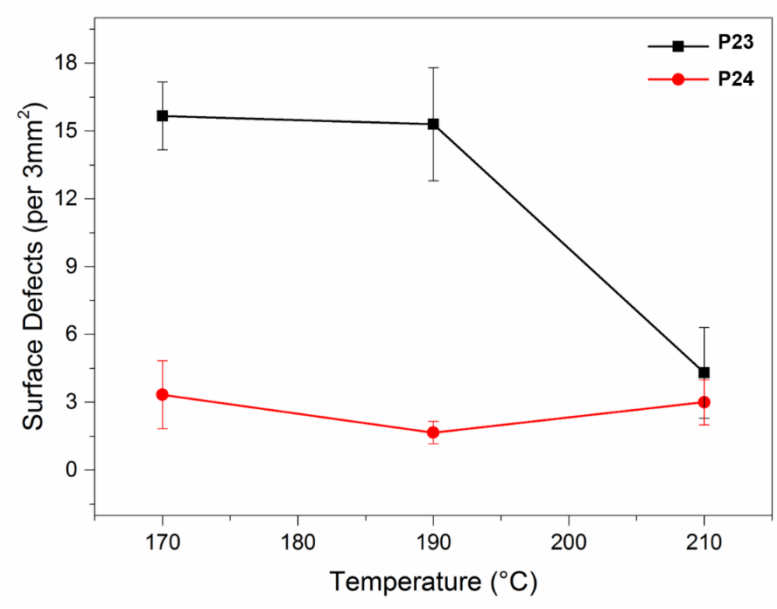

Figure 3.28 Graph depicting the number of pinholes in the SEM surface micrographs of samples **P23**, **P24** across the temperature range 170-210 °C.

Sample **$P24_{170}$**, showed a relatively even texture, comparable to that observed in the control expanded formulation **P_{ADCA}**. This suggests an even distribution of additive **24** within the plastisol formulation. Minimal change in physical surface properties was observed between samples **$P24_{170}$** and **$P24_{190}$**. (d, e, Figure 3.27). That said, in the sample **$P24_{210}$** larger gas bubbles were detected on the surface, correlating to the phase observed at T_{max} of 222 °C and T_{DSC} at 223 °C (Figure 3.23). The average defect size was 0.92 mm, comparable to the approx. 0.80 mm defects observed in **P_{blank}**. The SEM surface micrographs for sample **P68**, suggest that the system is more favourable between the temperatures 170-190 °C, this is advantageous as manufacturing temperatures could be lowered resulting in cost savings.

3.4.4.2 Surface Gloss Analysis of the Semicarbazide Series

As in the previously mentioned, a smooth and matt finish, as observed in **P_{ADCA}** was desired for the product. This physical property is more appealing to the decorative wallpaper mass market[xiv]. The gloss of the surface of each coating in the semicarbazide series was analysed using a glossmeter and the data is tabulated below (Table 3.11).

Table 3.11 Gloss readings for samples **P23**, **P24** and **P_{ADCA}.**

Sample	85° Beam Angle Reading (GU)				
	130 °C	150 °C	170 °C	190 °C	210 °C
P23	20.8	10.2	8.5	9.9	8.2
P24	28.1	10.5	5.7	7.6	4.9
P_{ADCA}	28.5	28.5	7.6	3.5	1.3

In the case of **P23** and **P24**, the general gloss trend followed that observed for **P_{ADCA}**, where the coating surface became less glossy as the temperature was increased. All gloss values for samples above 170 °C were with the matt region of ≤10 GU. In the case of samples **$P23_{150}$** and **$P24_{150}$**, the gloss readings observed were on the border of the matt region with values of 10.2 GU and 10.5 GU respectively. (Figure 3.29)

[xiv] Graham & Brown market research

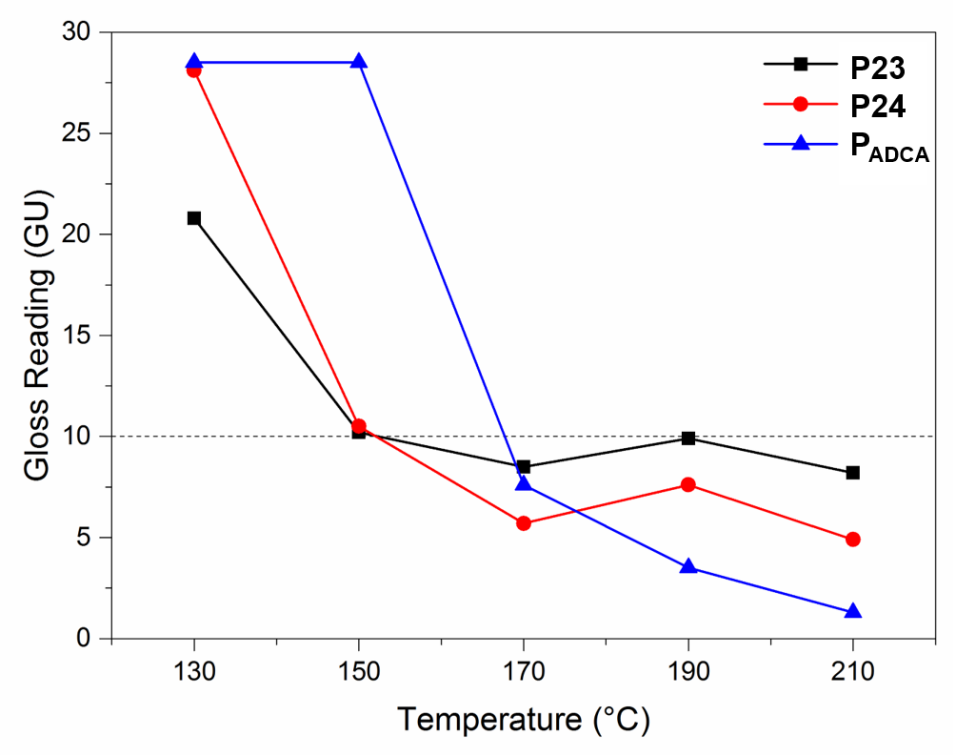

Figure 3.29 Graph depicting the gloss readings for samples **P23**, **P24** and **P_{ADCA}** with the upper region of the matt region (10 GU) highlighted.

Samples **$P23_{190}$** and **$P24_{190}$**, both showed a slight anomaly to the downward trend of the data. This is aligned with the SEM surface micrographs, which confirmed a smoother surface for both **P23** and **P24** at 190 °C (b, e, Figure 3.27). In the TGA data of additive **23**, 190 °C sits between the two stages of pyrolysis, whilst for **P24**, onset of decomposition is shown at the higher temperature of 210 °C (Figure 3.23). This provides explanation of the slightly glossier surfaces observed at the temperature of 190 °C. As less decomposition was occurring at this temperature range, less disorder was placed upon the formulation and subsequently minimal disruption was caused to the coating surface. The matt surface observed in **P_{ADCA}** is resultant of the texture exhibited on the surface.

3.4.4.3 Microstructure Analysis of the Semicarbazide Series

Cross-section micrographs provided information of the internal cellular structure. The blank control sample, **P_{blank}** (a, Figure 3.30), contained irregularly sized and unevenly distributed gas cells within the plastisol matrix. On the contrary the control expansion sample, **P_{ADCA}** (b, Figure 3.30), shows an even distribution of regularly sized gas pockets creating an overall expansion of the plastisol layer of approx. 400 µm. All additives in formulations **P23** and **P24** (c-f, Figure 3.30) showed the formation of gas pockets within the coating and

confirmed that the compounds release gas as a result of thermal decomposition and act as blowing agents. The control sample **P_{blank}**, shows minimal gas production by comparison.

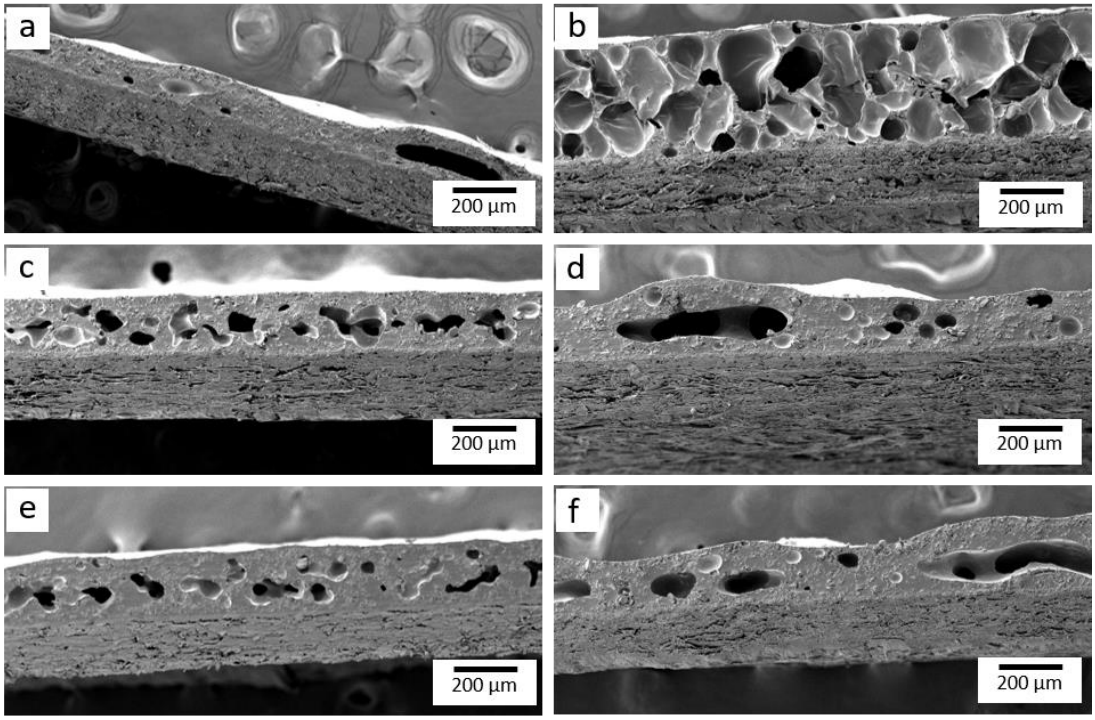

Figure 3.30 SEM cross-section micrographs of samples (a) **P_{blank}**, (b) **P_{ADCA}**, (c) **$P23_{190}$**, (d) **$P23_{210}$**, (e) **$P24_{190}$** and (f) **$P24_{210}$** at x75 Mag.

The cross-section micrographs of formulation **P23**, containing additive **23**, showed more regular cell formation at the lower curing temperature of 190 °C (c, Figure 3.30). This is conducive with the surface SEM images which showed that samples **$P23_{190}$** (b, Figure 3.27) exhibited a much smoother surface than the other analysed temperatures. The evenness of the cells within sample **P23** is advantageous and suggests that additive **23** aids distribution within the formulation. That said, the gas formed in the case of **P23**, is not sufficient enough to provide overall expansion of the coating layer.

Similarly, to sample **$P23_{190}$**, sample **$P23_{190}$** (e, Figure 3.30) showed a fairly even distribution of unevenly shaped gas cells throughout the plastisol matrix. Sample **$P24_{190}$** formed a more dense coating layer, with less gas cells produced overall. As the temperature was increased, **$P24_{210}$** (f, Figure 3.30) showed the formation of large, irregular gas pockets within the coating layer. Subsequently the upper surface of the plastisol became more uneven as a result of these large gas cells. This internal cellular structure is conducive with the surface properties

observed in the SEM micrographs of the corresponding surfaces (e, f, Figure 3.27). As with **P23**, the gas formed within the plastisol layer for **P24** provided no significant expansion of the coating.

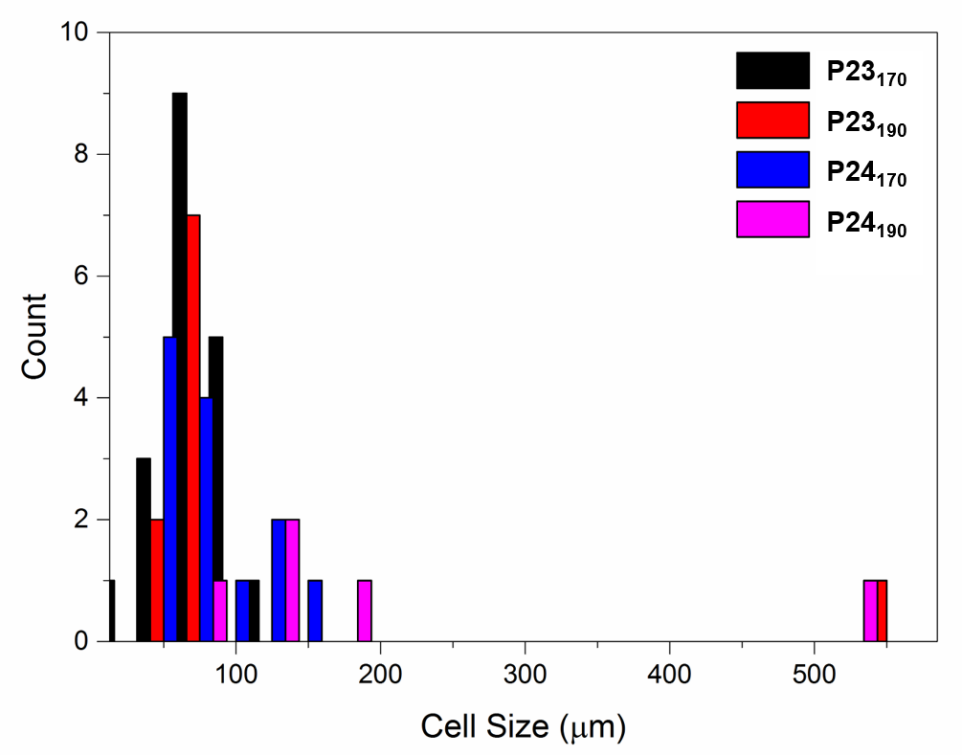

Figure 3.31 Graph depicting the cell size distribution in the SEM cross-section micrographs of samples **P23$_{190}$**, **P23$_{210}$**, **P24$_{190}$** and **P24$_{210}$**.

The distribution graph (Figure 3.31) clearly shows that the general trend of the semicarbazide series forms cells in the region of 50 µm to 200 µm.

In general, the formulations containing additive **23**, showed a smaller cell size than in the formulations **P24**. At both 190 °C and 210 °C, the majority of observed cells in **P23** SEM micrographs were below 100 µm in diameter, with cells in sample **P24** appearing in sizes up to 200 µm. However, some anomalies are observed. In sample **P23$_{210}$** and **P24$_{210}$** larger cells over 500 µm were visible in the cross-section micrographs. This suggests that the system is more favourable in the case of the semicarbazide materials at temperatures below 210 °C. This supports the defects observed in the surface SEM micrographs and the TGA data which showed T_{max} around 220 °C in both cases. This further suggests that the large gas cells and surface defects are resultant of thermal decomposition.

3.4.5 Conclusions of the Semicarbazide Series

The semicarbazide compounds **23-25** have been successfully synthesised and characterised. In the case of compound **25**, the compound was determined unstable in solution due to observed colour changes over sustained periods in solution. Synthesis of the compounds **23** and **24** was effectively scaled up to approx. 25 g in excellent yields of up to 96%.

The TGA and DSC data confirmed that thermal degradation of compounds **23** and **24**, occurred within a suitable range for implementation in PVC applications. PVC plastisol's containing compounds **23-24** were prepared and physical properties of the final formulations were tested at different curing temperatures.

In the case of all materials, gas cells were formed within the plastisol layer of the coating; however, this gas formation was not significant enough to increase the observed expansion of the coating. The even gas formation with the plastisol samples of **P23** and **P24**, produced a smooth, matt coating surface at temperatures 170 – 210 °C. However, significant surface defects were evident in the SEM surface images of samples $\mathbf{P23_{170}}$ and $\mathbf{P23_{210}}$, providing evidence that the system was not stable.

Compounds **23-24** did not significantly affect the colouration of the coating surface, suggesting that these additives are suited well to colour sensitive and decorative applications. Further investigation into suitable concentrations of optical brightener within the formulation could determine the efficiency of the material for batch colour matching ($\Delta E \leq 0.2$)

The study outlined in the chapters above proved that the incorporation of the compounds **23-24** into commercial PVC plastisol's for wallpaper applications directly affects the physical properties of the resultant coating. However, insufficient gas production and subsequent expansion of the plastisol layer upon thermal decomposition of the additives, resulted in an unsuitable alternative to ADCA in all cases.

3.5 Toluene Sulfonate Derivatives

Toluenesulfonyl hydrazide (TSH) **10** and toluenesulfonyl semicarbazide (TSSC) **11** are known alternatives to azodicarbonamide (ADCA) listed in the Austrian Dossier published in 2012, which led to the inclusion of ADCA as a Substance of Very High Concern (SVHC). Toluenesulfonyl hydrazide **10** decomposes readily at 110 °C to form nitrogen and water vapour. [68] The low decomposition temperature of TSH limits its application as a blowing agent, whilst toluenesulfonyl semicarbazide **11** decomposes at the much higher temperature of 235 °C.

Despite its efficiency in foam formation for other applications such as process foam injection moulding, [68] previous studies (Chapter 3.2.3) proved that TSSC **11** was not suitable in place of ADCA in wallpaper manufacturing, neither could it be used as a co-blowing agent in formulations containing both TSSC and ADCA. That said, synthetic modification of materials including the toluenesulfonate structural backbone could improve efficiency within the desired application by combining the advantageous properties of both TSH and TSSC within a suitable decomposition temperature that coincides with the melt viscosity of PVC plastisol formulations. Toluenesulfonyl chloride **26** provides a versatile platform for the synthesis of these toluenesulfonate materials.

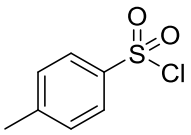

26

It was hypothesised that modified structures can alter the decomposition temperature and improve the expansion quality of the plastisol coating. Full decomposition of the materials below the curing temperature, and within the melt viscosity range [37, 127], could result in the formation and retention of more gas pockets within the plastisol matrix.

Toluenesulfonyl chloride **26** is a cost effective starting material[xv] that fits the scope of the project. Furthermore, it was predicted that the decomposition products would pose less acute toxicity than the previously synthesised aromatic derivatives as toluene would be produced in place of benzene vapour. [137]

[xv] Based on Sigma-Aldrich price April 2018.

TSSC is currently used as a chemical additive within the chemical industry [138, 139] and it was therefore predicted that toluene containing chemical additives would conform to the current industrial regulatory restrictions.

3.5.1 Synthesis and Characterisation of the Sulfonate Derivatives

Toluenesulfonyl chloride **26** was reacted with phenylhydrazine **27** in the first instance (**15**, Figure 3.32). Phenylhydrazine was used to develop an efficient synthesis for the sulfonate series; however, relatively low yields of <23% were observed. The toluenesulfonyl chloride was subsequently reacted with carboxyl containing reagents in attempt to maximise carbon dioxide produced upon thermal decomposition. Ethyl carbazate **28**, 2-hydrazoisobutyric acid **29** and 2-hydrazocitric acid **30** were used as the carboxyl containing reagents in reaction with toluenesulfonyl chloride. (Scheme 3.2)

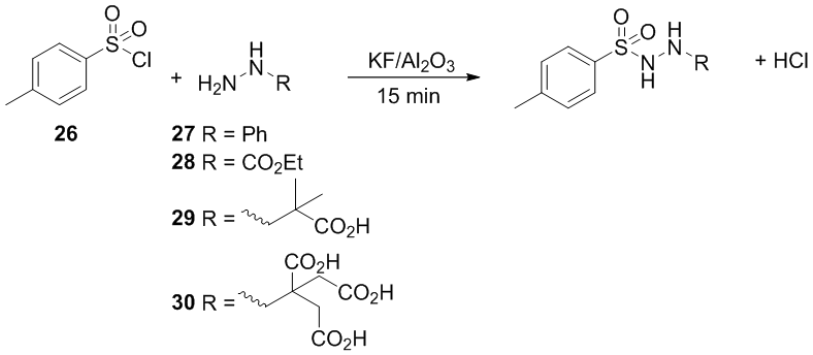

Scheme 3.2 Generic scheme of the synthesis of the sulfonate series

The following target compounds **31-32** were synthesised. (Figure 3.32)

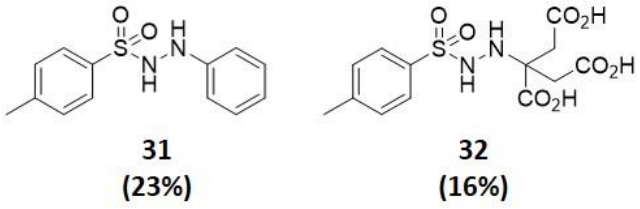

Figure 3.32 Synthesized aromatic **31** and acid **32** sulfonate derivatives

Although low yields were obtained in the case of compound **31** and **32**, an efficient synthetic strategy was developed to yield compound **31**. Both IR and NMR spectra of compound **31** were in agreement with the proposed structures.

Significant bands in the IR spectra for the sulfonate series are tabulated below. (Table 3.12)

Table 3.12 IR data for compounds **31** and **34.**

Compound	N-H[a] (bend)	N-H[b] (stretch)	S=O[c]
31	1494	3314	1321

a Typical region 1490-1650 cm^{-1}
b Typical region 3300-3500 cm^{-1}
c Typical region 1350 cm^{-1}

The synthesis of compounds **33** and **34**, was attempted under the same reaction conditions. (Figure 3.33)

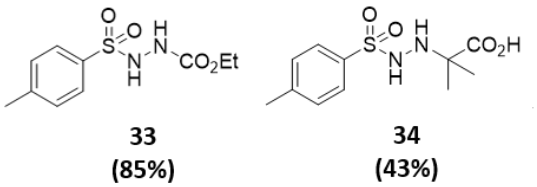

33 (85%) **34** (43%)

Figure 3.33 Unsuccessful sulfonate derivatives **33** and **34**.

Reactions to yield compounds **33** and **34** resulted in highly complex mixtures. Although significant peaks were present in the IR spectra of the mixtures, it was clear from the ^{1}H NMR spectra of the materials that multiple compounds were present. Besides the starting material, the side-products also included a potential adduct with the solvent, ethanol. The aromatic region of the proton NMR spectra clearly showed separate aromatic compounds in the case of mixture **33** and mixture **34** (Figure 3.34).

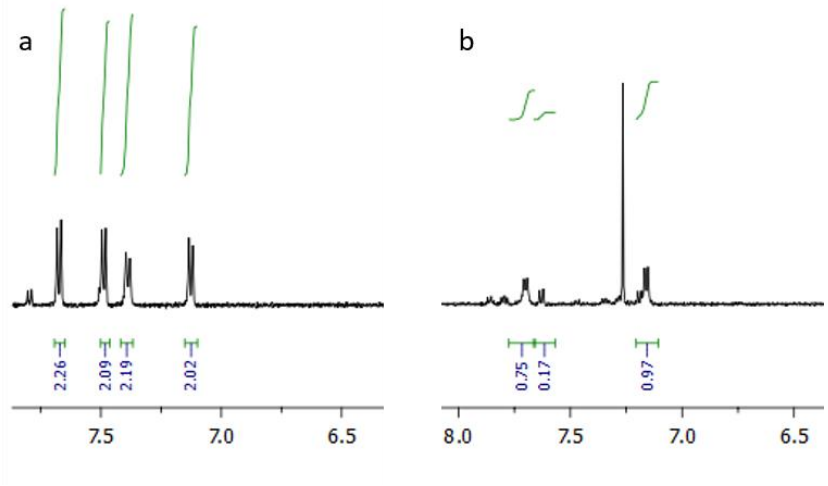

Figure 3.34 Aromatic regions of the ^{1}H NMR spectra of (a) compound **33** and (b) compound **34** showing non-isolated mixtures.

Attempts to isolate the desired product proved unsuccessful, within the remits of the synthetic strategy. Furthermore, despite isolation in high purity on the small scale, scale up attempts proved unsuccessful in the case of compound **32**. The unsuccessful synthetic scale up for compound **32**, resulted in the material not meeting the outlined requirements set out for the project to ensure efficient commercialization was possible. (Chapter 3.1) Subsequently compound **32** could not be analysed within the plastisol coating.

Despite the synthetic difficulties associated with the sulfonate series, compound **31** was taken forward for plastisol testing in attempt to identify potential advantageous physical properties of the sulfonate series. If this was the case, the synthetic pathways to yield compounds **32-34** could be re-evaluated in detail in order to carry out a fully comprehensive plastisol study.

3.5.2 Thermal Behaviour, Stability and Decomposition Pathway of Compound 31

Thermal gravimetric analysis (TGA) and differential scanning calorimetry (DSC) were used to evaluate the thermal properties of compound **31** and the typical temperatures are summarized in Table 3.13.

Table 3.13 TGA and DSC data for compound **31**.

Compound	TGA		DSC
	$T_{-10\%}$[a]	T_{max}[b]	T_{DSC}[c]
31	142	151, 197	160

a Temperature at 10% mass loss in the TGA
b Maximum thermal degradation temperature from the 1st derivative of the TGA
c Phase transition temperature in the DSC

For the aromatic compound **31**, the thermal degradation based on TGA is a two-step process, characterised by T_{max}, and occurs in the range of 151 °C and 197 °C (Figure 3.35). These values of the maximum degradation temperatures are in a correlation with the value obtained from DSC analysis compound **31**, where T_{DSC} is 160 °C (a, Figure 3.36). Both transition steps observed in the DTG spectrum of compound **31**, correlate to the optimum melt viscosity range of the PVC plastisol formulation. The TGA showed a total of 69% weight loss below the 210 °C manufacturing temperature.

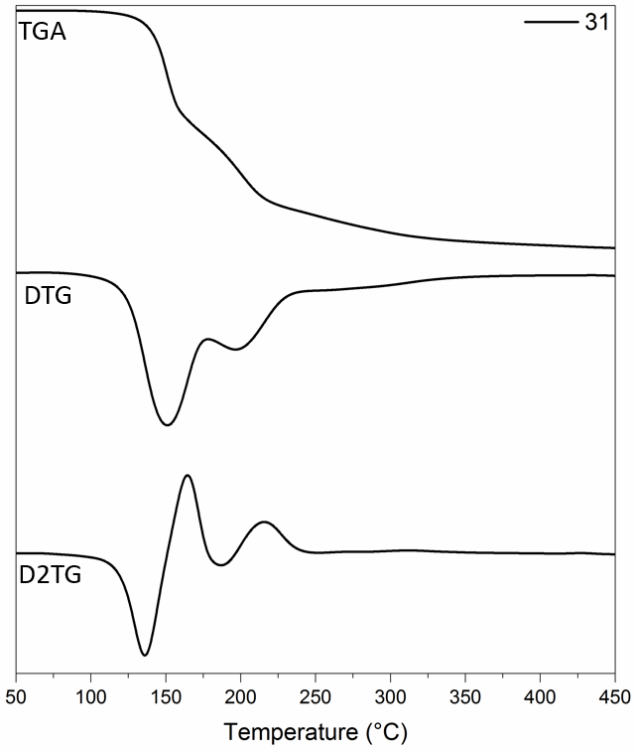

Figure 3.35 TGA, first derivative of the TGA (DTG) and second derivative of the TGA (D2TG) for compound **31**.

The DSC analysis for compound **31** (Figure 3.36), support the ^{1}H NMR spectra that showed the isolation of pure compounds due to the well-defined phase transition peaks.

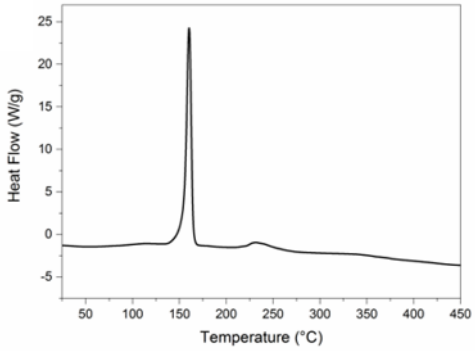

Figure 3.36 DSC analysis for compound **31**.

The occurrence of T_{max} and T_{DSC} for compound **31** within the suitable melt viscosity for PVC plastisol, suggests the suitability of compound **31** within the desired application process.

3.5.3 PVC Coating Formulations, Temperature Dependency and Colour Correlation of the Sulfonate Series

Conversely to the results observed for the previous phenyl containing materials, compound **31** was isolated as an off white solid. In attempt to maximize distribution of the powdered material, the compound was finely ground using a pestle and mortar before implementation into the plastisol formulation. The use of fine grade powders is essential as large particle sizes can disrupt the application of a 200 µm coating layer by hindering drawdown of the k-bar.

To study the sulfonate derivative **31** within polymer matrix, the plastisol containing compound **31** was formulated to a standard specification, manufactured and analysed to determine the effect on coating efficiency, surface wetting and coating coverage. The formulation had been cured at 130-210 °C to correspond with the melt viscosity range of the PVC plastisol. This allowed temperature dependency studies to be carried out. Table 3.14 shows L*a*b* and ΔE data for the thermally cured plastisol **P31**. The L*a*b* values are given for the formulated plastisol cured at 130 °C and was set as the control sample $\mathbf{P31_{130}}$ to monitor temperature dependent colour change (ΔE) of the formulation.

Table 3.14 L*a*b* data and ΔE values of **P31** and $\mathbf{P_{ADCA}}$.

	130 °C			ΔE			
Entry	**L***	**a***	**b***	**150 °C**	**170 °C**	**190 °C**	**210 °C**
P31	91.03	0.83	10.68	4.64	11.71	6.85	20.23
$\mathbf{P_{ADCA}}$	92.55	-0.96	11.55	0.51	0.53	1.18	6.81

Sample **P31** formulated with **31** shows a significant increase in ΔE at 170 °C and at 210 °C curing temperatures (Table 3.14), these figures coincide with the two-step pyrolysis observed in the first derivative TGA of compound **31**. The control sample $\mathbf{P31_{130}}$ showed significant yellow saturation (b* = 10.68) before the any thermal decomposition of additive **31**. (Figure 3.37)

Figure 3.37 Photographic images of samples **P31$_{130}$** – **P31$_{210}$**.

This suggested that the ΔE values observed across the temperature range of **P31$_{130}$-P31$_{210}$** were outside the suitable range for correction using optical brighteners or bleaching agents. This data confirms that the additive **31** is not suitable for colour sensitive applications such as the decorative industry. All samples in the analysed temperature range for **P31**, showed significantly more colouration than the control expanded coating **P$_{ADCA}$**.

As seen in the graph below (Figure 3.38), the colouration of sample **P31** did not follow a straight-line trend as the temperature increased.

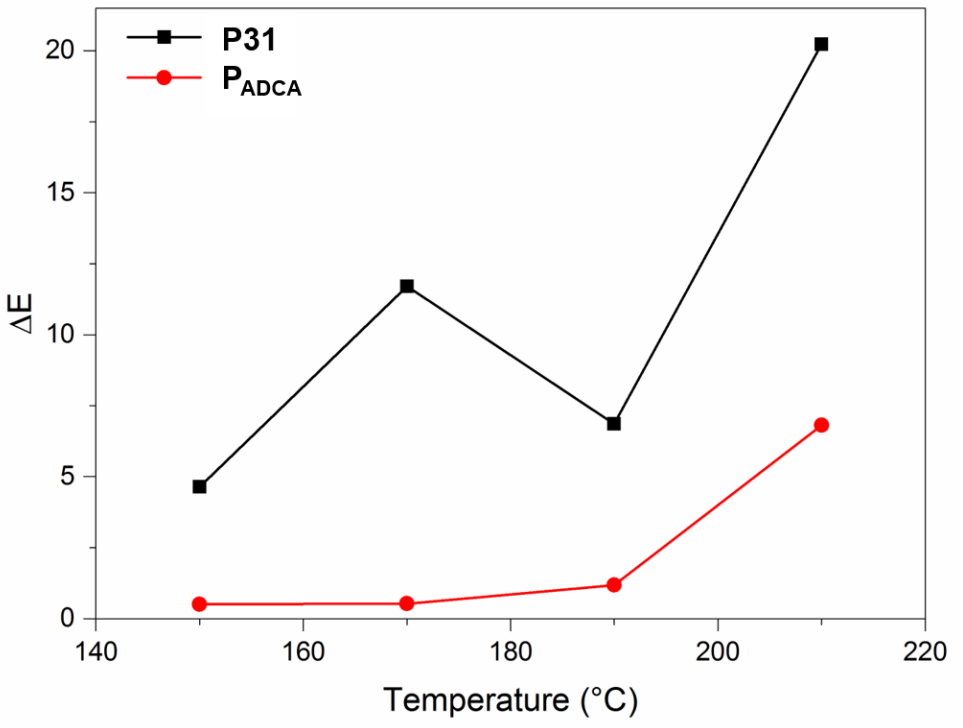

Figure 3.38 Graph depicting ΔE for samples **P31** and **P$_{ADCA}$**.

Significant spikes in ΔE were observed at 170 °C and 210 °C. The correlation with T_{DSC} at 160 °C (a, Figure 3.36) and T_{max} at 197 °C (Figure 3.35) confirmed that the colour changes observed in the plastisol's **P31** were resultant of the thermal degradation of compound **31**.

3.5.4 Surface Texture and Microstructure of the Sulfonate Series

3.5.4.1 Surface Texture Analysis of the Sulfonate Series

The surface textures of the formulations containing additive **31**, were analysed by scanning electron microscopy (SEM). This allowed any surface defects or properties to be identified. As previously mentioned to desired physical properties of the plastisol coatings were evenly expanded, smooth and matt surfaces. The blank formulation $\mathbf{P_{blank}}$, showed large defects across the surface coating caused by irregular gas cells within the formulation layer. The control material $\mathbf{P_{ADCA}}$ showed an even and level surface with a visible texture, leading to a matt surface effect. (Figure 3.39)

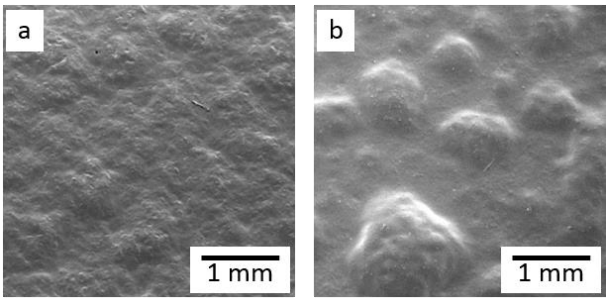

Figure 3.39 SEM surface micrographs of the controls (a) $\mathbf{P_{ADCA}}$ and (b) $\mathbf{P_{blank}}$ at x18 Mag.

The sulfonate series additive, **31**, showed varied surface properties when analysed microscopically (Figure 3.40). Samples $\mathbf{P31_{170\text{-}210}}$ showed a mixture of both raised surface bubbles and pinholes.

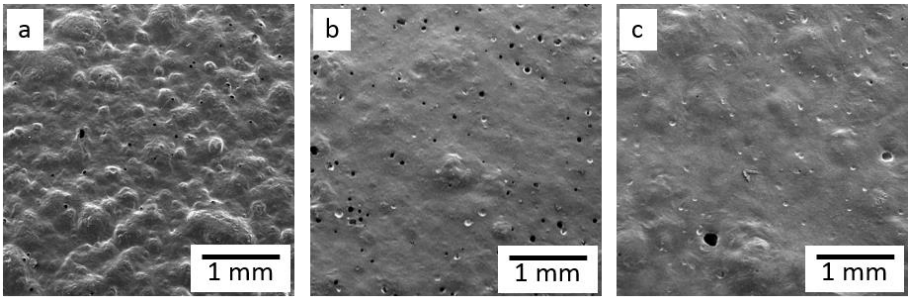

Figure 3.40 SEM Surface micrographs of samples (a) $\mathbf{P31_{170}}$, (b) $\mathbf{P31_{190}}$, (c) $\mathbf{P31_{210}}$ at x18 Mag.

Coating sample $\mathbf{P31_{190}}$ (b, Figure 3.40) exhibited significantly more pinhole defects across its surface, suggesting that this temperature was not conducive with even distribution of compound **31**. Less colouration was observed in sample

P31$_{190}$, further confirming that a manufacturing temperature of 190 °C is not optimised for the decomposition of additive **31**. At 210 °C (c, Figure 3.40), pinhole defects were still observed; however, in significantly lower quantity. In general, the surface of sample **P31$_{210}$** was smoother than that of the other temperatures. Sample **P31$_{170}$**, shows a rougher textured surface, with an even distribution of defects, most likely as a result of increased interactions within the formulation at this temperature.

3.5.4.2 Surface Gloss Analysis of the Sulfonate Series

As in the previously analysed series', a smooth and matt finish was desired for the end product. This physical property is more appealing to the decorative wallpaper mass market[xvi]. The gloss of the surface of each coating was analysed using a glossmeter and the data is tabulated below (Table 3.15).

Table 3.15 Gloss readings for plastisol samples **P31** and **P$_{ADCA}$**.

Sample	85° Beam Angle Reading (GU)				
	130 °C	150 °C	170 °C	190 °C	210 °C
P31	20.0	5.3	2.0	11.5	15.5
P$_{ADCA}$	28.5	28.5	7.6	3.5	1.3

The plastisol sample containing additive **31**, showed a semi-gloss surface at 130 °C. The gloss reading significantly lowers between 130 °C and 150 °C, with both **P31$_{150}$** and **P31$_{170}$** reading well within the matt surface range (GU ≤10). This result suggests that decomposition of additive **31** does not initiate until 150 °C and this is conducive with the thermal degradation data obtained from the DTG that shows a step at 151 °C (Figure 3.35) with the phase transition in the DSC at 160 °C (Figure 3.36). This suggested that the first pyrolysis step of the additive **31** yields the most advantageous physical properties in terms of surface gloss. This data is also conducive with the SEM surface micrographs of sample **P31$_{170}$** which showed a significantly rougher coating surface.

Sample **P31** does not follow the trend of **P$_{ADCA}$** where gloss units decrease as the temperature is increased (Figure 3.41).

[xvi] Graham & Brown market research

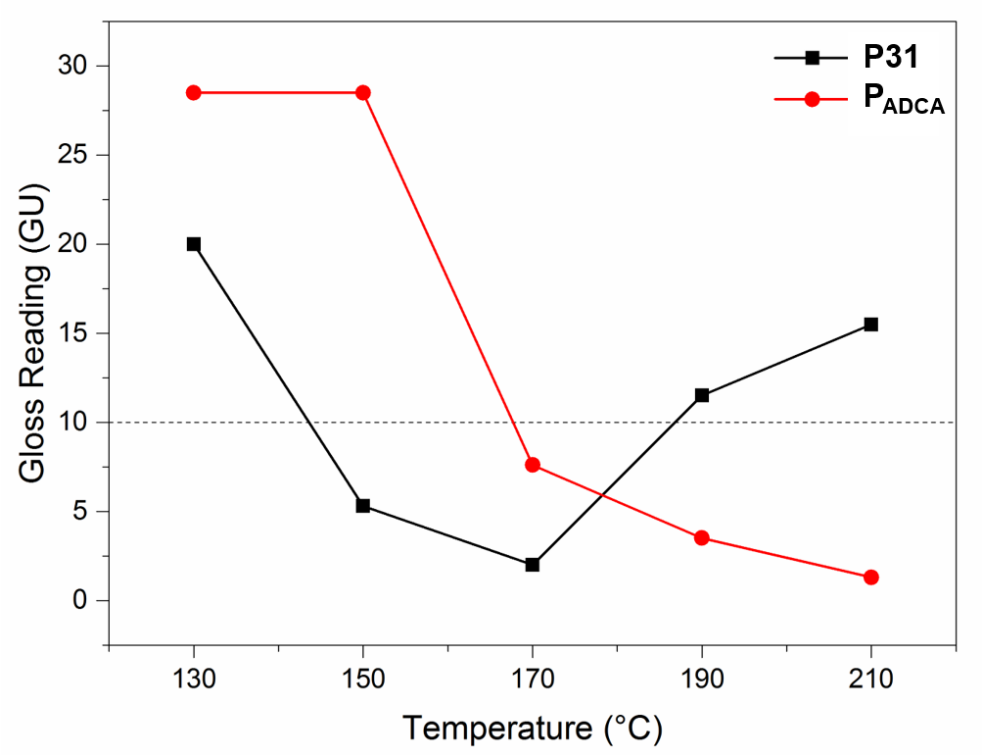

Figure 3.41 Graph depicting the gloss readings of **P31** and **P_{ADCA}** with the upper region of the matt region (10 GU) highlighted.

When the temperature is raised above 170 °C, the surface of coating sample **P31** becomes glossier. **$P31_{170}$** gave a gloss reading most closely matched with that of the control sample **P_{ADCA}** at the standard manufacturing temperature.

3.5.4.3 Microstructure Analysis of the Sulfonate Series

Cross-section micrographs provided information of the internal cellular structure. The blank control sample, **P_{blank}**, and the control expansion sample, **P_{ADCA}**, (Figure 3.42) are shown below.

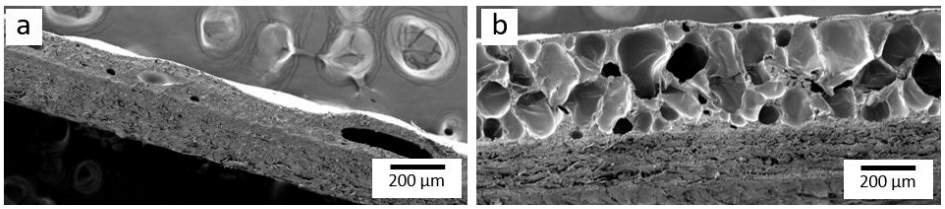

Figure 3.42 SEM cross-section micrographs of the control samples (a) **P_{blank}** and (b) **P_{ADCA}** at x75 Mag.

Additive **31** showed the formation of gas pockets within the coating layer of samples **P31** and confirmed that the compound release gas as a result of thermal decomposition and acts as a blowing agent. (Figure 3.43)

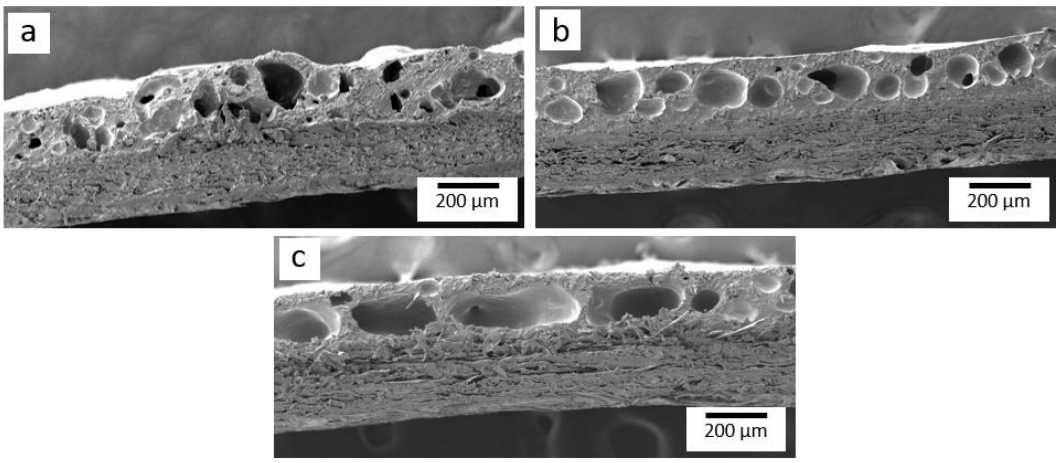

Figure 3.43 SEM cross-section micrographs of the plastisol coatings (a) **P31$_{170}$** (b) **P31$_{190}$**, and (c) **P31$_{210}$** at x75 Mag.

In the case of sample **P31**, the cross-section analysis indicated that the additive **31** forms evenly sized and distributed gas cells through the coating layer when cured at 190 °C (b, Figure 3.43). **P31$_{190}$** shows an average cell size of 90 µm, which is similar to that shown by the expanded control sample (b, Figure 3.42); however, the gas cells formed in sample **P31$_{190}$** do not provide sufficient expansion of the plastisol layer as an increase of only 30 µm is observed when compared to the blank control. The desired expansion level is approx. 400 µm, an increase of 100% compared to the 200 µm drawdown level. In the case of samples **P31$_{170}$** and **P31$_{190}$**, the cell range was typically between 20 µm and 150 µm, with some anomaly results observed above this range.

When the temperature was increase to 210 °C, the cells formed by additive **31**, became larger and elongated, with a number of cells appearing between 200-450 µm. The cells observed in **P31$_{210}$** (c, Figure 3.43) are significantly less in number than those seen in the corresponding samples heated to 190 °C (b, Figure 3.43). This result was conducive with the previously analysed thermal decomposition data, which suggested that the first phase of thermal decomposition occurred at temperatures lower than 210 °C. This is advantageous as lower temperatures are more economically favourable during the manufacturing process of commercial products.

3.5.5 Conclusions of the Sulfonate Series

The sulfonate derivative **31** was successfully synthesised in high purity and characterised. Despite the low yield associated with the synthesis, the material was effectively scaled up to approx. 25 g. If further study of compound **31** was required within the plastisol formulation, further investigation into developing an alternative synthetic pathway would be required to ensure the synthesis was both time and cost effective. The sulfonate derivatives **32-34**, were not efficiently synthesised in high yields or purities and were therefore eliminated from the study.

The TGA and DSC data confirmed that thermal degradation of compound **31**, occurred within suitable range for implementation in PVC applications. PVC plastisol's of **31** were prepared and physical properties of the final formulation were tested at different curing temperatures.

At all analysed temperatures, gas cells were formed within the plastisol layer of the coating containing compound **31**; however, expansion of the coating was observed. The even gas formation with the plastisol samples **P31$_{150\text{-}170}$**, produced a smooth, matt coating surface within the desired GU region. However, at higher temperatures samples **P31$_{190\text{-}210}$** showed a semi-gloss surface. Furthermore, pinhole defects were evident in the SEM surface images of sample **P31$_{210}$**, providing evidence that the formulation system was not stable.

P31 showed significant colouration in all analysed plastisol samples. In particular, significant colour change was observed in samples **P31$_{170}$** and **P31$_{210}$**. Thermal degradation data of the individual additive **31** and observed colour changes in the plastisol samples containing **31** were in an excellent agreement supporting a thermal decomposition between 150 °C and 200 °C curing temperatures. This result eliminates compound **31** as a potential additive within formulations for decorative applications.

The study outlined in the chapters above proved that the incorporation of compound **31** into the wallpaper formulation directly affects the physical properties of the resultant coating. However, low expansion as well as strong colouration of the plastisol layer upon thermal decomposition of the additive, resulted in an unsuitable alternative to ADCA in all cases.

3.6 Triazine Derivatives

The 1,3,5-triazine ring is a commonly used fragment in agricultural, [140] biological [141] and electronic applications, [142] to name a few. The triazine ring can be synthesised by green methods such microwave irradiation. [143] Triazine derivatives decompose readily to yield mixtures of NO, NO_2, CO_2 and H_2O gases dependant on substituents. [144]

The 1,3,5-triazine derivative cyanuric acid **4**, is a known decomposition product of ADCA. The decomposition temperatures of such compounds are typically high, however rearrangements can occur from as low as 120 °C. [145] It is therefore hypothesised that modification to contain carbonyl functions, could allow interaction with temperature lowering kicker complexes, as in ADCA.

The natural products urea **2** and glycine **36**, a readily available amino acid, [146] were chosen for reaction with the 1,3,5-triazine building block. The addition of the carbonyl containing substituents was predicted to yield carbon dioxide upon thermal decomposition of the raw material within the plastisol.

3.6.1 Synthesis and Characterisation of the Triazine Derivatives

Cyanuric chloride **35** was reacted with the natural products urea **2** and glycine **36**. (Scheme 3.3)

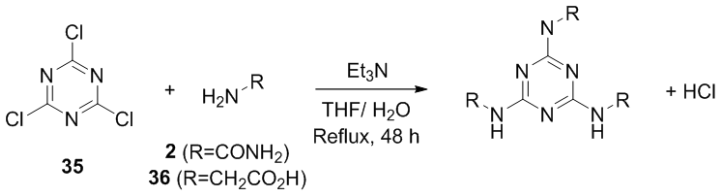

Scheme 3.3 Generic scheme for the synthesis of the triazine series

The following target compounds were synthesised **37-38** (Figure 3.44).

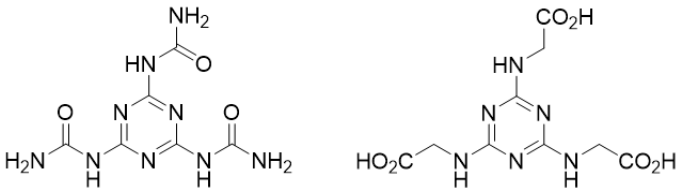

37 **(63%)** **38** **(<1%)**

Figure 3.44 Chemical structures of the target triazine compounds **76** and **70**

Attempts to produce compound **38** were unsuccessful in yields over 1%. A catalytic study was carried out, investigating the effect of varying equivalents of triethylamine, to no avail.

Compound **37** was isolated in good yield and purity was confirmed by ^{1}H NMR spectroscopy. Due to the limited number of proton environments present in compound **37**, multiple analytical techniques were required for characterisation of the material. The IR data was in excellent agreement confirming the formation of the C-N bond (Table 3.16). HRMS was used to identify the formation of the tri-substituted derivative of the triazine.

Table 3.16 IR data for compounds **37** and **38**.

Compound	C-N[a]	N-H[b] (bend)	N-H[c] (stretch)	C=O[d]
37	1056	1633	3458, 3542	1733
38	1233	1515	3273	1627

a Typical region 1000-1300 cm^{-1}
b Typical region 1490-1650 cm^{-1}
c Typical region 3300-3500 cm^{-1}
d Typical region 1600-1750 cm^{-1}

The complications in the synthesis, and subsequent scale up, of compound **38**, resulted in the material not meeting the outlined requirements set out in the project to ensure efficient commercialization was possible. This led to its exclusion from the analysed series. As previously mentioned, success of the series in the manufacturing process, would lead to further investigation of the materials.

3.6.2 Thermal Behaviour, Stability and Decomposition Pathway of Compounds 37 and 38

Thermal gravimetric analysis (TGA) and differential scanning calorimetry (DSC) were used to evaluate the thermal properties of compound **37** as these techniques can be used to predict the behaviour of the additives within the coating formulation at various cure temperatures.

Typical thermal analysis temperatures, such as $T_{-10\%}$, T_{max} and T_{DSC} are summarized below in Table 3.17.

Table 3.17 TGA and DSC data for compounds **37** and **38**

Compound	TGA		DSC
	$T_{-10\%}$[a]	T_{max}[b]	T_{DSC}[c]
37	293	211, 354	433
38	47	274, 376	276

a Temperature at 10% mass loss in the TGA
b Maximum thermal degradation temperature from the 1st derivative of the TGA
c Phase transition temperature in the DSC

The thermal decomposition data showed that modification of the cyanuric chloride significantly increased the decomposition temperature of the derivative. As shown in the table above, when modified with urea, the corresponding derivative **37** showed an initial onset set of pyrolysis at 211 °C; however, this step only accounts for a total of 10% mass loss with the main phase appearing at 354 °C (Figure 3.45).

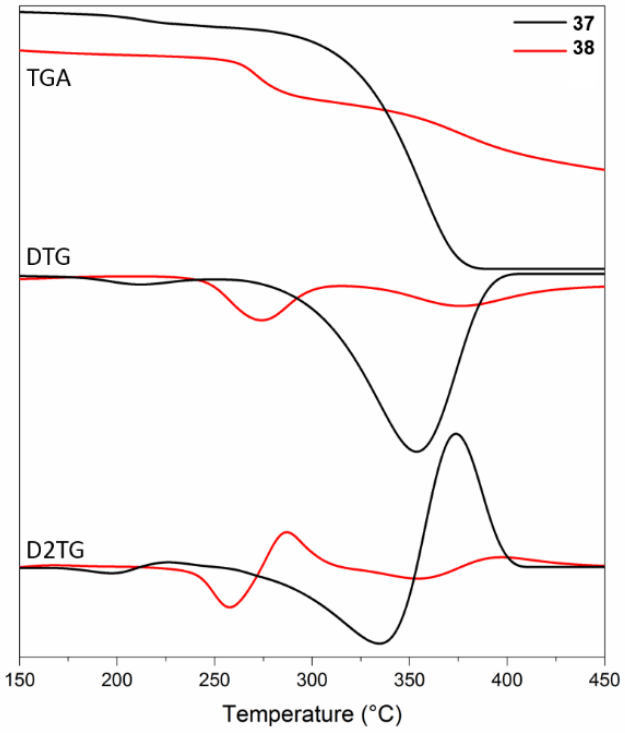

Figure 3.45 TGA, first derivative TGA (DTG), and second derivative TGA (D2TG) of compounds **37** and **38**.

Compound **38** also showed an increase in decomposition temperature compared to the starting triazine. T_{max} onset of pyrolysis was observed at 274 °C. In the case of compound **38**, only an approx. 60% mass loss was observed by 450 °C (Figure 3.45). These temperatures do not correspond with the suitable melt viscosity range of the PVC plastisol. This information coupled with the synthetic difficulties associated with compound **38** supported the decision to exclude the material from the study.

The DSC data for compound **37** showed a potential sublimation transition from approx. 350 °C, with a maximum of 433 °C. (Figure 3.46) Concurrent with the TGA data showing a transition in the region of 350 °C.

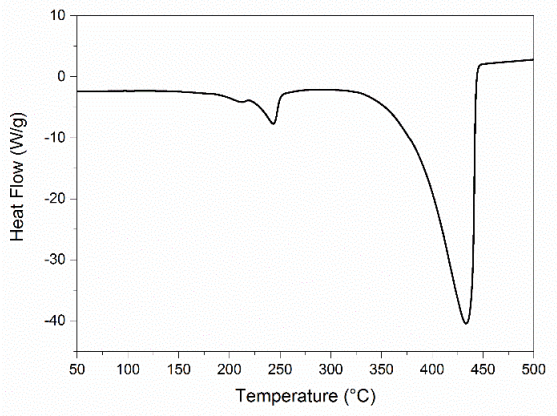

Figure 3.46 DSC data for compound **37**

Despite the high temperatures of thermal decomposition, the chemical structure of compound **37** allows for the potential coordination with metal ions. In the case of ADCA, the decomposition temperature of 225 °C, is lowered to ca. 160-175 °C, through coordination with potassium and zinc containing ‘kicker’ additives within the formulation. The urea fragment in compound **37**, could allow for similar coordination, subsequently lowering any observed decomposition temperature by TGA analysis. For this reason, the compound was scaled up for implementation within the plastisol formulation to identify if compound **37** had any effect on the physical properties of the coatings < 210 °C.

3.6.3 PVC Coating Formulations, Temperature Dependency and Colour Correlation of the Triazine Series

Despite high levels of nitrogen within the compound, compound **37** was isolated as an off white solid. This is beneficial in colour sensitive, decorative applications. As carried out in the case of all solid products, the compound was finely ground using a pestle and mortar before implementation into the plastisol formulation in attempt to aid distribution. The use of fine grade powders is an essential step of the manufacturing process as large particle sizes can disrupt the application of a 200 µm coating layer by hindering drawdown of the k-bar.

To study the triazine derivative **37** within polymer matrix, the novel plastisol containing compound **37** was formulated to a standard specification, manufactured and analysed to determine the effect on coating efficiency, surface wetting and coating coverage. The formulation had been cured at 130 °C, 150 °C, 170 °C, 190 °C and 210 °C to correspond with the melt viscosity range of the PVC plastisol. This allowed colour-temperature dependency studies to be carried out. L*a*b* and ΔE data for the thermally cured plastisol **P37**. The L*a*b* values are given for the formulated plastisol cured at 130 °C which was set as the control to monitor temperature dependent colour change (ΔE) of the formulation. (Table 3.18)

Table 3.18 L*a*b* data and ΔE for samples **P37** and $\mathbf{P_{ADCA}}$.

	130 °C			ΔE			
Entry	**L***	**a***	**b***	**150 °C**	**170 °C**	**190 °C**	**210 °C**
P37	92.98	-0.04	-0.08	0.08	0.39	0.33	1.30
$\mathbf{P_{ADCA}}$	92.55	-0.96	11.55	0.51	0.53	1.18	6.81

Minimal colour change was observed across the analysed temperature range of **P37**. The control sample $\mathbf{P37_{130}}$ also showed very little colouration, with both a* and b* detection very close to white (0.00). A slight increase in ΔE was observed in the sample $\mathbf{P37_{210}}$ conducive with the T_{max} observed at 211 °C in the first derivative TGA graph. This value was within the region for correction with optical brighteners and/or bleaching agents.

Conversely the control sample **P_{ADCA}** shows high levels of colouration in the 130 °C control sample where no decomposition had taken place. This colouration is due to the high b* detection caused by the strong yellow colour of the ADCA raw material. As the temperature increased, as does ΔE (Figure 3.47). However, in the case of ADCA the high ΔE value represents a colour change towards the white region of the colour space.

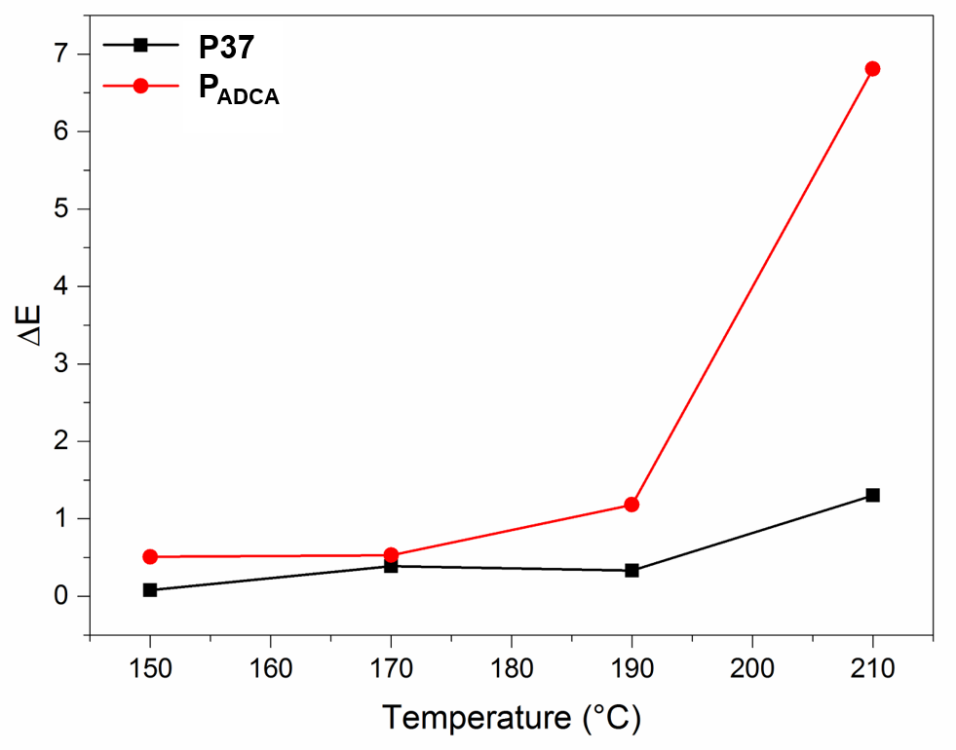

Figure 3.47 Graph Depicting ΔE for samples **P37** and **P_{ADCA}**.

The colour index data for **P37**, could represent limited thermal decomposition within the temperature range 130 – 210 °C as indicted in the thermal gravimetric analysis results. Conversely, if 'kicker' compounds within the formulation were actively lowering the decomposition point of compound **37**, the L*a*b* data could be an indication that non-coloured by-products were formed. Further investigation into the microscopic structure of the coating samples could identify if any gas was produced throughout the temperature range in the case of **P37**. The colour values observed in the case of **P37** suggest that it could be used in colour sensitive applications, if all other physical property standards are met.

3.6.4 Surface Texture and Microstructure of the Triazine Series

3.6.4.1 Surface Texture Analysis of the Triazine Series

The surface textures of the formulations containing additive **37**, were analysed by scanning electron microscopy (SEM). This allowed any surface defects or properties to be identified. As previously mentioned to desired physical properties of the plastisol coatings were evenly expanded, smooth and matt surfaces. The blank formulation $\mathbf{P_{blank}}$, and the control expanded formulation $\mathbf{P_{ADCA}}$ are shown below (Figure 3.48).

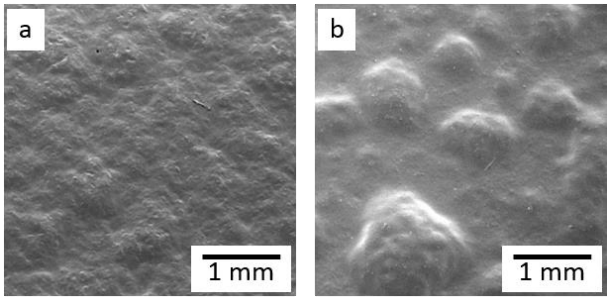

Figure 3.48 SEM surface micrographs of the control samples (a) $\mathbf{P_{ADCA}}$ and (b) $\mathbf{P_{blank}}$ at x18 Mag.

As the interaction of the 'kicker' complexes on the additive **37** were unknown, samples $\mathbf{P37_{130}}$ – $\mathbf{P37_{210}}$ were analysed by SEM in attempt to identify any pattern of decomposition. The surface SEM micrographs (Figure 3.49) showed different surface properties to those exhibited in the sample, $\mathbf{P_{blank}}$.

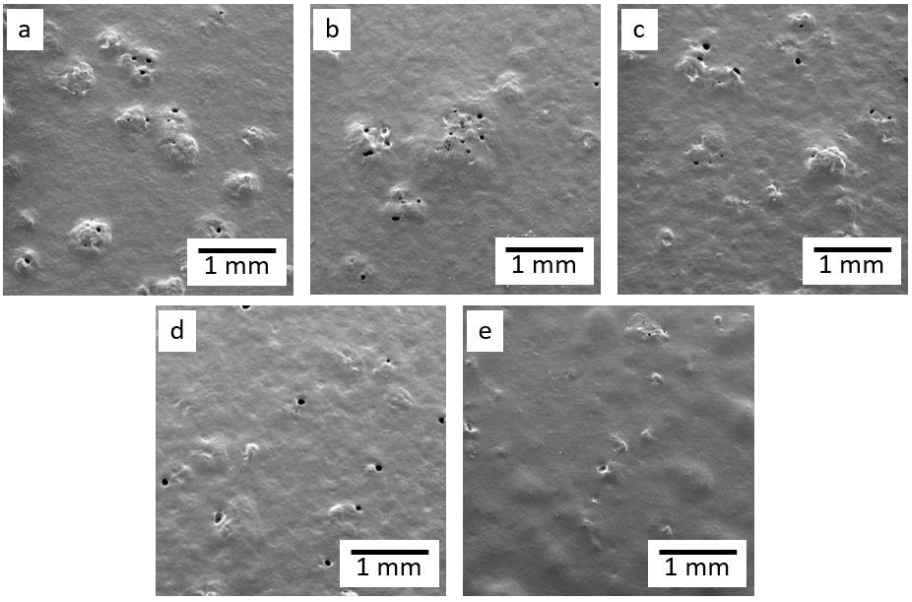

Figure 3.49 SEM surface micrographs of samples (a) $\mathbf{P37_{130}}$, (b) $\mathbf{P37_{150}}$, (c) $\mathbf{P37_{170}}$, (d) $\mathbf{P37_{190}}$ and (e) $\mathbf{P37_{210}}$ at x18 Mag.

Conversely to the bubble-like defects shown in **P_{blank}**, (Figure 3.48) **P37** exhibited a number of raised defects coupled with pinhole defects. This suggests that additive **37** has some influence on the formulation. It is unclear if thermal decomposition and the subsequent formation of gas, or disruption of the distribution of the formulation across the surface is responsible for these surface properties.

In general, as the temperature increased, fewer defects were detected on the surfaces of the coatings **P37** (Figure 3.50).

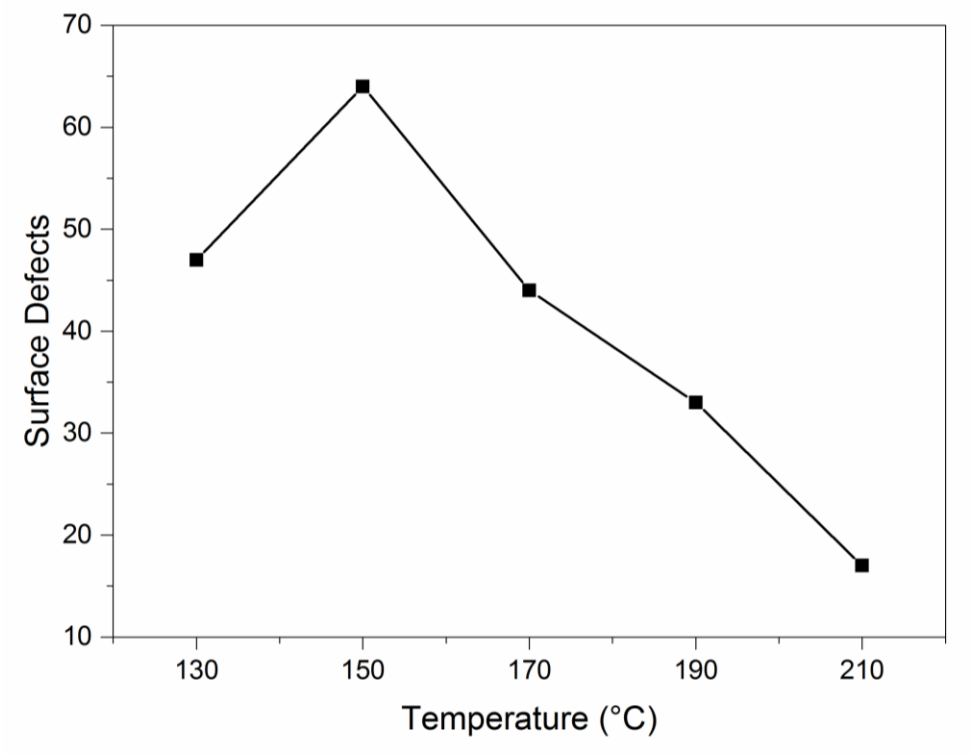

Figure 3.50 Graph depicting observed surface defects in sample **P37**.

This suggests that as the temperature was increased, fewer interactions occurred within the formulation. This further suggests that the 'kicker' complexes did not have a significant influence on the decomposition of additive **37** as observed in the case of ADCA.

3.6.4.2 Surface Gloss Analysis of the Triazine Series

As in the previously analysed series, a smooth and matt finish was desired for the target product. This physical property is more appealing to the decorative coatings mass market[xvii]. A matt surface is characterised as having GU <10. The

[xvii] Graham & Brown market research

gloss of the surface of each coating was analysed using a glossmeter and the data is tabulated below (Table 3.19).

Table 3.19 Gloss readings for plastisol samples **P76** and **P_{ADCA}**.

Sample	85° Beam Angle Reading (GU)				
	130 °C	150 °C	170 °C	190 °C	210 °C
P37	19.2	10.0	12.0	10.9	15.5
P_{ADCA}	28.5	28.5	7.6	3.5	1.3

Similar to the observed colour index data, the gloss readings for **P37** show minimal change across the analysed temperature range. All values sit within the semi-gloss (10+ GU) region, (Figure 3.51) which is undesirable within the wallpaper industry. As shown in the graph, little correlation between temperature change and gloss reading was observed. In contrast the control expanded sample **P_{ADCA}** showed significant change, conclusive with the decomposition of ADCA and the increased interaction within the plastisol matrix contributing to a matt and textured surface.

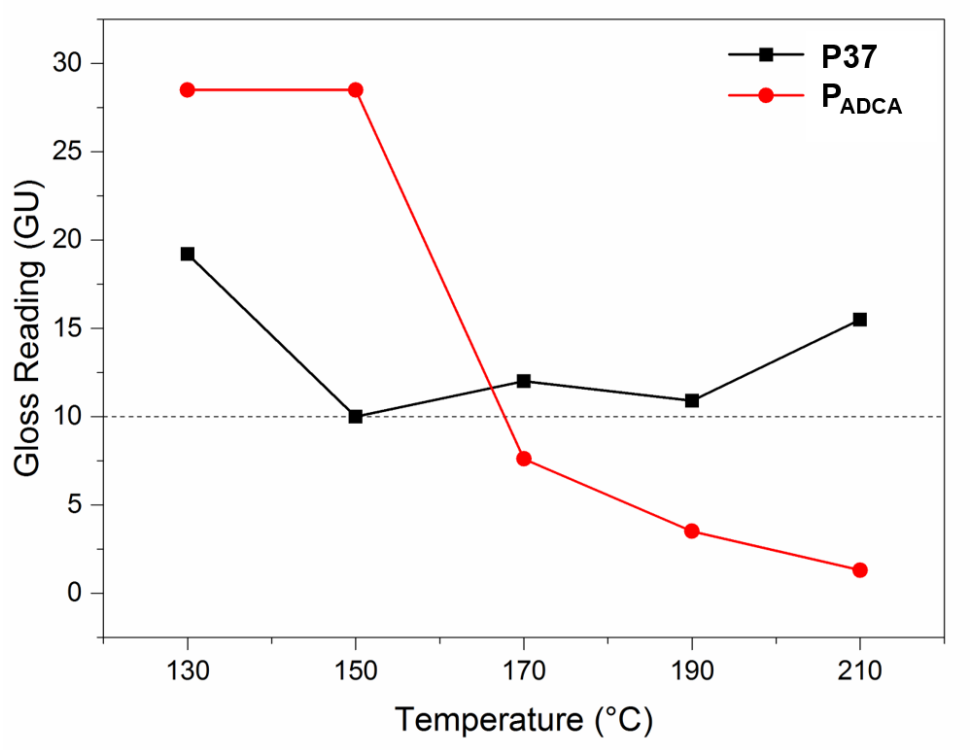

Figure 3.51 Graph depicting gloss readings for samples **P37** and **P_{ADCA}**.

This data provides further evidence that decomposition of additive **37**, does not occur within the suitable range of the desired use and that the kicker complexes do not significantly affect the properties exhibited by additive **37**.

3.6.4.3 Microstructure Analysis of the Triazine Series

Cross-section micrographs provided information of the internal cellular structure and any gas formed within the matrix. The blank control sample, $\mathbf{P_{blank}}$, (a, Figure 3.52) contained irregularly sized and unevenly distributed gas cells. The control expansion sample, $\mathbf{P_{ADCA}}$, (b, Figure 3.52) shows an even distribution of regularly sized gas cells with an overall expansion of approx. 400 µm.

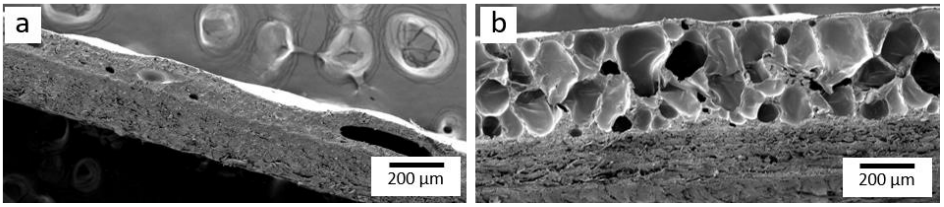

Figure 3.52 SEM cross-section micrographs of the control samples (a) $\mathbf{P_{blank}}$ and (b) $\mathbf{P_{ADCA}}$ at x75 Mag.

The plastisol samples containing additive **37**, $\mathbf{P37_{130}}$ **–** $\mathbf{P37_{210}}$ all showed gas formation within the plastisol matrix (Figure 3.53), suggesting that the material does act as a blowing agent in some capacity.

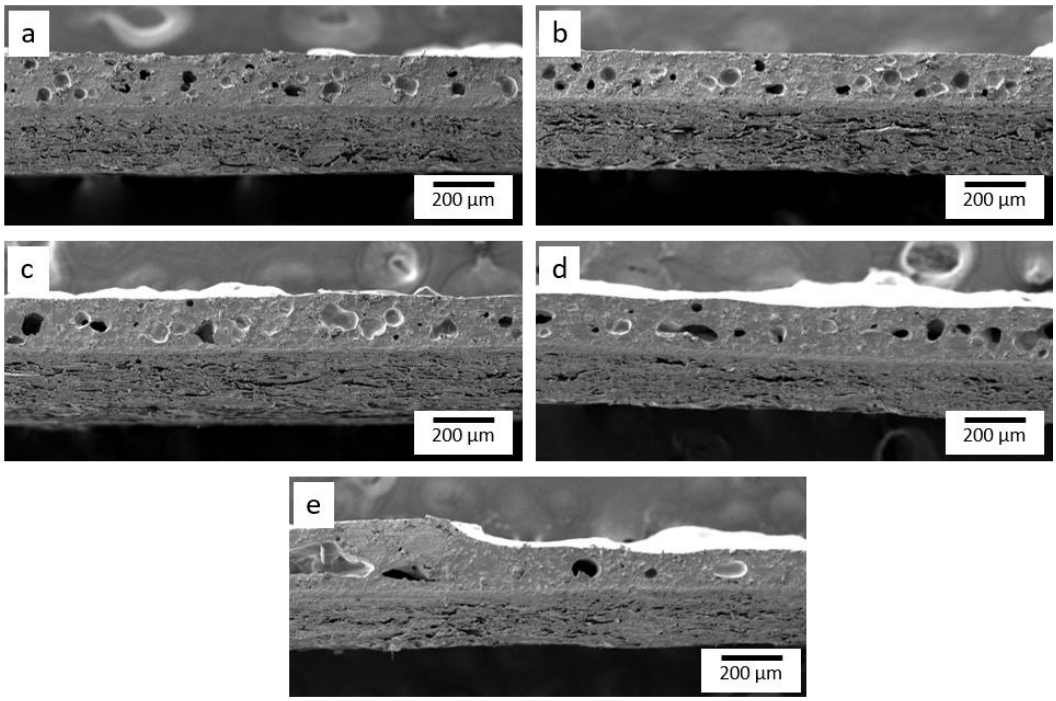

Figure 3.53 SEM cross-section micrographs of samples (a) $\mathbf{P37_{130}}$, (b) $\mathbf{P37_{150}}$, (c) $\mathbf{P37_{170}}$, (d) $\mathbf{P37_{190}}$ and (e) $\mathbf{P37_{210}}$ at x75 Mag.

In the case of samples **P37$_{130}$**, and **P37$_{150}$**, (a, b, Figure 3.52) the gas cells formed were evenly distributed and of a regular cell size. This suggests that at lower temperatures the additive **37** aids distribution within the plastisol matrix. The even gas cell formation did not contribute to any significant expansion of the coating layer.

As the temperature increased, more irregularity was observed within the coating layer of the samples. This could contribute to the fewer number of surface defects observed in the corresponding surface micrographs of samples **P37$_{170}$** and **P37$_{190}$**, (c, d, Figure 3.53) as fewer regions of concentrated gas pockets were present.

In the case of **P37$_{210}$**, very minimal gas cells were observed; however, a highly irregular surface was shown in the cross-section micrograph. This uneven surface, is characteristic of high surface tension [32] and can be attributed to the increased hydrogen bonding caused by more disorder within the system at higher temperatures. The ‘waves’ across the surface of the cross-section attribute to the smoother bubbles shown in the surface micrographs (Figure 3.54).

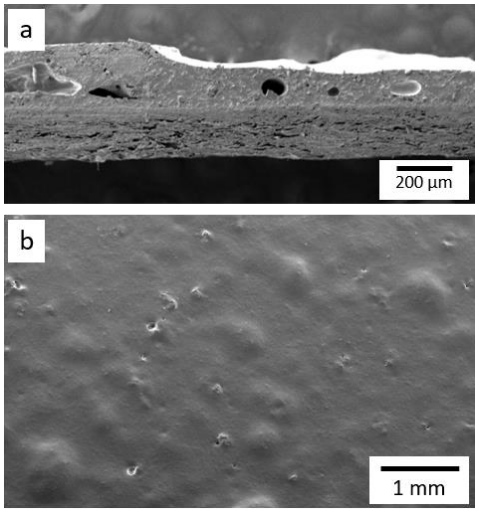

Figure 3.54 SEM (a) cross-section at x75 Mag and (b) surface at x18 Mag, micrographs of sample **P37$_{210}$**.

3.6.5 Conclusions of the Triazine Series

The triazine compound **37** was successfully synthesised and characterised. Synthesis of the compound was effectively scaled up to approx. 5 g in good yields of up to 63%. The triazine derivatives **38**, was not obtained in acceptable yields, therefore scale up of the material was not possible in accordance with the synthetic parameters of the project.

The TGA and DSC data showed that thermal degradation of both compounds **37** and **38** occurred outside the suitable melt viscosity range of the PVC plastisol. This lead to the exclusion of compound **38** from the study. It was predicted that the decomposition temperature of compound **37** could be reduced, as in ADCA, using ‘kicker’ complexes. Therefore, PVC plastisol’s containing compound **37** were prepared and physical properties of the final formulation were tested at different curing temperatures.

Gas cells were formed within the plastisol layer of the coating suggesting some interaction with the ‘kicker’ complexes. However, this gas formation was not significant enough to increase the observed expansion of the coating. Furthermore, as the temperature increased the gas yield decreased, directly affecting the observed defects on the sample surfaces. The SEM data provided evidence that the system was unstable.

The implementation of compound **37** within the formulation had little effect on gloss reading of colouration of the coating samples. However, the semi-gloss finish was not desired in this application. In terms of colour, a* and b* values close to 0.00 at all temperatures, suggest that additive **37** was well suited to colour sensitive and decorative applications. Further study would be required to identify if the physical properties were result of the thermal decomposition of **37** within the formulation as the TGA only provides information on the decomposition of the raw material.

Compound **37** directly affects the physical properties of the wallpaper coating. However, the high decomposition temperature of additive **37** resulted in insufficient gas production and expansion of the plastisol layer across the analysed temperature range. Additive **37** was an unsuitable alternative to ADCA in the desired application.

3.7 Citric Acid Derivatives

Citric acid **18** is an inexpensive and renewable additive readily available from both synthetic and natural resources, such as fruits [147] and bacteria. [148] Citrates are, in general terms, cost effective, non-toxic and meet the listed specifications of a potential new blowing agent. The decomposition pathway of citric acid is well known and documented in the literature dating back as far as 1930. [149, 150] This information can be used to help predict the decomposition behaviour of novel derivatives. Furthermore, carbon dioxide gas is a by-product of the decomposition of polycarboxylic acids, such as citric acid [151], this gas production could lead to the formation of a cellular structure within the plastisol matrix as desired. (Figure 3.55)

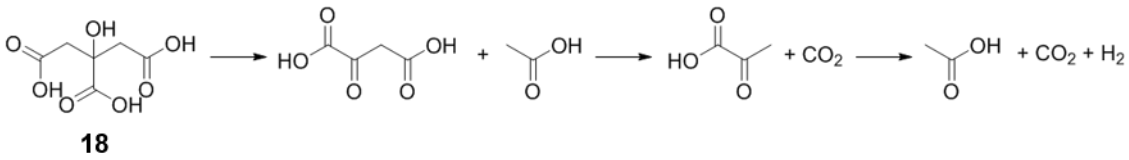

Figure 3.55 Thermal decomposition mechanism of citric acid **18**, adapted from Cody *et al.* [151]

The citrate derivatives also provide water-solubility, which allows for greater diversity in formulation modifications. Furthermore, the green properties of the citrate derivatives are also essential, both in production and recycling to maintain the sustainability of the manufacturing process. [152]

Based on its availability and non-toxic nature, citric acid and its derivatives have been widely studied and used in the fields of resins, [153] coatings and plasticisers, [20, 21] and cosmetics to name a few. As outlined in chapter 3.2.4, citric acid is not suitable as an alternative to azodicarbonamide in wallpaper applications due to its strong discoloration of the coating. That said the sample coatings containing citric acid showed evidence of gas formation in the SEM cross-section analysis (Figure 3.9, Chapter 3.2.4). It was therefore hypothesised that modification of the citric acid backbone to include a hydrazo group could lead to more gas formation by allowing for the production of both nitrogen and carboxylic acid gases. [91]

3.7.1 Synthesis and Characterisation of Citric Derivatives

Citric acid can be regarded as a versatile platform for structural modification, as its scaffold allows a variety of chemical transformations with various species. Citric acid and its ethyl ester **39** are common reagents and were selected for use in the reaction with the hydrazine derivatives (hydrazine monohydrate **40** and phenyl hydrazine **27**). Hydrazine monohydrate **40** reacted with both citric acid **18** and triethyl citrate **39** to yield compounds **41** and **43**, respectively. (Scheme 3.4)

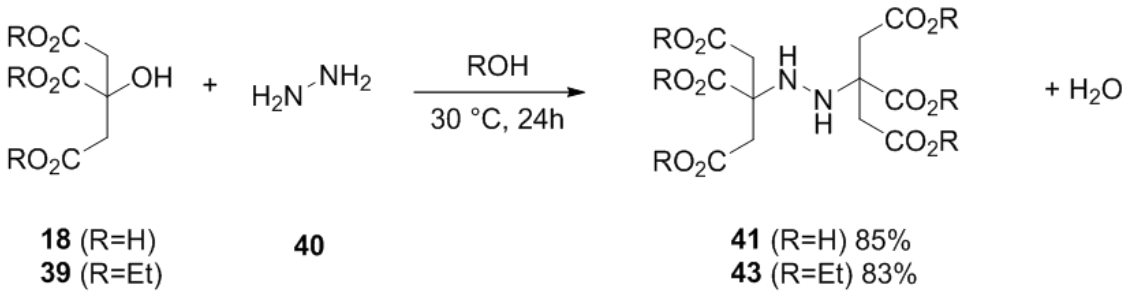

Scheme 3.4 Generic scheme of the reaction of citric acid **18** and triethyl citrate **39** with hydrazine monohydrate **40**.

Phenylhydrazine **27**, reacted similarly with the citrate derivatives yielding corresponding products **42** and **44**. (Scheme 3.5)

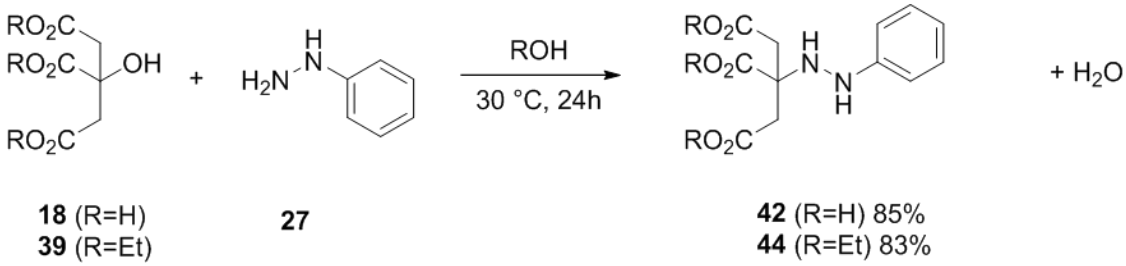

Scheme 3.5 Generic scheme of the reaction of citric acid **18** and triethyl citrate **39** with phenylhydrazine **27**.

The excellent chemical purity and yields make this synthetic pathway highly practical allowing cost-efficient scale-up (50 g) of the compounds **41-44**.

The characterisation of the citrate derivatives was carried out using a combination of analytical techniques. The ^{1}H NMR data of the materials **41-44** highlight a shift in the peak corresponding to the aliphatic protons (circled, Figure 3.56). A typical shift of 0.15-0.30 ppm (Figure 3.56) from the corresponding hydroxyl-precursors is observed in hydrazo derivatives **41-42** indicating the

successful conversion to the hydrazo group. Due to the highly polar nature of the compounds they proved to be insoluble in chloroform and the NMR experiments were subsequently carried out in D_2O or DMSO. A proton exchange between the OH and NH groups and the solvent molecules, resulted in the absence of the corresponding peaks in the ^1H NMR spectra and reinforced the need for multiple characterisation techniques to confirm the successful synthesis of the desired product.

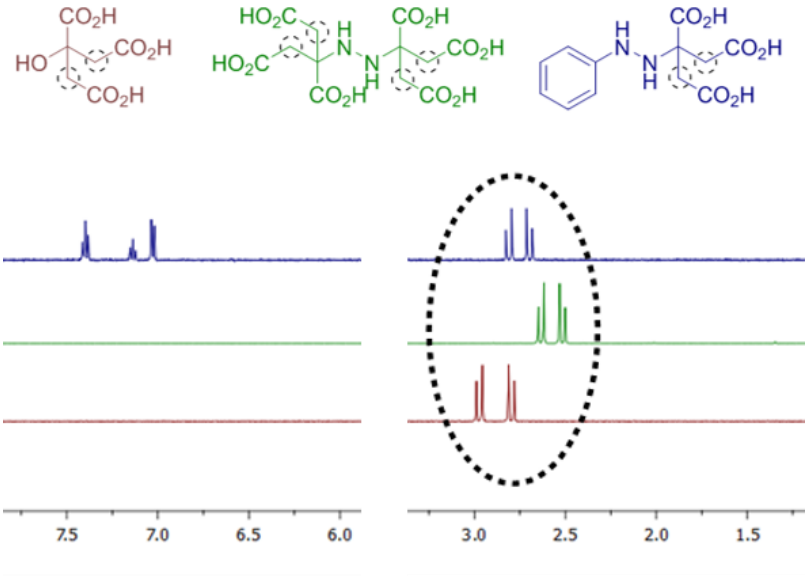

Figure 3.56^1H NMR spectrum in DMSO of citric acid (red), compound **41** (green) and compound **42** (blue) overlaid to show shift of the AB system shown between 2.4-3.0 ppm corresponding to the aliphatic CH_2 groups, circled in the structural diagrams.

The ^{13}C NMR spectrum can typically be utilised to identify the up field shift of the HN-C carbon; as opposed to the HO-C carbon in the starting material due to the difference in electronegativity of the adjacent nitrogen and oxygen atoms. [135]However; in this case the adjacent hydrazo function (HN-NH) exhibits significantly more electronegativity than the corresponding amine group, furthermore the hydrazo group is highly electron withdrawing resulting in a minimal up field shift (approx. 5 ppm) in the ^{13}C spectrum. [135]

Furthermore, the citrate compounds are volatile and sensitive to ionisation and therefore fragmented into corresponding decomposition products during the electrospray ionisation step of the mass spectroscopy. The mass spectrum for

compound **41** shows the presence of both the monomer (**41a**) and dimer (**41**) structures with peaks seen at 254.9840 and 402.8871 respectively.

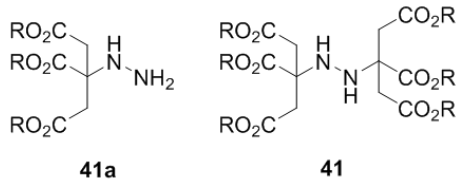

Figure 3.57 Chemical structures of the monomer **41a** and dimer **41** observed in the mass spectrum

The ^{1}H NMR spectrum clearly indicated that only one product was present and it was concluded that the mixture observed in the mass spectrum was due to the fragmentation upon ionisation of the sample. Similar results were observed in the mass spectrum of compounds **42**-**44**. The experimental errors of the mass analysis were larger than generally accepted due to the impurity of residual solvent, however, this purity was accepted by the industrial sponsor and further purification was disregarded as per the synthetic strategy. (Chapter 3.3)

The IR data supports the characterisation of the materials. Significant peaks in the IR spectrum for the characterisation of hydrazo molecules account for a contemporaneous presence of the C-N, N-H and N-N stretching vibrations. The essential IR peaks for characterisation are listed in Table 3.20. All compounds **41-44** exhibited a strong peak in the region of 1000-1300 cm^{-1} (C-N). The absence of the sharp peak between 3590 cm^{-1} and 3650 cm^{-1} [136] confirmed that no starting material remained.

Table 3.20 IR data for compounds **41-44**

Compound	C-N[a]	N-H[b] (bend)	N-H[c] (stretch)	C=O[d]
41	1184	1653	3436	1704
42	1082	1551	3252	1702
43	1022	1619	3497	1730
44	1096	1598	3490	1731

a Typical region 1000-1300 cm^{-1}
b Typical region 1490-1650 cm^{-1}
c Typical region 3300-3500 cm^{-1}
d Typical region 1600-1750 cm^{-1}

3.7.1.1 Oxidation of the Citrate Derivatives

The N=N azo bond in azodicarbonamide contributes to the decomposition of the molecule and the production of the nitrogen gas. [154] Therefore, oxidation of the hydrazo compounds was attempted where hydrogen peroxide acts as an oxidising agent in the presence of $TiCl_3$ and HBr. [155] (Figure 3.58)

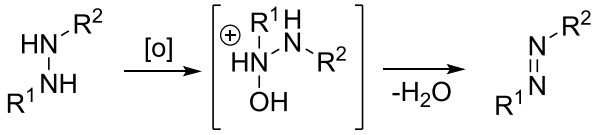

Figure 3.58 Oxidation of hydrazo compounds to the corresponding azo derivative.

The published work reported success of the reaction in yields of 85-95% for a number of R groups. [155] Despite these findings, the oxidation reaction in the citrate series resulted in the cleavage of the N-N bond in compounds **41** and **43**, suggesting that this synthetic strategy was not viable.

3.7.2 Thermal Behaviour, Stability and Decomposition Pathway of Compounds 41-44

Thermal gravimetric analysis (TGA) and differential scanning calorimetry (DSC) were used to evaluate the thermal properties of compounds **41-44** and predict their behaviour. Typical temperatures are shown in Table 3.21.

Table 3.21 TGA and DSC data for compounds **41-44**

Compound	TGA		DSC
	$T_{-10\%}$[a]	T_{max}[b]	T_{DSC}[c]
41	116	198	199
42	79	139, 201	207
43	141	188	209
44	126	189	205

a Temperature at 10% mass loss in the TGA
b Maximum thermal degradation temperature from the 1st derivative of the TGA
c Phase transition temperature in the DSC

Differences in the thermal stability are observed between the acids **41**, **42** and esters **43**, **44** (Figure 3.59).

For the ester compounds **43** and **44**, the thermal degradation based on TGA is a one-step process, characterised by T_{max}, and occurs at a similar range of 188 °C and 189 °C, respectively. These values of the maximum degradation temperatures are in a correlation with the values obtained from DSC analysis for the corresponding compounds **43** (209 °C) and **44** (205 °C).

In both cases, T_{max} and T_{DSC} are observed within the suitable melt viscosity range of PVC plastisol. Acid compounds **41** and **42** showed an earlier onset of thermal degradation, compared to the esters **43** and **44**, and occur over two steps. The two-steps observed in compounds **41-42** could be due to the decarboxylation of the acids which does not occur in the ester derivatives **43-44**.

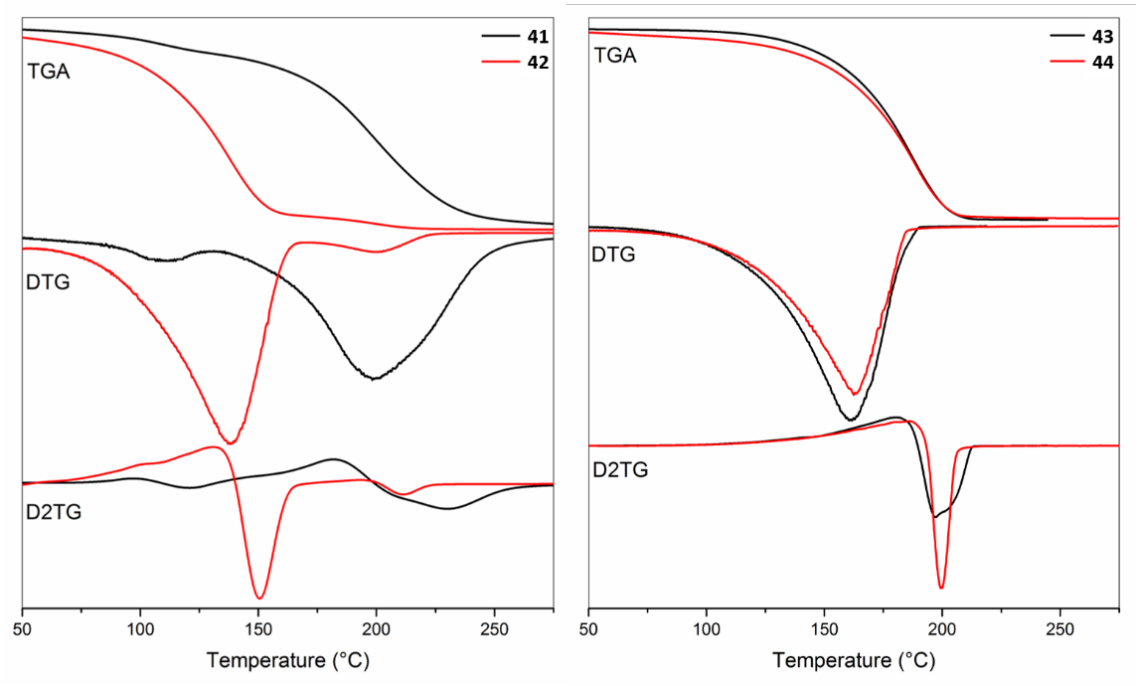

Figure 3.59 TGA, first derivative TGA (DTG), and second derivative TGA (D2TG) of compounds **41-44**

Compound **41** exhibits 10% mass loss at the lower temperature of 116 °C, due to water volatilisation, also observed as a small shoulder in the first derivative graph. However, T_{max} onset of the pyrolysis happens at the much higher temperature of 198 °C and coherent with T_{DSC} 199 °C (as observed in **43-44**).

In the case of the acid compound **42**, its thermal degradation process can be divided into two distinct stages characterised by two values of T_{max}. The first step occurs in the range of 100-160 °C, which is much lower than that of the other citrate derivatives, and accounts already for almost 70% mass loss. DSC

data supports this finding showing a broad band approx. 100 °C wide within the same range, which may be attributed to the subsequent decarboxylation steps.

3.7.3 PVC Coating Formulations, Temperature Dependency and Colour Correlation of the Compounds 41-44

To study derivatives **41-44** within polymer matrix, the novel plastisols containing compounds **41-44** have been formulated to a standard specification, manufactured and analysed to determine the effect on coating efficiency, surface wetting and coating coverage. The formulations have been cured at a range of temperatures between 130 °C and 210 °C to correspond with the melt viscosity range of the PVC plastisol. This allowed colour-temperature dependency studies to be carried out for each of the materials. Table 3 shows L*a*b* and ΔE data for the thermally cured plastisol's **P41-P44** (Table 3.22)

Table 3.22 L*a*b* data and ΔE data for samples **P41-P44** and **P_{ADCA}**.

	130 °C			**ΔE**			
Entry	**L***	**a***	**b***	**150 °C**	**170 °C**	**190 °C**	**210 °C**
P41	93.95	-0.27	0.43	1.61	4.55	10.01	22.19
P42	93.75	-0.68	4.07	1.44	6.76	22.87	27.70
P43	94.43	-0.08	-0.39	0.40	0.33	0.31	0.74
P44	89.39	1.45	18.62	0.46	0.40	2.38	3.77
P_{ADCA}	92.55	-0.96	11.55	0.51	0.53	1.18	6.81

Sample **P41** formulated with **41** shows a significant increase in ΔE between 170 °C, 190 °C and 210 °C curing temperatures (Figure 3.60), which coincides with the TGA and DSC data of the individual compound **41**.

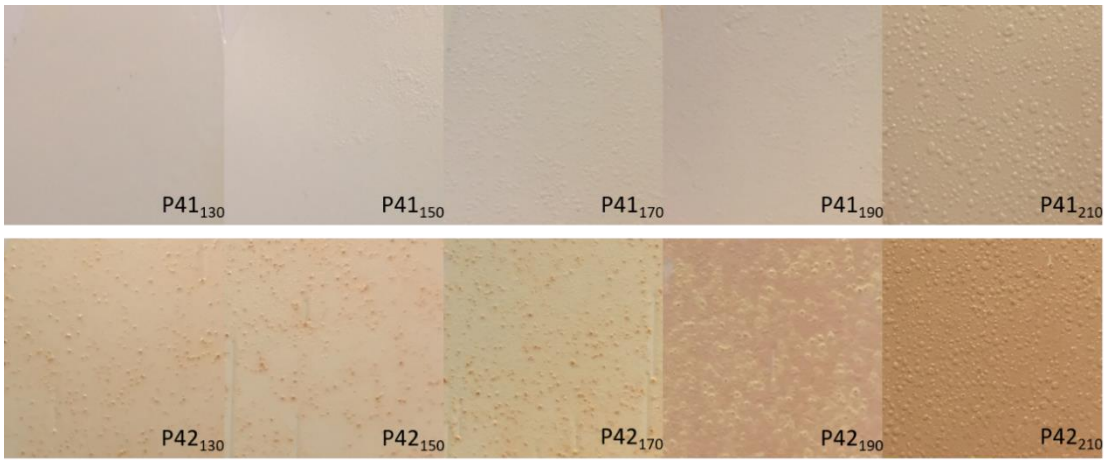

Figure 3.60 Photographic images of the samples **P41** and **P42** at 130-210 °C.

The yellow saturation (b*) in **P41** increases from 130 °C, evident in the TGA shoulder of **41** from 110 °C upwards. The colour indexing coupled with the TGA data confirms that the full decomposition of compound **41** occurs within the range of 170-200 °C.

The sample **P42$_{130}$** shows a stronger initial colouration (Table 3.22), this is due to the lower decomposition temperature observed in the TGA of the compound **42** accounting for a 70% weight loss between 100-160 °C. Similarly, sample **P42** shows a strong colour change from 170 °C to 210 °C demonstrated by a significant increase in ΔE. This corresponds to the second thermal decomposition step, which occurs within this T range. With ΔE_{210} values of 22.54 and 30.85, for **P41** and **P42** respectively, the colour changes observed are beyond the limit for corrections, such as bleaching, to be effective (Figure 3.60).

The results observed for **P41** and **P42** are similar to that observed in the citric acid control sample, providing evidence that modification of the hydroxyl alcohol group on citric acid has little influence on the thermal decomposition effects of the materials within the wallpaper coating. As in citric acid (chapter 3.2.4) the colouration of the coating is outside the range for correction with bleaching and whitening agents and therefore the material would be unsuitable in colour sensitive applications. This data concludes that at the temperatures above 175 °C, strong colouration renders these additives unsuitable.

In contrast, the ester derivatives **43** and **44** do not show a significant colour change during the heating process (Figure 3.61).

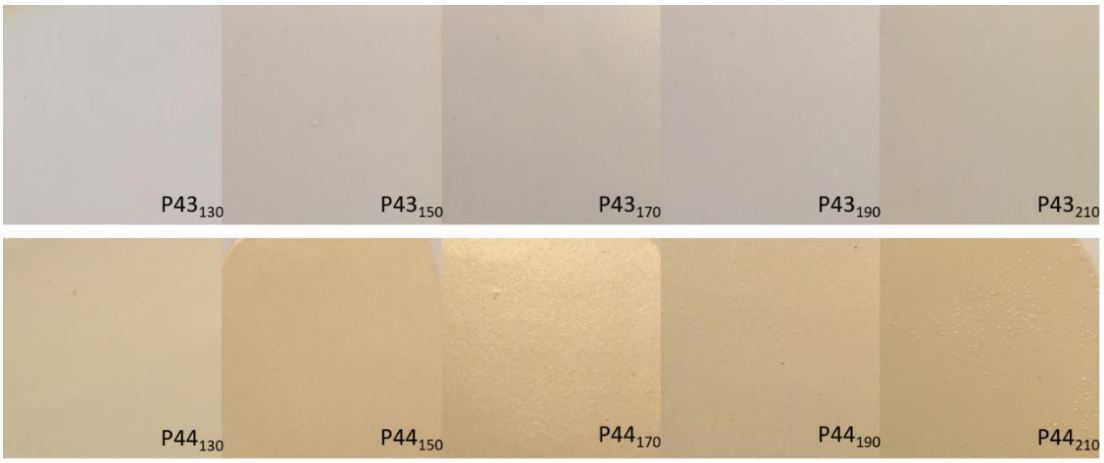

Figure 3.61 Photographic images of the samples **P43** and **P44** at 130-210 °C.

The ΔE values for formulated plastisol **P43** (0.31-0.74) show that the colour change is negligible across the analysed temperature range (ΔE<1). Similarly, formulation **P44** shows an insignificant colour change up to 170 °C; however, a noticeable change in ΔE is observed at a higher temperature. Sample **P44**, ΔE_{210} shows a slight increase in colour intensity, conducive with T_{DSC} 205 °C. Unlike the compounds **41** and **42**, the ester derivatives **43** and **44** would be suitable for colour sensitive applications based on their colour indexing data. The colour changes across the temperature range can be seen clearly in the graph below. (Figure 3.62)

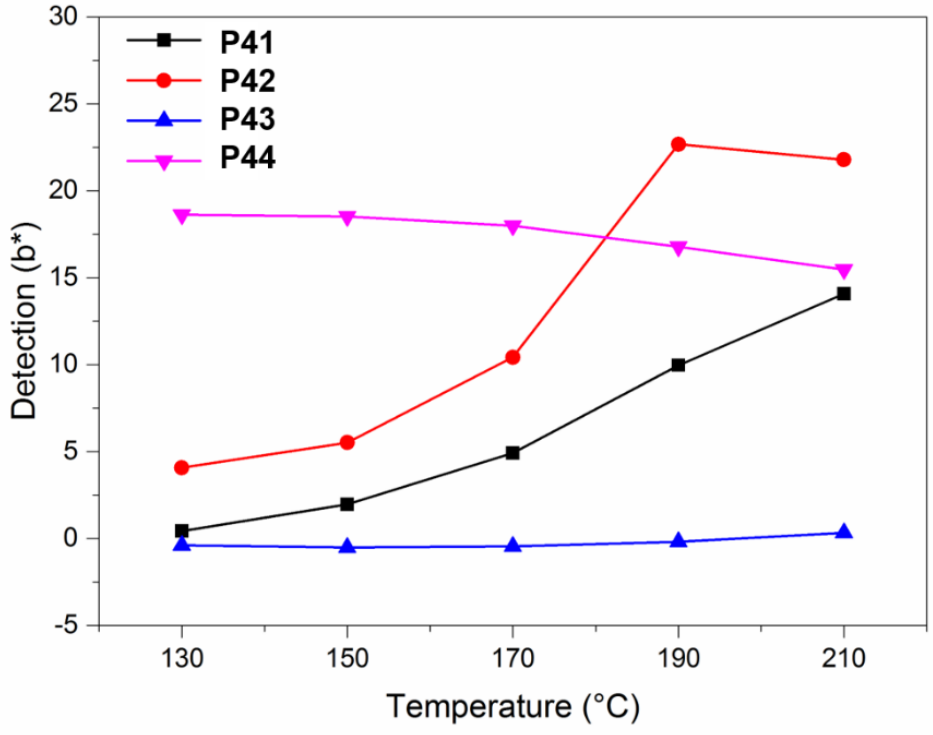

Figure 3.62 Graph depicting b* detection for samples **P41-P44** at 130-210 °C.

3.7.4 Surface Texture and Microstructure of the Citrate Series

As well as the surface colouration, the texture of the surface is equally important. The external surface topography and the internal cellular structure of the paper samples **P41$_{210}$-P44$_{210}$**, formulated with compounds **41-44** and cured at 210 °C, were analysed with scanning electron microscopy (SEM). The desired physical properties obtained from the synthesised additives **41-44**, were a controllable expansion with evenly distributed gas pockets within the plastisol matrix. The coating surface must be smooth, and matt as seen in the current expansion control **P$_{ADCA}$**. A standard 'blank' formulation (**P$_{blank}$**) containing no chemical blowing additives was prepared via the same method for comparisons.

3.7.4.1 Surface Texture Analysis of the Citrate Series

The control expanded plastisol (**P$_{ADCA}$**, a, Figure 3.63) showed an evenly textured surface. The control 'blank' sample, **P$_{blank}$** presented an uneven surface (b, Figure 3.63), which was the result of irregularly sized gas pockets throughout the sample. The defects were observed across the sample surface ranging from 0.31-1.46 mm with the average defect size ca. 0.80 mm.

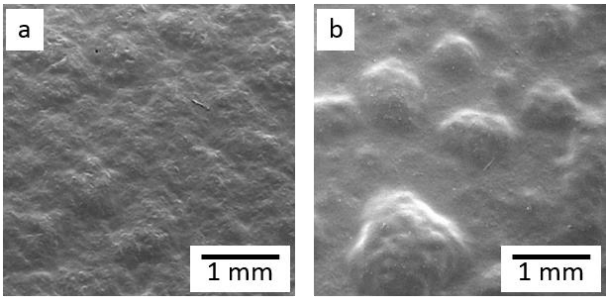

Figure 3.63 SEM surface micrographs of the control samples (a) **P$_{ADCA}$** and (b) **P$_{blank}$** at x18 Mag.

Samples **P41$_{210}$** and **P42$_{210}$** (a, b, Figure 3.64) showed a reduction in the average size of the gas bubbles on the surface of the coating, when compared to **P$_{blank}$**; however, more defects were observed across the entirety of the surface. Sample **P41$_{210}$** showed an average defect size of ca. 0.59 mm. In the case of sample **P42$_{210}$**, the unevenness caused by the gas bubbles consisted of both raised defects and craters (Figure 3.64); however, these were generally of a smaller size than seen in the control sample **P$_{blank}$** (Figure 3.63). Whilst it was evident from this data that the additives **41** and **42** did influence the surface

properties of the resulting plastisol coating, the surfaces of both **P41$_{210}$** and **P42$_{210}$** did not replicate the desired smooth effect seen in **P$_{ADCA}$**.

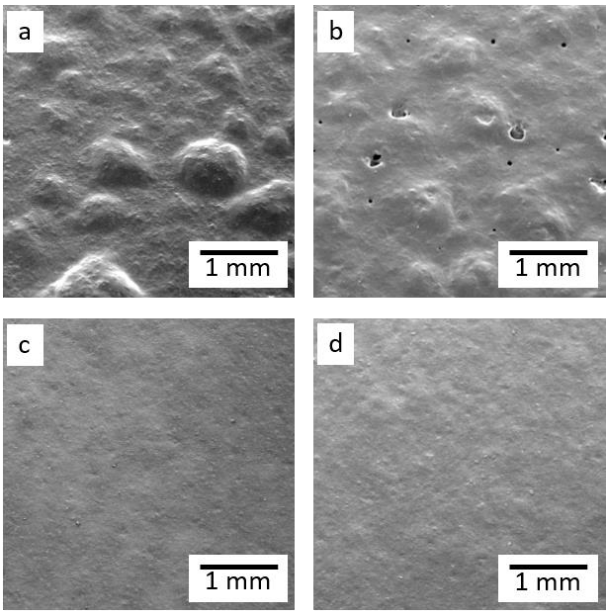

Figure 3.64 SEM surface micrographs of samples (a) **P41$_{210}$**, (b) **P42$_{210}$**, (c) **P43$_{210}$** and (d) **P44$_{210}$** at x18 Mag.

All three samples exhibited a wide range in surface defect size. That said **P41$_{210}$** and **P42$_{210}$** showed a higher concentration of defects within the lower region of 0.1-0.6 mm compared to **P$_{blank}$**, which displayed a higher number of defects above 0.6 mm. This suggested that gas formation is more controlled and evenly distributed with the presence of additives **41** and **42**. Improved distribution of the chemical additive could result in a higher quality coating. The quantity of the observed gas bubbles increased as the temperature was increased, confirming that the colouration and gas formation were both a direct result of the thermal decomposition of additives **41** and **42** within with formulation.

Both the ester formulations, **P43** and **P44** produced very smooth and evenly dispersed coatings. No surface defects were observed for coatings **P43** and **P44**, either with the naked eye or microscopically, much like in the case of **P$_{ADCA}$**. In the acid compounds **41** and **42** the main contributing force is hydrogen bonding around the N-H donor site, as well as the HOOC- site in the carboxylic acid derivatives. Despite being significantly weaker than covalent bonds, hydrogen bonds exhibit strong dipole-dipole interactions creating stability within the system and thus contributing to a relatively high surface tension. The esterification of the carboxylic acid group (as in compounds **43** and **44**) limited the available H-

bonding sites and therefore reduced the surface tension effects, creating a levelling effect and a smooth coating surface (Figure 3.64).

3.7.4.2 Surface Gloss Analysis of the Citrate Series

As well as a smooth, defect free surface, market research identified that a matt finish is desirable for the final foamed coating product. The gloss reading of the surface of each coating sample was measured using a glossmeter. Gloss readings are based on the amount of light reflected on the surface relative to a polished glass reference standard, measured in Gloss Units (GU). Surfaces ≤10 GU are considered matt, whilst readings between 10 and 75 GU are regarded as semi- gloss, whereas 75-100 GU depicts a glossy surface. The gloss values for samples **P41**-**P44** are tabulated below. (Table 3.23)

Table 3.23 Gloss reading values for samples **P41**-**P44**, and the control sample $\mathbf{P_{ADCA}}$.

Sample	85° Beam Angle Reading (GU)				
	130 °C	150 °C	170 °C	190 °C	210 °C
P41	21.9	9.1	6.7	5.7	3.7
P42	25.3	8.3	7.8	6.7	8.9
P43	26.9	25.1	21.7	25.1	31.6
P44	27.3	21.9	18.8	22.0	24.1
$\mathbf{P_{ADCA}}$	28.5	28.5	7.6	3.5	1.3

The acidic derivatives **41** and **42**, showed a significant loss in gloss as the temperature was increased from 130-210 °C. (Figure 3.65).

In the case of compounds **P41** and **P42**, the gloss data was conducive with the observed surface defects at high temperatures, giving further evidence that a thermal decomposition reaction was occurring in this temperature range. Although the gloss readings were within the acceptable range for samples $\mathbf{P41_{150}}$-$\mathbf{P41_{210}}$ and $\mathbf{P42_{150}}$-$\mathbf{P42_{210}}$, the samples were not viable as alterative to ADCA due to unsuccessful results in the other areas.

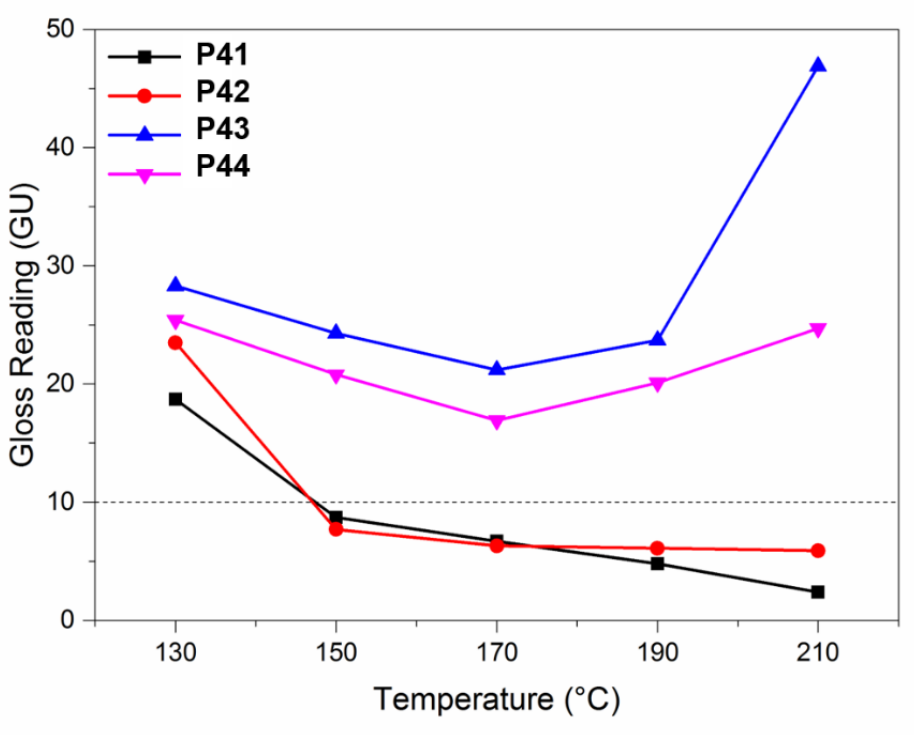

Figure 3.65 Graph depicting gloss values for samples **P41-P44** with the upper region of the matt region (10 GU) highlighted.

Samples **P43** and **P44**, were smooth and defect free, the low surface tension and even distribution of the additives **43** and **44** resulted in a 'semi-gloss' surface, with little correlation to temperature This provided further evidence that the reduced level of hydrogen bonding within the system allowed the esterified materials to aid dispersion due to a lower surface tension. Despite not being the target physical properties for this application, compounds **43** and **44** show potential for application as levelling agents in smooth surface applications.

In all cases the observed gloss readings were above that observed for $\mathbf{P_{ADCA}}$ which showed an extremely matt surface with GU = 1.3. $\mathbf{P41_{210}}$ showed the closest GU reading to the desired value. The graph clearly shows that in the case of the ester materials **43** and **44**, samples at all temperatures appear significantly above the desired matt region (≥10 GU, Figure 3.65).

3.7.4.3 Microstructure Analysis of the Citrate Series

Cross-section images provided information of the internal cellular structure of the coating samples. (Figure 3.66) The cross-sections confirmed that the observed surface defects are resultant of gas pockets within the coating and that the compounds did act as blowing agents in some capacity.

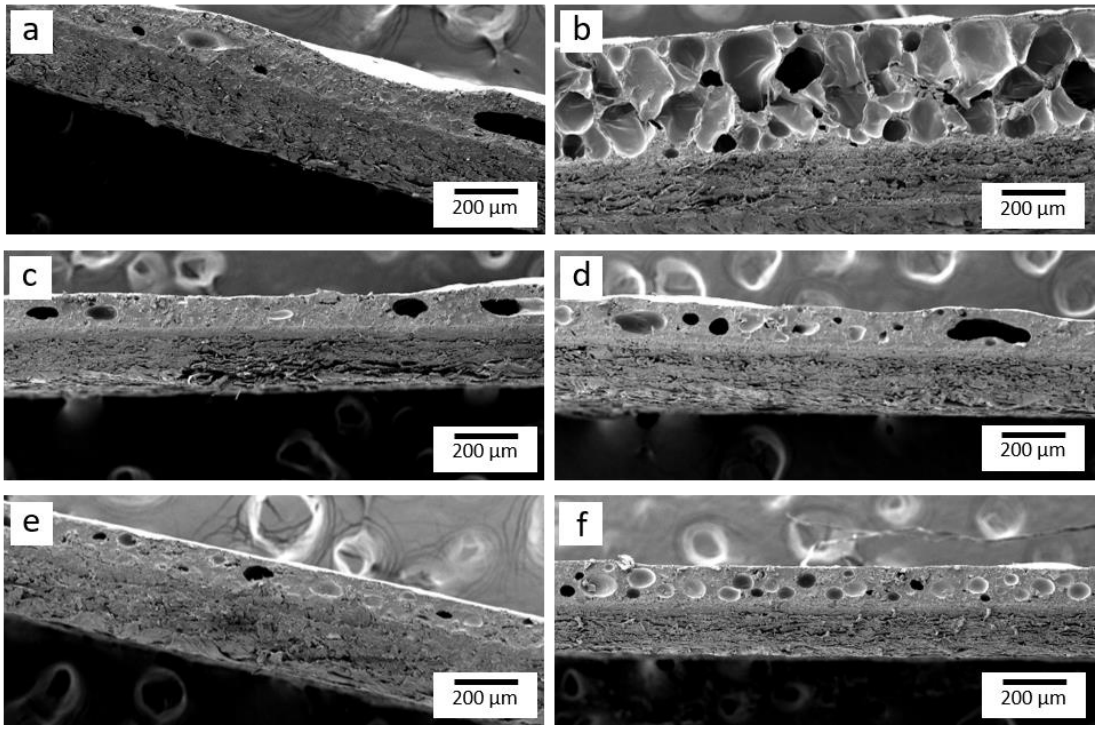

Figure 3.66 SEM cross-section micrographs of samples (a) $\mathbf{P_{blank}}$, (b) $\mathbf{P_{ADCA}}$, (c) $\mathbf{P41_{210}}$, (d) $\mathbf{P42_{210}}$, (e) $\mathbf{P43_{210}}$, (f) $\mathbf{P44_{210}}$ at x75 Mag.

In the case of sample $\mathbf{P41_{210}}$, the cross-section analysis (c, Figure 3.66) indicates that the additive **41** not only presents a negative result in terms of blowing ability but it also hindered the distribution of the internal gas pockets that were formed (Figure 3.67). Although fairly regularly dispersed on the surface, the internal pockets were not evenly dispersed and exhibited a large cell size range.

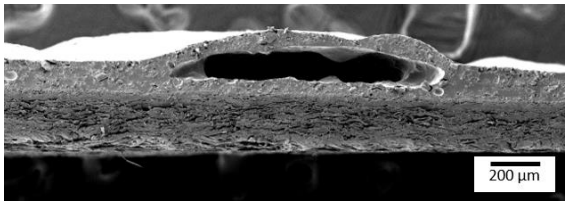

Figure 3.67 SEM cross-section micrograph of sample $\mathbf{P41_{210}}$ showing large irregular gas pocket at x75 Mag.

In comparison, $\mathbf{P_{blank}}$ showed more evenly distributed internal gas bubbles, within a narrower cell size range (Figure 3.66). That said, the gas pockets observed in $\mathbf{P41_{210}}$ did not result in any significant expansion of the coating, mainly due to their irregular distribution.

As mentioned, in contrast to the rough uneven surface observed in the blank, sample $\mathbf{P43_{210}}$ appeared to be smooth and even (Figure 3.64). The cross-

section micrograph of **P43$_{210}$** showed that gas pockets were still formed in the formulation (Figure 3.66); however, the pockets were significantly smaller, with a narrower size range, and more evenly dispersed, thus not defecting the external surface. The distribution graph (Figure 3.68) shows that, in general, the internal cell sizes were below 200 µm. The control expanded sample **P$_{ADCA}$** contained cells with an average size of approx. 150 µm, thus contributing to the overall expansion of the plastisol layer. **P43$_{210}$** and **P44$_{210}$** exhibited no anomaly results with all analysed cells between 50 µm and 150 µm.

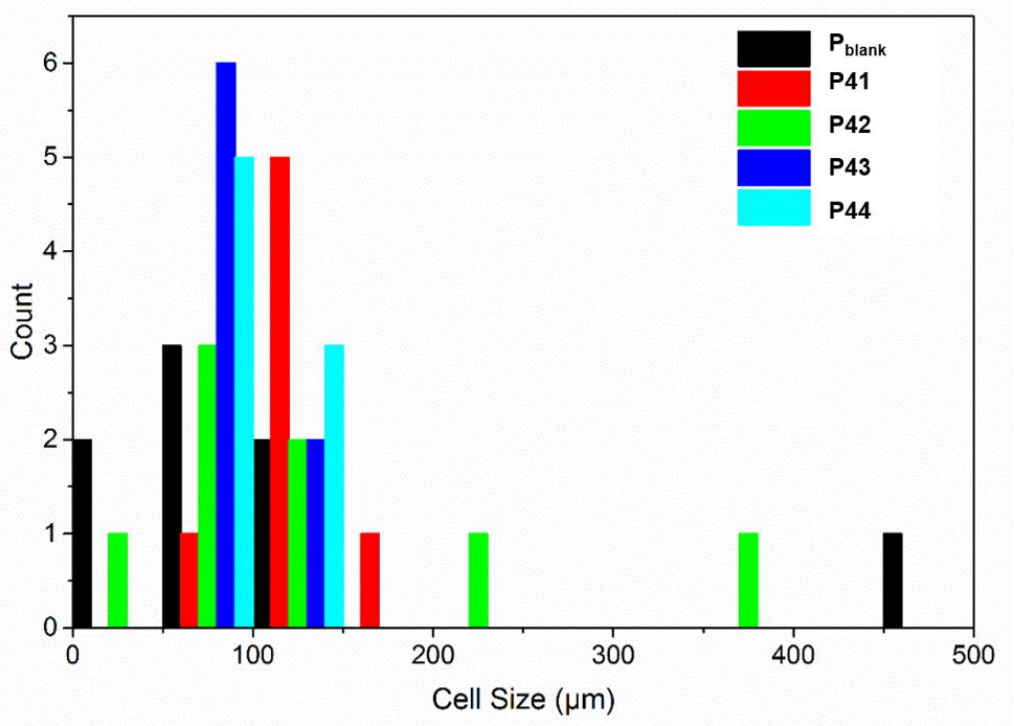

Figure 3.68 Distribution graph showing the cell size range observed in the SEM cross-section micrographs of samples **P$_{blank}$** and **P41**-**44** at 210 °C.

This data confirmed that compounds **43** and **44** aided the even distribution of the various formulation components across the coating whilst inhibiting larger gas pocket formation. This allowed even distribution of small gas pockets throughout the coating, resulting in a smooth even surface. Contrastingly, **P$_{blank}$**, **P41$_{210}$** and **P42$_{210}$** contained several larger gas pockets. These larger gas pockets contributed to the uneven defects on the coating surface (Figure 3.64). The micrographs confirmed that the distribution and regularity of the internal cell structure was fundamental to the surface appearance. Whilst all formulations showed evidence of gas formation during heating, the cross-section analysis provided evidence that compounds **43** and **44** inhibit the formation of large gas pockets which limits the disruption to the surface.

3.7.5 Conclusions of the Citrate Series

The citrate compounds **41-44** have been successfully synthesised and characterised. Synthesis of the compounds was effectively scaled up to approx. 50 g in excellent yields of up to 80%.

The TGA and DSC data confirmed that thermal degradation of compounds **41-44**, occurred within suitable range for implementation in PVC applications. PVC plastisol's containing compounds **41-44** were prepared and physical properties of the final formulations were tested at different curing temperatures.

In the case of all materials, gas cells were formed within the plastisol layer of the coating; however, this gas formation was not significant enough to increase the observed expansion of the coating. Compounds **41** and **42**, showed irregular cell production, leading to surface defects observed in the SEM surface micrographs. In the case of compounds **43** and **44** the increased gas dispersion coupled with decreased cellular size, observed in the SEM cross-sections, resulting in a low expansion rate

Compounds **43-44** did not significantly affect the colouration of the coating surface, suggesting that these additives are suited well to colour sensitive and decorative applications. Furthermore, the plastisols **P43** and **P44** exhibited smooth gloss surfaces. Although not the target result for this application the addition of additives **43** or **44** was beneficial to the overall appearance of the coating surface and they could potentially be utilised as naturally derived, non-toxic levelling agents for many other industrial processes.

In the case of **41** and **42**, a significant colour change was observed as the temperature was increased. Thermal degradation data of compounds **41** and **42** and observed colour changes in the plastisol samples were in an excellent agreement supporting thermal decomposition between 170 °C-210 °C.

The study outlined in the chapters showed that compounds **41-44** directly affects the physical properties of the PVC wallpaper coating. However, insufficient gas production and subsequent expansion of the plastisol layer upon thermal decomposition of the additives, resulted in an unsuitable alternative to ADCA in all cases.

3.8 Tartronic Acid Derivatives

The initial tests of the citrate series confirmed that gas pockets were produced but the high level of hydrogen bonding within the system increased the surface tension to inhibit expansion and even distribution of the additives. It was therefore hypothesised that with additives with fewer carboxylic acid groups may limit the negative effects observed due to hydrogen bonding yet still allow the production of gas. Tartronic acid was chosen as the backbone structure of the second series of novel agents. Tartronic acid is a natural product present in foodstuffs such as potato and mung bean. [156]

Tartronic acid does not strictly fit the costing specification set about in this project[xviii] However, literature suggests that in-house synthesis of tartronic acid is routine. [157] To ensure both time and resources were spent economically within this study, the initial starting material was purchased with the strategy to further investigate a routine in-house synthesis if the resulting synthesised materials proved to be of significant industrial interest.

Due to the similarities in chemical structure, and the presence of multiple carboxylic acid groups, it was predicted that the decomposition of tartronic acid would follow a similar mechanism to that of citric acid to yield carbon dioxide and hydrogen gases as well as nontoxic small molecule by products.

3.8.1 Synthesis and Characterisation of Tartronic Derivatives

Although more uncommonly referenced in the literature, similar to citric acid, tartronic acid can be regarded as a versatile platform for structural modification. Hydrazine monohydrate **40** was reacted with the tartronic acid **20** and diethyl tartronate **45**. (Scheme 3.6)

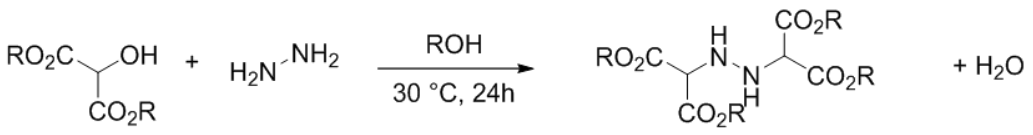

20 (R=H)
45 (R=Et)

40

46 (R=H) 79%
48 (R=Et) 79%

Scheme 3.6 Generic scheme of the reaction of tartronic acid **20** and diethyl tartronate **45** with hydrazine monohydrate **40**.

[xviii] Based on Sigma-Aldrich price April 2018.

The diethyl tartronate **45** was prepared in the yield of 74%, through the reaction of tartronic acid **20**, with ethanol in the presence of H_2SO_4. The tartronic acid **20** and diethyl tartronate **45** were reacted with phenylhydrazine under the same conditions as the hydrazine monohydrate. (Scheme 3.7)

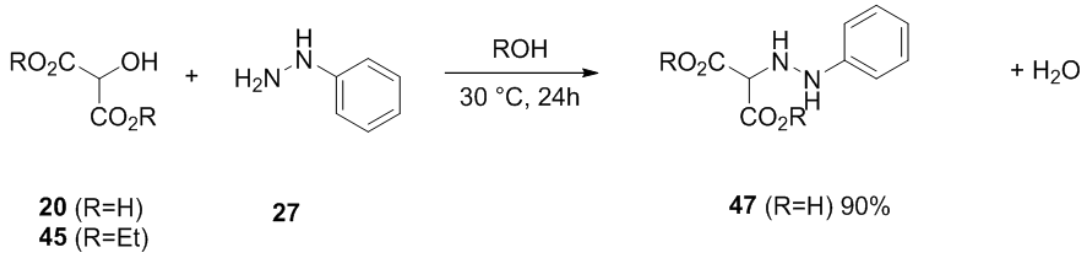

Scheme 3.7 Generic scheme of the reaction of tartronic acid **20** and diethyl tartronate **45** with phenylhydrazine **27**.

In this series, diethyl tartronate appeared not to react with phenylhydrazine. The excellent chemical purity and yields of the two compounds (**46-47**) make this synthetic pathway highly practical and the compounds were synthesised and scaled up to 30 g in the case of compound **46**.

As in the previously discussed series, the characterisation of the tartronate derivatives was carried out using a combination of analytical techniques (NMR, IR and MS).

As seen in the case of the citrate series, the tartronate derivatives proved insoluble in organic solvent and consequently the ^1H NMR experiments were carried out in D_2O. This again, resulted in proton exchange occurring at the OH and NH groups. Despite the minimal proton regions within the tartronate series, the ^1H NMR data of the materials **46-47** supported the characterisation made by IR and highlighted a shift in the peak corresponding to the aliphatic protons. A typical shift of approx. 0.30 ppm from the corresponding hydroxyl-precursors is observed in hydrazo derivatives **46-47** indicating the successful conversion to the hydrazo group. The scale up of compound **48**, did not fit the criteria set-out for the synthesis of commercial materials within this project (Table 3.7, chapter 3.3) and it was therefore not taken forward for analysis within the plastisol coatings.

The essential IR peaks for the characterisation of the novel compounds are listed in Table 3.24.

Table 3.24 IR data for compound **46-47**.

Compound	C-N[a]	N-H[b] (bend)	N-H[c] (stretch)	C=O[d]
46	1086	1546	3329	1601
47	1317	1491	3289	1602

a Typical region 1000-1300 cm^{-1}
b Typical region 1490-1650 cm^{-1}
c Typical region 3300-3500 cm^{-1}
d Typical region 1600-1750 cm^{-1}

3.8.2 Thermal Behaviour, Stability and Decomposition Pathway of Compounds 46-47

Thermal gravimetric analysis (TGA) and differential scanning calorimetry (DSC) were used to evaluate the thermal properties of compounds **46-47**. Typical experimental temperatures are summarized in Table 3.25.

Table 3.25 TGA and DSC data for the compounds **46-47**.

Compound	TGA		DSC
	$T_{-10\%}$[a]	T_{max}[b]	T_{DSC}[c]
46	100	148, 228	176
47	114	156, 235	174

a Temperature at 10% mass loss in the TGA
b Maximum thermal degradation temperature from the 1st derivative of the TGA
c Phase transition temperature in the DSC

The thermal degradation data was used to predict the behaviour of the additives within the coating formulation at various cure temperatures. (Figure 3.69)

All the materials in the tartronate series showed a 10% mass loss at approx. 100 °C, which could be due to the loss of residual solvent. In all cases the first derivative DTG analysis identified a two-step decomposition process, which supports the theory that multiple decarboxylation steps occur in polycarboxylic acids. This result was comparable to that seen in **P23**, which contained the same

polycarboxylic functional group and showed a two-step pyrolysis process with T_{max} observed at 155 °C and 223 °C (Chapter 3.4.2).

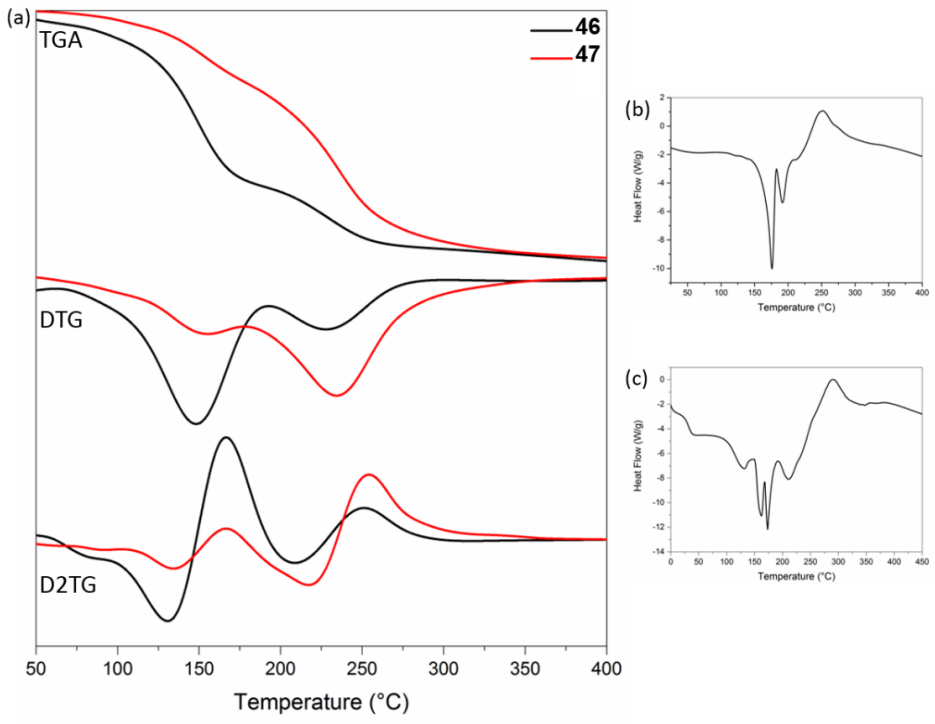

Figure 3.69 (a) TGA, DTG and D2TG data for compounds **46-4**, (b) DSC data for compound **46**, (c) DSC data for compound **47**.

T_{max} occurred within the suitable melt viscosity range of PVC for additives **46** and **47**.The second derivative (D2TG) data for compounds **46** and **47** were conducive with the DSC data (b, c, Figure 3.69), confirming a phase transition at ca 170-180 °C for both materials.

3.8.3 PVC Coating Formulations, Temperature Dependency and Colour Correlation of the Tartronate Series

Despite the unsuccessful synthesis of compound **48**, compounds **46-47** were analysed under the standard manufacturing conditions to produce plastisol coated samples containing each additive. It was decided that if successful results were obtained, the synthesis of compound **47**, and its phenylhydrazine derivative, would be investigated and, if successful, further analysed as part of the series.

Contrary to the citrate series, which produced pale coloured oils in the case of the symmetrical derivatives **41** and **43** (chapter 3.7), the tartronate series produced highly coloured powders. In attempt to obtain a more even distribution the powders were milled using a pestle and mortar before being implemented

into the plastisol formulation as coarse powders could disrupt the drawdown process by blocking the k bar.

To study derivatives **46-47** within polymer matrix, the novel plastisols containing compounds **46-47** have been formulated to a standard specification, manufactured and analysed to determine the effect on coating efficiency, surface wetting and coating coverage. The formulation **P46**, had been cured at 130 °C, 150 °C, 170 °C, 190 °C and 210 °C to correspond with the melt viscosity range of the PVC plastisol. This allowed temperature dependency studies to be carried out for the material.

Table 3.26 shows L*a*b* and ΔE data for the thermally cured plastisol **P46**. The L*a*b* values were given for the formulated plastisol cured at 130 °C and set as the control sample $\mathbf{P46_{130}}$ to monitor temperature dependent colour change (ΔE). The plastisol formulation **P47**, containing additive **47**, was cured at 210 °C only to determine the influence on the colouration properties caused by the phenyl ring before large scale up of the material.

Table 3.26 L*a*b* data and ΔE for samples **P46** and $\mathbf{P_{ADCA}}$.

	130 °C			ΔE			
Entry	**L***	**a***	**b***	**150 °C**	**170 °C**	**190 °C**	**210 °C**
P46	93.92	-0.51	1.49	0.57	0.42	1.88	1.32
$\mathbf{P_{ADCA}}$	92.55	-0.96	11.55	0.51	0.53	1.18	6.81

The colour changes in **P46** were insignificant when compared to $\mathbf{P_{ADCA}}$ (Figure 3.70) and it was predicted that the higher ΔE values observed in $\mathbf{P46_{190\text{-}210}}$ were correctable by alteration of the optical brightener content within the formulation.

Compound **46**, showed very little colour change at the lower curing temperatures; however, an increase in ΔE was observed in sample $\mathbf{P46_{190}}$. This result was in agreement with the DSC analysis of compound **46** (b, Figure 3.69) which indicated that phase transition occurred above 170 °C. This shows that the colouration of samples **P46** is directly related to the full thermal decomposition of additive **46** within the plastisol matrix, which occurred in the range of 180-230 °C.

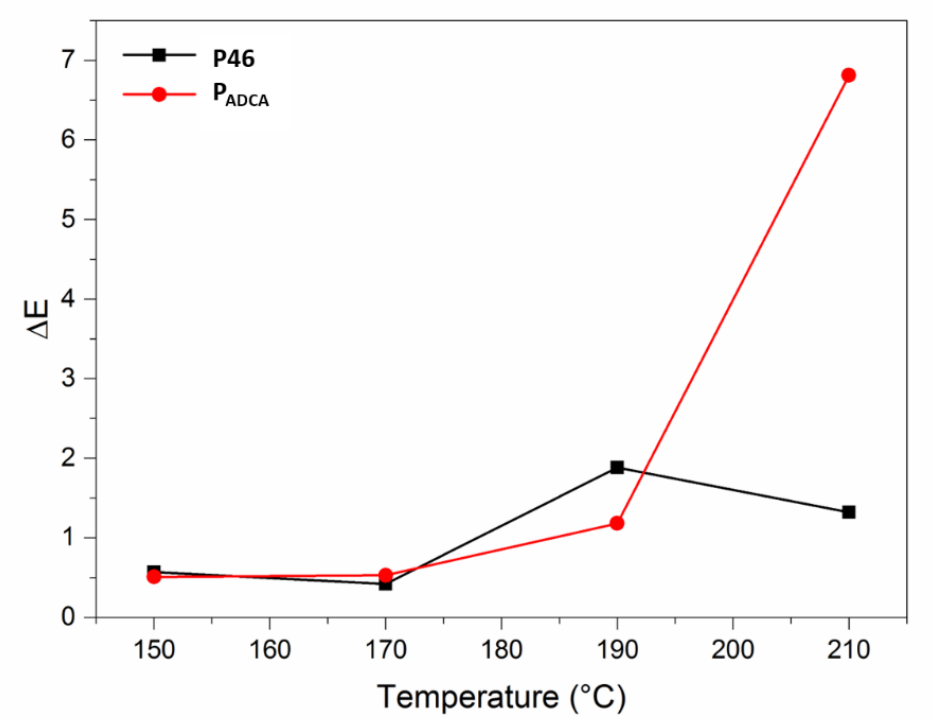

Figure 3.70 Graph depicting ΔE for samples **P46$_{150}$** – **P46$_{210}$** and **P$_{ADCA}$**.

The T_{max} onset of the first step, shown in the DTG data at 148 °C, did not contribute to a colouration of the plastisol coating (ΔE = 0.57 at 150 °C). This first step accounted for 40% mass of the additive **46**, the low colouration across this decomposition suggests that colourless by-products are formed and that a lower curing temperature could be advantageous to the manufacturing process of the plastisol coating **P46**.

Although minimal colour changes are observed in the ΔE data for samples **P46$_{130\text{-}210}$**, it was clear from the photographic images of the samples that the particle size caused disruption of the surface layer. (Figure 3.71)

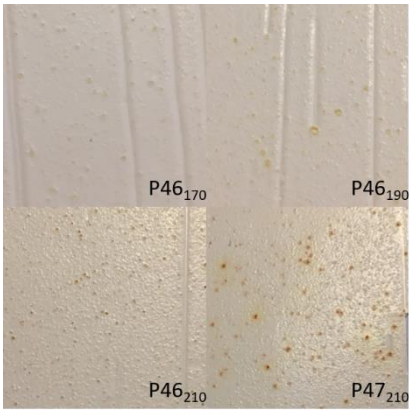

Figure 3.71 Photographic images of samples **P46$_{170}$** – **P46$_{210}$** and **P47$_{210}$**.

This result was due to the low solubility and insufficient distribution of the particles within the plastisol formulation. The dissolution of additive **46**, within a compatible solvent, before addition to the formulation could aid the distribution of the material throughout the plastisol. However, this could be disadvantageous as significant lowering of viscosity could lead to disruption of the curing process. Furthermore, volatile solvents must be pre-blown at 130 °C for 20 seconds[xix] to limit any disruption to the expansion process and the surface properties of the coating.

As shown in the photographic images (Figure 3.71), sample **P47$_{210}$** showed significantly more colouration when compared to the symmetrical derivative **P46$_{210}$**. This was confirmed by a significant increase observed in b*, where b* = 10.36 in sample **P47$_{210}$**, compared to b* = 2.38 in the case of **P46$_{210}$**. This strong b* detection further confirms the theory that the phenyl ring, in additive **47**, actively contributes to the colouration of the plastisol coating.

3.8.4 Surface Texture and Microstructure of the Tartronate Series

3.8.4.1 Surface Texture Analysis of the Tartronate Series

The external and the internal cellular structure of the paper samples **P46$_{130\text{-}210}$**, were analysed with scanning electron microscopy (SEM).

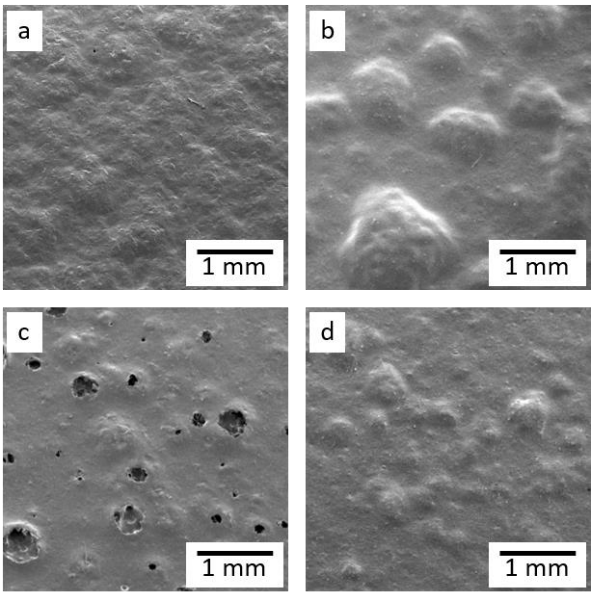

Figure 3.72 SEM surface micrographs of samples (a) **P$_{ADCA}$**, (b) **P$_{blank}$**, (c) **P46$_{210}$** and (d) **P47$_{210}$** at x18 Mag.

[xix] Graham & Brown standard manufacturing procedure

As in the previous series', the micrographs were compared to the standard expanded plastisol coating, $\mathbf{P_{ADCA}}$ which exhibited a smooth and matt surface. A 'blank' control, $\mathbf{P_{blank}}$, containing no chemical blowing additive was also prepared for comparison. (a, b, Figure 3.72)

In the case of sample $\mathbf{P47_{210}}$ (d, Figure 3.72) the SEM surface micrograph shows a similar appearance to the control sample, $\mathbf{P_{blank}}$. 'Bubble-like' defects were evident on the coating surface. In general, the defects observed in sample $\mathbf{P47_{210}}$ were reduced in size, with an average size of 0.30 mm, compared to the average of 0.80 mm in sample $\mathbf{P_{blank}}$.

The SEM surface micrograph for sample $\mathbf{P46_{210}}$ (c, Figure 3.72), showed significant surface defects across the coating. Large craters had formed suggesting a high incompatibility within the system. This is likely due to the low dissolution of additive **5** within the formulation disrupting even distribution. This effect can also be seen in the photographic images of the coating surface (Figure 3.71)

As shown in Figure 3.73, significant craters are observed on the surface of coating **P46** across the temperature range 170-210 °C.

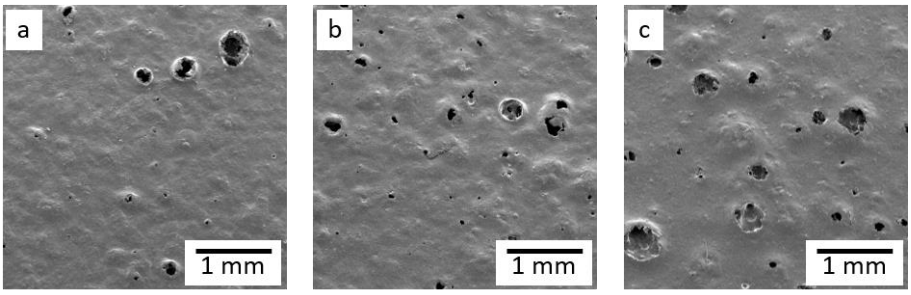

Figure 3.73 SEM surface micrographs of samples (a) $\mathbf{P46_{170}}$, (b) $\mathbf{P46_{190}}$ and (c) $\mathbf{P46_{210}}$ at x18 Mag.

This is in agreement with thermal data which suggests that decomposition occurs from 150 °C. Due to the low distribution of the particles within the formulation, it is possible that increased gas production around these particles as they decompose would create an increase in pressure and subsequently break the surface tension, resulting in the large crater defects. This surface topography concludes that the tartronate derivative **46**, is incompatible with the current formulation.

3.8.4.2 Surface Gloss Analysis of the Tartronate Series

The plastisol surfaces were also analysed for gloss readings. The desired effect is a smooth but matt finish as this proves most popular with consumers in the wallpaper markets[xx]. The samples were analysed using a glossmeter, where GU ≤10 corresponds to an observed matt effect. The gloss readings are shown in Table 3.27 below.

Table 3.27 Gloss readings for samples **P46**, **P47** and **P_{ADCA}**.

Sample	85° Beam Angle Reading (GU)				
	130 °C	**150 °C**	**170 °C**	**190 °C**	**210 °C**
P46	23.8	13.7	8.4	6.8	6.6
P47	-	-	-	-	14.7
P_{ADCA}	28.5	28.5	7.6	3.5	1.3

In general, **P46** followed the trend of the control sample **P_{ADCA}**. As the temperature was increased, the gloss reading of the surface coating was reduced (Figure 3.74).

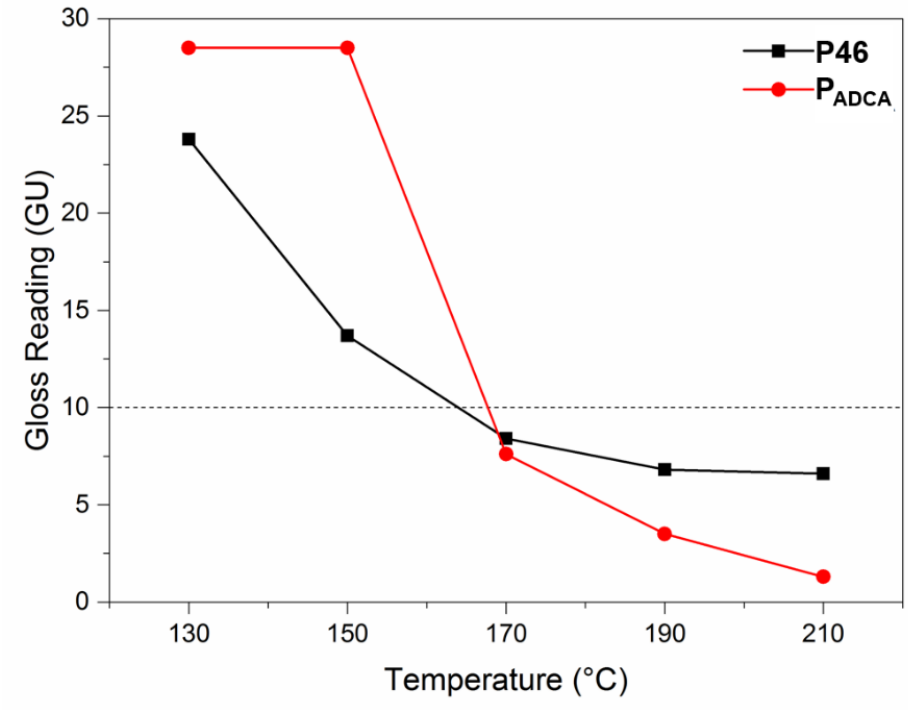

Figure 3.74 Graph depicting the gloss readings of **P46** and **P_{ADCA}** across the temperature range 130-210 °C.

[xx] Graham & Brown market research data

This effect was observed because, as the temperature was increased, thermal decomposition of the additive was initiated, creating more disorder within the system through the formation of gas particles, thus disrupting the smooth and glossy surface. **P47$_{210}$** showed a significantly glossier surface with the observed gloss reading outside of the matt region.

The gloss readings for **P46** are conducive with the L*a*b* and thermal data which showed that significant decomposition occurs above 170 °C. The gloss data is advantageous as it represents the desired matt surface, within the appropriate curing temperatures.

3.8.4.3 Microstructure Analysis of the Tartronate Series

Cross-section images provide information of the internal cellular structure, confirming that the surface effects can be resultant of gas pockets within the coating. As before, the novel formulations **P46** and **P47** were compared with the control samples **P$_{ADCA}$** (expanded) and **P$_{blank}$** (no additive). (a, b, Figure 3.75)

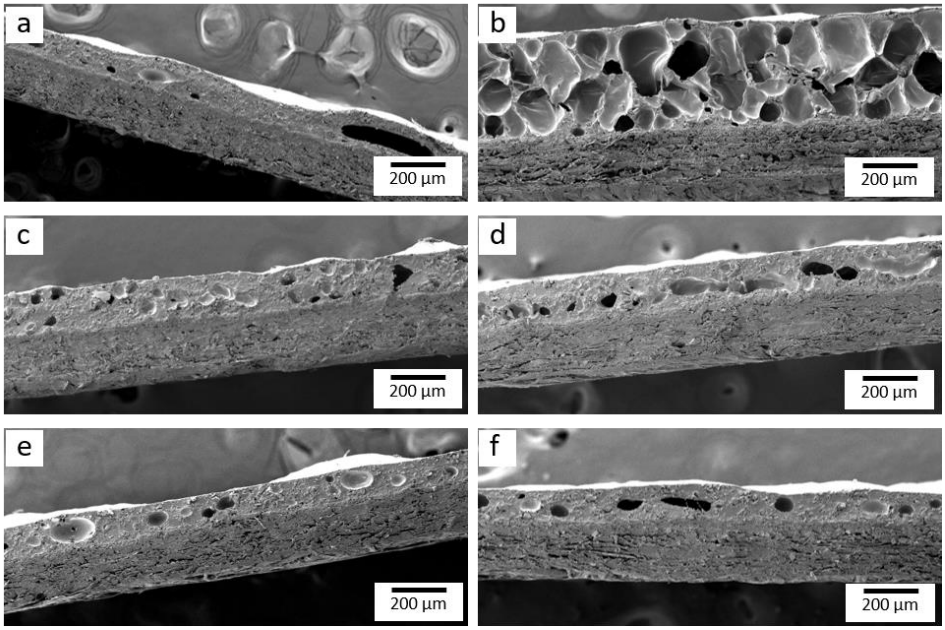

Figure 3.75 SEM cross-section micrographs of samples (a) **P$_{blank}$**, (b) **P$_{ADCA}$**, (c) **P46$_{170}$**, (d) **P46$_{190}$**, (e) **P46$_{210}$** and (f) **P47$_{210}$** at x75 Mag.

The observed cellular structure in the cross-section micrographs of samples **P46** and **P47** confirmed that the compounds do act as blowing agents in some capacity. That said, the gas production by the additives does not aid significant expansion of the plastisol layer, with average coating depths of

160 µm observed across the samples. This analysis shows a contraction from the initial applied coating depth of 200 µm before curing. This suggests that the inclusion of additives **46** and **47**, hinders expansion within the formulation. Further confirming, that compounds **46** and **47** are not suitable as direct replacements to ADCA within polymer coating formulations.

Despite this, the gas pockets formed in samples **P46$_{170}$** – **P46$_{210}$** (c-e, Figure 3.75) were consistent across the analysed temperature range. The cell sizes are small and evenly distributed, contrary to the surface results. This suggests that the material is evenly dispersed within the formulation despite evidence of formulation incompatibility shown in the surface SEM micrographs. This further supports the theory that the surface defects were due to the undissolved particle matter within the system, rather than an internal incompatibility of the dissolved matter.

To resolve the issue of particle surface defects, such as craters and fish-eyes, a finer particle grade could be obtained through the extensive milling of the material. Alternatively, the material can be pre-dissolved in a suitable solvent, such as isopropanol or the plasticizer DINP. In this case however, the solvent effects on the surface must be considered and the standard manufacturing process must be adapted to remove excess solvent from within the formulation. To investigate such adaptations to the formulation, the standard manufacturing process would have to be altered. This was not beneficial in this case as the observed expansion levels did not suggest that these modifications could solidify additive **46** as a suitable alternative blowing agent to ADCA.

Sample **P47$_{210}$**, also showed regularly sized cells within the plastisol coating layer. This similarly suggests that the dissolved material is evenly dispersed within the formulation, which is conclusive with the SEM surface micrographs which showed minimal defects upon the surfaces. However, despite fewer observed defects, in the case of **P47**, high coloration levels eliminate the additive from application within decorative coatings.

3.8.5 Conclusions of the Tartronate Series

The tartronate compounds **46-48** have been successfully synthesised and characterised. Synthesis of the compounds **46** and **47** was effectively scaled up to approx. 30 g in excellent yields of up to 90%. That said, the scale up of compound **48** was unsuccessful for implementation into the plastisol formulations, due to unworkability of the material.

The TGA and DSC data confirmed that thermal degradation of compounds **46-47**, occurred within suitable range for implementation in PVC applications. PVC plastisol's containing compound **46** were routinely prepared and physical properties of the final formulations were tested at different curing temperatures. Compound **47**, was prepared in formulation for testing at 210 °C due to concern of colouration. It was subsequently discovered that compound 6 was incompatible with the system due to low solubility.

In the case of all samples, gas cells were formed within the plastisol layer of the coating; however, this gas formation was not significant enough to increase the observed expansion of the coating. The cellular structure was regular in size and distribution, suggesting some dispersion within the system. That said surface defects were observed at all temperature for sample **P46**.

High coloration was observed in the sample **P47$_{210}$**, rendering it unsuitable for implementation in decorative coating applications. While **P46** showed little colouration across the temperature range, large particle defects were observed in the plastisol coatings, including substantial disturbance to the application of the coating using a k-bar which resulting in the paper substrate being visible in areas of the coating surface. This effect is detrimental in decorative coatings and the use of additive **46** within formulation would require substantial further investigation into the compatibility of the formulation.

The study outlined in the chapters above proved that the incorporation of the compounds **46-47** into commercial PVC plastisol's for wallpaper applications directly affects the physical properties of the resultant coating. However, insufficient gas production, low expansion of the plastisol layer and significant surface defects, renders the materials unsuitable alternatives to ADCA in all cases.

3.9 2-Hydroxyisobutyric Acid Derivatives

Following the results of the citrate and the tartronate series', 2-hydroxyisobutyric acid **21** was chosen as a starting material with a single carboxylic acid functional group.

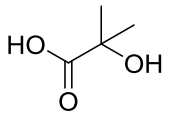

21

The 2-Hydroxyisobutyric acid was also hypothesised to work well within the formulation as the presence of aliphatic side chains, such as two methyl groups, can potentially further lower the surface tension of the coating and allow for evenly distributed gas pockets. Furthermore, the reduced polarity of the molecule allows for increased solubility, and therefore workability, when compared to the citrate and tartronate series. This workability is essential when working on industrial scale productions as it allows for easier, faster and more cost-effective scale up synthesis.

2-Hydroxyisobutyric acid and its ethyl ester **49** are readily commercially available and cost effective[xxi] starting materials that fit the scope of the project.

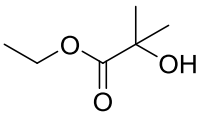

49

As with the previously investigated starting materials, 2-hydroxyisobutyric acid is a versatile structural backbone that can yield various derivatives. 2-Hydroxyisobutyric acid is characterised as natural product that can be effectively biosynthesised from renewable carbon sources. [158]

Furthermore, the structure of 2-hydroxyisobutyric acid suggests a decomposition mechanism to nontoxic small molecule by products. Domingo *et al* theoretically characterised the gas phase of decomposition of 2-hydroxyisobutyric acid to yield carbon monoxide, water and corresponding carbonyls. [159]

[xxi] Based on Sigma- Aldrich price December 2017

3.9.1 Synthesis and Characterisation of the Isobutyrate Derivatives

The 2-hydroxyisobutyric acid **20** and ethyl 2-hydroxyisobutyrate **49** were reacted with the hydrazine monohydrate **40** (Scheme 3.8) and phenyl hydrazine **27**. (Scheme 3.9)

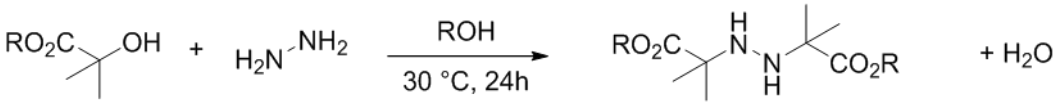

21 (R=H)
49 (R=Et)

40

50 (R=H) 84%
52 (R=Et) 59%

Scheme 3.8 Generic scheme for the synthesis of the isobutyric acid **21** and ethyl isobutyrate **49** with hydrazine monohydrate **40**.

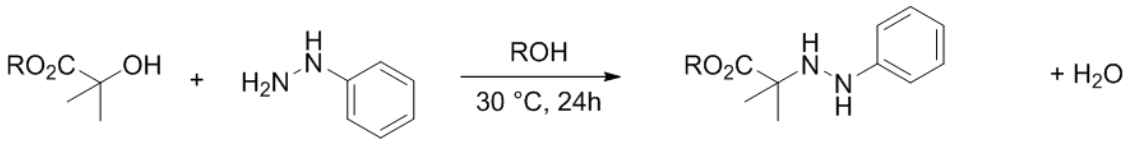

21 (R=H)
49 (R=Et)

27

51 (R=H) 68%
53 (R=Et) 72%

Scheme 3.9 Generic scheme for the synthesis of the isobutyric acid **21** and ethyl isobutyrate **49** with phenylhydrazine **27**.

The excellent chemical purity and yields make this synthetic pathway highly practical allowing cost-efficient scale-up (100 g) of the compounds **50-53**.

As previously mentioned the ethyl ester of 2-hydroxyisobutyric acid is a readily available commercial product and subsequently the Fischer-Speier esterification step, carried out in the citrate and tartronate series, was not chosen, in favour of purchasing the starting material. As observed previously the small-scale reactions in the isobutyrate series resulted in excellent chemical purities and yields of up to 98%. The practicality of these reactions allowed the synthesis of up to 100 g of the compound **50**, in similarly good yields of up to 95%.

As documented in the previous chapters, the characterisation of the isobutyrate derivatives was carried out using a combination of analytical techniques. Significant peaks in the IR spectrum for the characterisation of hydrazo molecules account for the C-N, N-H and N-N stretching vibrations. The quaternary carbon alpha to the hydroxyl group in 2-hydroxyisobutyric acid

eliminated formation of isomeric derivatives and consequently no C=N bonds were observed in the IR spectra of the isobutyrate series. All compounds **50-53** exhibit a strong peak in the region of 1000-1300 cm^{-1} (C-N) confirming the formation of the new bond. The essential IR peaks for the characterisation of the novel compounds are listed in Table 3.28.

Table 3.28 IR data for compounds **50-53**

Compound	C-N[a]	N-H[b] (bend)	N-H[c] (stretch)	C=O[d]
50	1171	1546	3324	1651
51	1174	1551	3302, 3377	1600
52	1189	1504	3347	1639
53	1139	1522	3301, 3377	1601

a Typical region 1000-1300 cm^{-1}
b Typical region 1490-1650 cm^{-1}
c Typical region 2300-3500 cm^{-1}
d Typical region 1600-1750 cm^{-1}

As in the previously series', proton exchange occurred between the NH and OH protons and the NMR solvent. This made identification of these protons impossible in the ^{1}H NMR. Due to this exchange only one signal was present in the aliphatic region of the spectrum for the isobutyrate compounds. Compound **51** was further confirmed by the presence of the aromatic peaks between 7.4 ppm and 6.8 ppm. Although the ^{1}H NMR data did not provide sufficient evidence for structural characterisation it confirmed that for the compounds **50-53** were present in high purity. The mass spectrometry data further confirms the characterisation of compounds **50-53**.

3.9.1.1 Oxidation of the Isobutyrate Derivatives

As previously mentioned, it is understood that a high percentage of the gas evolved upon the decomposition of ADCA is nitrogen gas generated primarily from the azo, nitrogen-nitrogen double bond. In attempt to replicate this behaviour compounds attempt was made to oxidise the hydrazo bond in compounds **50** and **52** to the corresponding derivatives **50.1** and **52.1**. (Figure 3.76)

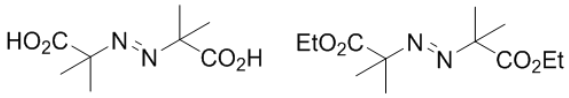

50.1 **52.1**

Figure 3.76 Chemical structure of the oxidised compounds **50.1** and **52.1**.

3.9.1.1.1 Oxidation of Hydrazo Compounds with Copper Acetate

The 1999 publication by M. Hristova-Kazmierski and J. Kepler in the Journal of Labelled Compounds and Radiopharmaceuticals [160] reports the oxidation of biurea to azodicarbonamide with copper acetate in the presence of ammonium nitrate at 115 °C in yields up to 86%.

An attempt to oxidise compounds **50** and **52** under these conditions did not lead to azo derivatives **50.1** and **52.1**. (Figure 3.76) Multiple issues during work up of the reaction including inefficient separation of copper catalyst as well as sensitivity of the target azo compound to basic conditions have been identified.

This suggests that this method was not a viable oxidation technique for the hydrazo bond in these compounds.

3.9.1.1.2 Oxidation of Hydrazo Compounds with Potassium Fluoride

The work of Mihara *et al* in 2007 [161] presents a solvent free oxidation of hydrazo compounds in the presence of potassium fluoride on aluminium oxide (KF/Al_2O_3). This reaction was carried out on compound **50**, in attempt to yield the azo derivative **50.1**, at 80 °C for 1 hour. Low solubility of compound **50.1** in diethyl ether resulted in no separation of the compound from the catalyst. Alternative solvents were attempted. (Table 3.29)

Table 3.29 Work up conditions and results for the oxidation reaction of compound **50.1** in the presence of KF/Al_2O_3.

Solvent	**Result**
Diethyl ether	No product obtained
Ethyl acetate	No product obtained
Ethanol	Yellow solid isolated
Dichloromethane	No product obtained

The wash with ethanol yielded a yellow solid; however, as well as dissolving the product; ethanol partly dissolved the catalyst, not allowing for separation of the two materials. The solubility issues of the product made the use of the solid-state oxidation impractical.

Attempts to yield to oxidised, azo compounds proved unsuccessful; however, the potential for the hydrazo derivatives to yield both by nitrogen and carbon dioxide gases was investigated through the formulation testing of the derivatives **50**-**53**.

3.9.2 Thermal Behaviour, Stability and Decomposition Pathway of Compounds 50-53

Thermal gravimetric analysis (TGA) and differential scanning calorimetry (DSC) were used to evaluate the thermal properties of compounds **50-53** and predict the behaviour of the additives within the coating formulation at various cure temperatures. Typical temperatures are summarized in Table 3.30.

Table 3.30 TGA and DSC data for the compounds **50-53**.

Compound	TGA		DSC
	$T_{-10\%}$[a]	T_{max}[b]	T_{DSC}[c]
50	111	168	179
51	106	129, 211	230
52	38	66, 152	85
53	54	74, 231	144

a Temperature at 10% mass loss in the TGA
b Maximum thermal degradation temperature from the 1st derivative of the TGA
c Phase transition temperature in the DSC

The isobutyrate series showed significant differences in the thermal stability between the acids **50** and **51** and the esters **52** and **53** (Figure 3.77). Compound **52** showed an uncharacteristically low first T_{max} in the first derivative of the TGA analysis. It was determined from the TGA data that compound **50** underwent a one-step thermal decomposition process, characterised by T_{max} at 168 °C. Compounds **51**-**53** showed evidence of a two-step process due to the presence of a clear second band in the DTG data.

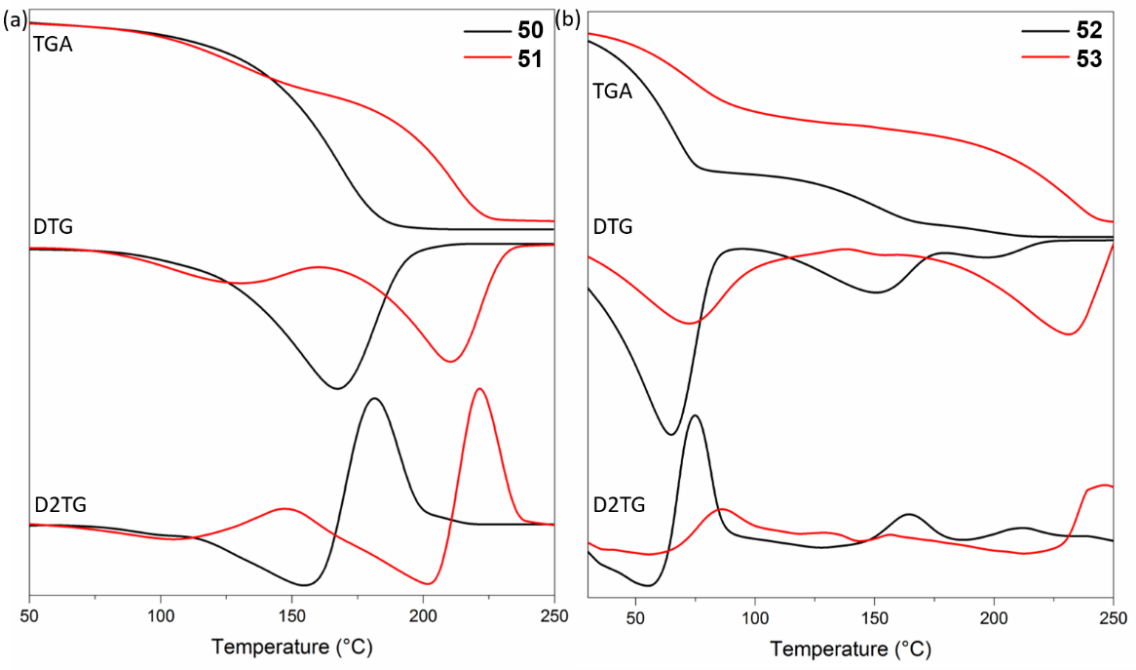

Figure 3.77 TGA, first derivative DTG and second derivative D2TG data for (a) compounds **50**-**51** and (b) compounds **52**-**53**.

Compound **51** showed T_{max} in the ranges of 129 °C and 211 °C, correlating T_{DSC} at 128 °C and 230 °C. As predicted in the case of citric acid, this two-step pattern could be a result of the decarboxylation of the acidic group during decomposition. Compound **51** exhibits 10% mass loss at the lower temperature of 106 °C, which can be attributed to water volatilisation, as this occurs at lower temperature than decomposition as observed in the first derivative graph, T_{max} onset of the first pyrolysis was observed at 129 °C, whilst the second pyrolysis step (accounting for approx. 65% weight loss) happens at the much higher temperature of 211 °C and coherent with T_{DSC}=230 °C (Figure 3.78). Although at the higher end, this temperature still coincides with melt viscosity range of PVC.

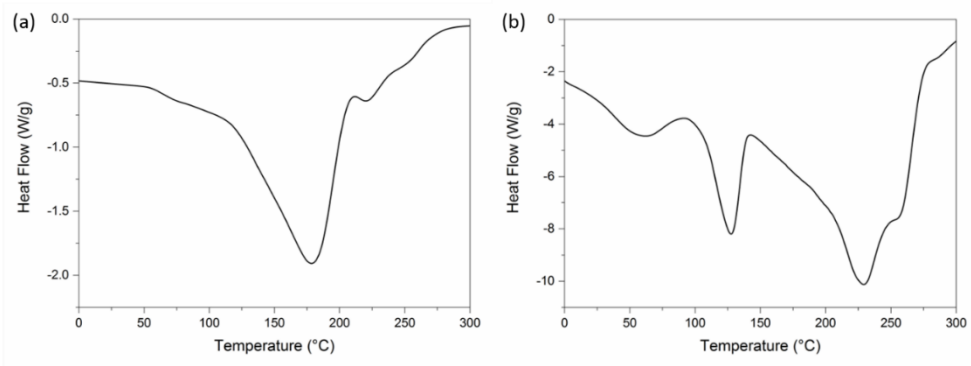

Figure 3.78 DSC data for (a) compound **50** and (b) compound **51**.

In the case of compound **52**, T_{max} was uncharacteristically low, showing at 66 °C; however, the second band appearing at 152 °C, and attributing to a 30% mass loss was within the melt viscosity range of the PVC plastisol. That said, a lower decomposition temperature could result in a more economic process as manufacturing temperatures could be reduced. Therefore, it was beneficial to analyse the efficiency of compound **52** at the suitable range of curing temperatures to investigate if the gas pockets were retained within the plastisol throughout the heating and curing process.

Compound **53** also showed a two-step process in the first derivative data. The two bands in the DTG analysis appeared at 74 °C and 231 °C. The large range between these transitions could be attributed to a melt and subsequent decomposition/ evaporation. The melt transition can clearly be seen in the DSC data, represented by a sharp peak at 144 °C. (Figure 3.79)

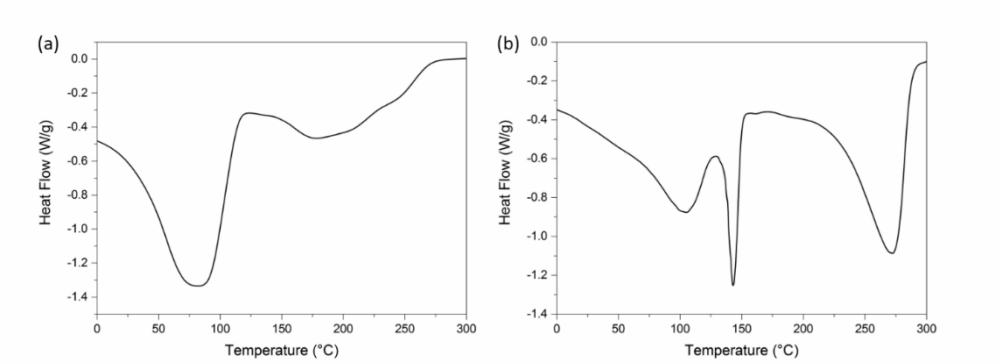

Figure 3.79 DSC data for (a) compound **52** and (b) compound **53**.

In the case of the acid compounds **50** and **51** both T_{max} and T_{DSC} were observed within the suitable melt viscosity range of PVC plastisol. Both compounds showed an onset of thermal degradation temperature in the range of 150 °C. The TGA analysis of compound **50** showed a plateau at 194 °C, showing a total loss of 99%. This is advantageous when compared to the control ADCA. In the TGA of ADCA is was identified that mass loss initiated at 200 °C. This suggests that kicker additives would be required at lower temperatures in the case of compound **50**. The lower decomposition temperature observed in the case of compound **50** would lead to a more economical industrial process.

3.9.3 PVC Coating Formulations, Temperature Dependency and Colour Correlation of the Isobutyrate Series

The isobutyrate series produced pale and dark orange oils, and a strongly coloured solid in the case of compound **51**. It was predicted that, similarly to the citrate and tartronate series, the highly coloured materials would retain their colour during the formulation and curing stages of the coating process. For this reason, compounds **50** and **52**, the pale coloured oils, were scaled up for multiple coatings tests. In the first instance the strongly coloured aromatic compounds **51** and **53**, were analysed at 210 °C only, with a view to scale up for further analysis if the initial tests identified a workable colouration after curing.

The compounds **50-53** were formulated under the standard manufacturing conditions to produce plastisol coated samples containing each additive (**P50**-**P53**) at molar equivalent concentrations to azodicarbonamide in the control $\mathbf{P_{ADCA}}$. Furthermore, efficient scale up of compounds **50** and **52**, allowed for a greater scope of tests to be carried out. The compounds were tested under the standard concentration (**P50-P53**), at double concentration (**P50a** and **P52a**) and at double concentration without the presence of kickers (**P50b** and **P52b**). Expansion levels, gloss and colour of the manufactured samples were compared for all cases.

Samples **P50-P53** were formulated to a standard specification, manufactured and analysed to determine the effect on coating efficiency, surface wetting and coating coverage. The formulations have been cured at 130 °C, 150 °C, 170 °C, 190 °C, 210 °C and 230 °C to correspond with the melt viscosity range of the PVC plastisol. This allowed temperature dependency studies to be carried out for each of the materials. **P51** and **P53** were treated at 210 °C only to determine the initial potential of these materials as lower yields were observed in the large-scale reactions. Furthermore, it was decided that the presence of aromatic rings, increased exposure to benzene gas during decomposition which was unbeneficial to the overall manufacturing process. These compounds were subsequently ruled out as potential alternatives to ADCA.

The phenyl derivatives **51** and **53** were tested and measured for L*a*b* data at 210 °C. The samples showed significantly more colouration than their symmetrical counterparts (**50** and **52**). (Figure 3.80)

Figure 3.80 Photographic images of samples **P50-53$_{210}$**.

Increased b* values of 8.34 and 8.52 for compounds **51** and **53** respectively, were observed. These increased b* saturations were evident as a stronger yellow colour was observed with the naked eye. These results agree with the L*a*b* values observed for the phenyl derivatives in both the citrate and the tartronate series' and further support the decision to eliminate phenyl derivatives as potential alternatives to ADCA.

Table 3.31 shows L*a*b* and ΔE data for the thermally cured plastisols **P50** and **P52** containing compounds **50** and **2**. As in the previous series the L*a*b* values obtained for the formulated plastisols cured at 130 °C have been set as the control samples **P50$_{130}$** and **P52$_{130}$** to monitor temperature dependent colour change (ΔE) for each formulation.

Table 3.31 L*a*b* data and ΔE for samples **P50**, **P52** and **P$_{ADCA}$**.

	130 °C			**ΔE**				
Entry	**L***	**a***	**b***	**150 °C**	**170 °C**	**190 °C**	**210 °C**	**230 °C**
P50	93.36	-0.32	1.74	1.07	0.48	0.53	2.25	3.27
P52	93.76	-0.50	2.46	0.70	1.08	1.81	0.12	2.82
P$_{ADCA}$	92.55	-0.96	11.55	0.51	0.53	1.18	6.81	

Samples **P50** and **P52** formulated with **50** and **52** respectively, showed minimal colour changes across the temperature range. (Figure 3.81) This suggested that full thermal decomposition of compounds **50** and **52** produced no strongly coloured residual by-products. This property is advantageous in colour sensitive applications such as the wallpaper industry. The ΔE values across the range of 130 – 230 °C, is correctable using bleaching agents such as titanium dioxide or various optical brighteners. Although little change was observed in the surface colour over the temperature range, it was noted that in the case of compound **50** the lowest ΔE values of 0.48 and 0.53 (for samples **$P50_{170}$** and **$P50_{190}$**) coincided with T_{max} = 168 °C and T_{DSC} = 179 °C, further suggesting that the surface colour is resultant of the decomposition of compound **50**.

Figure 3.81 Photographic images of samples **$P50_{130}$** – **$P50_{230}$** and **$P52_{130}$** – **$P52_{230}$**.

The initial coating samples were made with molar concentrations of compounds **50**-**53** equivalent to the control formulation **P_{ADCA}**. However, further plastisol formulations containing double molar concentrations of compound **50** and compound **52** were prepared with (**P50a** and **P52a**) and without (**P50b** and **P52b**) kicker additives. The double concentration samples were cured at 170 and 190 °C, in agreement with the observed TGA decomposition ranges of the raw materials and the results of the molar equivalent samples, **P50** and **P52**. ΔE was calculated to analyse any difference in colour between the 1M (**P50** and **P52**) and 2M (**P50a**, **P50b** and **P52a**, **P52b**) samples at each temperature.

The L*a*b* data for the range of samples tested at 170 and 190 °C is tabulated below (Table 3.32).

Table 3.32 L*a*b* data for samples **$P50_{170}$** – **$P50_{190}$** and **$P52_{170}$** – **$P52_{190}$** with ΔE for **P50a**, **P50b**, **P52a** and **P52b**.

	Temp (°C)	L*	a*	b*	ΔE a[1]	ΔE b[2]
50	170	93.78	-0.34	1.5	**0.28**	**0.69**
	190	93.58	-0.46	2.2	**0.28**	**0.46**
52	170	93.98	-0.76	3.49	**1.91**	**2.54**
	190	93.86	-0.92	4.22	**2.14**	**3.20**

1 ΔE a = P50a and P52a containing double concentration of additive
2 ΔE b = P50b and P52b containing double concentration of additive and no kicker complexes

The observed colour data for sample **P50** remained constant. This confirmed that compound **50**, produced little to no colour and was not influenced by the presence of the kicker additives. If the trend follows, it would suggest that the concentration of compound **50** could be increased or decreased to the desired requirements, without influencing the surface colour of the coating. This is a very advantageous property in the manufacture of decorative and colour sensitive products. Furthermore, it suggests that the presence of compound **50**, should have little/no influence on further colouration of the formulation with pigments and dyes. This colouration test could be carried out as future work, by comparing the L*a*b* data of coloured formulations containing compound **50** in various concentrations.

P52a, shows an increase in ΔE when the concentration of compound **52** is doubled. ΔE is further increased in **P52b**, where compound **52** is doubled and the kicker additives are removed. Although higher ΔE values are observed, the colour change is from lower b* saturation. In this case less colour is observed on the surface of samples **P52a** and **P52b**. ΔE only measures the change in colour and higher numbers do not necessarily represent more colouration in the samples. This suggested that the surface colour was influenced by the novel additives and that higher concentrations of **52**, dispersed colour from the formulation. The levels of coloration observed in all samples in the isobutyrate series are correctable using optical brighteners and bleaching processes.

3.9.4 Surface Texture and Microstructure of the Isobutyrate Series

3.9.4.1 Surface Texture Analysis of the Isobutyrate Series

The external and the internal cellular structure of the paper samples **P50**-**P53**, formulated with compounds **50**-**53**, were analysed with scanning electron microscopy (SEM). The samples were compared to the control expanded plastisol $\mathbf{P_{ADCA}}$ which has a smooth, matt finish. These were the desired physical properties in the cases of **P50**-**P53**. A standard 'blank' formulation $\mathbf{P_{blank}}$ was also prepared via the same method for comparisons. $\mathbf{P_{blank}}$ presents an uneven surface. (Figure 3.82)

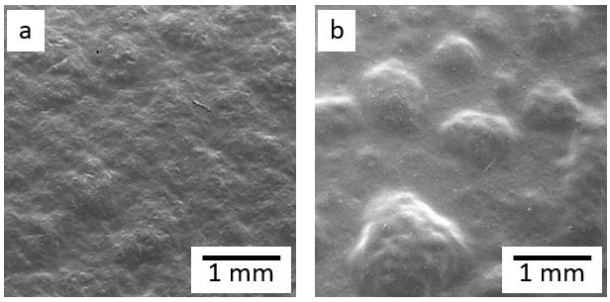

Figure 3.82 SEM surface micrographs of the controls (a) $\mathbf{P_{ADCA}}$ and (b) $\mathbf{P_{blank}}$ at x18 Mag.

All compounds in the isobutyrate series showed a relatively smooth external surface in the SEM micrographs of the 210 °C samples (Figure 3.83).

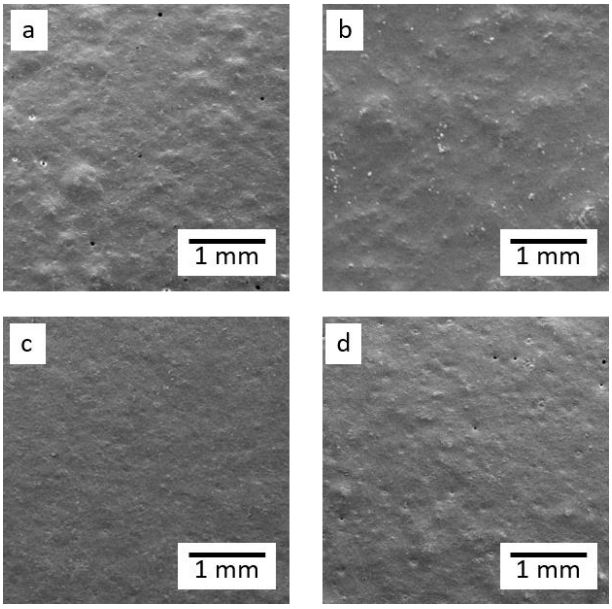

Figure 3.83 SEM surface micrographs of samples (a) $\mathbf{P50_{210}}$, (b) $\mathbf{P51_{210}}$, (c) $\mathbf{P52_{210}}$ and (d) $\mathbf{P53_{210}}$ at x18 Mag.

Small pinhole defects were observed on the surfaces of samples **P50** and **P53**; however, the structure of the surfaces was homogeneous, which is an advantageous result.

The trivial synthesis of compounds **50** and **52** allowed for a range of sample tests to be ran. Across the temperature range, variances were observed in the surface micrographs of **P50** and **P52**. (Figure 3.84)

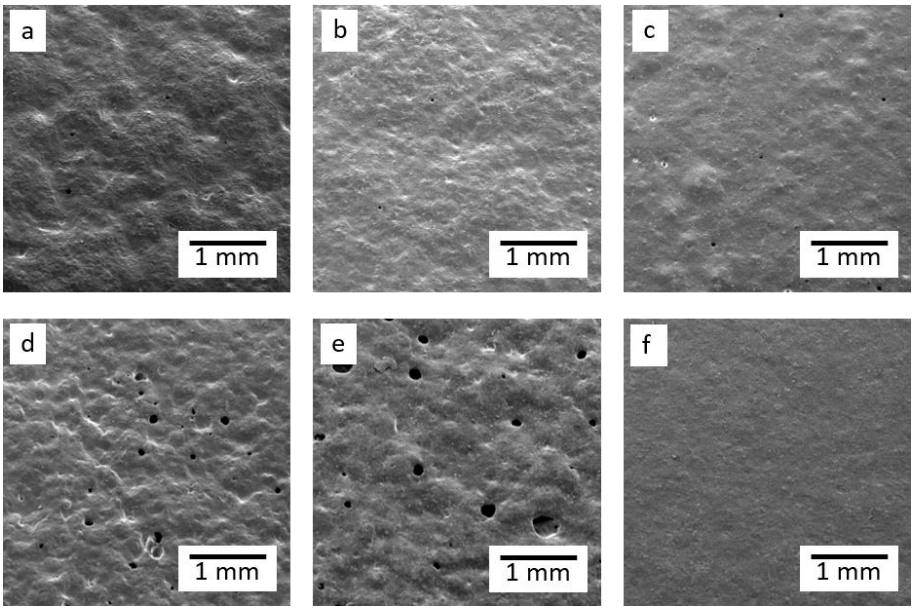

Figure 3.84 SEM Surface micrographs of samples (a) **P50$_{170}$**, (b) **P50$_{190}$**, (c) **P50$_{210}$**, (d) **P52$_{170}$**, (e) **P52$_{190}$** and (f) **P52$_{210}$** at x18 Mag.

At the lower temperatures, **P50$_{170}$** and **P50$_{190}$** (a, b, Figure 3.84) showed a similar surface topography to that observed in the control sample **P$_{ADCA}$** (Figure 3.82) the smooth but homogeneous texture is a desired physical property in the decorative wallcoverings industry. [xxii] The surfaces shown for the lower temperatures exhibit significantly more texture than the corresponding P9$_{210}$ coating. (c, Figure 3.84) this is in agreement with the thermal analysis, which shows T_{max} at 168 °C and T_{DSC} at 179 °C. Decomposition around these temperatures would create more disorder within the system and consequently disrupt the surface of the formulation coating.

[xxii] Graham & Brown – Market Research

In the case of compound **52**, significant surface defects were observed in the lower temperature micrographs when compared to sample **P52$_{210}$**. (f, Figure 3.84). This result is likely due to the low decomposition point of compound **52**, observed in the TGA and DSC analysis. At lower temperatures the plastisol has a lower viscosity[xxiii] and this can lead to increased disruption of the surface by gases formed. The size of the surface defects was increased in sample **P52$_{190}$** when compared to **P52$_{170}$**, suggesting a higher level of incompatibility at 190 °C.

The double concentration tests were also analysed by SEM. The below image (Figure 3.85) shows the surface micrographs for samples **P50**, **P50a** (double concentration) and **P50b** (double concentration minus kickers) for both 170 °C and 190 °C.

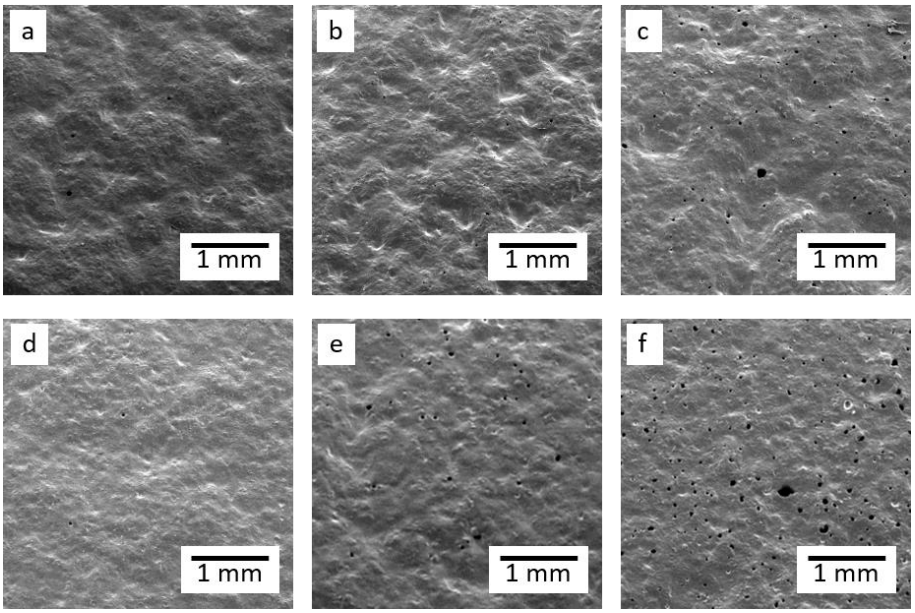

Figure 3.85 SEM surface micrographs of samples (a) **P50$_{170}$**, (b) **P50a$_{170}$**, (c) **P50b$_{170}$**, (d) **P50$_{190}$**, (e) **P50a$_{190}$** and (f) **P50b$_{190}$** at x18 Mag.

The SEM micrographs for the concentration investigation showed that as the concentration is doubled (**P50a** – b, e, Figure 3.85) more pinholes are present on the coating surface. At 170 °C (b, Figure 3.85), the pinholes are significantly smaller than observed in the corresponding 190 °C sample. Furthermore, the 170 °C sample, **P50a$_{170}$**, had retained its textured surface, observed in the single concentration sample **P50$_{170}$**.

[xxiii] Private communication – Information from Graham & Brown Viscosity Study 2015

When the kickers were removed, the number of pinholes increased significantly, with an average number of 92.7 and 136.7 per 3mm^2 for samples **P50b$_{170}$** and **P50b$_{190}$** respectively. (Figure 3.86)

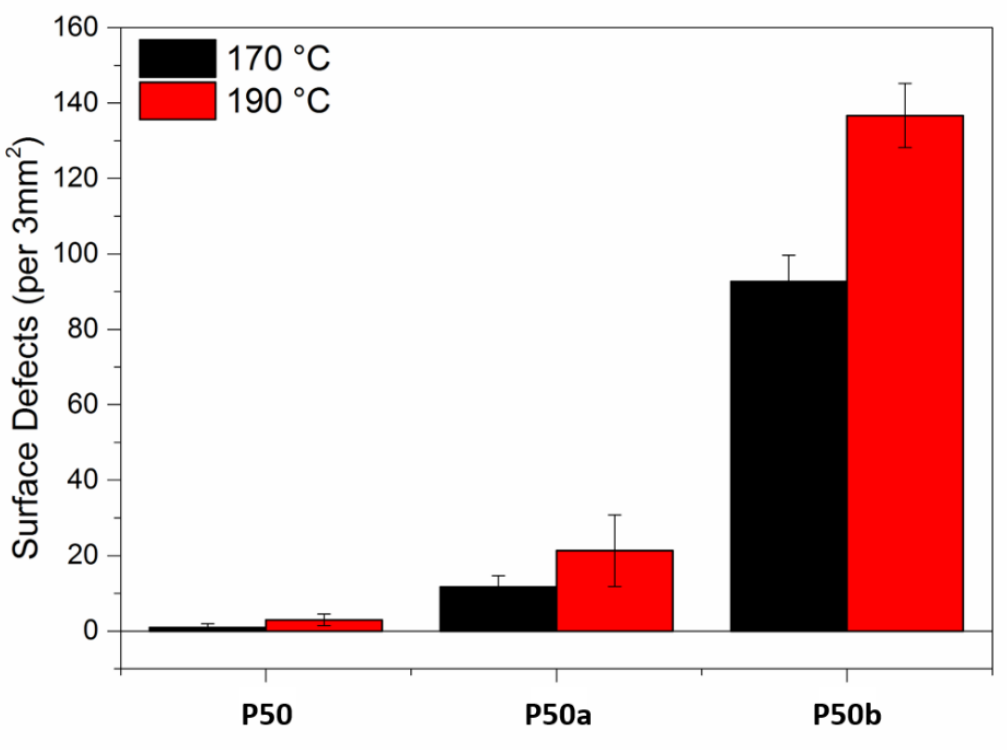

Figure 3.86 Bar graph depicting the number of pinhole defects per 3mm^2 for samples **P50**, **P50a** and **P50b** at 170 °C and 190 °C.

This significant difference between the samples with and without kickers provides evidence that the kicker complexes add stability to the formulation. Although tailored to suit the requirements of ADCA, the materials prove to even out the distribution and gas production of additive **50** also. As in the double molar equivalent samples **P50a**, the samples without kickers **P50b**, showed significantly more pinhole defects in the 190 °C sample. With the exception of the molar equivalent samples which both show minimal defects (a, d Figure 3.85), on average 70% more pinhole defects were observed in the 190 °C sample. This confirms that the system is more unstable at 190 °C and is in agreement with the thermal analysis data.

The samples **P52**, showed the opposite effect to **P50**, when the concentration was doubled (**P52a**) and the kickers were removed (**P52b**). At both temperatures when the concentration was doubled, the resultant coating was significantly smoother with almost no visible pinhole defects. (Figure 3.87)

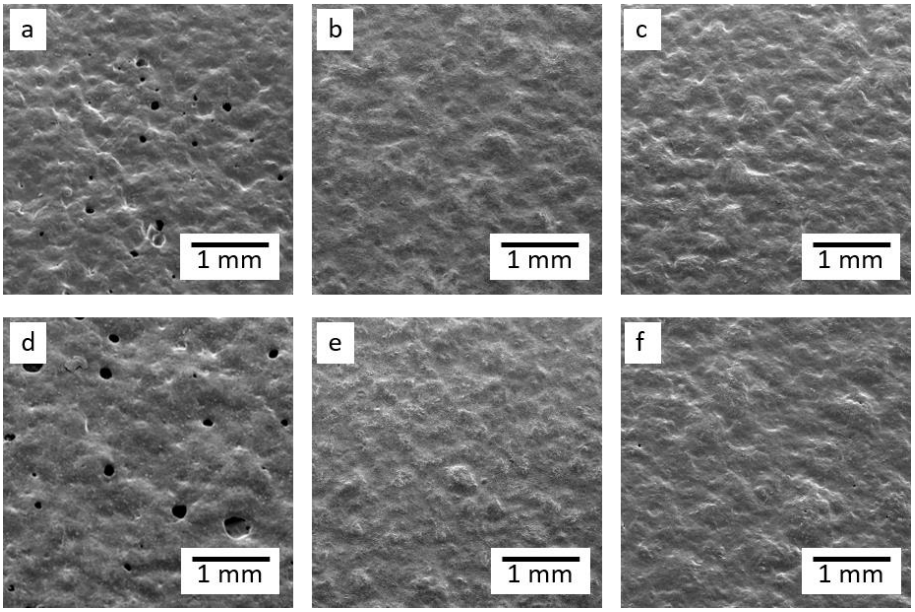

Figure 3.87 SEM surface micrographs of samples (a) **P52$_{170}$**, (b) **P52a$_{170}$**, (c) **P52b$_{170}$**, (d) **P52$_{190}$**, (e) **P52a$_{190}$** and (f) **P52b$_{190}$** at x18 Mag.

This data suggests that at higher concentrations the material acts as a levelling agent by reducing the surface tension and increasing the distribution of the formulation. This effect was also observed in the ethyl ester derivatives in the citrate series (chapter 3.7.4). Further confirming the theory that reduced hydrogen bonding allows for more even distribution and levelling effects by the additives. In the case of **P52**, limited differences were observed between the samples with and without the kicker complexes.

3.9.4.2 Surface Gloss Analysis of the Isobutyrate Series

The glossmeter readings of the plastisol coatings **P50$_{130}$-P50$_{230}$**, **P52$_{130}$-P52$_{230}$**, **P51$_{210}$** and **P53$_{210}$** were taken to analyse the gloss of each sample surface and identify trends in their physical properties. The glossmeter readings, measured in Gloss Units (GU) were taking using an 85° beam angle, GU readings under 10.0 are considered matt, which is the desired physical property for this application.

The gloss data for the various plastisol samples of **P50** and **P52** are tabulated below (Table 3.33).

Table 3.33 Gloss readings for compounds **P50**-**P53**.

Sample	85° Beam Angle Reading (GU)					
	130 °C	150 °C	170 °C	190 °C	210 °C	230 °C
P50	14.0	4.4	3.2	5.6	8.1	3.6
P50a	-	-	2.9	3.9	1.7	-
P50b	-	-	2.8	4.1	2.3	-
P52	4.0	2.1	2.3	3.9	27.0	11.9
P52a	-	-	5.3	4.0	3.1	-
P52b	-	-	4.2	4.3	4.3	-
P51	-	-	-	-	12.8	-
P53	-	-	-	-	19.6	-

The graph (Figure 3.88) shows that no linear trend was observed in the cases of **50** and **52**.

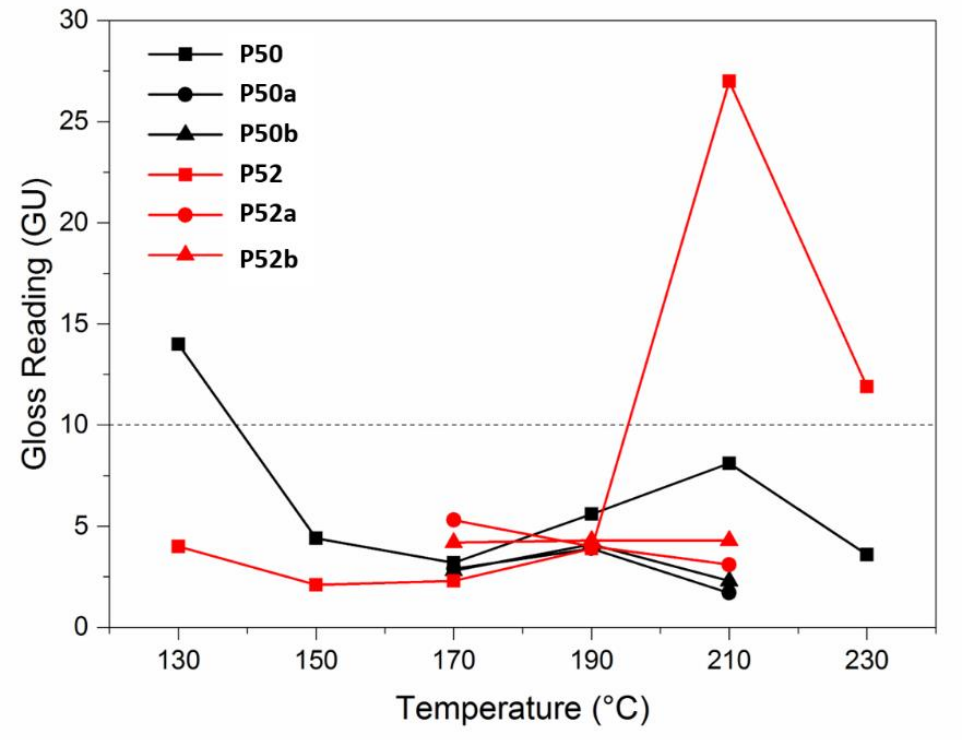

Figure 3.88 Graph depicting gloss values for samples **P50** and **P52**, with the upper region of the matt region (10 GU) highlighted.

However, it was observed that at curing temperatures 150-210 °C for compound **50** and 130-190 °C for compound **52**, the formulated coatings are within the matt region. This is in agreement with the thermal degradation and colour indexing data of compound **50** that suggests that decomposition of the material occurs within this range. Despite compound **52** demonstrating significant weight loss at lower temperatures in its TGA graph, the glossmeter readings, along with the L*a*b* data suggest that changes in the physical properties are still observed in the samples at higher temperatures.

The significant jump in GU between samples **P52$_{190}$** and **P52$_{210}$**, suggested that the levelling properties of the additives within the formulation had changed. This could be resultant of the residual decomposition products of compound **52** within the formulation. Stability at these higher temperatures could allow these residual materials to act as levelling agents, increasing distribution across the coating and resulting in a glossier surface. This result is concurrent with the SEM surface micrographs that show a significantly smoother surface in the case of **P52$_{210}$**.

As the temperature was further increased 230 °C, the gloss of both **P50$_{230}$** and **P52$_{230}$**, was reduced significantly. This result correlates with the surface topography which showed that when the temperature increased, the evenly distributed expansion collapsed to form large gas pocket defects upon the coating surface (Figure 3.81). These defects therefore, disrupted the gloss of the coating surface.

When the concentration of compounds **50** and **52** was doubled (**P50a** and **P52a**) and the kicker complexes removed (**P50b** and **P52b**), the gloss reading of the coating surfaces remained constant across the temperature range analysed. In the case of both compound **50** and **52**, the samples analysed at 170 °C and 190 °C all showed very little change in GU. That said at a curing temperature of 210 °C, doubling the concentration (**P50a$_{210}$** and **P52a$_{210}$**) resulted in a significantly less glossy coating surface when compared to the corresponding molar equivalent formulation. (**P50$_{210}$** and **P52$_{210}$**). This suggests that increasing the concentration of the additives, increases the uniform gas formation with in the plastisol matrix. The formation of small, evenly dispersed cells creates a smooth, matt coating surface as observed in samples **P50a$_{170\text{-}190}$**

and **P52a$_{170\text{-}190}$**. This result further suggested that the optimised temperature for compounds **50** and **52** is between 170 °C and 190 °C. The removal of the kickers from the formulation at 210 °C (**P50b$_{210}$** and **P52b$_{210}$**) showed a slight increase in GU from the double concentration corresponding sample (**P50a$_{210}$** and **P52a$_{210}$**), but still shows a significant reduction in GU when compared to the molar equivalent samples (**P50$_{210}$** and **P52$_{210}$**). This result suggests that the kicker compounds act as levelling agents within the formulation in increase distribution and therefore increase observed gloss levels.

Formulations containing compounds **51** and **53**, were treated at 210 °C to give **P51$_{210}$** and **P53$_{210}$** respectfully. Both of these samples were within the semi-gloss region (10-75 GU). As shown in the symmetrical derivatives (**50** and **52**), the acid compound **51** gave a lower GU result than the corresponding esterified derivative **53**. This result is conclusive with the results observed in the previous series, further confirming that the esterified materials allow for a reduced surface tension due to the reduced number of H-bonding sites. This lower surface tension allows the materials to be more evenly dispersed across the coating surface, producing a glossier effect.

3.9.4.3 Microstructure Analysis of the Isobutyrate Series

Cross-section micrographs provided information of the internal cellular structure of samples **P50-P53**. As in the previous series the additives **50-53** formed gas pockets within the coating confirming that the compounds do act as blowing agents in some capacity. The novel formulations were compared with the controls **P$_{blank}$** and **P$_{ADCA}$** as in the previous series. (Figure 3.89)

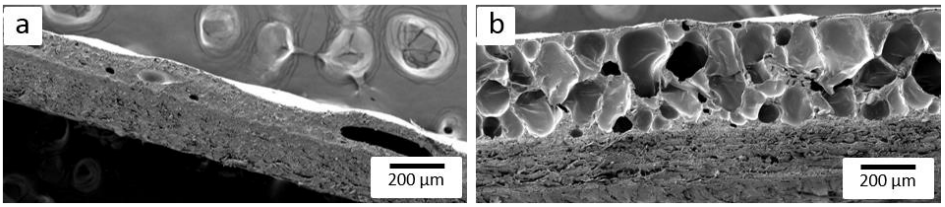

Figure 3.89 SEM cross-section micrographs of samples (a) **P$_{blank}$** and (b) **P$_{ADCA}$** at x75 Mag.

In the case of sample **P50$_{210}$**, (a, Figure 3.90) the cross-section analysis indicated that the additive **50** formed minimal gas cells within the plastisol matrix, resulting in no expansion of the formulation layer. The cells observed in the cross-section micrograph are evenly distributed and show a small cell size range

of 33-83 µm. That said the formulation layer had contracted from an initial 200 µm, to approx. 170 µm after curing at 210 °C. This suggests that compound **50** is not evenly dispersed within the plastisol coating, resulting in telegraphic effects across the coating surface.

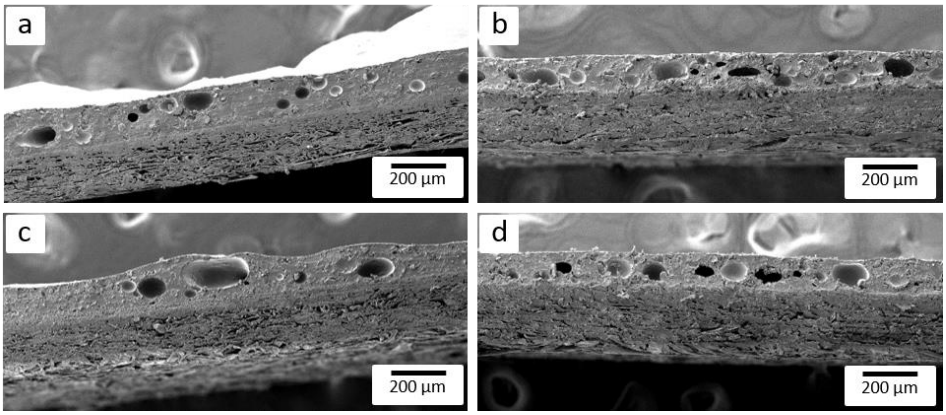

Figure 3.90 SEM cross-section micrographs of samples (a) **P50$_{210}$**, (b) **P51$_{210}$**, (c) **P52$_{210}$**, and (d) **P53$_{210}$** at x75 Mag.

The cross-section micrograph of **P52$_{210}$**, (b, Figure 3.90) again shows that minimal gas cells have formed and even distribution was not obtained within the plastisol matrix. In the case of **P52$_{210}$** the observed cells are larger than those in sample **P50$_{210}$** with an average cell size of 125 µm.

In the case of the phenyl derivatives, **P51** and **P53**, (c, d, Figure 3.90) the dispersion of the gas cells is more even than in the aliphatic derivatives **50** and **52**. This suggests that the system is more favourable; however, the cells produced do not contribute to the expansion of the material with plastisol depths of 126 µm and 115 µm observed for samples **P51** and **P53** respectively. This is significantly lower than the 200 µm initial draw down depth.

Despite the formation of cells within the formation, the results of the samples **P50$_{210}$**-**P53$_{210}$** suggest that the additives **50**-**53** have little effect on the overall microstructure of the coatings. This conclusion can be drawn from the similarity in cross-section micrographs containing the synthesised additives **P50$_{210}$**-**P53$_{210}$** compared with the blank sample **P$_{blank}$**. To further investigate the properties of the additives, compounds **50** and **52** were analysed at a range of temperatures and concentrations, the cross-section micrographs for samples **P50$_{170\text{-}190}$**, **P50a$_{170\text{-}190}$** and **P50b$_{170\text{-}190}$**, are shown below in Figure 3.91.

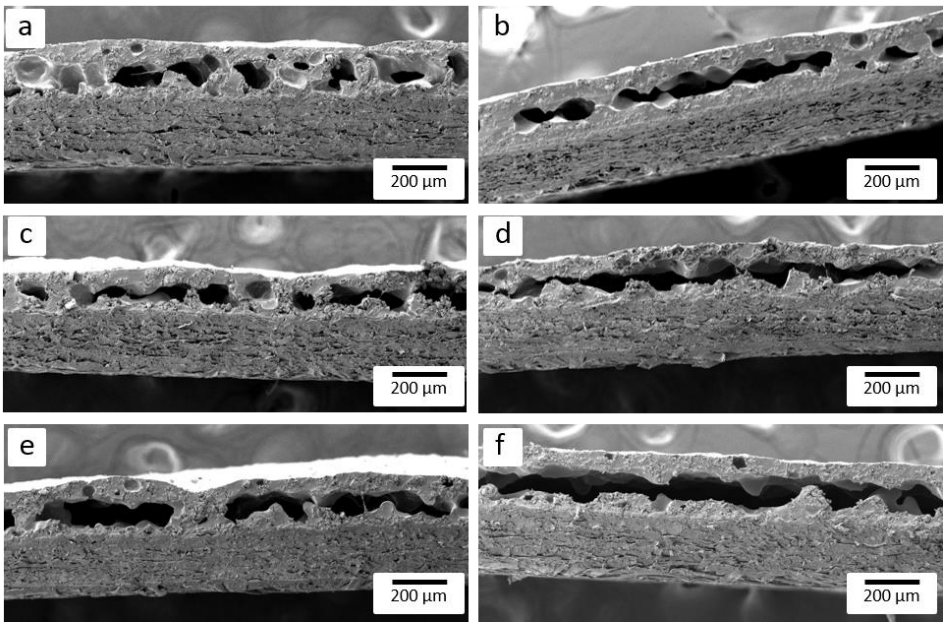

Figure 3.91 SEM cross-section micrographs of samples (a) **P50$_{170}$**, (b) **P50$_{190}$**, (c) **P50a$_{170}$**, (d) **P50a$_{190}$**, (e) **P50b$_{170}$** and (f) **P50b$_{190}$** at x75 Mag.

Molar equivalents **P50$_{170}$** and **P50$_{190}$** (a, b, Figure 3.91) showed an increase in expansion of approx. 30 µm when compared to the corresponding 210 °C sample. However, no overall expansion was observed from the 200 µm starting point. This is insignificant when compared to the desired expansion of approx. 400 µm, observed in the case of **P$_{ADCA}$**.

More evenly distributed cells were observed in the 170 °C samples. In the case of sample **P50$_{190}$**, (b, Figure 3.91) the gas produced had formed an open cell structure within the formulation. An open cell structure is the result of two or more gas cells merging together and forming open cellular channels with in the plastisol matrix. The presence of open cell channels within the plastisol is not an ideal property as the risk of surface collapse is increased. That said, if the coating fit the commercial specification, the open cellular structure would not present a regulatory issue in non-safety related products.

At both temperatures (c = 170 °C and d = 190 °C in Figure 3.91), doubling the concentration of compound **50** within the formulation had little influence on the internal structure. This suggests that the blowing capability of additive 9, had reached it capacity and that further increase in concentration would not affect the overall expansion of the plastisol layer of the coating.

When the kickers were removed (**P50b$_{170}$** and **P50b$_{190}$**) the cellular structure became more open. (e, f, Figure 3.91). This confirms the results of the

surface analysis that showed increased number of pinhole defects when the kicker compounds were removed from the formulation.

For all formulations, the corresponding 190 °C sample (b, d, f, Figure 3.91) showed a more open cell structure when compared to the 170 °C samples. (a, c, e, Figure 3.91) This confirms that additive **50**, is optimised to lower manufacturing temperatures. This data is conclusive with the findings of the TGA and DSC analysis which show decomposition temperatures within the range of T_{max} = 168 °C.

As observed in the case of compound **50**, **P52$_{170}$** showed an increase of approx. 50 µm in expansion, when compared to the sample cured at 210 °C (**P52$_{210}$**) higher temperatures. (Figure 3.92)

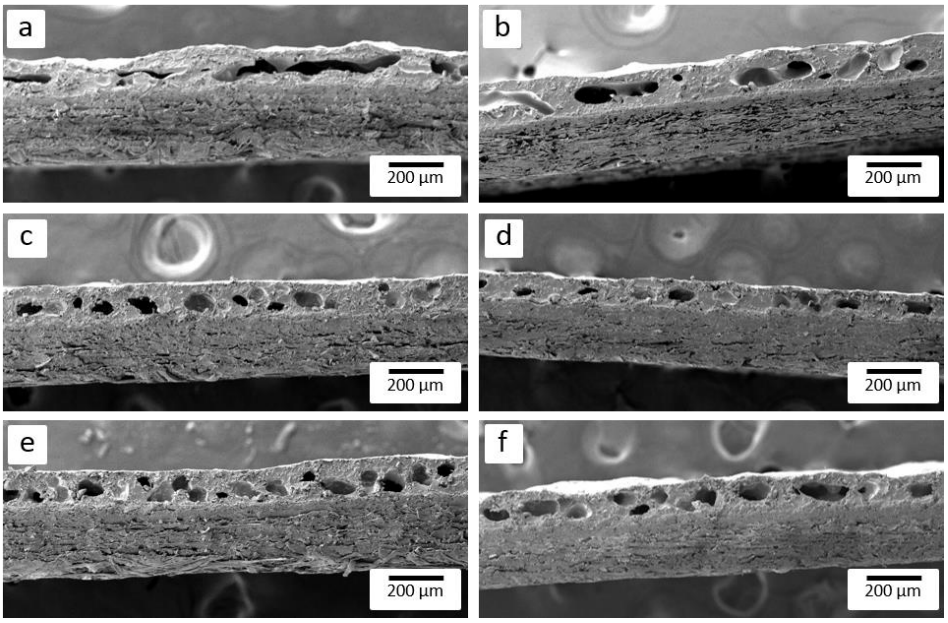

Figure 3.92 SEM cross-section micrographs of samples (a) **P52$_{170}$**, (b) **P52$_{190}$**, (c) **P52a$_{170}$**, (d) **P52a$_{190}$**, (e) **P52b$_{170}$** and (f) **P52b$_{190}$** at x75 Mag.

That said, the structure of the cells was more irregular at 170 °C (a, Figure 3.92) compared to higher temperatures. This result is conclusive with the DSC data for compound **52** which shows a secondary phase transition in the region of 175 °C and suggests more disorder within the formulation at this temperature. (Figure 3.79)

When the concentration of compound **52** was doubled (c, d, Figure 3.92) the distribution of cells within the plastisol matrix became more even. This suggests that increased levels of compound **52**, allows the material to act more

as a levelling agent. This is in agreement with the surface micrographs (Figure 3.87) which showed significantly smoother surfaces for sample **P52a** (double concentration) compared to **P52** (single concentration) at both 170 °C and 190 °C.

In sample **P52b**, where the concentration was doubled, and the kickers were removed, (e, f Figure 3.92) the cross-section micrographs are comparable to those of sample **P52a** (double concentration). This suggests that the kickers have little influence on the distribution of additive **52** within the system and that the concentration of the additive is the contributing factor.

Unlike in sample **P50** no significant open cellular channels were formed within the matrix of any of the formulations containing additive **52**. This could be resultant of the minimized H-bonding within the system, due to the esterification of the carboxylic acid group in compound **52**.

3.9.5 Conclusions of the Isobutyrate Series

The isobutyrate compounds **50-53** have been successfully synthesised and characterised. Synthesis of the compounds **50** and **52** was effectively scaled up to approx. 100 g in excellent yields of up to 80%. Attempts made to oxidise the hydrazo bond proved unsuccessful, as purification of the materials was not possible within the set synthetic guidelines in chapter 3.3

The TGA and DSC data confirmed that thermal degradation of compounds **50**, **51** and **53**, occurred within suitable range for implementation in PVC applications. In the case of compound **52**, lower temperatures were observed in the TGA data, but phase transitions in the region of 175 °C suggested some suitability to the melt viscosity of PVC.

PVC plastisol formulations containing compounds **50-53** have been prepared and thermal stability of the final formulations have been tested at different curing temperatures. The incorporation of the compounds **50-53** into commercial PVC plastisols directly affects the physical properties of the resultant coating. Despite the lower onset thermal decomposition temperature of compound **52**, formulation **P52** showed evidence of thermal degradation across the range of temperatures (130-230 °C) with the best results observed in correlation with the shoulder observed in the DSC *ca* 175 °C.

Thermal degradation data of the additive **50** and observed colour changes in the plastisol sample containing **P50** (ΔE, Table 3) were in an excellent agreement supporting a thermal decomposition between 150 °C and 190 °C curing temperatures. Furthermore, the L*a*b* data showed minimal colour change and was within a suitable range for decorative applications for compounds **50** and **52**. The efficiency of synthesis for compounds **50** and **52** allowed for variable formulations to be analysed including the addition of 2M equivalents of **50** and **52** (**P50a** and **P52a**) and the removal of kicker complexes (**P50b** and **P52b**).

In the case of all samples, gas cells were formed within the plastisol layer of the coating; however, in the samples cured at 210 °C a contraction of the initial 200 µm coating layer was observed. In the case of **P50**, an unfavourable open cellular structure was observed in the samples treated at 190 °C. Furthermore, the increased concentration of additive **50**, and the removal of the kicker complex had little effect on the physical properties observed in the cross-section micrographs, despite a significant increase in surface defects. This suggests that the formulation was not optimised to compound **50** in terms of maximising the potential blowing efficiency.

In the formulations containing additive **52**, doubling the concentration (**P52a**) benefited the physical properties of the coating by increasing distribution of the internal gas cells and creating a smoother surface. However, the gas formation was not significant enough to increase the observed expansion of the coating. The cellular structure was regular in size and distribution, suggesting some dispersion within the system for samples **P52a** and **P52b** at both 170 °C and 190 °C.

The study outlined in the chapters above proved that the incorporation of the compounds **50-53** into commercial PVC plastisols for wallpaper applications directly affects the physical properties of the resultant coating. However, the low expansion levels eliminate the compounds as direct replacements for ADCA. That said, additive **50**, showed potential in terms of both gas production and temperature range. Furthermore, the desired textured, matt surface was observed. Modification of various components in the formulation could optimise the system to maximise the results observed in the case of compound **50**.

3.10 Influences of the Formulation

3.10.1 Control Formulations

Formulations are complex matrixes, designed to fulfil the many requirements of a commercial product. A flexible coating formulation typically contains 10+ chemical components that work simultaneously to produce the desired physical and chemical properties of the specific design.[xxiv]

For simplicity and reproducibility all novel additives were analysed after addition to a standardised control plastisol. As expansion level is the focus of this project, the highest expanded manufactured plastisol[xxv] was selected as the control plastisol (**P_{ADCA}**) as these are the properties that need to be replicated by a novel additive. That said, the current standardised plastisol formulation is modified to suit the blowing capability of azodicarbonamide specifically. As mentioned previously azodicarbonamide undergoes a specific thermal decomposition mechanism to release nitrogen gas when heated. Kickers have been added to the control formulation to lower the decomposition temperature of azodicarbonamide and prevent the formation of hydrogen chlorides by thermal decomposition. This works by introducing a coordinating metal, typically K or Zn, which promotes an alternative decomposition pathway which occurs at lower temperatures, shown below in the case of Zn (Figure 3.93).

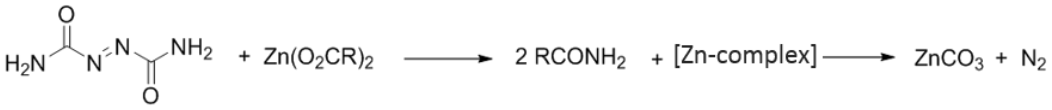

Figure 3.93 Proposed decomposition scheme of azodicarbonamide in the presence of ‘kicker’ Zn ions.

Furthermore, due to the commercial nature, the control plastisol has been formulated with several considerations other than performance, one of which is cost. The high percentage of filler in the control formulation, 100 parts per hundred of resin, is one contributing factor to ensuring that low costs are maintained. However, one consequence of increased filler concentrations is the restriction of cell formation by azodicarbonamide.

[xxiv] Graham & Brown Standard Formulation

[xxv] Graham & Brown formulation currently used for the high blown products was set as the control **P_{ADCA}**.

3.10.1.1 Selection of the Alternative Blowing Agent for Formulation Investigation

Although this control formulation is optimised in the case of azodicarbonamide, it is unknown if its components are inhibiting the gas formation of the novel additives. Once initial screening of each novel additive had been completed using the control formulation, with no significant success, the most promising additive (Compound **50**) was scaled up to investigate the significance of numerous variables within the formulation. Compound **50** was chosen as the alternative blowing agent to ADCA for the factorial experiment as it showed potential gas formation within the plastisol matrix during initial tests. Molar equivalent concentrations of compound **50** showed a semi open cellular structure within the plastisol. Increasing the concentration of compound x did not increase the observed gas yield, giving evidence that components within the formulation may inhibit the cell formation of compound **50**. The factorial experiment will identify if the various formulation components influence the blowing capability of compound **50** and ADCA.

3.10.2 Design of the Factorial Experiment

A factorial design experiment is an experimental method used to analyse combinations of experimental conditions and their interaction with one another. The principle components are manipulated experimentally, thus creating the independent variables within the experiment. These variables are the factors in the design. If an experiment had three factors, each with two experimental levels a 2x2x2, or 2^3, factorial design is created. In such a design 8 different experimental conditions would be investigated ($2^3 = 8$).[xxvi]

Screening designs can be used to identify the key variables; however, these experiments do not necessarily highlight interactions between variables. In many applications screening designs are of great value as the number of potential variables affecting process quality, can be too high to feasibly study. The screening process can provide vital information on the most important factors, which can be developed by optimization experiments that provide a more conclusive overlook of the relationships between the factors and the responses.

[xxvi] https://methodology.psu.edu/ra/most/factorial

For this study a screening design experiment was designed using 'Stat-Ease Design Expert® Software' to identify the major influential factors within the formulation. A 2-level factorial designed experiment with 5 variable factors was carried out. The 5 initial factors considered were as follows:

- Plasticiser: DINP
    - Controls the elasticity of the product
- Kicker stabiliser: Potassium/ Zinc
    - Controls decomposition
- Blowing Agent Concentration
    - Controls the amount of expansion
- Filler: $CaCO_3$
    - Controls the cost of the product
- Blowing Agent Type
    - ADCA vs novel additives

The extremes (-1 and +1) were analysed to establish if the responses were significant. The following formulations were prepared and tested:

Table 3.34 Formulation factorial experiment samples **1-8**.

Sample	Plasticizer	Kicker	Blowing Agent Type	Blowing Agent Amount	Filler
1	-1	-1	Compound **50**	-1	+1
2	+1	+1	Compound **50**	+1	+1
3	+1	+1	Compound **50**	-1	-1
4	-1	-1	Compound **50**	+1	-1
5	+1	-1	ADCA	-1	-1
6	-1	+1	ADCA	+1	-1
7	+1	-1	ADCA	+1	+1
8	-1	+1	ADCA	-1	+1
ADCA Control	-1	-1	ADCA	-1	+1

3.10.3 Screening Design Experimental Results

The 8 factorial design experiment samples (**F1**-**F8**) were manufactured under that standard conditions and analysed for the following parameters:

- Colour
- Gloss
- Coating Depth
- Surface Defects
- Cross-section Cells

Table 3.35 Tabulated results obtained from the factorial design experiment runs, **F1-8**.

Analysis		F1	F2	F3	F4	F5	F6	F7	F8
Colour	L*	93.82	93.79	94.65	94.02	95.25	94.60	94.49	94.58
	a*	-0.39	-0.42	-0.14	0.08	-0.05	-0.06	-0.02	-0.05
	b*	0.51	0.34	1.94	1.12	1.91	2.75	3.81	2.41
Gloss	60°	8.1	5.6	10.1	7.7	7.9	3.1	4.7	2.6
	85°	4.6	2.7	8.1	5.0	9.7	0.8	2.0	0.5
Coating Depth	(µm)	206	272	200	239	689	1538	1100	675
Surface Defects (mm)	Number ($5mm^2$)	18	11	18	13	0	14	0	15
	Average Size	0.78	1.05	0.78	0.79	0.00	0.92	0.00	0.88
	Size Range	0.61	1.48	0.78	0.44	0.00	0.70	0.00	0.44
Cross-section Cells (µm)	Number (1mm)	9	15	10	14	63	47	42	34
	Average Size	62.22	98.88	155.54	73.36	148.94	66.70	200.00	295.00
	Size Range	55.56	166.65	399.96	133.38	111.15	900.00	300.00	1000.00

3.10.3.1 Formulations Containing Compound 50

As previously mentioned, Compound **50** showed promising results when analysed within the formulation as a direct swap for ADCA. The effects of increasing the concentration of compound **50**, as well as the influence of kicker compounds was investigated during the initial study. This work showed that the physical properties of the coatings **P50** were modifiable dependant on the formulation. This work is discussed in detail in chapter 3.9. Although this initial work suggested that increasing the concentration of the blowing agent, compound **50** did not have an advantageous result in term of expansion level, it is hypothesised that altering supplementary components in the formulation could increases the observed gas yield and subsequent expansion levels. This work provided evidence that additive **50** was a suitable starting point for a formulation modification study.

In terms of coating depth, the formulation components investigated in this experiment showed no significant influence on the expansion level of samples **F1-4**. All samples were prepared by applying a 200 µm coating to a non-woven paper backing, using an automatic K-bar[xxvii]. Analysis of the cured coatings containing compound **50** show coating depths between 200 and 272 µm. As expected, samples **F2** and **F4** show a greater coating depth than samples **F1** and **F3** due to increased levels of blowing agent within these formulations. The +1 blowing agent formulations show an increase in coating depth of between 39 and 72 µm. This shows that compound **50** does have some effect on expansion levels; however, the surface levels are very uneven. (Figure 3.94)

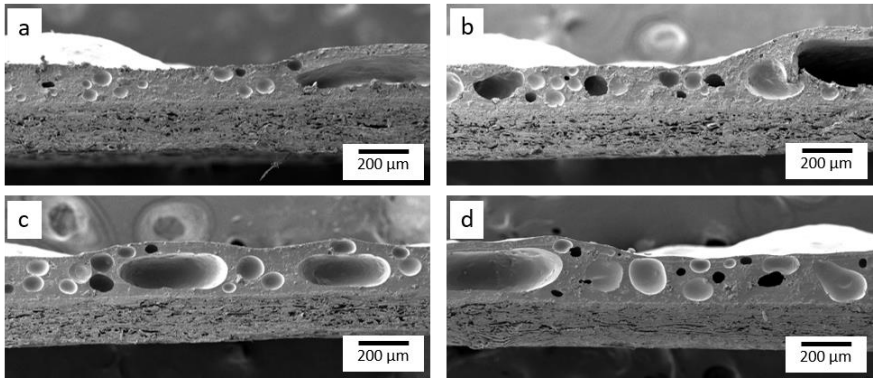

Figure 3.94 SEM cross-section micrographs of samples (a) **F1**, (b) **F2**, (c) **F3** and (d) **F4** at x75 Mag.

[xxvii] As per the standard manufacturing process

It was known that the presence of the filler component inhibits the blowing capability of ADCA. That said, the opposite result was observed in the case of compound **50**. Samples **F1** and **F2** both contained +1 levels of filler. When comparing the +1 blowing agent samples (**F2** and **F4**), sample **F2**, with +1 levels of filler showed an increased coating depth of 33 µm. Although an increase in expansion was observed, no significant change in cell distribution was observed. Large gas pockets were observed in the cross-section SEM in all cases, resulting in large cell size ranges of up to 399.96 µm. This is shown in the x33 magnified cross-section micrographs shown in Figure 3.95. Despite a large range in cell sizes there was no overall influence on the coating depth.

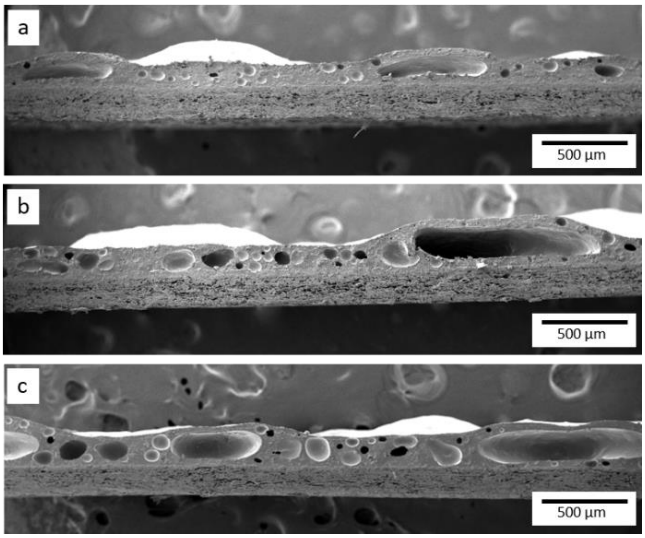

Figure 3.95 SEM cross-section micrographs of (a) **F1**, (b) **F2** and (c) **F4** at x33 Mag.

The surface images obtained by SEM, showed that in all formulations containing compound **50**, surface defects were present resultant of the gas pockets formed within the coating (Figure 3.96). The highest number of defects were observed in samples **F1** and **F3**, which contain -1 levels of blowing agent. This suggests that as the level of blowing agent increases, as does the level of distribution within the system. Sample **F2** showed the highest average defect size as well as the biggest range in defect size across the surface coating. Sample **F2** contains +1 levels of all components, suggesting that there is incompatibility within the formulation of sample **F2**. The defect sizes observed for samples **F1**, **F3** and **F4**, were more consistent with sizes ranging from approx. 0.45-1.3 mm.

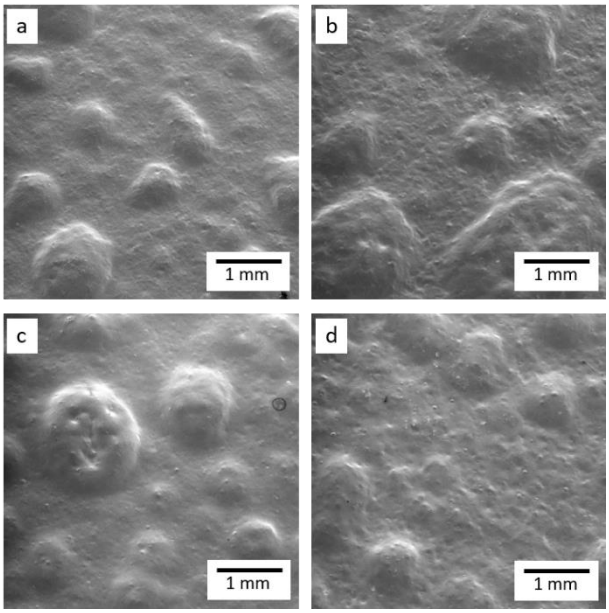

Figure 3.96 SEM surface micrographs of samples (a) **F1**, (b) **F2**, (c) **F3** and (d) **F4** at x18 Mag.

The colour and gloss level of the sample coatings were also analysed. The colour index data for the formulations containing compound **50** showed no significant colour change across the variables. Samples **F3** and **F4** showed a slight increase in yellow saturation (b*), both formulations contain -1 levels of filler, suggesting that decreased levels of the filler component had a direct effect on the yellowing of the coating surface. Glossmeter readings identified that all formulations produced a matt surface with GU ≤10. As expected the gloss level was reduced in samples **F1** and **F2** which contain +1 levels of filler.

3.10.3.2 Formulations Containing ADCA

The screening formulations containing ADCA were also compared to the control ADCA plastisol (**P_{ADCA}**, Figure 3.97) currently used in standard polymer coating manufacturing.

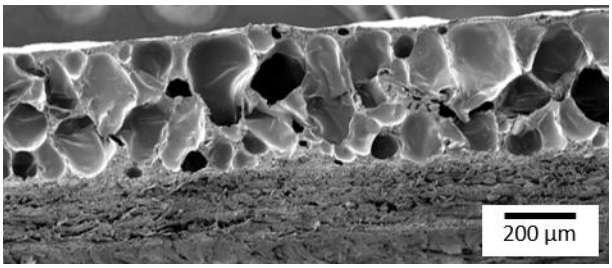

Figure 3.97 SEM cross-section micrograph of the control expanded sample **P_{ADCA}** at x75 Mag.

The modification of the formulation had a direct result on the physical properties of the coatings **F5-8** containing ADCA. Sample **F5** (a, Figure 3.98), showed the most similar cellular structure to that of the control sample **P_{ADCA}**. That said, in the case of **F5**, the observed expansion level had increased by approx. 300 µm when compared to **P_{ADCA}**. This result was likely due to the -1 level of filler within the formulation **F5**.

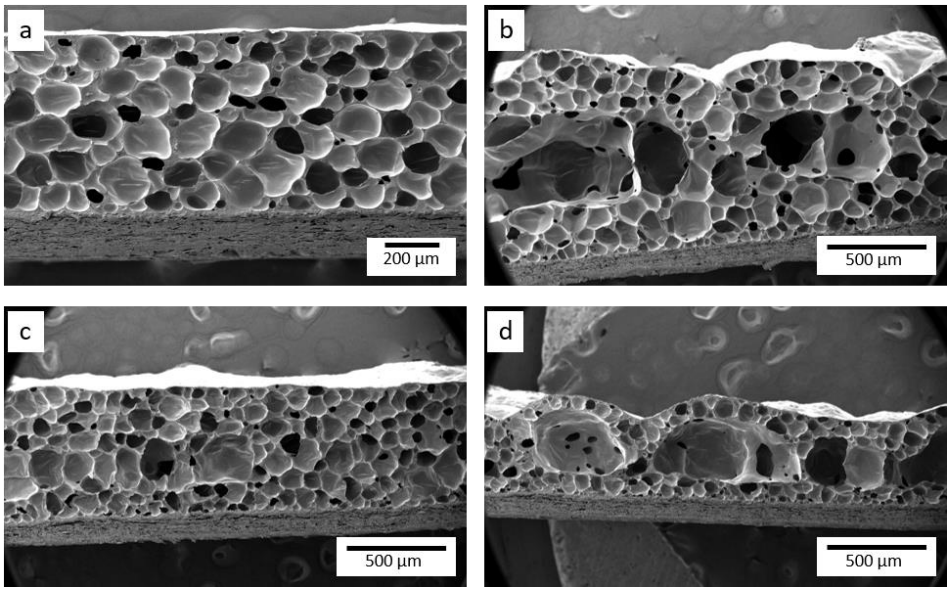

Figure 3.98 SEM cross-section micrographs of samples (a) **F5** at x75 Mag. and (b) **F6**, (c) **F7** and (d) **F8** at x33 Mag.

Significant increase in expansion levels was observed in the samples containing +1 blowing agent levels. **F6** and **F7**, showed expanded plastisol coating levels of 1538 µm and 1100 µm respectively (b, c, Figure 3.98). This is substantial when compared to the observed level of 400 µm in **P_{ADCA}**. This result is conducive with the fact that the filler inhibits gas production of ADCA as **F6** (-1 filler) showed significantly more expansion than **F7**.

The formulation also showed to have significant effect on the cell sizes within the formulation. In samples **F6** and **F8**, where plasticizer levels are low, but kicker levels are high, large open cell vacuoles were formed (b, d, Figure 3.98). This is because the plasticizing agent aids distribution of the formulation additives leading to uneven cell distribution within the system upon thermal decomposition. Furthermore, the kicker complexes activate the blowing capability of ADCA creating more gas production. The combination of these effects results in large cell ranges (< 1 mm) and uneven distribution.

The evenly distributed cells in sample **F5**, actively contributed to the smooth surface observed in the surface micrograph (a, Figure 3.99).

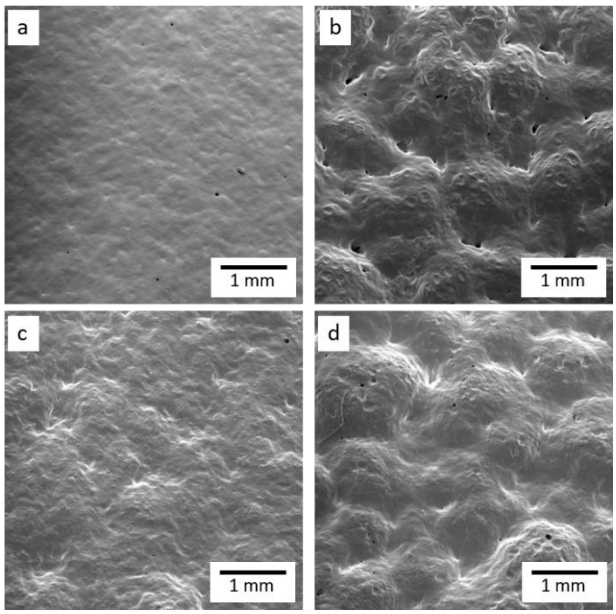

Figure 3.99 SEM surface micrographs of samples (a) **F5**, (b) **F6**, (c) **F7** and (d) **F8** at x18 Mag.

The irregular cellular structure observed in the cross-section analysis of samples **F6** and **F8**, resulted in the irregular texture observed in the surface micrographs (b, d, Figure 3.99). This uneven surface can be attributed to the increased disorder within the system caused by increased kicker levels. The texture observed on the surface of sample **F7**, was due to +1 levels of filler, which created a denser coating. This surface result (c, Figure 3.99) is similar to that observed in the case of the control ADCA sample $\mathbf{P_{ADCA}}$.

As expected the concentration of ADCA contributed to the coloration of the coating with elevated b* levels observed in the +1 blowing agent samples **F6** and **F7**. As was the case with the samples containing compound **50**, samples **F5**-**8** all appeared within the matt region, GU ≤10. The lowest gloss readings were observed in samples **F6** and **F8**, conducive with the disorder observed within the surface of cross-section micrographs. This result confirms that the amount of gas produced, reduces the gloss level of the surface by creating more disorder within the system and subsequently disruption to the coating surface.

3.10.3.3 Statistical Analysis of the Screening Design Experiment

The Stat-Ease Design Expert® program allows for statistical analysis of the obtained results. The most important physical properties within the scope of this project were:

1. Expansion Level
2. Cell Size Range
3. Colour (b*)
4. Gloss (85°)

The software was used to identify which factors, if any, had significant influence on each result. Due to the limited parameters set in the screening design experiment, it was not possible to identify if the responses followed a linear trend. However, a one-factor plot could be made showing the relationship between the factor and the response. When no significant response was detected a straight line one-factor plot was observed. As shown below for the influence of the kicker compounds on the observed colour (L*) (Figure 3.100).

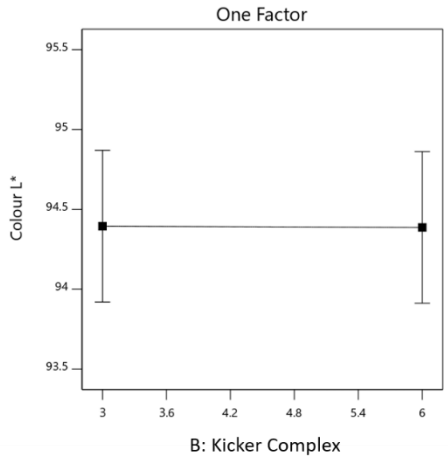

Figure 3.100 One factor plot of the effects of the kicker complex on the colour L* in the screening design experiment.

In the case of expansion, the most appropriate model was the Shapiro-Wilk test. (Figure 3.101) This identified the most significant contributing factor was ‘blowing agent type’. The observed p-value of 0.835 showed that further investigation would be required to identify the full extent of the influence. This is common in a two-level screening design experiment.

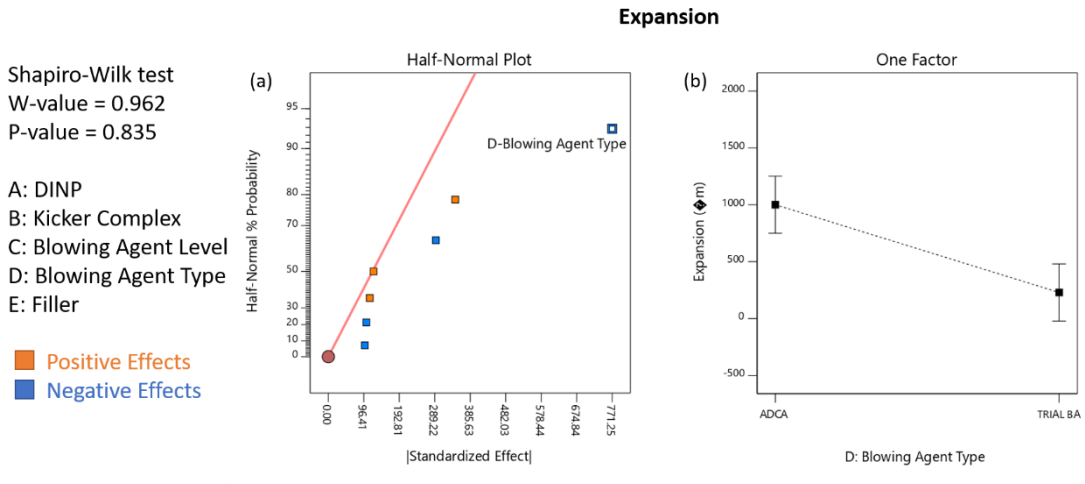

Figure 3.101 (a) Half-Normal plot of the Shapiro-Wilk test results for expansion in the screening design experiment and (b) One factor plot of the effects of the blowing agent type on the expansion

From the half-normal plot, a one factor plot was extrapolated which showed the relationship between blowing agent type and expansion. As seen in the one-factor plot (b, Figure 3.101) the samples containing ADCA showed a significantly higher expansion response than the samples containing the trial blowing agent, compound **50**. This result corresponds to the observed SEM data which shows significant expansion in the case of the ADCA samples **P5-8** and confirms that blowing agent type is more of a determining factor than blowing agent level.

Cell size range was measured using the SEM cross-section micrographs and the resulting data was statistically analysed using the Stat-Ease Design Expert® Program. (Figure 3.102)

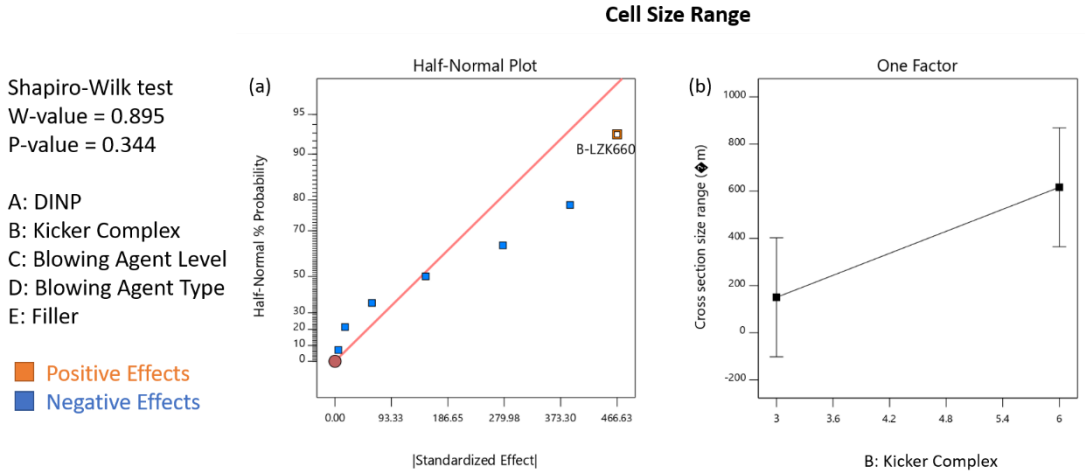

Figure 3.102 (a) Half-Normal plot of the Shapiro-Wilk test results for cell size range in the screening design experiment and (b) One factor plot of the effects of the kicker complex on the cell size range.

In this case, the statistical analysis showed that a more conclusive result was observed as p = 0.344. P-values closer to 0.00 show that the data is reliable without further investigation. In terms of the cell size range, none of the factors exhibited a significant change on the observed response; however, the 'kicker' complexes showed the most variation within the data set. The one factor plot showed that as the level of kicker increased as did the observed cell size range. This is conclusive with the fact that the kicker complexes initiate gas formation by the blowing agents and create more disorder within the system.

The third important response was colour detection, in particular b* which showed particularly high detection in the control formulation **P_{ADCA}**. As seen in the statistical analysis of the expansion response, the blowing agent type was identified as the most significant contributing factor (Figure 3.103). The p-value for the association of blowing agent type with colour b* detection is 0.214, this suggests that the data is more accurate than the other results. However, the value still suggests that further investigation is required to give a conclusive correlation.

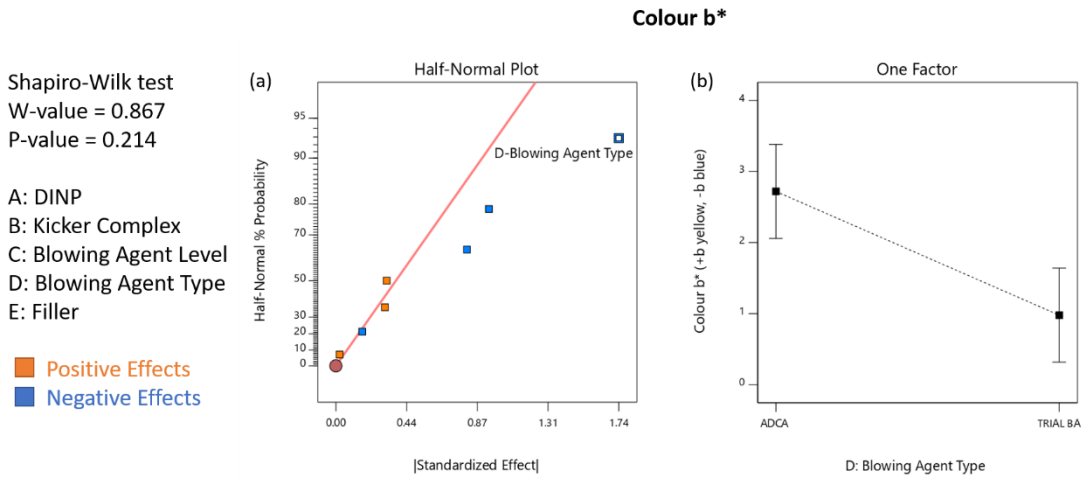

Figure 3.103 (a) Half-Normal plot of the Shapiro-Wilk test results for colour b* in the screening design experiment and (b) One factor plot of the effects of the blowing agent type on the colour b*.

This result was expected due the inherent strong yellow colouration of the ADCA raw powder. Further factorial experiments could extend the experimental levels to determine links between the factors and the observed colour response. For example, clarifying the interaction between the blowing agent level and the

kicker complex which show adverse effects in terms of colour b* detection (Figure 3.104).

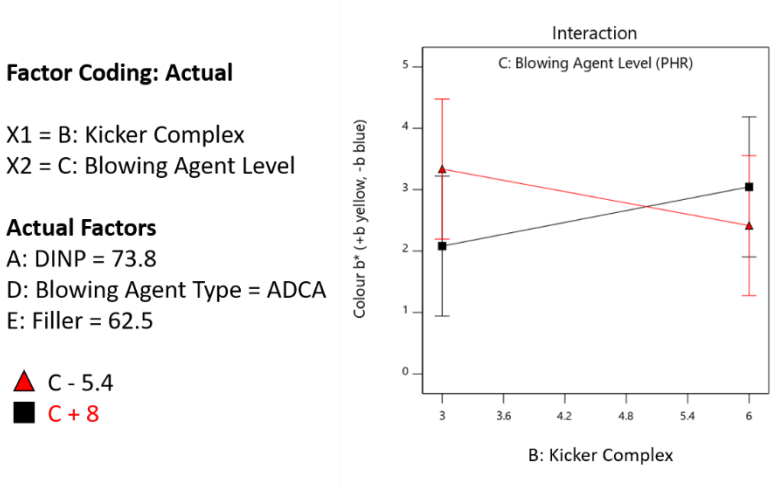

Figure 3.104 Interaction plot of the effects of the blowing agent level and the kicker complex on the colour b*.

The final response of significance within this project was the gloss reading. The values observed at 85° were inputted into the statistical analysis software. In general, the 85° beam angle is used to analyse matt surfaces, as this is the desired effect, this beam angle is of most importance. The Pareto chart of the gloss response shows the significance of each factor. (Figure 3.105)

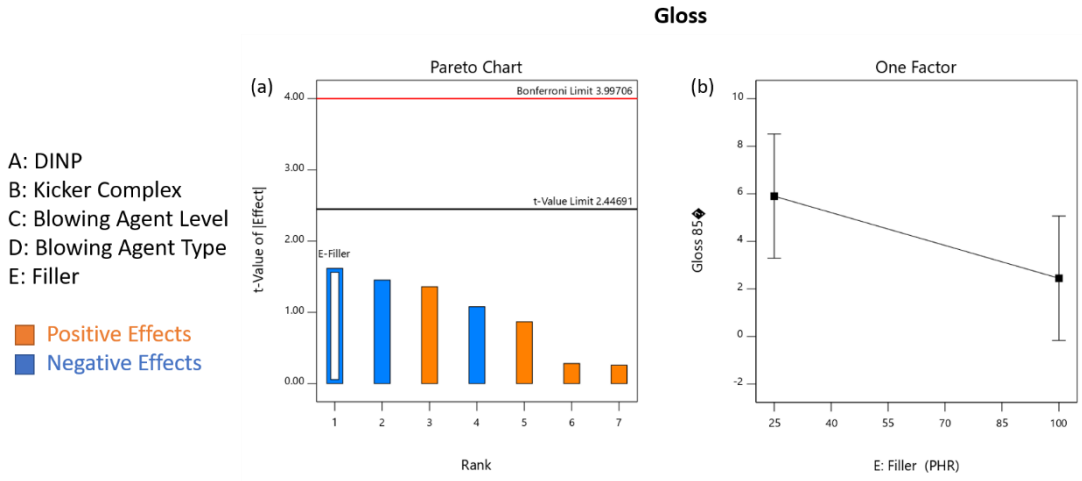

Figure 3.105 (a) Pareto chart of the results for gloss in the screening design experiment and (b) One factor plot of the effects of the Filler on the gloss value.

The size of the bar in the graph represents the significance of the factor. The Pareto chart calculates two limits, the upper limit is the Bonferroni Limit (shown in red) and any value above this this almost certainly significant to the

response. The lower limit is the t-Value Limit (shown in blank), values above this limit are classified as probably significant. It was observed that in the case of the gloss response, none of the factors showed a significant influence. The highest t-Value was observed for the filler. The one factor graph shows this influence of the filler on the gloss response. This result is conducive with the theory that the increased viscosity created by the filler compound, actively contributes to the textured surface in the SEM micrographs.

3.10.4 Conclusions of the Factorial Design Experiment

In general, the statistical results of the screening design experiment identified that further investigation would be required to conclusively identify the relationship between the factors and the response. However, that said the most significant factor was the blowing agent type. The change between blowing agents ADCA and compound **50** showed to influence many responses including expansion, cell range, colour and gloss effects. This initial data suggests that irrespectively of considerable formulation modification, compound **50** would not be an equivalent substitute for ADCA. However, in absence of a direct equivalent compound **50** could have potential in this application.

Chapter 4 Conclusions and Future Work

This study has provided evidence that alternative, naturally derived chemical additives can replicate some of the physical properties generated by azodicarbonamide in polyvinylchloride formulated coatings. For example, regular cellular structures were observed in the case of samples **P23** and **P37** under some conditions. Whilst, smooth matt surfaces have been displayed by samples **P50** and **P52**, furthermore low colouration effects were shown in the case of the semicarbazide series.

That said, no alternative chemical additive was able to replicate the multitude of simultaneously desired physical properties, quite as efficiently as azodicarbonamide itself. The ability to create not only an expanded and regular cell structure, but also a smooth, defect free and matt surface, makes the effectiveness of azodicarbonamide unparalleled in the desired application.

As developments move forward to reduce the levels of azodicarbonamide in a range of commercial applications, this study has highlighted the effectiveness of co-blowing agents. In particular, an azodicarbonamide and sodium hydrogen carbonate formulation that provides sufficient, yet controllable, expansion, surface topography and gloss results for the target coatings application. Furthermore, the fundamentals for the development of a quantitative study for the detection of residual azodicarbonamide within final products, utilising ultra-performance convergence chromatography (UPC^2) methodology, have been provided.

It is also important to consider alternative applications for those additives that do not offer a direct alternative to azodicarbonamide for the purpose of producing a polymer foamed coating. Properties such as smooth, defect free, glossy surfaces (as observed in the cases of materials **P43** and **P44**) can be beneficial to numerous applications where surface defects pose a significant problem. This application can be further considered with aim to investigate the efficiency of additives **43** and **44** as levelling agents for such coatings.

Chapter 5 Experimental

The chemical purity of all materials was within accepted range for the industrial sponsor, in accordance with requirements for the desired application.

5.1 Materials

The materials listed in Table 5.1 were used without further purification unless otherwise stated.

Table 5.1 List of materials used

Chemical	**Grade (%)**	**Supplier**
2-Aminoisobutyric acid	99+	Fisher Scientific
2-Hydroxyisobutyric acid	99	Alfa Aesar
4,4'-oxybis(benzenesulfonyl hydrazide)		Graham & Brown
Acetone	100	VWR International
Azodicarbonamide	90+	Graham & Brown
Chloroform	99.8	Sigma Aldrich
Citric acid	99+	Sigma Aldrich
Cyanuric chloride	99	Sigma Aldrich
Diethyl ether	≥99.8	Sigma Aldrich
Dimethyl sulfoxide	≥99.7	Sigma Aldrich
Ethanol	99.9	VWR International
Ethyl Acetate	99.8	VWR International
Ethyl 2-hydroxyisobutyrate	98	Alfa Aesar
Hydrazine monohydrate	98+	Alfa Aesar
KF/Al_2O_3		Sigma Aldrich
Methanol	≥99.9	Sigma Aldrich
Phenylhydrazine	97	Alfa Aesar
p-Toluenesulfonyl chloride	≥98	Sigma Aldrich
Semicarbazide hydrochloride	99	Alfa Aesar
Sodium acetate	100	VWR International
Sodium hydrogen carbonate		Graham & Brown
Sodium Sulphate	99-100	Sigma Aldrich
Tartronic acid	≥97	Sigma Aldrich
Tetrahydrofuran	99.99	Fisher Scientific
Toluenesulfonyl semicarbazide		Graham & Brown
Triethyl citrate	99	Alfa Aesar
Triethylamine	≥99.5	Sigma Aldrich
Urea	≥99.5	Sigma Aldrich

5.2 Instruments

5.2.1 Colour Analysis

L*a*b* colour values were collected from raw cured plastisol samples on an X-RITE, Color i7 Benchtop Spectrophotometer and analysed using the Color Master FMIII V7 Software. Values were taken from the D65/10° light source.

ΔE was calculated using the 1976 formula:

$$\Delta E^*_{ab} = \sqrt{(L^*_2 - L^*_1)^2 + (a^*_2 - a^*_1)^2 + (b^*_2 - b^*_1)^2}$$ [162]

5.2.2 Differential Scanning Calorimetry (DSC)

All differential scanning calorimetry (DSC) analysis was carried out using a TA Q20 instrument. Temperature range from 0 °C – 500 °C at a rate of 10 °C per minute in an open Al pan lid, under a controlled N_2 atmosphere.

5.2.3 Glossmeter

All surface testing readings were taken using a Gloss Meter PCE-GM 50, accuracy ± 1.2 GU, repeatability ± 0.4 GU, measurement range 15 x 32 mm. All sample readings were taken at room temperature and at an optical angle of 85° unless otherwise stated.

5.2.4 High Performance Liquid Chromatography (HPLC)

All HPLC samples were run on an Agilent Technologies 1290 Infinity Liquid Chromatography System under the following conditions;

Column: Brownlee Si 5 µ 80Å column 22 cm x 4.6 mm with holder

Guard: Si Aquapore 7 µm spherical 15 mm cartridge with holder

Mobile Phase: 95% ethyl acetate and 5% DMSO (HPLC grade)

Flow Rate: 1 mL/min

Temperature: 30 °C

Injection volume: 10 µL

Detection: UV detection, PDA at 270 nm

5.2.5 Infrared (IR)

All spectra were recorded on a Bruker Platinum FTIR-ATR spectrometer. 16 scan experiments were run for all samples. Samples were analysed neat unless otherwise stated

5.2.6 Mass Spectroscopy (ESI-MS)

Positive electrospray (ESI) mass spectrometry (MS) was carried out on a Bruker Daltronics microTOF spectrometer.

5.2.7 Nuclear Magnetic Resonance (NMR)

All ^{1}H and $^{13}C^{1}H$ NMR spectra were collected on a Bruker Avance 500 MHz spectrometer or Bruker Avance 300 MHz spectrometer unless otherwise stated. All chemical shifts are quoted in parts per million (ppm) and coupling constants are reported in Hertz (Hz). All NMR experiments were carried out in $CDCl_3$ or *d*-DMSO solvents unless otherwise stated.

5.2.8 Plastisol Drawdowns

All blowing agents were added to the Graham & Brown standard chemically expanded foam plastisol at concentrations of 0.161 mmol/g. Co-blowing agent ratios were premixed and ratios were determined by molar equivalents. The plastisol mixture was pre-made without the azodicarbonamide component and consisted of the following;

PVC (100 eq)

Plasticizer (70 eq)

Fine grade calcium carbonate (105 eq)

Titanium Oxide (12 eq)

Isopropyl alcohol (8.5 eq).

Potassium/Zinc Kicker (3 eq) (‘kickers’ were used as standard unless otherwise stated)

All plastisol formulations were coated as a 200 µm film on preheated (5 seconds at 210 °C) FSC Double Coated Peelable Duplex Paper (140 g/m^2) using a Werner Mathis LTE-S Labcoater k-bar and heated for 24 seconds in a Werner Mathis Thermosol Oven, 220 v, 3 phase, 60 Hz, 9 KW.

5.2.9 Scanning Electron Microscopy (SEM)

Cross-section samples were prepared using a Pilling Weck WECPREP Surgical Blade and coated with 30 nm gold using a Quorum Q15OR S Coater. All scanning electron micrographs were generated using a Geol JSM 6610 Lv Scanning Electron Microscope under the following parameters:

Accelerating voltage = 5 kV

Working distance = 10 mm

Spot size = 40

Magnification = x75 (unless otherwise stated)

5.2.10 Thermal Gravimetric Analysis (TGA)

All TGA analysis was carried out using a TA Q50 instrument. Temperature range from 25 °C – 450 °C at a rate of 10 °C per minute in an open Pt pan, under a controlled N_2 atmosphere.

5.2.11 Ultra-Performance Convergence Chromatography (UPC^2)

All UPC^2 samples were run on a Waters ACQUITY UPC^2 system with QDa and ISM under the following conditions:

Column: ACQUITY UPLC® Torus Diol 3.0x100 mm

Mobile phase: Liquid carbon dioxide

Strong wash: methanol

Weak wash: methanol/ IPA

Column temperature: 30 °C

Flow rate: 1.2 mL/min

UV wavelength: 270 nm

Methanol was used only as a co-solvent for screening purposes.

5.3 Synthesis of the Semicarbazide Series

5.3.1 Synthesis of semicarbazide tartronate (23)[xxviii]

Semicarbazide hydrochloride (1.11 g, 10 mmol) and sodium acetate (0.85 g, 10 mmol) were dissolved in methanol (50 mL) at 30 °C with stirring. Tartronic acid (1.23 g, 10 mmol) was added slowly. The reaction was left to stir for 24 hours at 40 °C. White precipitate was isolated by vacuum filtration. Filtrate was concentrated under vacuum to yield the product as a yellow oil **23** (0.52 g, 29%)

$C_4H_7O_5N_3$. IR ν_{max}/cm^{-1} (neat): 3348 cm^{-1} (m), 3210 cm^{-1} (m), 2914 cm^{-1} (m), 1717 cm^{-1} (s), 1623 cm^{-1} (s), 1237 cm^{-1} (s), 1119 cm^{-1} (s); δ_H (300 MHz, $CDCl_3$): 1.19 (s, 1H, CH); ESI-MS: *m/z* 228.06 (100%, $M+Na_2+2H_2+H^+$); (Found 228.0590, $C_4H_7O_5N_3$ requires $M+Na_2+2H_2+H^+$ 228.0567).

5.3.2 Synthesis of semicarbazide isobutyrate (24)[xxix]

Semicarbazide hydrochloride (2.78 g, 25 mmol) was dissolved in ethanol (100 mL). Sodium acetate (2.05 g, 25 mmol) was added in portions and left to stir for 10 minutes at 30 °C. 2-hydroxyisobutyric acid (2.6 g, 25 mmol) was added and the solution was left to stir for 24 at 40 °C. Solids were filtered by gravity and filtrate was concentrated under vacuum to yield a colourless oil **24** (3.78 g, 94%)

$C_4H_{11}O_3N_3$. IR ν_{max}/cm^{-1} (neat): 3367 cm^{-1} (m), 3212 cm^{-1} (s), 2983 cm^{-1} (m), 1666 cm^{-1} (s), 1588 cm^{-1} (s), 1168 cm^{-1} (s); δ_H (300 MHz, $CDCl_3$): 1.53 (s, 6H, 2 x CH_3); δ_C (100 MHz, DMSO): 179.3, 169.5, 71.3, 28.1; ESI-MS: *m/z* 184.07 (100%, M+Na); (Found 184.0690, $C_4H_{11}O_3N_3$ requires M+Na, 184.0698).

[xxviii] Dufresne, C., *et al.,* Bulletin de la Societe Chemique de France, 1972, (6), 2547-54

[xxix] Chang, P., Journal of Organic Chemistry, 1958, (23), 1951-53

5.4 Synthesis of the Sulfonate Series

5.4.1 Synthesis of Toluenesulfonyl phenylhydrazine (31)[xxx]

p-Toluenesulfonyl chloride (0.19 g, 1 mmol) was combined with basic KF/ Al_2O_3 (0.23 g), the solid were ground with a pestle and mortar, phenylhydrazine (0.11 mL, 1 mmol) was added dropwise, while mixing over 5 minutes. Ethanol (2 mL) was added and the mixture was ground for 15 minutes. After this time the mixture was dissolved in ethanol (15 mL) and the solid alumina was filtered by vacuum. The filtrate was concentrated under vacuum to yield the crude material as a yellow solid (0.12 g, 46%). The crude material was recrystallised in aqueous ethanol to yield a pale-yellow powder **31** (0.06 g, 23%)

$C_{13}H_{14}O_2N_2S$. m.p. 151.6-152.2 °C (from EtOH); IR ν_{max}/cm^{-1} (neat): 3314 cm^{-1} (s), 3240 cm^{-1} (s), 1919 cm^{-1} (w), 1602 cm^{-1} (s), 1494 cm^{-1} (s), 1321 cm^{-1} (s), 1156 cm^{-1} (s); δ_H (300 MHz, DMSO): 7.74 (d, J = 9.3 Hz, 2H, 2 x Ar-H), 7.58 (s, 1H, Ar-H), 7.41 (d, J = 8.0 Hz, 2H, 2 x Ar-H), 7.17-7.01 (m, 2H, 2 x Ar-H), 6.79 (d, J = 8.6 Hz, 2H, Ar-H), 6.69 (t, J = 7.3 Hz, 1H, Ar-H), 2.42 (s, 3H, CH_3); δ_C (126 MHz, DMSO): 148.6, 143.1, 136.3, 129.5, 128.4, 127.5, 118.9, 112.7, 21.0; ESI-MS: *m/z* 285.07 (100%, M+Na); (Found 285.0668, $C_{13}H_{14}O_2N_2S$ requires M+Na, 285.0674).

5.5 Synthesis of the Triazine Series

5.5.1 Synthesis of 1,3,5-triazine-2,4,6-urea (37)

Cyanuric chloride (0.46 g, 1 mmol) and urea (0.45 g, 3 mmol) was dissolved in THF (50 mL) and water (50 mL). Triethylamine (0.14 mL) was added dropwise. The solution was left to reflux for 48 hours. (Conversion monitored by LCMS) Liquid-liquid extraction with diethyl ether (3 x 50 mL), organic washes were combined and washed with brine (50 mL), dried with Na_2SO_4, filtered by gravity and concentrated under vacuum to yield the product as yellow oil **37** (0.4 g, 63%)

$C_6H_9O_3N_9$. IR ν_{max}/cm^{-1} (neat): 3542 cm^{-1} (m), 3458 cm^{-1} (m), 3199 cm^{-1} (m), 1733 cm^{-1} (m), 1633 cm^{-1} (s), 1056 cm^{-1} (m); δ_H (300 MHz, DMSO): 11.15

[xxx] Yan, Y., *et al*., Hournal of Organic Chemistry, 2017, **82** (15), 7957-63

(s, 6H, 3 x NH_2); δ_C (75 MHz, DMSO): 149.9; ESI-MS: *m/z* 282.28 (100%, M+Na+2H_2); (Found 282.2789, $C_6H_9O_3N_9$ requires M+Na+2H_2, 282.2198).

5.6 Synthesis of the Citrate Series

5.6.1 Synthesis of 2,2'-hydrazobiscitric acid (41)

Citric acid (16.52 g, 86 mmol) was dissolved in ethanol (95 mL) with vigorous stirring. The resulting solution was left to stir for 10 minutes, until all the solid material had fully dissolved. Hydrazine monohydrate (2.2 mL, 43 mmol) was added dropwise to the solution over 15 minutes. The solution was left to stir for 24 hours at 25 °C. Solvent was removed by rotary evaporation. A white sticky solid remained in yellow oil. The oil was dissolved in acetone, while solid remained. The resulting slurry was filtered and washed with acetone (3 x 10 mL), the filtrate was collected and concentrated by rotary evaporation. Analysis was carried out on both products identifying the yellow oil as the desired product. The product was isolated as yellow oil **41** (13.86 g, 85%)

$C_{12}H_{16}O_{12}N_2$. IR ν_{max}/cm^{-1} (neat): 3436 cm^{-1} (w), 2981 cm^{-1} (w), 2591 cm^{-1} (w), 1704 cm^{-1} (s), 1653 cm^{-1} (w), 1367 cm^{-1} (m), 1184 cm^{-1} (s); δ_H (500 MHz, D_2O): 2.58 (AB dd, 8H, *J* = 15.2 Hz, 4 x CH_2); δ_C (126 MHz, D_2O): 179.9, 176.6, 74.4, 57.2; ESI-MS: *m/z* 402.89 (39%, M+Na); (Found 402.8871, $C_{12}H_{16}O_{12}N_2$ requires M+Na, 403.0601).

5.6.2 Synthesis of 2-(2-phenylhydrazinyl)citric acid (42)

Citric acid (3.83 g, 20 mmol) was dissolved in ethanol (30 mL) under vigorous stirring. The resulting solution was left to stir for 10 minutes, until all the solid material had fully dissolved. Phenylhydrazine (2.5 mL, 20 mmol) was added dropwise to the solution and left to stir for 18 hours at 25 °C. The solvent was removed under reduced pressure to the give crude mixture. This crude product was further dried in a vacuum oven at 60 °C for 96 hours. Product was isolated as dark orange oil **42** (5.03 g, 89%)

$C_{12}H_{14}O_4N_2$. IR ν_{max}/cm^{-1} (neat): 3252 cm^{-1} (m), 2971 cm^{-1} (w), 2691 cm^{-1} (w), 1931 cm^{-1} (w), 1702 cm^{-1} (s), 1603 cm^{-1} (m), 1551 cm^{-1} (m), 1497 cm^{-1} (s), 1082 cm^{-1} (s); δ_H (500 MHz, $CDCl_3$): 7.36 (t, 2H, *J* = 8.5 Hz, 2 x Ar-H), 7.10 (t, 1H, *J* = 7.4 Hz, Ar-H), 7.01 (d, 2H, *J* = 8.5 Hz, 2 x Ar-H), 2.72 (AB dd, 4H, *J* =

15.4 Hz, 2 x CH_2); δ_C (126 MHz, DMSO): 197.4, 171.2, 130.2, 119.6, 114.6, 112.6, 69.4, 41.5, 25.9; ESI-MS: *m/z* 355.14 (63%, M+3Na+2H_2); (Found 355.1411, $C_{12}H_{14}O_4N_2$ requires M+3Na+2H_2, 355.0858).

5.6.3 Synthesis of 2,2'-hydrazobistriethyl citrate (43)

Triethyl citrate (10 mL, 41.2 mmol) was dissolved in ethanol (50 mL). Hydrazine monohydrate (1 mL, 20.6 mmol) was added dropwise over 15 minutes. The mixture was left to stir for 72 hours at 25 °C. The solvent was removed under vacuum to yield white oil. Oil dissolved in chloroform (75 mL) white precipitate formed, which was filtered under vacuum. Filtrate concentrated to yield yellow oil **43** (9.35 g, 83%)

$C_{24}H_{40}O_{12}N_2$. IR ν_{max}/cm^{-1} (neat): 3497 cm^{-1} (w), 2983 cm^{-1} (w), 2908 cm^{-1} (w), 1730 cm^{-1} (s), 1619 cm^{-1} (w), 1370 cm^{-1} (m), 1182 cm^{-1} (s), 1022 cm^{-1} (s); δ_H (500 MHz, $CDCl_3$): 4.22 (q, 4H, *J* = 7.1 Hz, 2 x CH_2), 4.08 (q, 8H, *J* = 7.1 Hz, 4 x CH_2), 2.77 (AB dd, 8H, *J* = 15.5 Hz, 4 x CH_2), 1.24 (t, 6H, *J* = 7.1 Hz, 2 x CH_3), 1.19 (t, 12H, *J* = 7.1 Hz, 4 x CH_3); δ_C (126 MHz, $CDCl_3$): 173.4, 169.7, 73.2, 60.9, 43.4, 14.0; ESI-MS: m/z 575.23 (22%, M+Na+2H_2); (Found 575.2276, $C_{24}H_{40}O_{12}N_2$ requires M+Na+2H_2, 575.2792).

5.6.4 Synthesis of 2-(2-phenylhydrazinyl)triethyl citrate (44)

Triethyl citrate (5.60 mL, 20 mmol) was dissolved in ethanol (30 mL). Phenylhydrazine (2 mL, 20 mmol) was added dropwise over 15 minutes and left to stir for 72 hours at 25 °C. Colour change from colourless to light orange. Solution was concentrated under vacuum and the product was isolated as yellow oil **44** (7.01 g, 96%)

$C_{18}H_{26}O_6N_2$. IR ν_{max}/cm^{-1} (neat): 3490 cm^{-1} (w), 2982 cm^{-1} (w), 2939 cm^{-1} (w), 2907 cm^{-1} (w), 1730 cm^{-1} (s), 1598 cm^{-1} (w), 1466 cm^{-1} (m), 1183 cm^{-1} (s), 1096 cm^{-1} (s); δ_H (500 MHz, $CDCl_3$)7.26-7.07 (m, 2H, 2 x Ar-H), 6.83-6.66 (m, 3H, 3 x Ar-H), 4.21 (q, 2H, *J* = 7.1 Hz, CH_2), 4.08 (q, 4H, *J* = 7.1 Hz, 2 x CH_2), 2.77 (AB dd, 4H, *J* = 15.5 Hz, 2 x CH_2), 1.30-1.21 (t, 3H, *J* = 8.6 Hz, CH_3), 1.18 (t, 6H, *J* = 8.6 Hz, 2 x CH_3); δ_c (126 MHz, $CDCl_3$) 173.5, 169.7, 129.2, 121.6, 119.5, 112.1, 74.2, 60.9, 43.4, 14.1; ESI-MS: m/z 385.25 (27%, M+H_2O+H^+); (Found 385.2333, $C_{18}H_{26}O_6N_2$ requires M+H_2O+H^+, 385.1969).

5.7 Synthesis of the Tartronate Series

5.7.1 Synthesis of 2,2'-hydrazobistartronic acid (46)

Tartronic acid (1.47 g, 12 mmol) was dissolved in ethanol (30 mL) with vigorous stirring. The resulting mixture was left until all solid had dissolved. Hydrazine monohydrate (0.3 mL, 6 mmol) was added dropwise over 15 minutes. The mixture was left to stir for 24 hours at 25 °C. After which time an off-white precipitate had formed, the solids were collected by vacuum filtration and recrystallised in aqueous ethanol. The pure product was isolated as an off-white powder **46** (1.12 g, 79%)

$C_6H_8O_8N_2$. m.p. 104.6-106.2 °C (from EtOH); IR ν_{max}/cm^{-1} (nujol mull): 3329 cm^{-1} (m), 3076 cm^{-1} (m), 2991 cm^{-1} (m), 1708 cm^{-1} (s), 1601 cm^{-1} (m), 1546 cm^{-1} (s), 1316 cm^{-1} (w), 1086 cm^{-1} (s); δ_H (500 MHz, D_2O): 4.55 (s, 2H, 2 x CH); δ_C (126 MHz, D_2O): 174.1, 72.3; ESI-MS: *m/z* 328.95 (100%, $M+4Na+H^+$); (Found 328.9469, $C_6H_8O_8N_2$ requires $M+4Na+H^+$, 328.9944).

5.7.2 Synthesis of 2-(2-phenylhydrazinyl)tartronic acid (47)

Tartronic acid (1.23 g, 10 mmol), was dissolved in ethanol (20 mL) under vigorous stirring. Phenylhydrazine (1.2 mL, 10 mmol) was added dropwise to the solution and left to stir for 18 hours at 25 °C. The solvent was removed under reduced pressure to the give crude mixture. This crude product was further dried in a vacuum oven at 60 °C for 96 hours to yield the final product as a yellow solid **47** (1.89 g, 90%).

$C_9H_{10}O_4N_2$. m.p 136.1-137.8 °C (from EtOH); IR ν_{max}/cm^{-1} (nujol mull): 3289 cm^{-1} (w), 3030 cm^{-1} (w), 1929 cm^{-1} (w), 1720 cm^{-1} (m), 1601 cm^{-1} (m), 1522 cm^{-1} (m), 1491 cm^{-1} (m) 1317 cm^{-1} (m); δ_H (500MHz, D_2O): 7.37 (t, 2H, *J* = 8.1 Hz, 2 x Ar-H), 7.10 (t, 1H, *J* = 7.5 Hz, Ar-H), 7.01 (d, 2H, *J* = 8.5 HZ, 2 x Ar-H), 4.55 (s, 1H, CH); δ_C (126 MHz, DMSO): 170.8, 168.1, 148.9, 128.6, 118.3, 113.8, 112.1, 71.3; ESI-MS: *m/z* 261.08 (55%, $M+Na_2+2H_2+H^+$); (Found 261.0847, $C_9H_{10}O_4N_2$ requires $M+Na_2+2H_2+H^+$, 261.0822).

5.8 Synthesis of the Isobutyrate Series

5.8.1 Synthesis of 2,2'-hydrazobis(2-hydroxybutyric acid) (50)[xxxi]

2-Hydroxyisobutyric acid (4.11 g, 40 mmol), was dissolved in Ethanol (20 mL) with vigorous stirring. The resulting solution was left to stir for 10 minutes, or until all solid material had fully dissolved. Hydrazine monohydrate (1 mL, 20 mmol) was added dropwise to the solution over 15 minutes. The solution was left to stir for 24 hours at 25°C. The mixture was concentrated under vacuum to yield a colourless oil as the crude product. The oil was dissolved in ethanol (60 mL), dried with sodium sulphate and concentrated on the rotary evaporator yielding a colourless oil **31** (3.41 g, 84%).

$C_8H_{16}O_4N_2$. IR ν_{max}/cm^{-1} (neat): 3324 cm^{-1}(w), 2973 cm^{-1} (m), 2933 cm^{-1} (w), 1713 cm^{-1} (m), 1651 cm^{-1} (w), 1546 cm^{-1} (s), 1171 cm^{-1} (s), 1141 cm^{-1} (s); δ_H (500 MHz*,* $CDCl_3$): 1.45 (s, 12H, 4 x CH_3); δ_C (75 MHz, DMSO): 180.5, 72.0, 28.3; ESI-MS: *m/z* 227.06 (28%, M+Na); (Found 227.0567, $C_8H_{16}O_4N_2$ requires M+Na, 227.1008).

5.8.2 Synthesis of 2-(2-phenylhydrazinyl)2-hydroxyisobutyric acid (51)

2-Hydroxyisobutyric acid (2.08 g, 20 mmol), was dissolved in ethanol (15 mL) under vigorous stirring. Phenylhydrazine (2.4 mL, 20 mmol) was added dropwise to the solution and left to stir for 18 hours at 25 °C. The solvent was removed under reduced pressure to the give crude mixture. This crude product was dried in a vacuum oven at 60 °C for 96 hours and recrystallised in aqueous ethanol. The product was isolated as an orangey/ brown solid **51** (2.64 g, 68%).

$C_{10}H_{14}O_2N_2$. m.p 105.6-106.8 °C (from EtOH); IR ν_{max}/cm^{-1} (nujol mull): 3077 cm^{-1} (w), 3303 cm^{-1} (w), 2972 cm^{-1} (w), 2120 cm^{-1} (w), 1600 cm^{-1} (m), 1551 cm^{-1} (s), 1496 cm^{-1} (m), 1174 cm^{-1} (s); δ_H (500 MHz, D_2O*):* 7.35 (t, 2H, *J* = 8.0 Hz, 2 x Ar-H), 7.08 (dd, 1H, *J* = 15.1, 7.6 Hz, Ar-H), 6.98 (d, 2H, *J* = 8.5 Hz, 2 x Ar-H), 1.29 (s, 6H, 2 x CH_3); δ_C (126 MHz, DMSO): 197.8, 129.0, 123.2, 118.8, 112.6, 72.4, 28.2; ESI-MS: *m/z* 195.11 (100%, $M+H^+$); (Found 195.1129, $C_{10}H_{14}O_2N_2$ requires $M+H^+$, 195.1128).

[xxxi] Kostyanovsky, R., et al., Russian Chemical Bulletin, 1997, **46** (7), 1291-99

5.8.3 Synthesis of 2,2'hydrazobis(ethyl 2-hydroxyisobutyrate) (52)

Ethyl 2-hydroxyisobutyrate (5 mL, 40 mmol) was dissolved in ethanol (40 mL). Hydrazine monohydrate (1 mL, 20 mmol) was added dropwise over 15 minutes. The solution was left to stir for 15 hours at 25 °C. Mixture was dried with sodium sulphate, decanted, filtered and concentrated under vacuum to yield a yellow oil **52** (3.08 g, 59%).

$C_{12}H_{24}O_4N_2$. IR ν_{max}/cm^{-1} (neat): 3347 cm^{-1} (m), 2975 cm^{-1} (m), 2933 cm^{-1} (m), 1639 cm^{-1} (s), 1504 cm^{-1} (s), 1189 cm^{-1} (s), 1142 cm^{-1} (s); δ_H (500 MHz, D_2O): 4.16 (q, 4H, *J* = 7.1 Hz, 2 x CH_2), 1.38 (s, 12H, 4 x CH3), 1.22 (t, 6H, *J* = 7.1 Hz, 2 x CH_3); δ_C (75 MHz, $CDCl_3$): 177.9, 77.5, 32.9, 30.1, 21.7; ESI-MS: *m/z* 339.19 (51%, $M+2K+H^+$); (Found 339.1958, $C_{12}H_{24}O_4N_2$ requires $M+2K+H^+$, 339.1083).

5.8.4 Synthesis of 2-(2-phenylhydrazinyl)ethyl 2-hydroxyisobutyrate (53)

Ethyl 2-hydroxyisobutyrate (2.50 mL, 20 mmol), was dissolved in ethanol (40 mL) under vigorous stirring. Phenylhydrazine (2 mL, 20 mmol) was added dropwise to the solution and left to stir for 18 hours at 25 °C. Colour change from colourless to pale yellow after 15 hours. The solvent was removed under reduced pressure to the give crude mixture. This crude product was further dried in a vacuum oven at 60 °C for 96 hours to yield the final product. Product was isolated as an orange oil **53** (3.21 g, 72%)

$C_{12}H_{18}O_2N_2$. IR ν_{max}/cm^{-1} (neat): 3377 cm^{-1} (m), 3301 cm^{-1} (m), 2980 cm^{-1} (w), 2540 cm^{-1} (w), 1724 cm^{-1} (s), 1601 cm^{-1} (s), 1522 cm^{-1} (m), 1176 cm^{-1} (s), 1139 cm^{-1} (s); δ_H (500 MHz, $CDCl_3$): 7.16 (dd, 2H, *J* = 10.0, 7.8 Hz, 2 x Ar-H), 6.83-6.70 (m, 3H, 3 x Ar-H), 4.16 (q, 2H, *J* = 7.1 Hz, CH_2), 1.36 (s, 6H, 2 x CH_3), 1.23 (t, 3H, *J* = 7.1 Hz, CH_3); δ_C (75 MHz, $CDCl_3$): 162.9, 130.8, 128.9, 119.5, 112.1, 72.6, 61.8, 27.1, 14.1; ESI-MS *m/z* 195.13 (93%, $M-(CH_3CH_2)+H^+$); (Found 195.1285, $C_{12}H_{18}O_2N_2$ requires $M-(CH_3CH_2)+H^+$, 195.1128).

5.9 Plastisol Formulations

Blowing agent (0.161 mmol) was added to the pre-mixed formulation (1 g) with the blowing agent removed. The mixture was stirred vigorously at speed 2000 rpm for 5 minutes using a mechanical stirrer with a radial turbine blade. The following quantities were added:

5.9.1 Control ADCA Formulation

Azodicarbonamide (9.5 g, 80.5 mmol) was added to the plastisol (500 g)

5.9.2 OBSH Formulations

5.9.2.1 100% OBSH Formulation (P9)

4,4'-oxybis(benzenesulfonyl hydrazide) (28.8 g, 80.5 mmol) was added to the plastisol (500 g)

5.9.2.2 OBSH: ADCA 1:1 Ratio Formulation ($P9_{1:1}$)

4,4'-oxybis(benzenesulfonyl hydrazide) (14.4 g, 40.25 mmol) and azodicarbonamide (4.7 g, 40.25 mmol) were added to the plastisol (500 g)

5.9.3 TSSC Formulations

5.9.3.1 100% TSSC Formulation (P11)

Toluenesulfonyl semicarbazide (18.4 g, 80.5 mmol) was added to the plastisol (500 g)

5.9.3.2 TSSC: ADCA 1:1 Ratio Formulation ($P11_{1:1}$)

Toluenesulfonyl semicarbazide (9.2 g, 40.25 mmol) and azodicarbonamide (4.7 g, 40.25 mmol) were added to the plastisol (500 g)

5.9.4 Citric Acid Formulations

5.9.4.1 100% Citric Acid Formulation (P18)

Citric acid (15.5 g, 80.5 mmol) was added to the plastisol (500 g)

5.9.4.2 Citric Acid: ADCA 1:1 Formulation ($P18_{1:1}$)

Citric acid (7.7 g, 40.25 mmol) and azodicarbonamide (4.7 g, 40.25 mmol) were added to the plastisol (500 g)

5.9.5 $NaHCO_3$ Formulations

5.9.5.1 100% $NaHCO_3$ Formulation (P19)

Sodium hydrogen carbonate (6.8 g, 80.5 mmol) was added to the plastisol (500 g)

5.9.5.2 $NaHCO_3$: ADCA 1:1 Formulation ($P19_{1:1}$)

Sodium hydrogen carbonate (3.4 g, 40.25 mmol) and azodicarbonamide (4.7 g, 40.25 mmol) were added to the plastisol (500 g)

5.9.5.3 $NaHCO_3$: ADCA 2:1 Formulation ($P19_{2:1}$)

Sodium hydrogen carbonate (4.5 g, 53.67 mmol) and azodicarbonamide (3.2 g, 26.83 mmol) were added to the plastisol (500 g)

5.9.5.4 $NaHCO_3$: ADCA 3:1 Formulation ($P19_{3:1}$)

Sodium hydrogen carbonate (5.1 g, 60.375 mmol) and azodicarbonamide (2.4 g, 20.125 mmol) were added to the plastisol (500 g)

5.9.5.5 $NaHCO_3$: ADCA 4:1 Formulation ($P19_{4:1}$)

Sodium hydrogen carbonate (5.4 g, 64.4 mmol) and azodicarbonamide (1.9 g, 16.1 mmol) were added to the plastisol (500 g)

5.9.6 Compound 23 Formulation (P23)

Compound **23** (2.8 g, 16.1 mmol) was added to the plastisol (100 g)

5.9.7 Compound 24 Formulation (P24)

Compound **24** (2.6 g, 16.1 mmol) was added to the plastisol (100 g)

5.9.8 Compound 31 Formulation (P31)

Compound **31** (2.5 g, 16.1 mmol) was added to the plastisol (100 g)

5.9.9 Compound 37 Formulation (P37)

Compound **37** (4.1 g, 16.1 mmol) was added to the plastisol (100 g)

5.9.10 Compound 41 Formulation (P41)

Compound **41** (18.4 g, 48.3 mmol) was added to the plastisol (300 g)

5.9.11 Compound 42 Formulation (P42)

Compound **42** (13.6 g, 48.3 mmol) was added to the plastisol (300 g)

5.9.12 Compound 43 Formulation (P43)

Compound **43** (26.5 g, 48.3 mmol) was added to the plastisol (300 g)

5.9.13 Compound 44 Formulation (P44)

Compound **44** (17.7 g, 48.3 mmol) was added to the plastisol (300 g)

5.9.14 Compound 46 Formulation (P46)

Compound **46** (11.4 g, 48.3 mmol) was added to the plastisol (300 g)

5.9.15 Compound 47 Formulation (P47)

Compound **12** (10.1 g, 48.3 mmol) was added to the plastisol (300 g)

5.9.16 Compound 50 Formulations (P50)

Compound **50** (16.4 g, 80.5 mmol) was added to the plastisol (500 g)

5.9.16.1 Double Concentration Compound 50 Formulation (P50a)

Compound **50** (23.8 g, 161 mmol) was added to the plastisol (500 g)

5.9.16.2 Double Concentration, No Kicker Compound 50 Formulation (P50b)

Compound **50** (23.8 g, 161 mmol) was added to the pre-mixed no kicker plastisol (500 g)

5.9.17 Compound 51 Formulation (P51)

Compound **51** (9.4 g, 48.3 mmol) was added to the plastisol (300 g)

5.9.18 Compound 52 Formulations (P52)

Compound **52** (20.9 g, 80.5 mmol) was added to the plastisol (500 g)

5.9.18.1 Double Concentration Compound 52 Formulation (P52a)

Compound **52** (41.8 g, 161 mmol) was added to the plastisol (500 g)

5.9.18.2 Double Concentration, No Kicker Compound 52 Formulation (P52b)

Compound **52** (41.8 g, 161 mmol) was added to the pre-mixed no kicker plastisol (500 g)

5.9.19 Compound 53 Formulation (P53)

Compound **17** (10.7 g, 48.3 mmol) was added to the plastisol (300 g)

5.10 HPLC and UPC^2 Sample Preparation

5.10.1 ADCA Calibration

Azodicarbonamide (5 mg) was dissolved in dimethyl sulfoxide (10 mL) and diluted 1:4 in DMSO to give a 100 µg/mL solution. A 5-level calibration curve was generated by injecting 2, 4, 6, 8 and 10 µL

5.10.2 Paper Samples

Paper samples containing 0.5, 1.0, 2.0 and 3.0 ADCA were dissolved in dimethyl sulfoxide to give 100 mg/mL solutions. (e.g. wallpaper (0.8025 g) was dissolved in dimethyl sulfoxide (8.025 mL)). Samples were diluted 1:4 in ethyl acetate and sonicated for 1 hour at 50 °C. Once sonicated the samples were filtered using a 0.22 µm nylon syringe filter.

Chapter 6 Notes and references

1. Codou, A., et al., *Glass transition dynamics and cooperativity length of poly(ethylene 2,5-furandicarboxylate) compared to poly(ethylene terephthalate).* Physical Chemistry Chemical Physics, 2016. **18**(25): p. 16647-16658.
2. Wei, L., N.M. Stark, and A.G. McDonald, *Interfacial improvements in biocomposites based on poly(3-hydroxybutyrate) and poly(3-hydroxybutyrate-co-3-hydroxyvalerate) bioplastics reinforced and grafted with [small alpha]-cellulose fibers.* Green Chemistry, 2015. **17**(10): p. 4800-4814.
3. Gandini, A. and T.M. Lacerda, *From monomers to polymers from renewable resources: Recent advances.* Progress in Polymer Science, 2015. **48**: p. 1-39.
4. Hong, S., et al., *High molecular weight bio furan-based co-polyesters for food packaging applications: synthesis, characterization and solid-state polymerization.* Green Chemistry, 2016. **18**(19): p. 5142-5150.
5. Quadrelli, E.A., et al., *Carbon Dioxide Recycling: Emerging Large-Scale Technologies with Industrial Potential.* ChemSusChem, 2011. **4**(9): p. 1194-1215.
6. Zhang, T., et al., *Zn electrode with a layer of nanoparticles for selective electroreduction of CO2 to formate in aqueous solutions.* Journal of Materials Chemistry A, 2016. **4**(42): p. 16670-16676.
7. Awadhiya, A., D. Kumar, and V. Verma, *Crosslinking of agarose bioplastic using citric acid.* Carbohydrate Polymers, 2016. **151**: p. 60-67.
8. Sagnelli, D., et al., *Cross-Linked Amylose Bio-Plastic: A Transgenic-Based Compostable Plastic Alternative.* International Journal of Molecular Sciences, 2017. **18**(10): p. 2075.
9. European Climate Foundation, *Understanding the Challenges and Opportunities for the Chemical Sector*, in *Europe's Low-Carbon Transition*, ECF, Editor. 2014. p. 31-32.
10. British Plastics Federation. *PVC Explained*. 2016 [cited 2016 25/08/2016]; Available from: http://www.bpf.co.uk/press/PVC_Explained.aspx.
11. Song, Z., et al., *Acetylene hydrochlorination over 13X zeolite catalysts at high temperature.* Green Chemistry, 2016. **18**(22): p. 5994-5998.
12. Lee, K.W., J.W. Chung, and S.-Y. Kwak, *Synthesis and characterization of bio-based alkyl terminal hyperbranched polyglycerols: a detailed study of their plasticization effect and migration resistance.* Green Chemistry, 2016. **18**(4): p. 999-1009.
13. European Climate Foundation, *Understanding the Challenges and Opportunities for the Chemical Sector*, in *Europe's Low-Carbon Transition*, ECF, Editor. 2014. p. 36.
14. Uysal Unalan, I., et al., *Nanocomposite films and coatings using inorganic nanobuilding blocks (NBB): current applications and future opportunities in the food packaging sector.* RSC Advances, 2014. **4**(56): p. 29393-29428.
15. Williams, K.S., *Plastic Packaging: Not a Throw-away Resource*, in *Waste as a Resource*. 2013, The Royal Society of Chemistry. p. 83-109.
16. *Wire and cable: some new developments.* Plastics, Additives and Compounding, 2004. **6**(3): p. 32-36.

17. Behboudi, A., Y. Jafarzadeh, and R. Yegani, *Enhancement of antifouling and antibacterial properties of PVC hollow fiber ultrafiltration membranes using pristine and modified silver nanoparticles.* Journal of Environmental Chemical Engineering, 2018. **6**(2): p. 1764-1773.
18. Czégény, Z., et al., *Pyrolysis of wood–PVC mixtures. Formation of chloromethane from lignocellulosic materials in the presence of PVC.* Journal of Analytical and Applied Pyrolysis, 2015. **113**: p. 123-132.
19. Ebnalwaled, A.A. and A. Thabet, *Controlling the optical constants of PVC nanocomposite films for optoelectronic applications.* Synthetic Metals, 2016. **220**: p. 374-383.
20. Zhang, X., et al., *The molecular interfacial structure and plasticizer migration behavior of "green" plasticized poly(vinyl chloride).* Physical Chemistry Chemical Physics, 2015. **17**(6): p. 4472-4482.
21. Tejasvi, R., M. Sharma, and K. Upadhyay, *Passive photo-catalytic destruction of air-borne VOCs in high traffic areas using TiO2-coated flexible PVC sheet.* Chemical Engineering Journal, 2015. **262**: p. 875-881.
22. Jiang, Z., et al., *Rigid cross-linked PVC foams with high shear properties: The relationship between mechanical properties and chemical structure of the matrix.* Composites Science and Technology, 2014. **97**: p. 74-80.
23. European Climate Foundation, *Understanding the Challenges and Opportunities for the Chemical Sector - Product Deep-Dives*, in *Europe's Low-Carbon Transition*, ECF, Editor. 2014. p. 3.
24. Jia, P., et al., *Synthesis and Application of Environmental Castor Oil Based Polyol Ester Plasticizers for Poly(vinyl chloride).* ACS Sustainable Chemistry & Engineering, 2015. **3**(9): p. 2187-2193.
25. Wilcken, R., et al., *Principles and Applications of Halogen Bonding in Medicinal Chemistry and Chemical Biology.* Journal of Medicinal Chemistry, 2013. **56**(4): p. 1363-1388.
26. Xu, Z., et al., *Utilization of Halogen Bond in Lead Optimization: A Case Study of Rational Design of Potent Phosphodiesterase Type 5 (PDE5) Inhibitors.* Journal of Medicinal Chemistry, 2011. **54**(15): p. 5607-5611.
27. Saiyad, M., N.M. Devashrayee, and R.K. Mewada, *The influence of stabilisers on resistance to gamma radiation for epoxy based polymeric composite material.* Composites Part B: Engineering, 2014. **57**: p. 71-79.
28. Vishnu, V.S., et al., *Synthesis and characterization of new environmentally benign tantalum-doped Ce0.8Zr0.2O2 yellow pigments: Applications in coloring of plastics.* Dyes and Pigments, 2009. **82**(1): p. 53-57.
29. Wypych, G., *10 - SELECTION OF FOAMING AND BLOWING AGENTS FOR DIFFERENT POLYMERS*, in *Handbook of Foaming and Blowing Agents*. 2017, ChemTec Publishing. p. 123-177.
30. Wood, K.A., *How can we effectively use accelerated methods to predict the decorative properties of PVDF-based coatings? – A practical approach.* Progress in Organic Coatings, 2014. **77**(12, Part B): p. 2140-2146.
31. Swarup, S. and C.K. Schoff, *A survey of surfactants in coatings technology.* Progress in Organic Coatings, 1993. **23**(1): p. 1-22.
32. Afcona Additives, *Slip and Leveling agent Surface Control*, Afcona Additives, Editor. 2009. p. 1.
33. Kornum, L.O. and H.K. Raaschou Nielsen, *Surface defects in drying paint films.* Progress in Organic Coatings, 1980. **8**(3): p. 275-324.

34. Petchwattana, N. and S. Covavisaruch, *Influences of particle sizes and contents of chemical blowing agents on foaming wood plastic composites prepared from poly(vinyl chloride) and rice hull.* Materials & Design, 2011. **32**(5): p. 2844-2850.
35. Marks, H.B., N., *Encyclopedia of Polymer Science and Engineering.* 1990: p. 532.
36. Bakeri, G. and M. Rahimnejad, *Kinetics study of hydrazodicarbonamide synthesis reaction.* Chemical Industry and Chemical Engineering Quaterly, 2013. **19**(2): p. 273-279.
37. Berins, M., *Plastics Engineering Handbook of The Society of the Plastics Industry*. 1991, New York: Van Nostrand Reinhold.
38. Exelby, J.H., et al., *Formulating Expanded Products*, in *Handbook of Vinyl Formulating*. 2007, John Wiley & Sons, Inc. p. 379-391.
39. Bledzski, A. and O. Faruk, *Injection molded microcellular wood fiber-polypropylene composites.* Composites Part A: Applied Science and Manufacturing, 2006. **37**: p. 1358.
40. Linde Plastics, *Polymer foaming with inert gases*, Linde Noth America Inc, Editor. 2012, The Linde Group: New Jersey. p. 3.
41. Sivertsen, K., *Polymer Foams*. 2007, MIT OpenCourseWare.
42. Riley, C.P., Jr., H.R. Lasman, and R. Strauss, *Activators for azodicarboxamide*. 1965, American Biltrite Rubber Co., Inc. . p. 22 pp.
43. Naguib, H., J. Xu, and C. Park. *Effects of Blending of Branched and Linear Polypropylene Materials on the Foamability*. in *Antec 2001 - Plastics: The lone star*. 2001. Dallas Texas: CRC Press.
44. Joiner, R., F. Vidal, and H. Marks, *A New powdered agent for flour maturing.* Journal of Cereal Chemistry, 1963. **40**(1): p. 539.
45. Eiwa Chemical Industry. *Properties of Blowing Agents*. 2014 [cited 2014 09 October]; Available from: http://www.eiwa-chem.co.jp/en/products/types.html.
46. Deng, Z., et al., *Preparation and application of heat-insulating powder coating materials*. 2015, Suzhou Yufeng Decorative Doors and Windows Co., Ltd., Peop. Rep. China; Suzhou Huashi Material Technology Service Co., Ltd. . p. 14pp.
47. Je, C.H., et al., *Waterproofing layer protective material for construction of buildings*. 2015, POSCO E & C Co., Ltd., S. Korea; Hanyang New Technology Co., Ltd. . p. 10pp.
48. Nezu, K., K. Adachi, and T. Suzuki, *Sealing materials and their manufacture*. 2011, Sekisui Chemical Co., Ltd., Japan . p. 12pp.
49. Koike, H., *Manufacture of decorative foamed wallpapers*. 2010, Dai Nippon Printing Co., Ltd., Japan . p. 13pp.
50. Prakash, A.S., W.A. Swam, and A.N. Strachan, *The thermal decomposition of azodicarbonamide (1,1[prime or minute]-azobisformamide).* Journal of the Chemical Society, Perkin Transactions 2, 1975(1): p. 46-50.
51. Yang, X., *Manufacture of environmentally friendly polyurethane leather and product thereof*. 2013, Jinjiang Mingao Textile Technology Co., Ltd., Peop. Rep. China . p. 8pp.
52. Herweh, J.E. and R.M. Fantazier, *1,1'-Azobisformamide. II. Thermal decomposition. Kinetics, products, and decomposition mechanism.* J. Org. Chem., 1974. **39**(6): p. 786-93.

53. Robledo-Ortiz, J.R., et al., *Non-isothermal decomposition kinetics of azodicarbonamide in high density polyethylene using a capillary rheometer.* Polymer Testing, 2008. **27**(6): p. 730-735.
54. Reyes-Labarta, J.A. and A. Marcilla, *Thermal Treatment and Degradation of Cross-Linked Ethylene Vinyl Acetate–Polyethylene–Azodicarbonamide–ZnO Foams. Complete Kinetic Modeling and Analysis.* Industrial & Engineering Chemistry Research, 2012. **51**(28): p. 9515-9530.
55. Riley, J.C.P., S. Richard, and H.R. Lasman, *Activated azodicarbonamide blowing agent compositions*. 1967, Google Patents.
56. Cameo Chemicals. *Azodicarbonamide - Chemical Data Sheet*. 2014 [cited 2014 17 October]; Available from: http://cameochemicals.noaa.gov/chemical/19157.
57. Sigma-Aldrich. *Azodicarboxamide*. 2014 [cited 2014 04 November]; Available from: http://www.sigmaaldrich.com/catalog/product/aldrich/a96606?lang=en&region=GB.
58. British Standards, *Decorative wallcoverings - Roll and panel form products*, in *15102:2007+A1*, Standards Policy and Strategy Committee, Editor. 2007, European Committee for Standardization: Brussels.
59. Austrian Competent Authority, *Identification of C,C'-azodi(formamide) (ADCA) as SVHC*, ECHA, Editor. 2012, Environment Agency Austria on behalf of the Austrian Competent Authority,: Austria.
60. Takahashi, M., et al., *Chronic toxicity and carcinogenicity of semicarbazide hydrochloride in Wistar Hannover GALAS rats.* Food and Chemical Toxicology, 2014. **73**(0): p. 84-94.
61. Nestmann, E.R., et al., *Safety assessment and risk-benefit analysis of the use of azodicarbonamide in baby food jar closure technology: Putting trace levels of semicarbazide exposure into perspective - A review.* Food Addit. Contam., 2005. **22**(9): p. 875-891.
62. Whitehead, L.W., et al., *Respiratory symptoms associated with the use of azodicarbonamide foaming agent in a plastics injection molding facility.* Am J Ind Med, 1987. **11**(1): p. 83-92.
63. Chemicalbook. *Material Safety Data Sheet*. 2013 [cited 2014 21 October]; Available from: http://www.chemicalbook.com/ProductChemicalPropertiesCB2494212_EN.htm#MSDSA.
64. Simpson, R., *Rubber Basics*. 2002: iSmithers Rapra Publishing.
65. PubChem. *Sodium Bicarbonate*. 2014 [cited 2014 13 October]; Available from: http://pubchem.ncbi.nlm.nih.gov/summary/summary.cgi?cid=516892.
66. Sigma-Aldrich. *Sodium bicarbonate*. 2014 [cited 2014 14 November]; Available from: http://www.sigmaaldrich.com/catalog/product/sial/s6014?lang=en&region=GB.
67. Acros Organics. *Material Safety Data Sheet*. 2009 [cited 2014 20 October]; Available from: https://www.fishersci.ca/viewmsds.do?catNo=AC263721000.
68. Park, C.B., et al., *Polymeric Foams*. Polymeric Foams Series, ed. S.-T. Lee. USA: CRC Press.

69. Chemicaland21. *4,4'-oxybis(benzenesulphonyl hydrazide)*. 2014 [cited 2014 17 October]; Available from: http://www.chemicalland21.com/specialtychem/perchem/4,4'-OXYBIS(BENZENESULPHONYL%20HYDRAZIDE).htm.
70. Ash, M. and I. Ash, *Handbook of Green Chemicals*. 2 ed. Vol. 1. 2004: Synapse Info Resources.
71. Alfa Aeser. *Material Safety Data Sheet*. 2012 [cited 2014 14 October]; Available from: http://www.alfa.com/content/msds/british/B23971.pdf.
72. Chemicaland21. *Benzenesulfonyl Hydrazide*. 2014; Available from: http://www.chemicalland21.com/specialtychem/perchem/BENZENESULFONYL%20HYDRAZIDE%20(BLOWING%20AGENT).htm.
73. United States Environmental Protection Agency, *Toxic Substances Control Act*, in *Chemical Substances Inventory*, Office of Toxic Substances, Editor. 1980, The Office: Michigan, USA.
74. Sheftel, V., *Indirect food additives and polymers: Migration and Toxicology*. 2000, London: CRC Press.
75. World Health Organisation. *FAO/WHO*. in *Technical Workshop on Residues on Veterinary Drugs Without ADI/MRL*. 2004. Bangkok, Thailand: Food and Agriculture Organisation.
76. Einhorn, I. *Recent Advances in Cellular Materials*. in *Cellular Plastics*. 1966. Natick, Massachusetts.
77. Chemicalbook. *p-toluenesulfonyl semicarbazide basic information*. 2008 [cited 2014 10 October]; Available from: http://www.chemicalbook.com/ProductChemicalPropertiesCB3382662_EN.htm.
78. Supuran, C., *Carbonic Anhydrase inhibitors - inhibitors with modifiec sulfonamido groups and their interaction with thye zinc enzyme.* Revue Romaine de Chemie,, 1991. **36**(11): p. 9.
79. Hunter Byron, A., *Sulfonyl Semicarbazides*, US3152176A, Editor. 1959.
80. Weissman, S. and G. Matthias, *Process of filling a rigis hollow structure with foamed-in-place foam*, in *US3155753A*. 1963.
81. Chemicalbook. *N,N'-Dinitrosopentamethylenetetramine(101-25-7)*. 2008 [cited 2014 08 October]; Available from: http://www.chemicalbook.com/ProductChemicalPropertiesCB2756327_EN.htm.
82. Sun, H. and E. Tang, *PVC plastic foam yoga mat and its preparation method*. 2011, Hebei Jiameile Plastic Products Co., Ltd., Peop. Rep. China . p. 6pp.
83. Miller, C.H., et al., *Printable compositions for manufacture of relief-printed decorative sheets*. 1986, Congoleum Corp., USA . p. 39 pp.
84. Kurti, L. and B. Czako, *Strategic Applications of Named Reactions in Organic Chemistry*, ed. E.J. Corey. 2005: Elsevier.
85. Sigma-Aldrich. *Material Safety Data Sheets*. Diethyl azodicarbonamide 2012 [cited 2015 5th January]; Available from: http://www.sigmaaldrich.com/MSDS/MSDS/DisplayMSDSPage.do?country=GB&language=en&productNumber=D90008&brand=ALDRICH&PageToGoToURL=http%3A%2F%2Fwww.sigmaaldrich.com%2Fcatalog%2Fproduct%2Faldrich%2Fd90008%3Flang%3Den.
86. Helmenstine, A.-M. *DEAD - diethyl azodicarboxylate*. Molecules with Strange names 2014 [cited 2015 5th January]; Available from: http://chemistry.about.com/cs/molecules/a/blmoldead.htm.

87. Wetzel, K., et al., *Propellant concentrate for thermoplastic synthetic materials*. 1981, VEB Chemiekombinat Bitterfeld, Ger. Dem. Rep. . p. 12 pp.
88. Ross, E., W. Jeblick, and H. Hurnik, *Azodicarbonamide-containing blowing agent for preparing foam plastic articles*. 1980, Bayer A.-G., Fed. Rep. Ger. . p. 22 pp.
89. Szmant, H. *Physical Properties of Dimethyl Sulfoxide and its Function in biological Systems*. DMSO Background Literature 2014 [cited 2014 13 November]; Available from: http://www.dmso.org/articles/information/szmant.html.
90. Yardley-Jones, A., D. Anderson, and D.V. Parke, *The toxicity of benzene and its metabolism and molecular pathology in human risk assessment.* Br J Ind Med, 1991. **48**(7): p. 437-44.
91. Massimo, S., P. Bortolotti, and M. Badali, *Process for producing pre-expandable plastic beads and their use as structural elements for household appliances*. 2012, Electrolux Home Products Corporation N. V., Belg. . p. 11pp.
92. Health and Safety Executive. *REACH Explained*. REACH 2015 [cited 2015 25 June]; Available from: http://www.hse.gov.uk/reach/about.htm.
93. Health and Safety Executive. *What is REACH?* REACH 2015 [cited 2015 25 June]; Available from: http://www.hse.gov.uk/reach/whatisreach.htm.
94. Health and Safety Executive. *The Registration Process*. REACH 2015 [cited 2015 25 June]; Available from: http://www.hse.gov.uk/reach/regprocess.htm.
95. Health and Safety Executive. *When to Comply with REACH*. REACH 2015 [cited 2015 25 June]; Available from: http://www.hse.gov.uk/reach/timeline.htm.
96. Health and Safety Executive. *Other REACH processes*. REACH 2015 [cited 2015 25 June]; Available from: http://www.hse.gov.uk/reach/otherreachprocesses.htm.
97. European Commission. *Evalutaion*. REACH 05/02/2013 [cited 2015 25 June]; Available from: http://ec.europa.eu/enterprise/sectors/chemicals/reach/evaluation/index_en.htm.
98. European Chemicals Agency. *Candidate List of Substances of Very High Concern for Autherisation*. 2012 16 June 2014 [cited 2014 31st October]; Available from: http://echa.europa.eu/candidate-list-table/-/substance/2101/search/+/term.
99. Health and Safety Executive, *REACH - Substances of Very High Concern*, HSE, Editor. 2014.
100. Health and Safety Executive. *Regime*. REACH 2015 [cited 2015 25 June]; Available from: http://www.hse.gov.uk/reach/regime.htm#a5.
101. Health and Safety Executive. *The UK enforcement regime for REACH*. REACH 2015 [cited 2015 25 June]; Available from: http://www.hse.gov.uk/reach/regime.htm.
102. Sittampalam, G.C., NP. Nelson, H. *Assay Guidance Manual [Internet]*. 2004 [cited 2015 25 June]; Available from: http://www.ncbi.nlm.nih.gov/books/NBK53196/.
103. Bonsall, J.L., *Allergic Contact Dermatitis to Azodicarbonamide.* Contact Dermatitis, 1984. **10**: p. 42.

104. ADCA Task Force, *ADCA and "equivalent concern"*, Team Mastery, Editor. 2018: UK.
105. ECHA, *Support Document for the Identification of Diazene-1,2-dicarboxamide as a Substance of Very High Concern/*, Member State Comittee, Editor. 2012.
106. Arts, J. and I. Kimber, *Azodicarbonamide (ADCA): A reconsideration of classification as a respiratory sensitiser.* Regulatory Toxicology and Pharmacology, 2017. **89**: p. 268-278.
107. Sigma-Alrdich. *Tetrahydrofuran Material Safety Data Sheet*. 2016 [cited 2018 20 April 2018]; Available from: https://www.sigmaaldrich.com/MSDS/MSDS/DisplayMSDSPage.do?country=GB&language=en&productNumber=T5267&brand=SIGMA&PageToGoToURL=https%3A%2F%2Fwww.sigmaaldrich.com%2Fcatalog%2Fproduct%2Fsigma%2Ft5267%3Flang%3Den.
108. Ye, J., et al., *Assessment of the Determination of Azodicarbonamide and Its Decomposition Product Semicarbazide: Investigation of Variation in Flour and Flour Products.* J. Agric. Food Chem., 2011. **59**(17): p. 9313-9318.
109. Yasui, A., et al., *Analysis of Azodicarbonamide in Wheat Flour and Prepared Flour Mixes.* Food Hygiene and Safety Science (Shokuhin Eiseigaku Zasshi), 2016. **57**(5): p. 133-138.
110. Health and Safety Executive, *Azodicarbonamide in Air*. HSE.
111. Brown, J.Q., et al., *Advances in Quantitative UV-Visible Spectroscopy for Clinical and Pre-clinical Application in Cancer.* Current opinion in biotechnology, 2009. **20**(1): p. 119-131.
112. Khorassani, H., F. Theraulaz, and O. Thomas, *Application of UV Spectrophotometry to the Study of Treated Wastwater Discharges in Rivers.* CLEAN - Soil, Air, Water, 1998. **26**(5).
113. Fountain, K., et al., *Beginner's Guide to Convergence Chromatography*. 2014, MA, USA: Waters Corporation.
114. Feng, L., et al., *A quantitative HPLC method for determining lactide content using hydrolytic kinetics.* Polymer Testing, 2009. **28**(6): p. 592-598.
115. Ferguson, G.K., *Quantitative HPLC Analysis of an Analgesic/Caffeine Formulation: Determination of Caffeine.* Journal of Chemical Education, 1998. **75**(4): p. 467.
116. Rahmani, A., S. Jinap, and F. Soleimany, *Qualitative and Quantitative Analysis of Mycotoxins.* Comprehensive Reviews in Food Science and Food Safety, 2009. **8**(3): p. 202-251.
117. Antwerp, J.V., *Convergence Chromatography: Solving Complex Chromatographic Challenges*. 2013, Waters.
118. Gong, X., et al., *Ultra-performance convergence chromatography (UPC2) method for the analysis of biogenic amines in fermented foods.* Food Chemistry, 2014. **162**: p. 172-175.
119. Waters, *Safe and Authentic Foodstuffs*, in *Business Solutions*, Waters, Editor. 2017, Waters: MA, USA.
120. Waters, *Chromatography Data System Solutions for the Food Industry*, in *Business Solutions*, Waters, Editor. 2017, Waters: MA, USA.
121. Waters, *Analytical Solutions for Cosmetics and Personal Care*, in *Business Solutions*, Waters, Editor. 2017, Waters: MA, USA.

122. Jones, J.W., et al., *Ultraperformance convergence chromatography-high resolution tandem mass spectrometry for lipid biomarker profiling and identification.* Biomed Chromatogr, 2017. **31**(3).
123. Waters, *Expanding SFC Applications at a Major Pharmaceutical Company*, in *Business Solutions*, Waters, Editor. 2016, Waters: MA, USA.
124. Sigma-Aldrich. *Azodicarbonamide Material Safety Data Sheet*. 2014 [cited 2014 13 October]; Available from: http://www.sigmaaldrich.com/catalog/product/aldrich/a96606?lang=en®ion=GB.
125. Salomão Garcia, P., et al., *Citric acid as multifunctional agent in blowing films of starch/PBAT*. Vol. 34. 2011. 1507-1510.
126. Sadik, T., et al., *Dsc studies on the decomposition of chemical blowing agents based on citric acid and sodium bicarbonate.* Thermochimica Acta, 2018. **659**: p. 74-81.
127. Speciality Coatings, *Hot Melt Vinyl Plastisols*, in *Technical Assistnace Brief*, PolyOne, Editor. 2010: Ohio, USA.
128. Stadler, R.H., et al., *Semicarbazide is a minor thermal decomposition product of azodicarbonamide used in the gaskets of certain food jars.* Analyst, 2004. **129**(3): p. 276-281.
129. O'Neil, M., *The Merck Index - An Encyclopedia of Chemicals, Drugs, and Biologicals*. 13th Edition ed, ed. M. O'Neil. 2001, Whitehouse Station, NJ: Merck and Co., Inc.
130. Abernethy, G.A., *Generation of semicarbazide from natural azine development in foods, followed by reaction with urea compounds.* Food Additives & Contaminants: Part A, 2015. **32**(9): p. 1416-1430.
131. Crews, C., *Potential Natural Sources of Semicarbazide in Honey*. 2012, The Food and Environment Research Agency: York, UK.
132. Hui, Y.-H., X. Zhang, and H.-j. Yu. *Investigation on the Natural Occurrence of Semicarbazide in Macrobrachium Nipponese Prawns*. in *2015 International Symposium on Material, Energy and Environment Engineering*. 2015. Atlantis Press.
133. Crook, A.J., E.C. Lisic, and D.D. Ensor, *Thiosemicarbazone and Semicarbazone Chelating Resins and Their Potential Use in Environmental Applications.* Separation Science and Technology, 2012. **47**(14-15): p. 2225-2229.
134. Nishat, N., et al., *Synthesis, characterization, and biocide properties of semicarbazide–formaldehyde resin and its polymer metal complexes.* European Journal of Medicinal Chemistry, 2010. **45**(4): p. 1287-1294.
135. Hesse, M., H. Meier, and B. Zeeh, *Spektroskopishe Methoden in der organischen Chemie*. Vol. 3. 1987, New York: Georg Thieme Verlag Stuttgart.
136. Reusch, W. *Infrared Spectroscopy*. Spectroscopy 2013 [cited 2015 6th January].
137. Uyeki, E.M., et al., *Acute toxicity of benzene inhalation to hemopoietic precursor cells.* Toxicology and Applied Pharmacology, 1977. **40**(1): p. 49-57.
138. Jeong, J., et al., *Sulfonyl hydrazide-based polymeric foaming agent nanoparticles.* Macromolecular Research, 2017. **25**(2): p. 128-134.
139. Wypych, G., *Handbook of Foaming and Blowing Agents*. Technology & Engineering. 2017, Toronto: Elsevier.

140. Parker, E.T., *Scope and Influence of Enhanced Triazine Degradation in U.S Soils*, in *Trace: Tennessee Research and Creative Exchange*. 2017, University of Tennessee: USA.
141. Singla, P., V. Luxami, and K. Paul, *Triazine as a promising scaffold for its versatile biological behavior.* Eur J Med Chem, 2015. **102**: p. 39-57.
142. Rothmann, M.M., et al., *Donor-Substituted 1,3,5-Triazines as Host Materials for Blue Phosphorescent Organic Light-Emitting Diodes.* Chemistry of Materials, 2010. **22**(7): p. 2403-2410.
143. Hoz, A. and A. Sánchez-Migallón, *Green synthesis of 1,3,5-triazines with applications in supramolecular chemistry and materials chemistry*. Vol. 20. 2017. 140-175.
144. Chakraborty, D., et al., *The Mechanism for Unimolecular Decomposition of RDX (1,3,5-Trinitro-1,3,5-triazine), an ab Initio Study.* The Journal of Physical Chemistry A, 2000. **104**(11): p. 2261-2272.
145. Dovlatyan, V.B., et al., *Synthesis and thermal decomposition of haloalkoxy-sym-triazines. 7. Thermal decomposition of 2-dialkylamino-4-(2-chloroethoxy)-6-methoxyamino-sym-triazines.* Chemistry of Heterocyclic Compounds, 1981. **17**(8): p. 838-841.
146. Glavin, D.P. and J.L. Bada, *Isolation of Amino Acids from Natural Samples Using Sublimation.* Analytical Chemistry, 1998. **70**(15): p. 3119-3122.
147. Chanukya, B.S., M. Prakash, and N.K. Rastogi, *Extraction of Citric Acid from Fruit Juices using Supported Liquid Membrane.* Journal of Food Processing and Preservation, 2017. **41**(1): p. e12790-n/a.
148. Vandenberghe, L.P.S., et al., *Microbial production of citric acid.* Brazilian Archives of Biology and Technology, 1999. **42**: p. 263-276.
149. Wiig, E.O., *THE DECOMPOSITION OF CITRIC ACID BY SULFURIC ACID.* Journal of the American Chemical Society, 1930. **52**(12): p. 4729-4737.
150. Apelblat, A., *Citric Acid*, ed. Ben-Gurion University of the Negev. 2014, Switzerland: Springer.
151. Cody, G.D., et al., *Geochemical roots of autotrophic carbon fixation: hydrothermal experiments in the system citric acid, H2O-(±FeS)−(±NiS).* Geochimica et Cosmochimica Acta, 2001. **65**(20): p. 3557-3576.
152. Barbooti, M. and D. Al-Sammerrai, *Thermal decomposition of citric acid.* Thermochimica Acta, 1986. **98**(1): p. 7.
153. Gogoi, P., et al., *Blends of Epoxidized Alkyd Resins Based on Jatropha Oil and the Epoxidized Oil Cured with Aqueous Citric Acid Solution: A Green Technology Approach.* ACS Sustainable Chemistry & Engineering, 2015. **3**(2): p. 261-268.
154. JunYing, Z.J.S.L.Z., *The mechanism of thermal decomposition of azodicarbonamide and the influence of zinc oxide.* Journal of Beijing University of Chemical Technology (Natural Science Edition), 2011. **3**: p. 009.
155. Drug, E. and M. Gozin, *Catalytic Oxidation of Hydrazo Derivatives Promoted by a TiCl3/HBr System.* Journal of the American Chemical Society, 2007. **129**(45): p. 13784-13785.
156. Schutte, H.R., *Progress in Botany*. 1 ed. Structural Botany, Physiology Genetics, Taxonomy and Geobotany, ed. H. Heidelberg, et al. 1992, Berlin: Springer-Verlag

157. Hartman, F.C. and F. Wold, *A new chemical synthesis of D-tartronic acid semialdehyde phosphate and D-glyceric acid 2-phosphate.* Biochimica et Biophysica Acta (BBA) - General Subjects, 1967. **141**(3): p. 445-453.
158. Rohwerder, T. and R.H. Müller, *Biosynthesis of 2-hydroxyisobutyric acid (2-HIBA) from renewable carbon.* Microbial Cell Factories, 2010. **9**(1): p. 13.
159. Zhu, H., H. Cao, and T. Li, *A theoretical study on the decomposition mechanisms of deprotonated glycolic acid.* Computational and Theoretical Chemistry, 2013. **1008**: p. 32-38.
160. Hristova-Kazmierski, M.K. and J.A. Kepler, *Synthesis of [14C]Azodicarbonamide.* Journal of Labelled Compounds and Radiopharmaceuticals, 1999. **42**(2): p. 203-206.
161. Mihara, M., et al., *Solvent-Free Basic or KF/Alumina-Assisted Dehydrogenation of Hydrazo Compounds.* Synlett, 2007. **2007**(13): p. 2124-2126.
162. Werner Backhaus, Reinhold Kliegl, and John Werner, *Colour Vision: Perspectives from Different Disciplines*, ed. Werner Backhaus. 1998, New York: Walter de Gruyter.

Chapter 7 Appendix

7.1 Compound 23

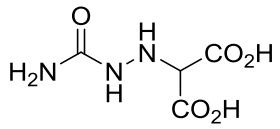

7.1.1 IR Spectrum of Compound 23

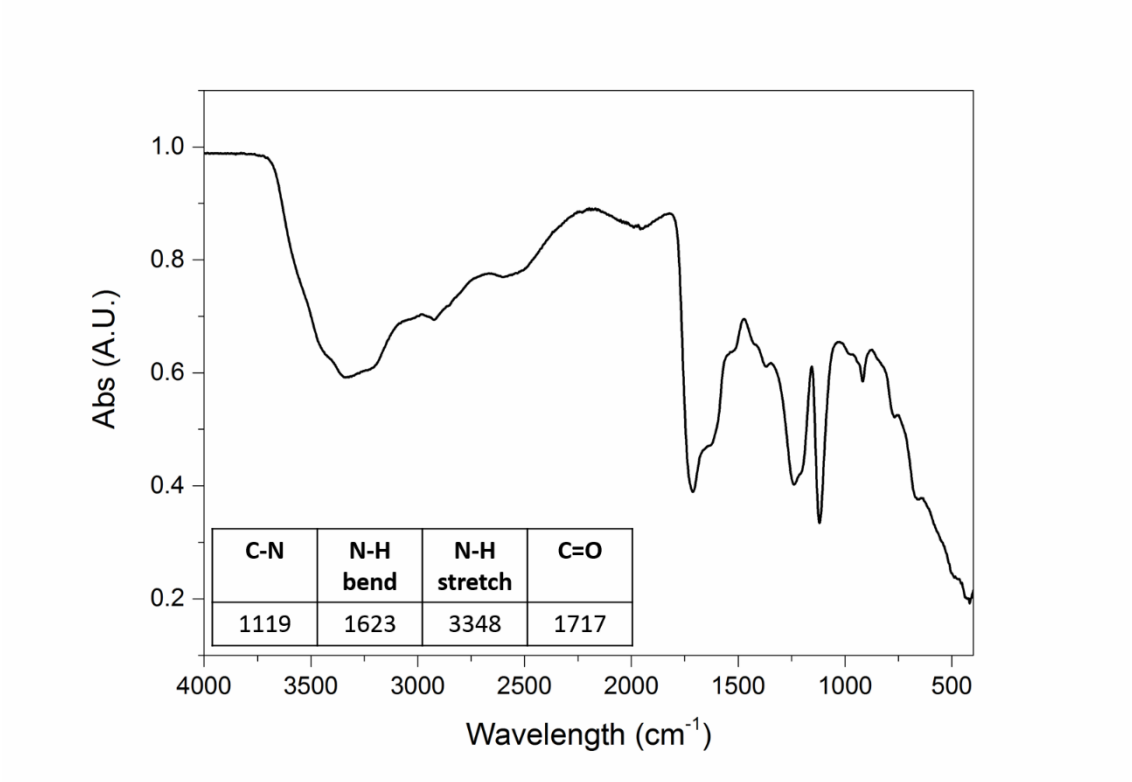

7.1.2 ^{1}H NMR Spectrum of Compound 23

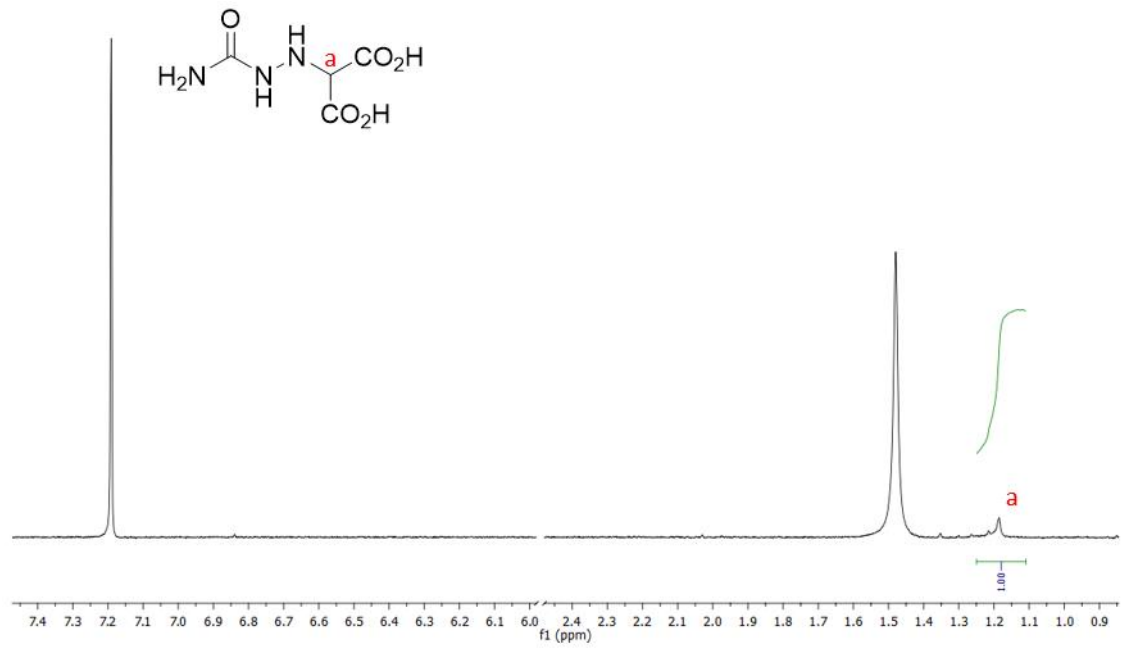

7.1.3 ^{13}C{^{1}H} NMR Spectrum of Compound 23[xxxii]

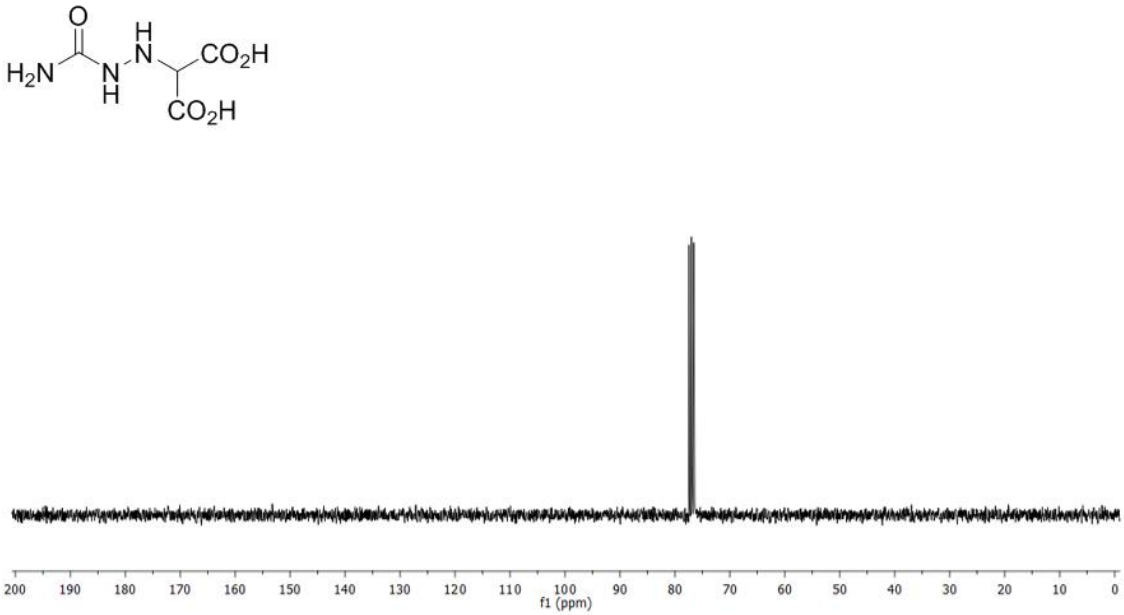

[xxxii] Low solubility of compound 23 prevented the acquirement of a strong ^{13}C{^{1}H} spectrum

7.2 Compound 24

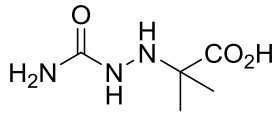

7.2.1 IR Spectrum of Compound 24

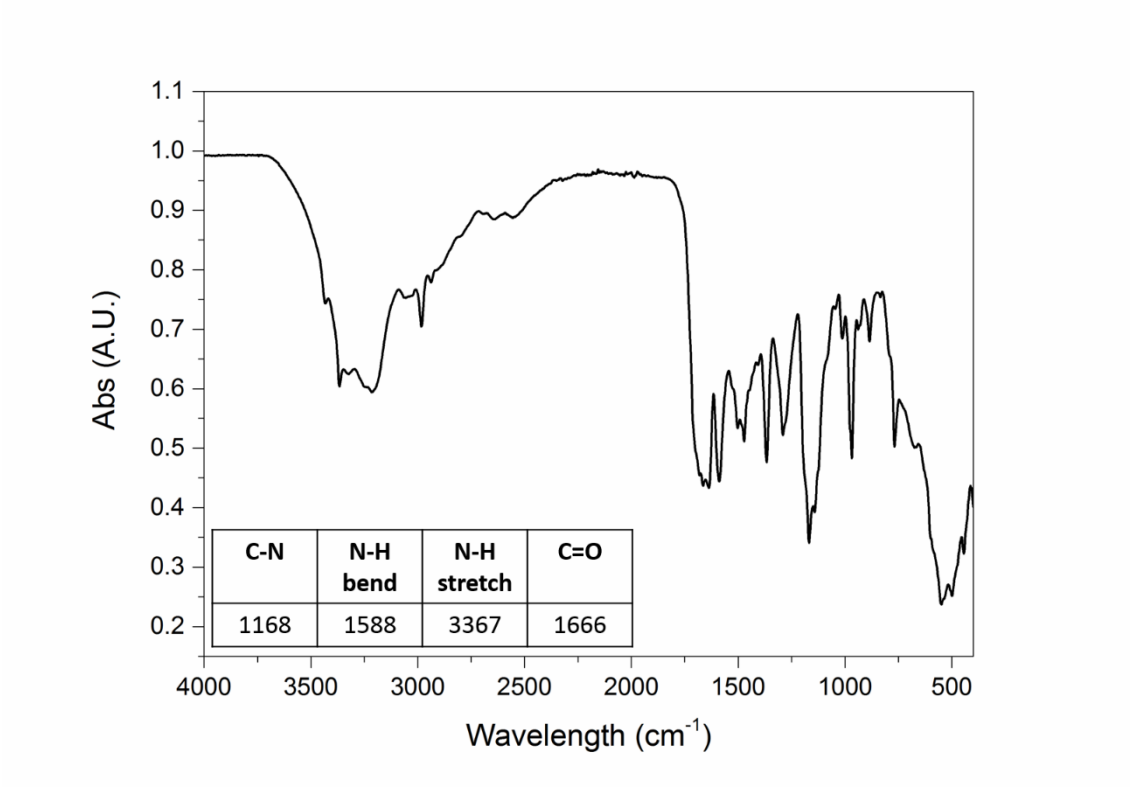

7.2.2 ^{1}H NMR Spectrum of Compound 24

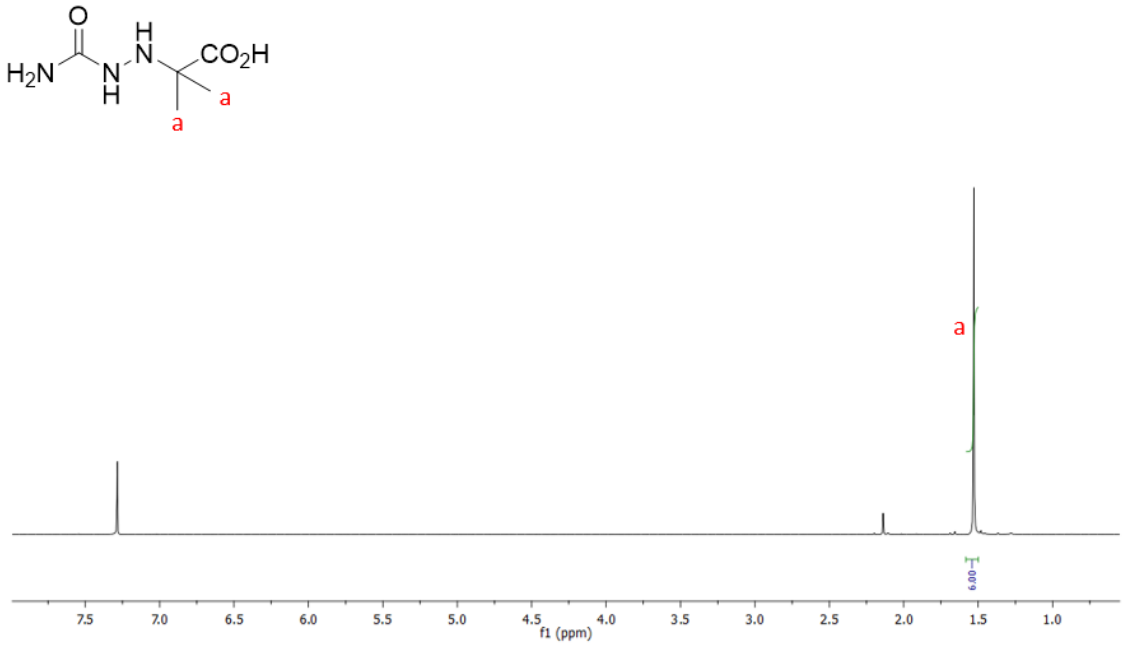

7.2.3 $^{13}C\{^{1}H\}$ NMR Spectrum of Compound 24

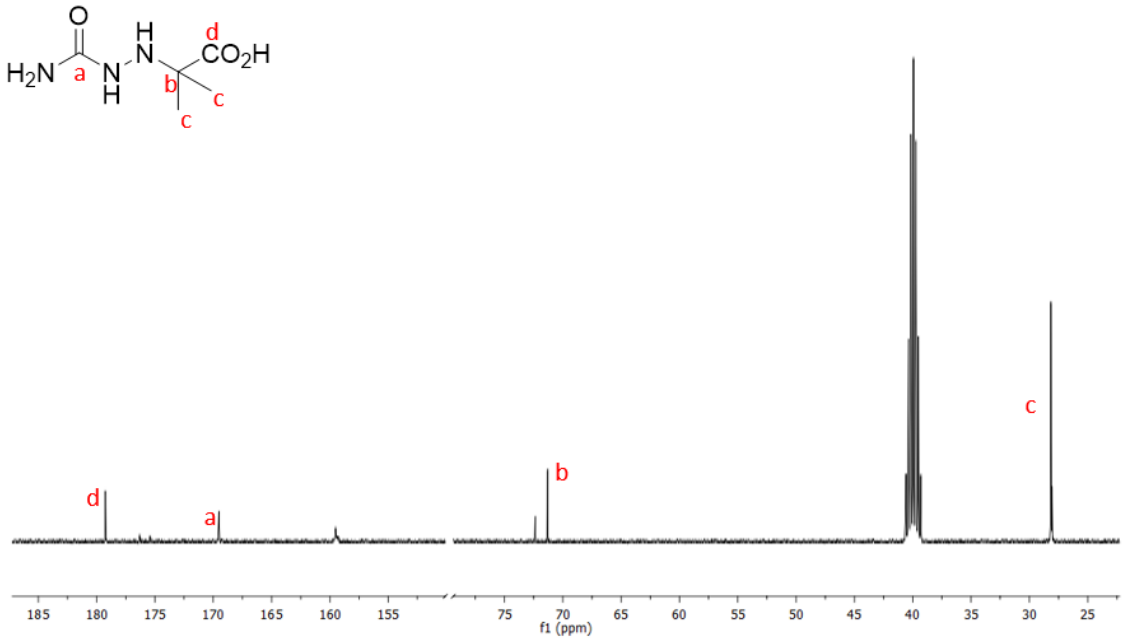

7.3 Compound 31

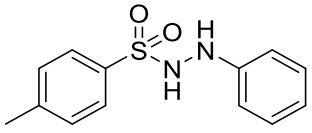

7.3.1 IR Spectrum of Compound 31

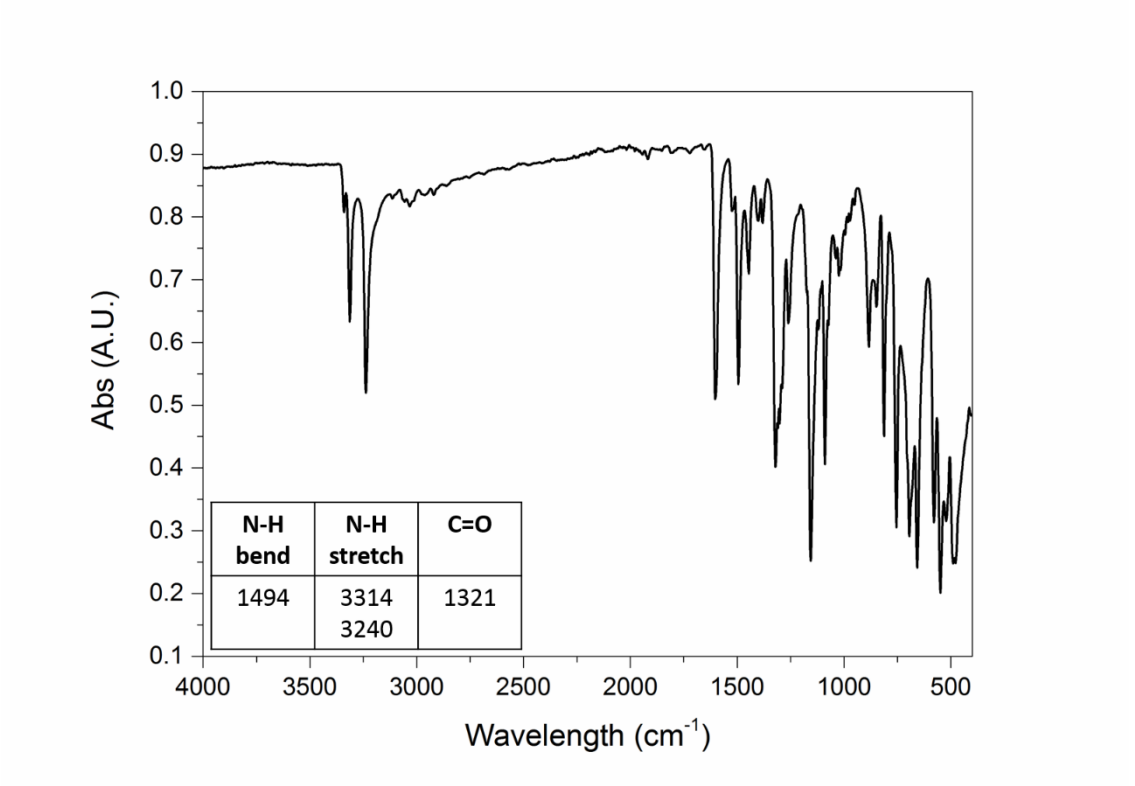

7.3.2 ^{1}H NMR Spectrum of Compound 31

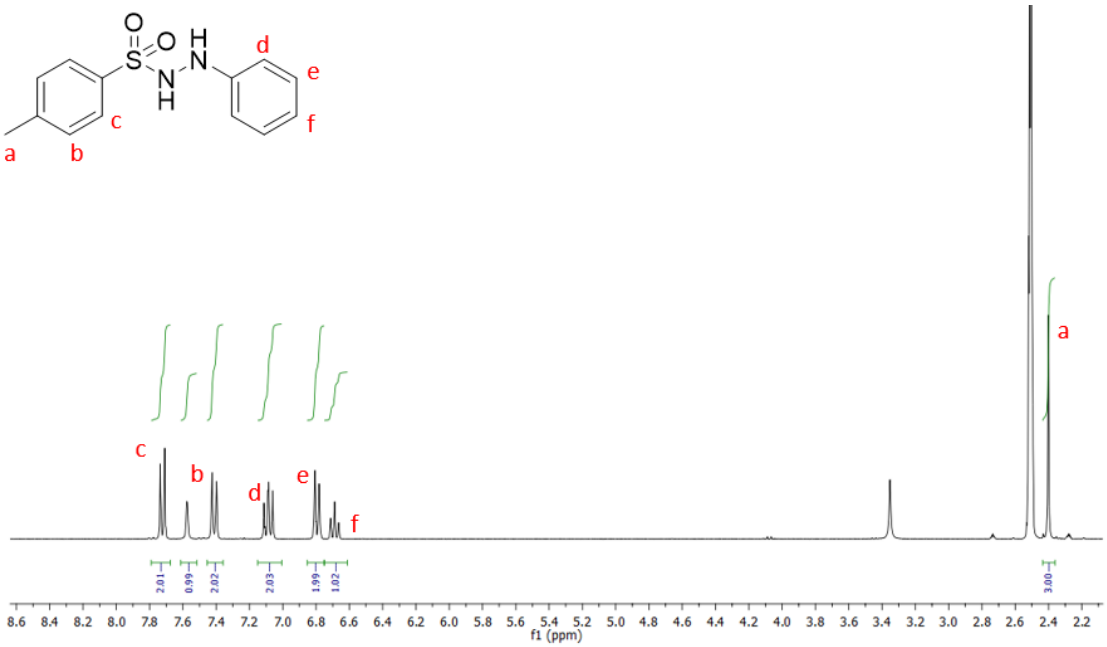

7.3.3 ^{13}C{^{1}H} NMR Spectrum of Compound 31

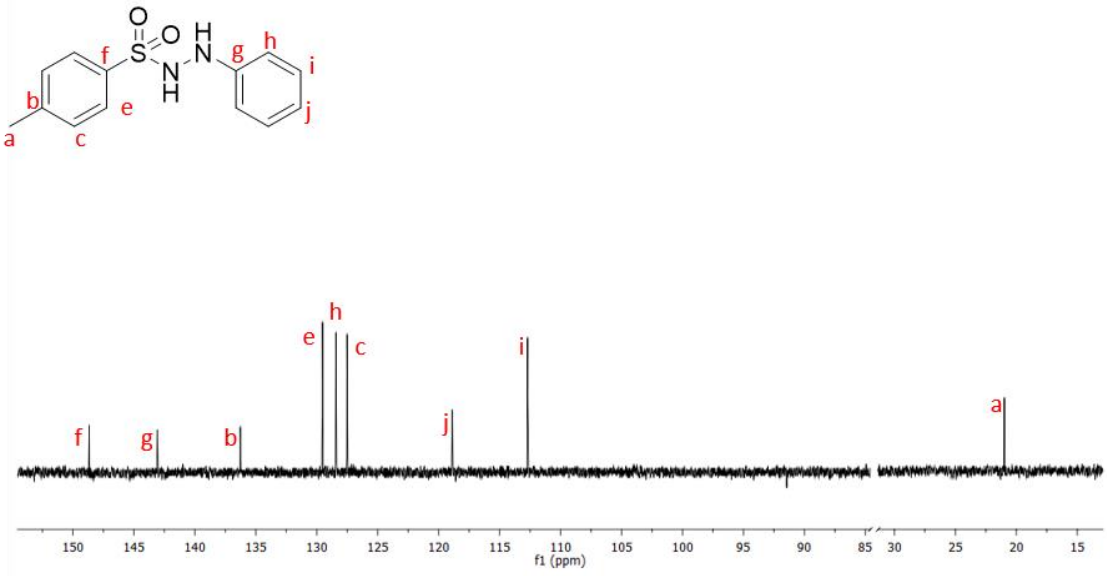

7.4 Compound 37

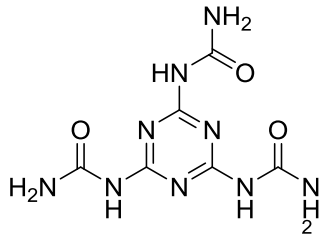

7.4.1 IR Spectrum of Compound 37

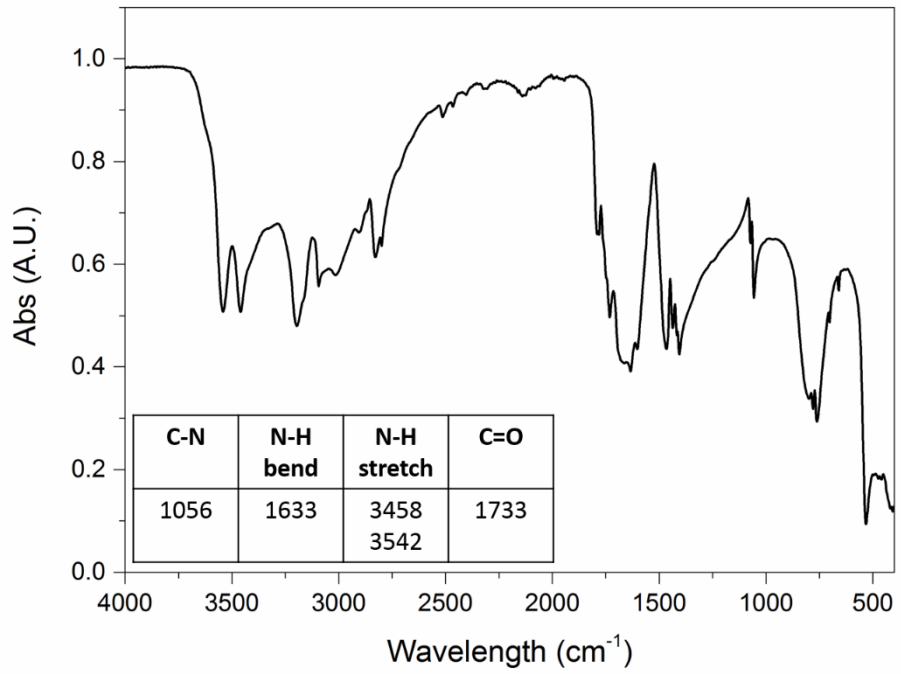

C-N	N-H bend	N-H stretch	C=O
1056	1633	3458 3542	1733

7.4.2 ^{1}H NMR Spectrum of Compound 37

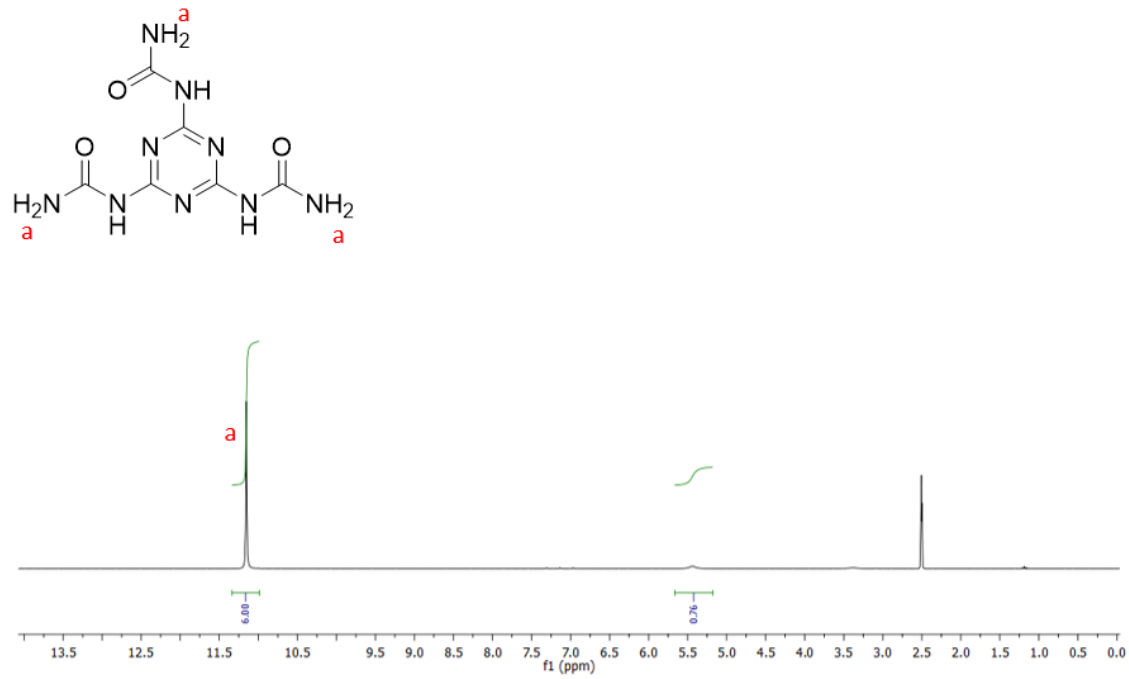

7.4.3 $^{13}C\{^{1}H\}$ NMR Spectrum of Compound 37

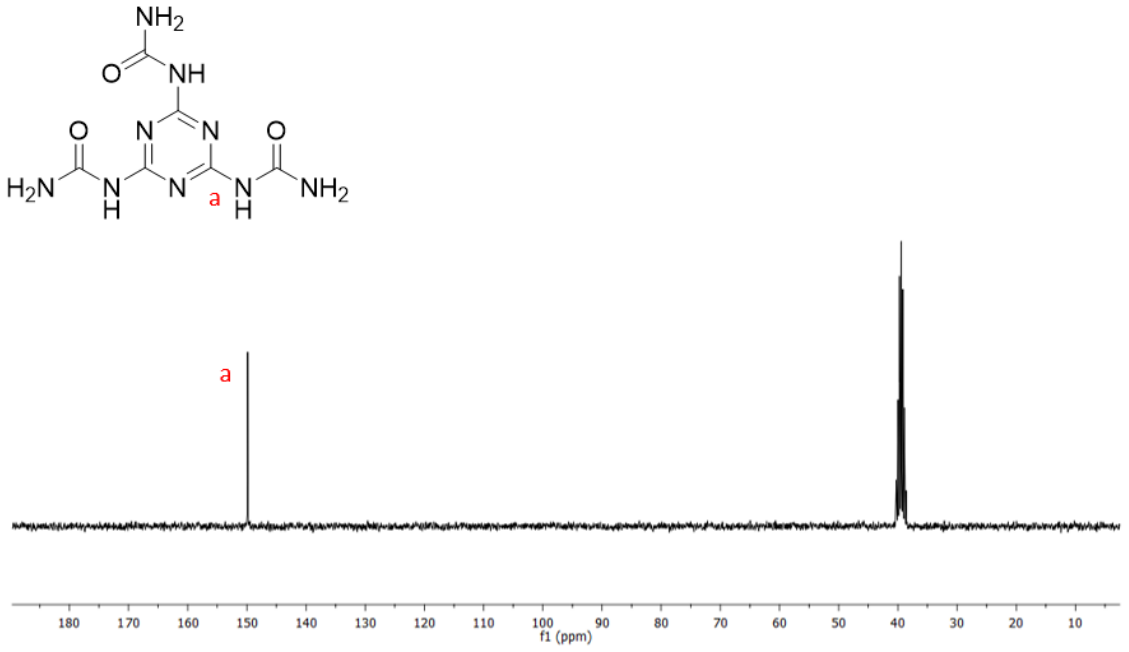

7.5 Compound 41

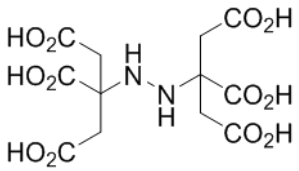

7.5.1 IR Spectrum of Compound 41

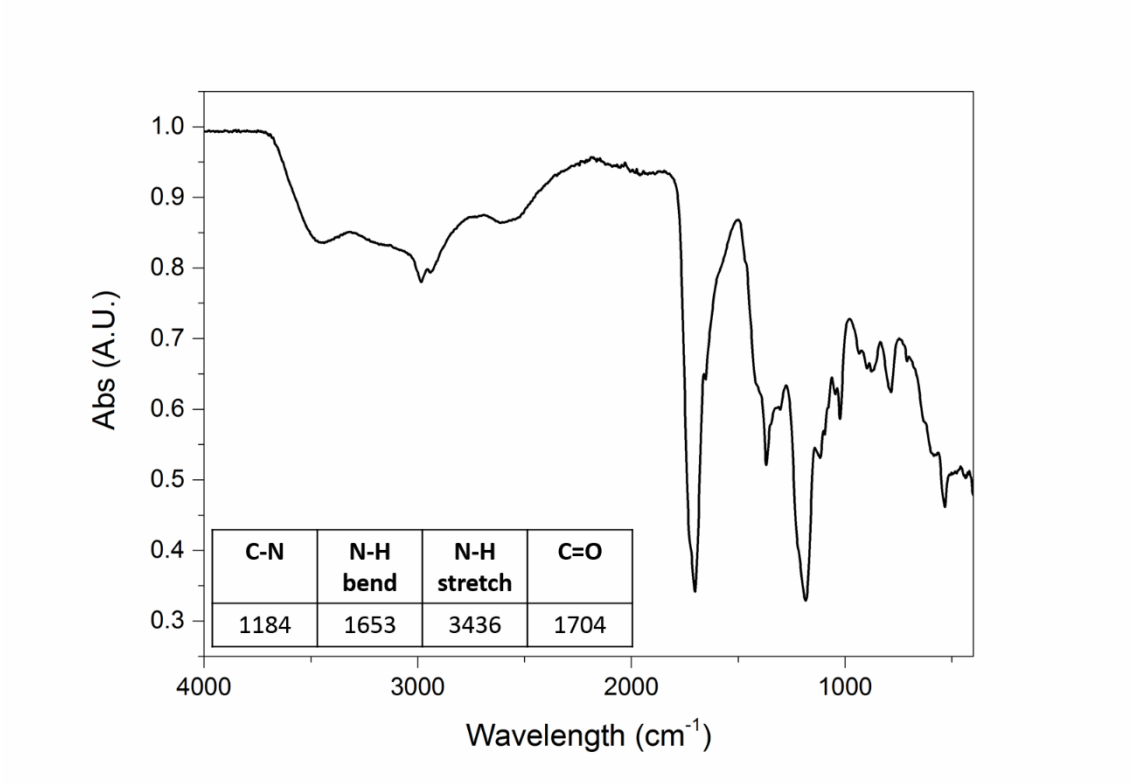

7.5.2 ^{1}H NMR Spectrum of Compound 41

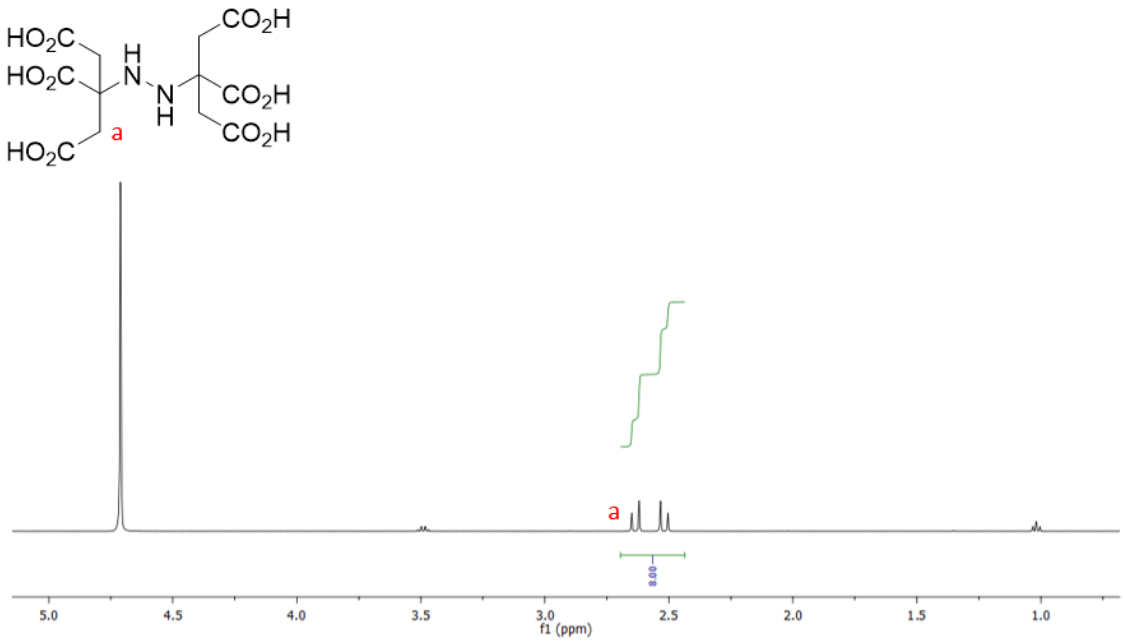

7.5.3 ^{13}C{^{1}H} NMR Spectrum of Compound 41

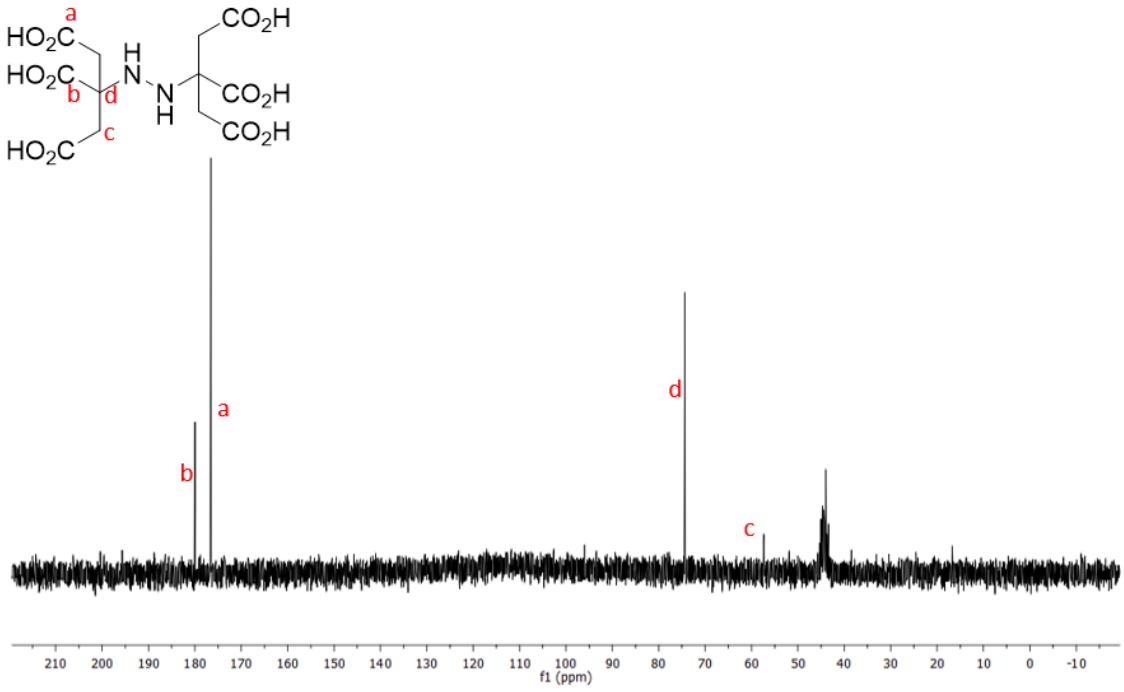

7.6 Compound 42

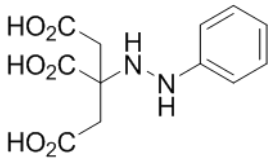

7.6.1 IR Spectrum of Compound 42

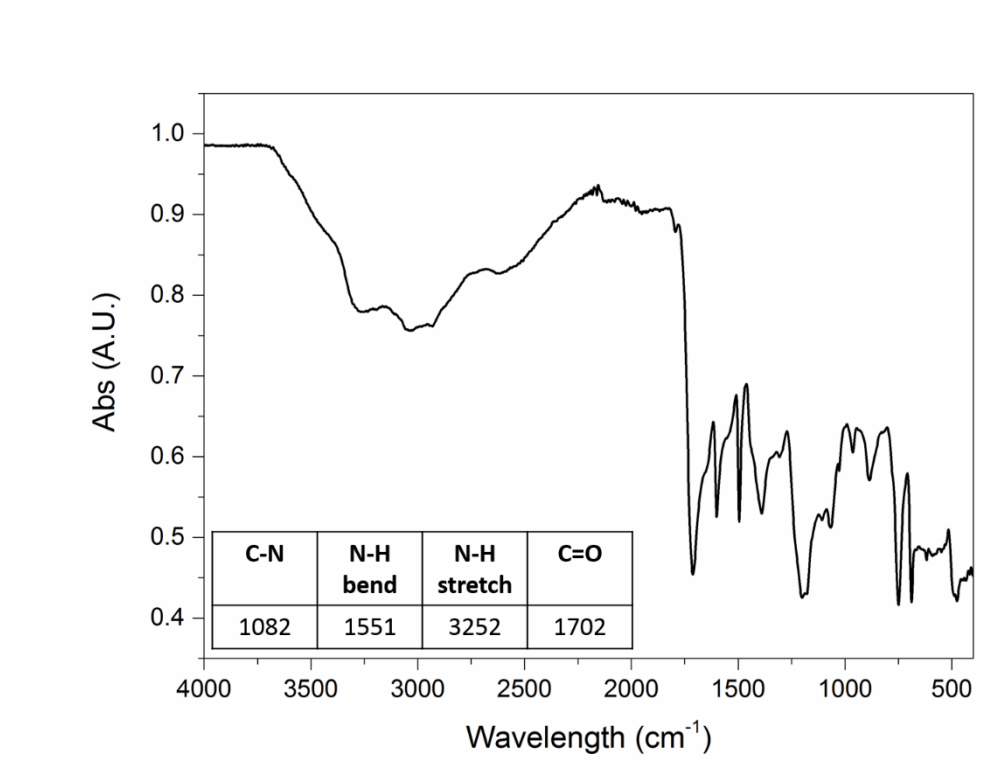

7.6.2 ^{1}H NMR Spectrum of Compound 42

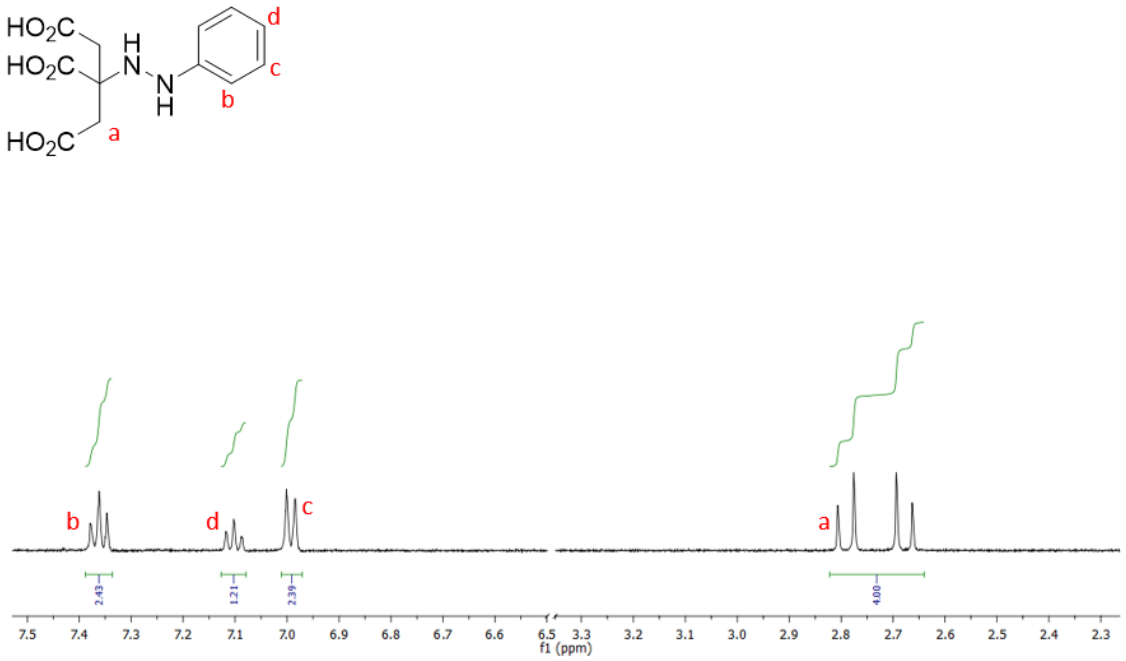

7.6.3 ^{13}C{^{1}H} NMR Spectrum of Compound 42[xxxiii]

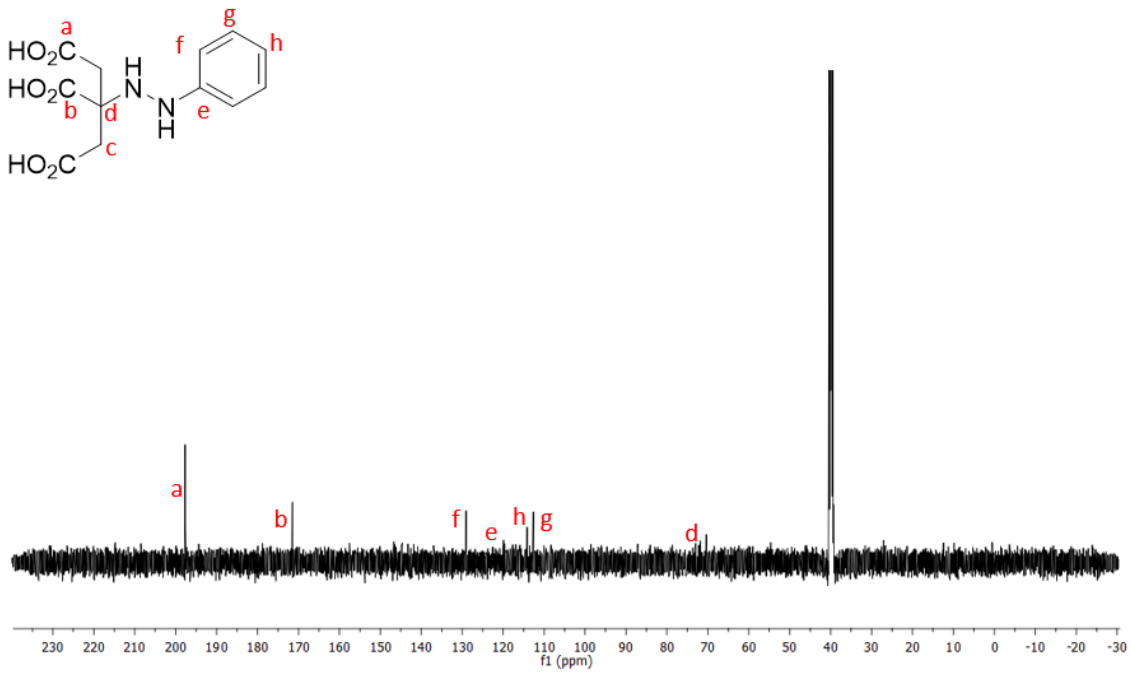

[xxxiii] Low solubility of compound 42 prevented the acquirement of a strong ^{13}C{^{1}H} spectrum

7.7 Compound 43

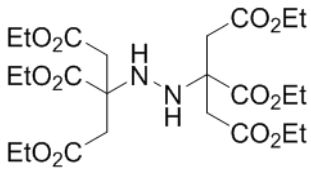

7.7.1 IR Spectrum of Compound 43

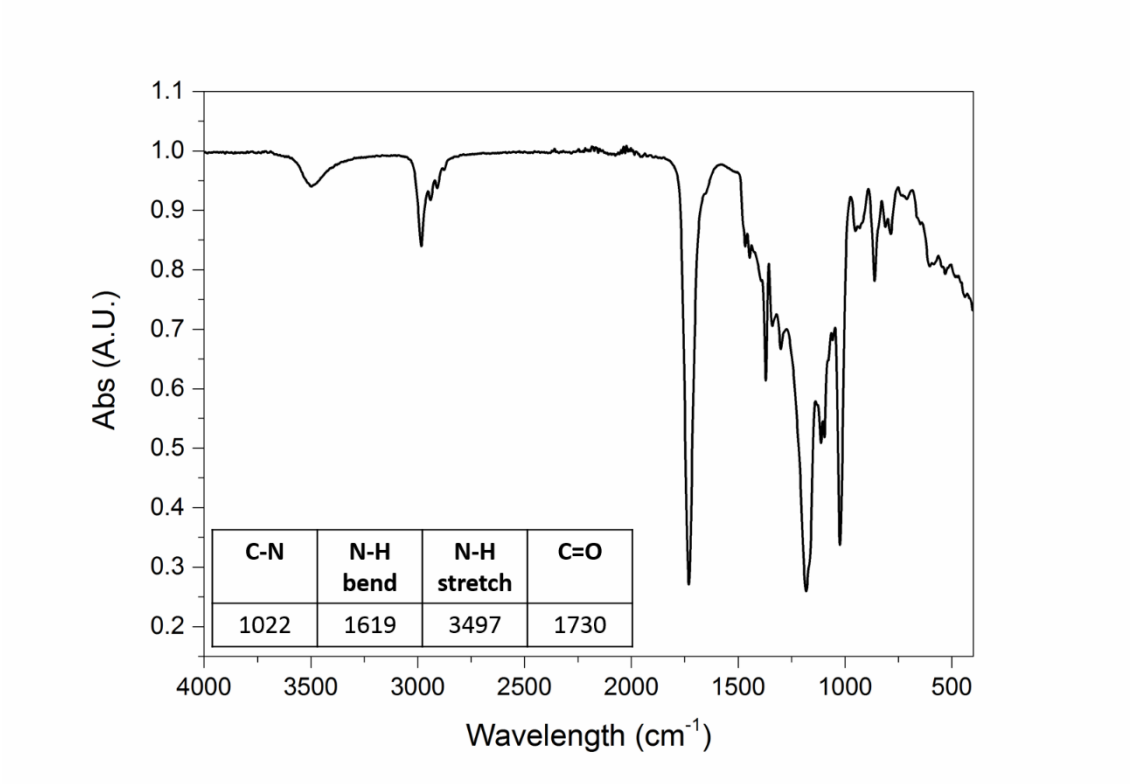

7.7.2 ^{1}H NMR Spectrum of Compound 43

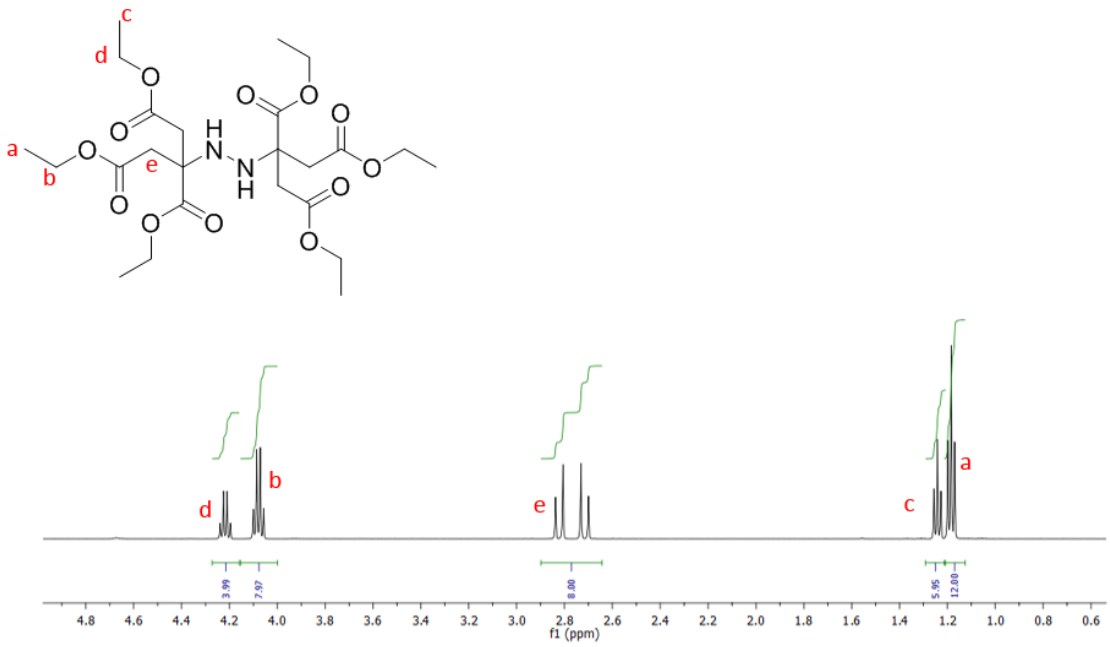

7.7.3 ^{13}C{^{1}H} NMR Spectrum of Compound 43

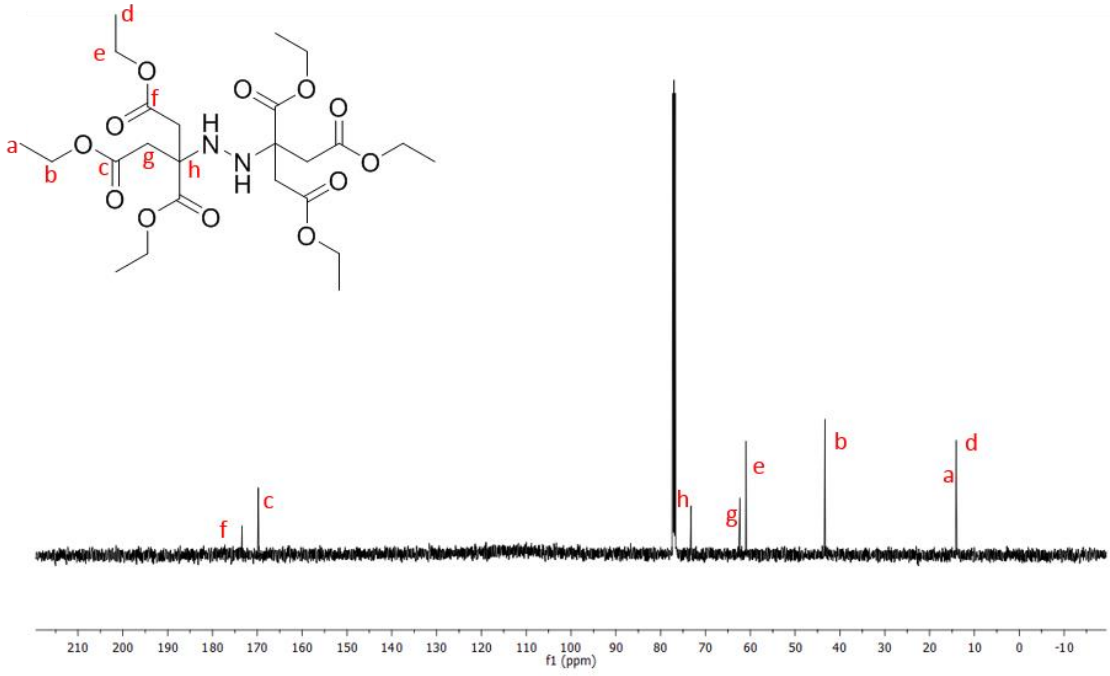

7.8 Compound 44

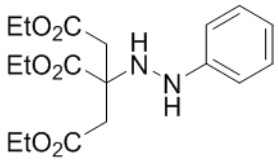

7.8.1 IR Spectrum of Compound 44

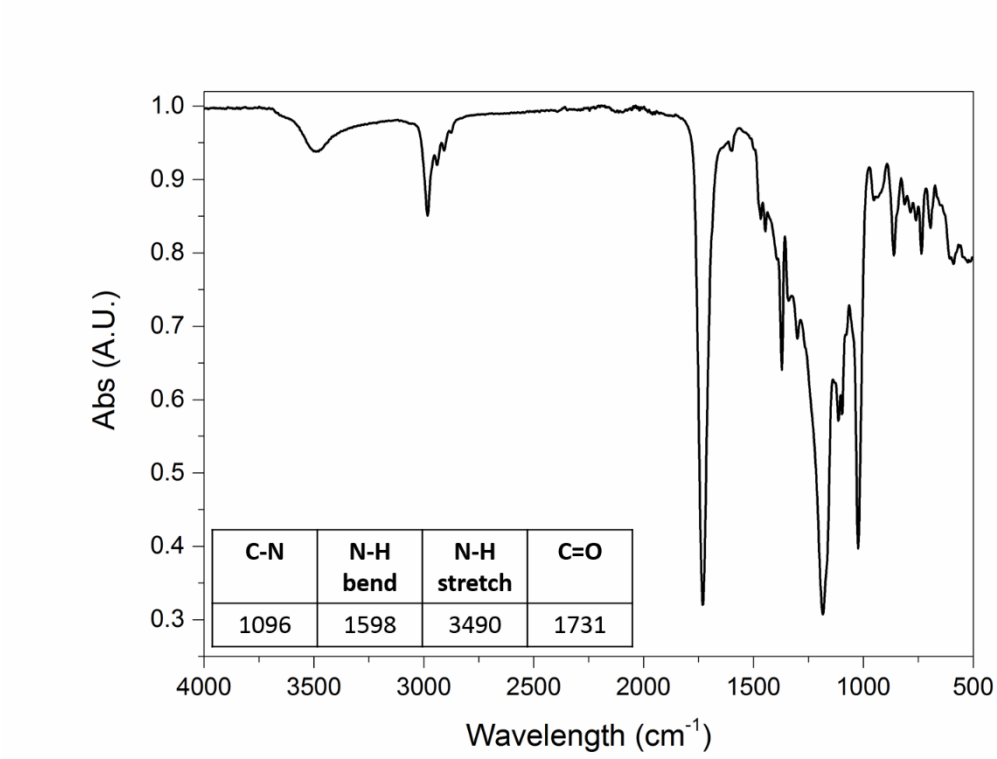

7.8.2 ^{1}H NMR Spectrum of Compound 44

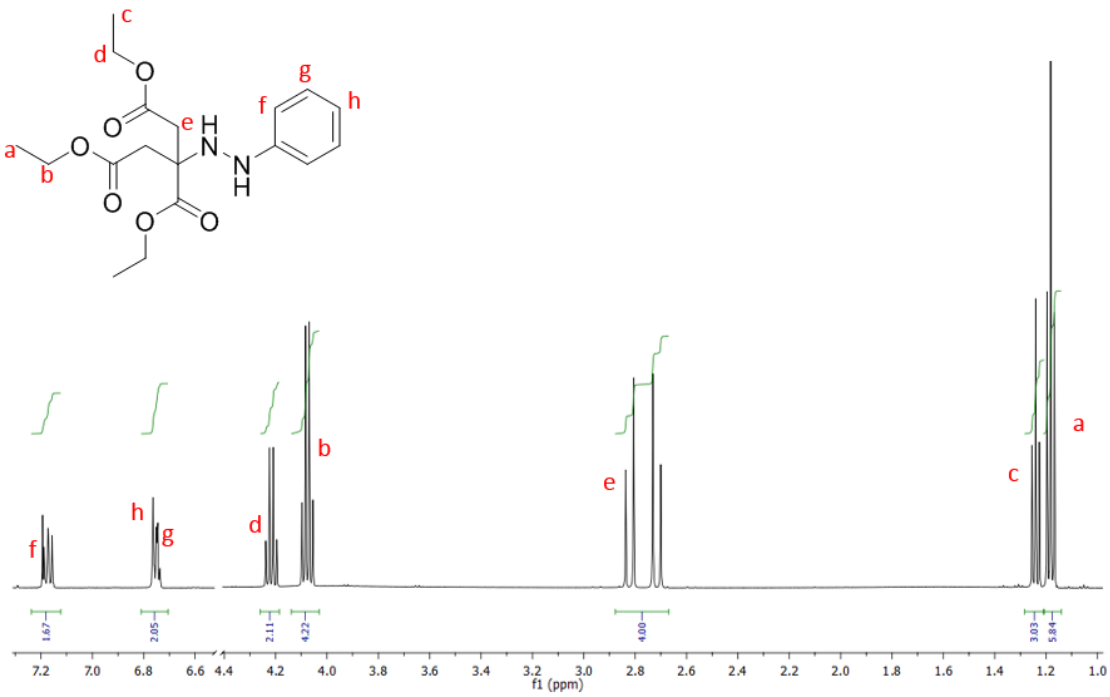

7.8.3 ^{13}C{^{1}H} NMR Spectrum of Compound 44

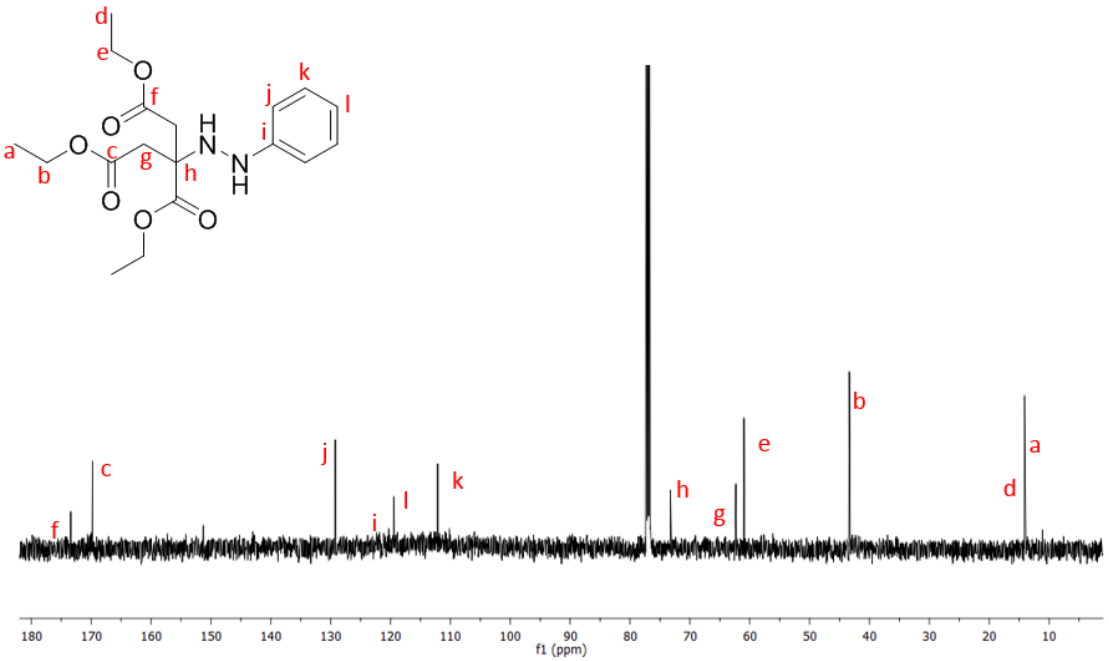

7.9 Compound 46

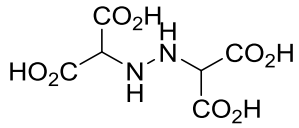

7.9.1 IR Spectrum of Compound 46

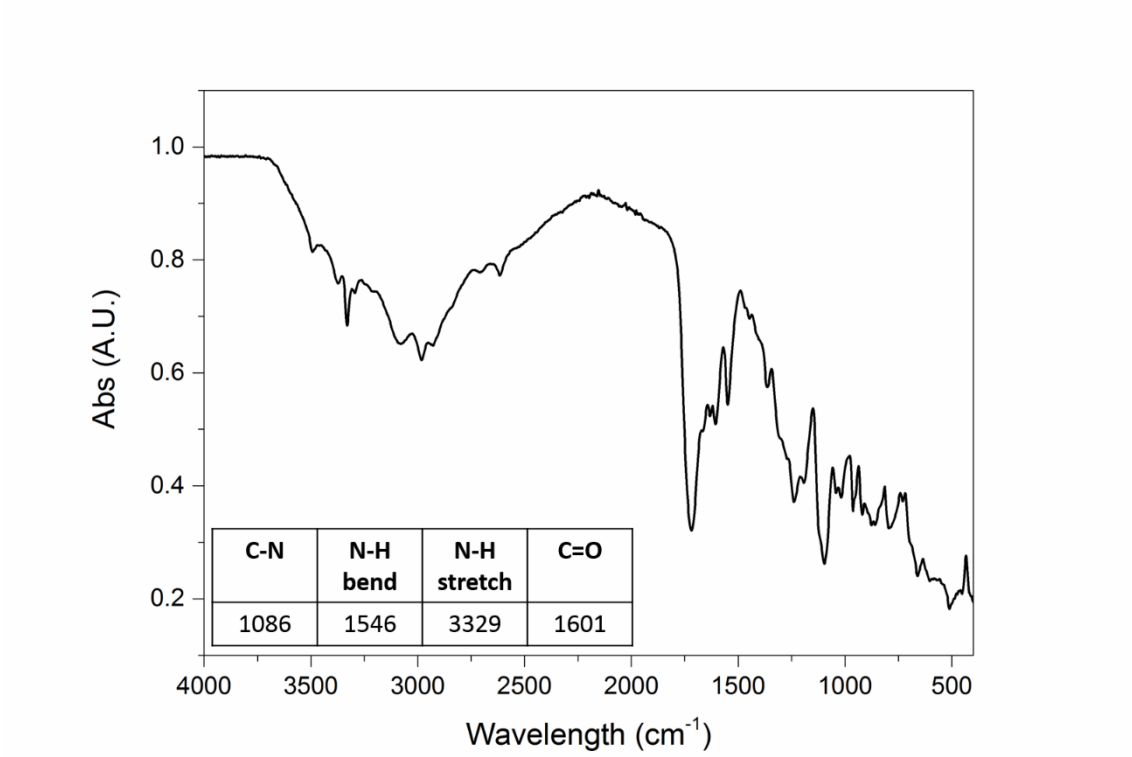

7.9.2 ^{1}H NMR Spectrum of Compound 46

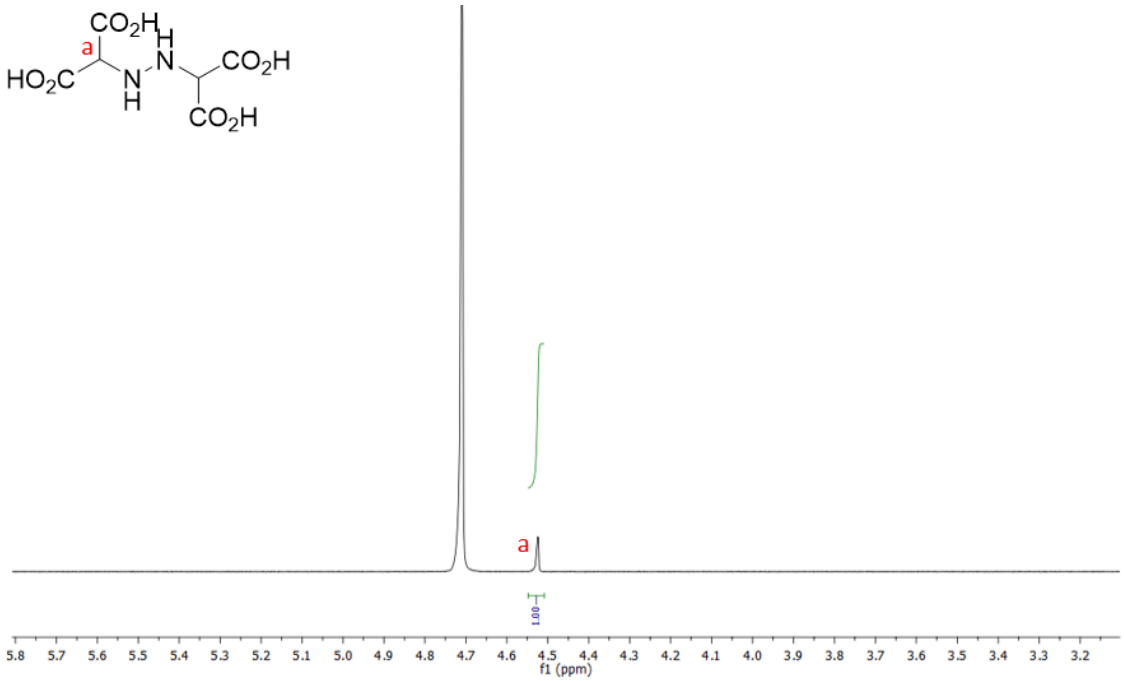

7.9.3 ^{13}C{^{1}H} NMR Spectrum of Compound 46

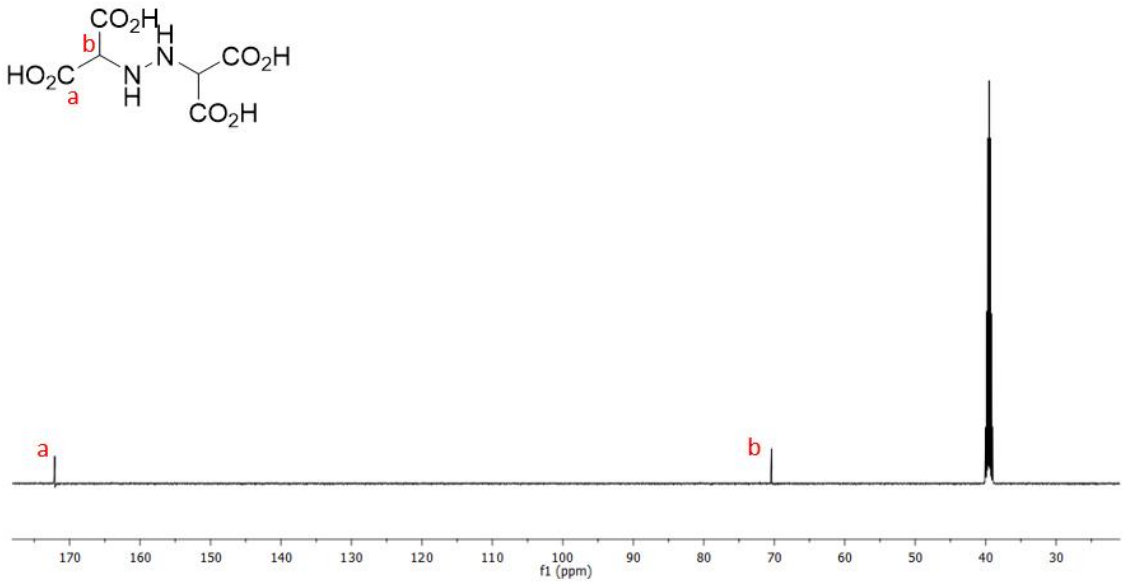

7.10 Compound 47

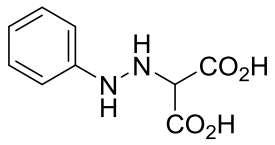

7.10.1 IR Spectrum of Compound 47

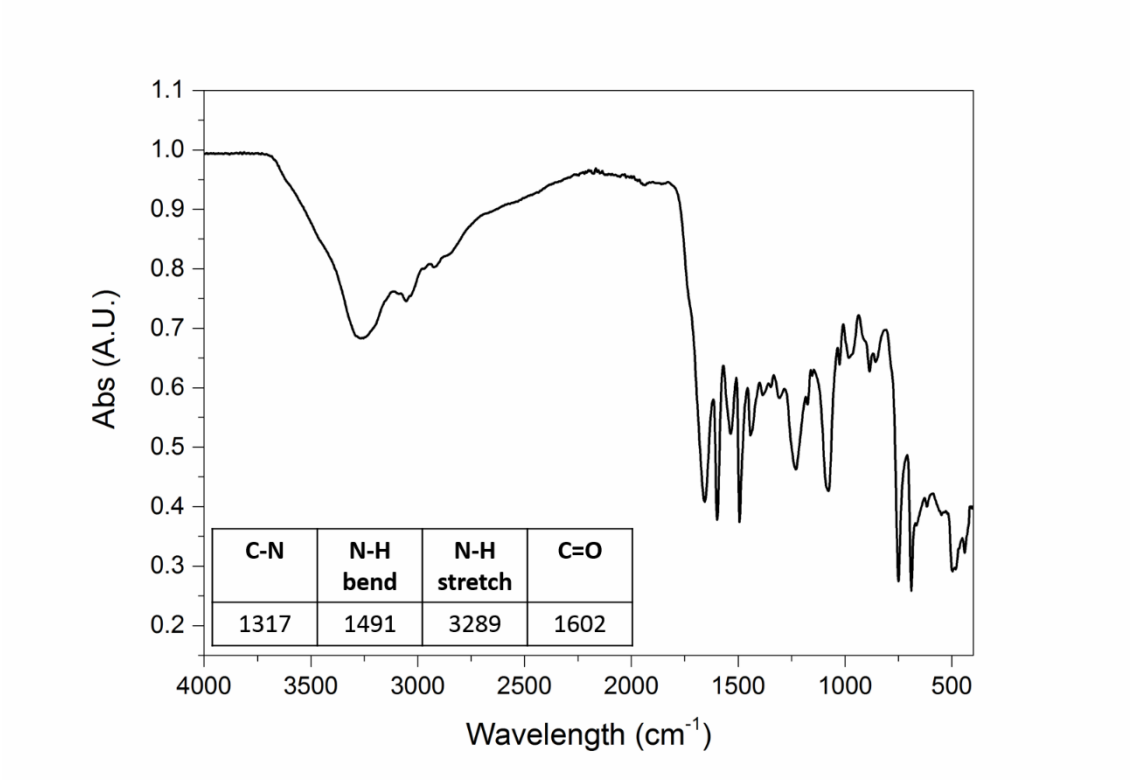

7.10.2 ^{1}H NMR Spectrum of Compound 47

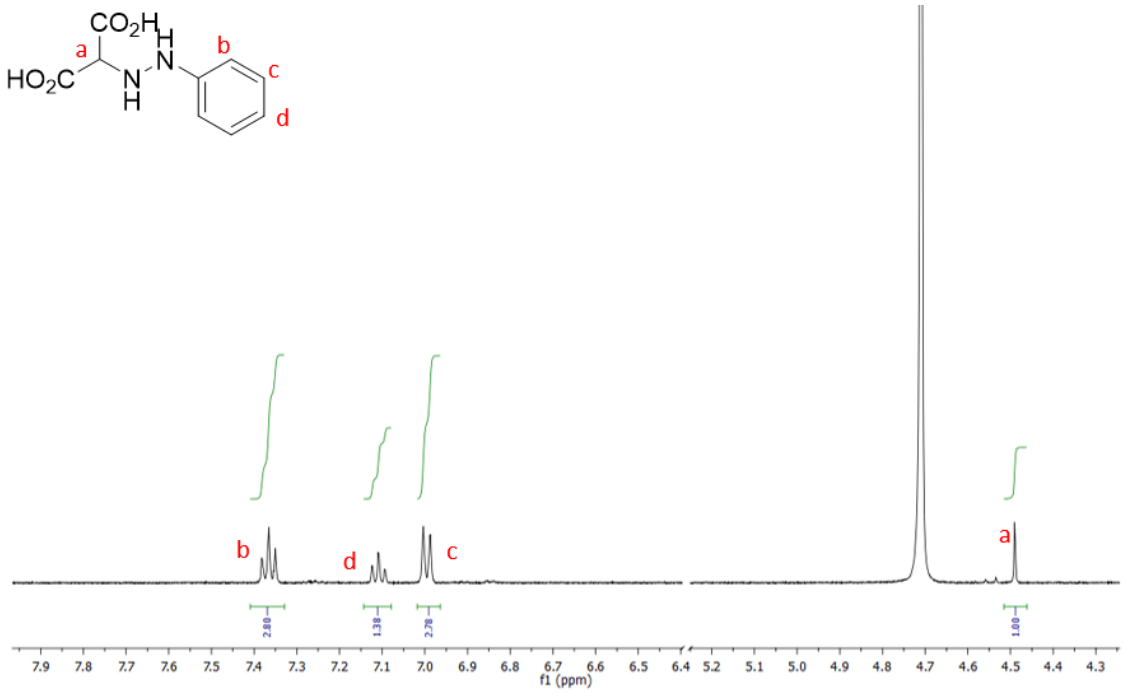

7.10.3 ^{13}C{^{1}H} NMR Spectrum of Compound 47

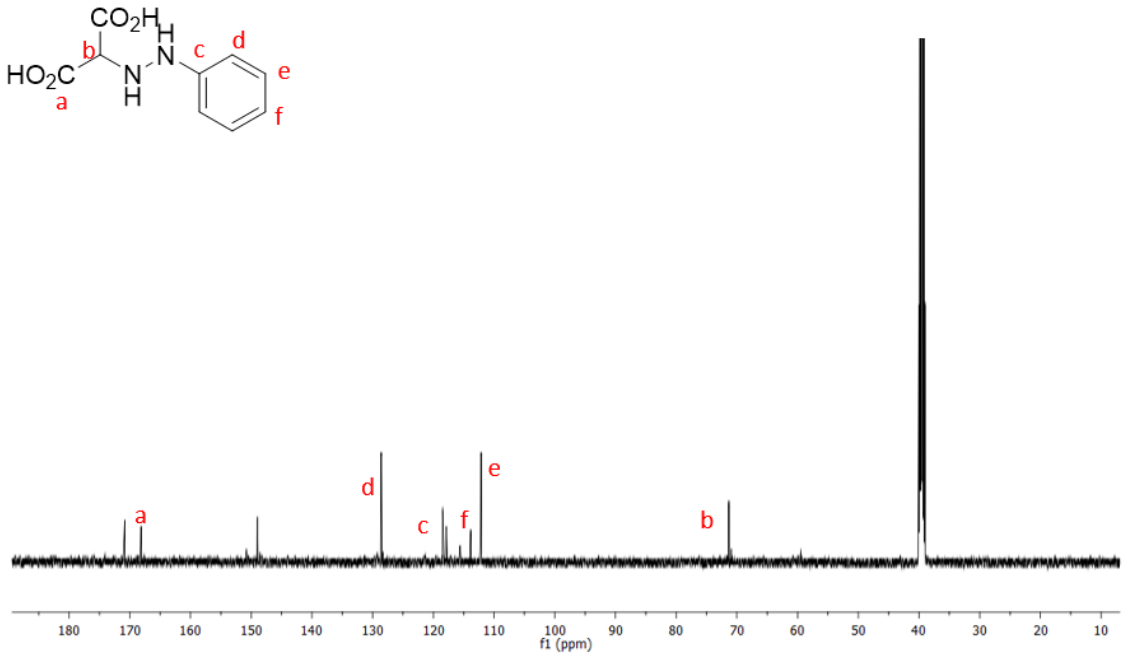

7.11 Compound 50

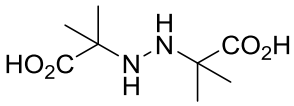

7.11.1 IR Spectrum of Compound 50

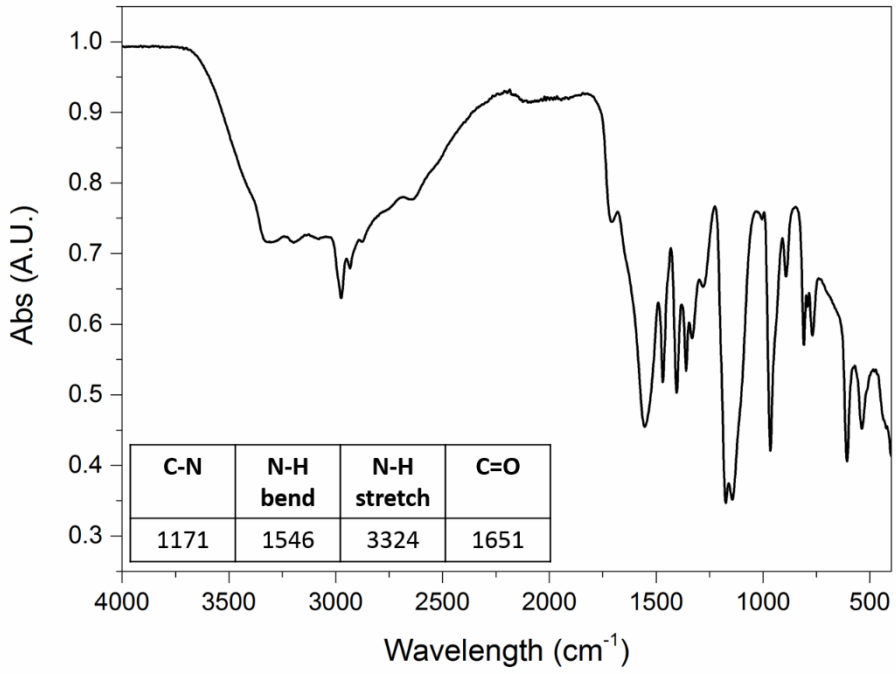

7.11.2 ^{1}H NMR Spectrum of Compound 50

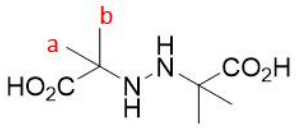

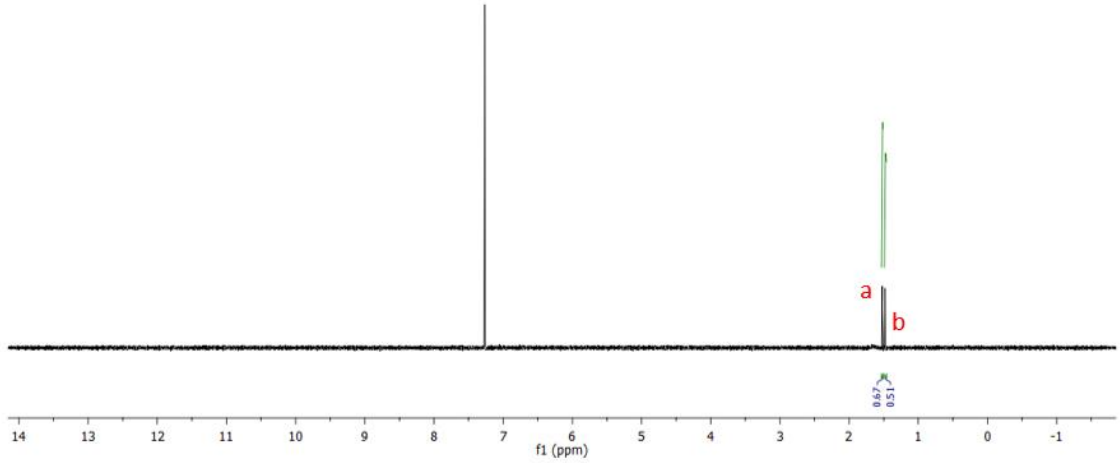

7.11.3 ^{13}C{^{1}H} NMR Spectrum of Compound 50

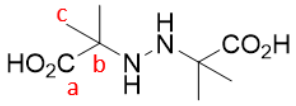

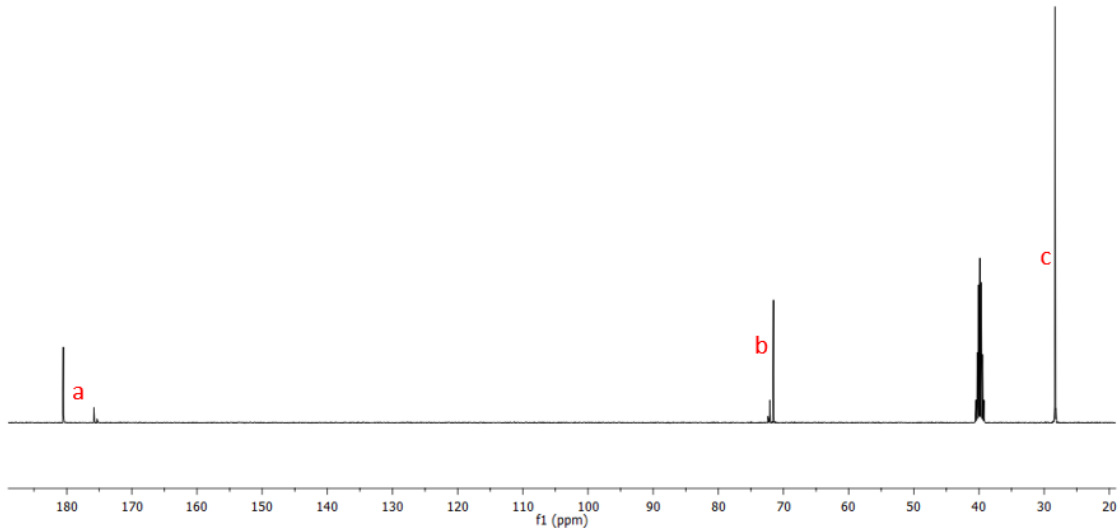

7.12 Compound 51

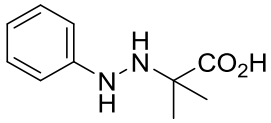

7.12.1 IR Spectrum of Compound 51

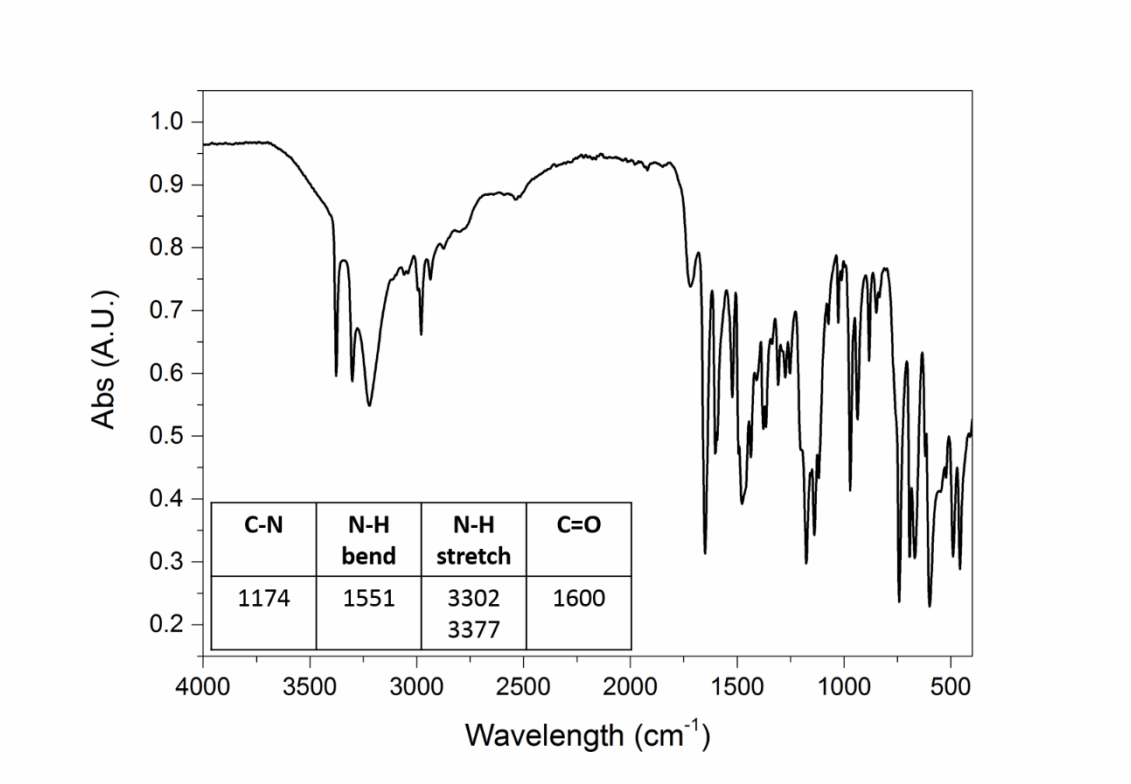

7.12.2 ^{1}H NMR Spectrum of Compound 51

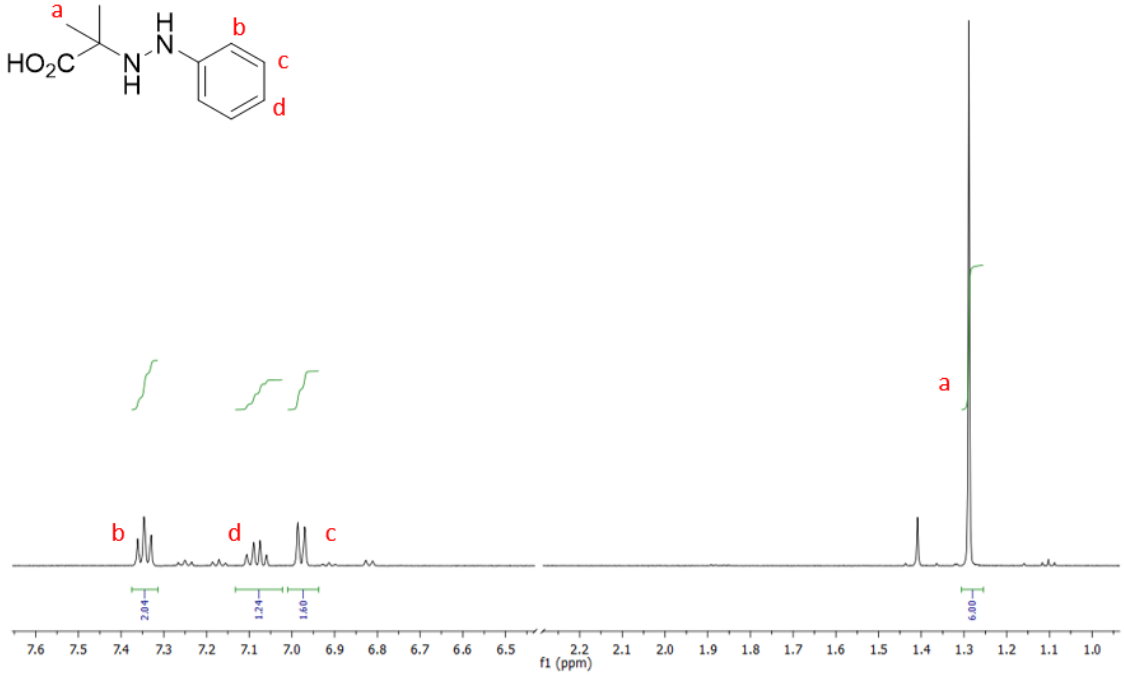

7.12.3 ^{13}C{^{1}H} NMR Spectrum of Compound 51[xxxiv]

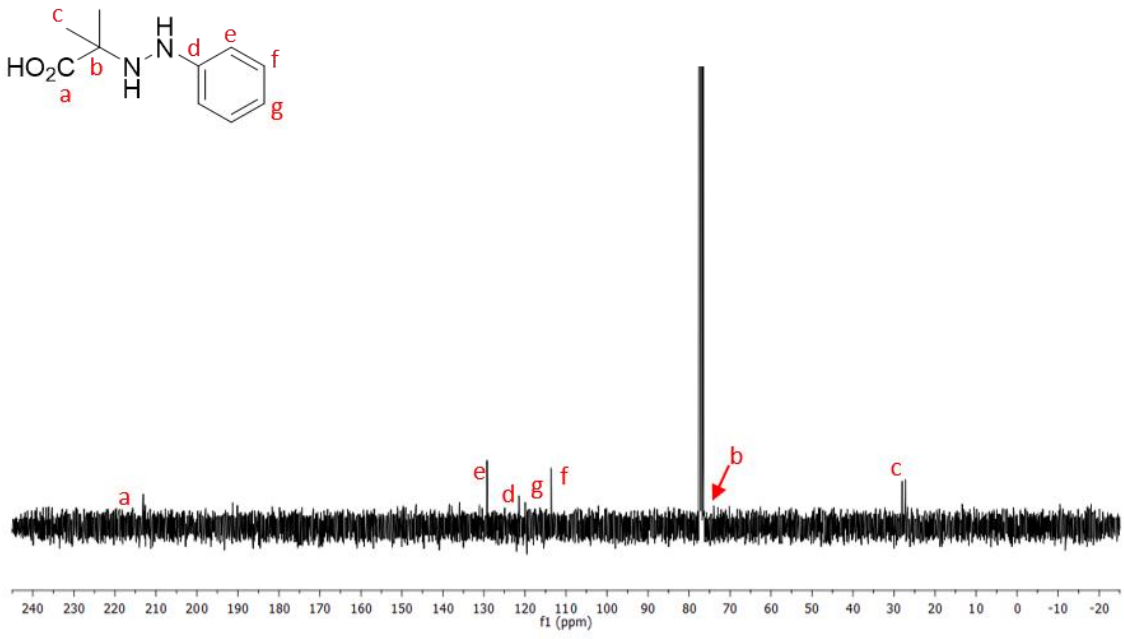

[xxxiv] Low solubility of compound 51 prevented the acquirement of a strong ^{13}C{^{1}H} spectrum

7.13 Compound 52

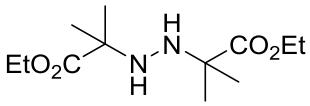

7.13.1 IR Spectrum of Compound 52

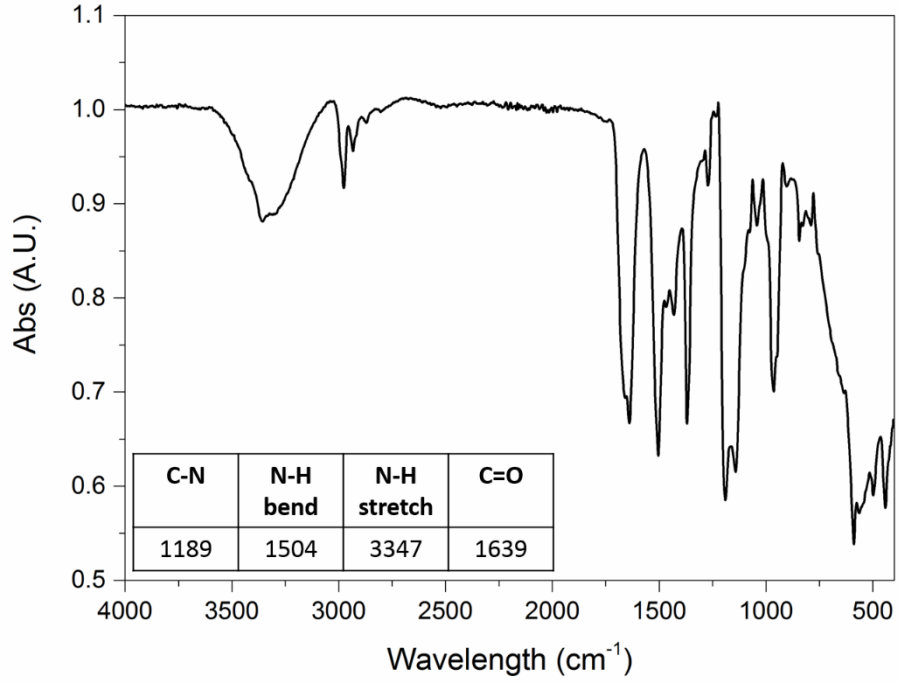

7.13.2 ^{1}H NMR Spectrum of Compound 52

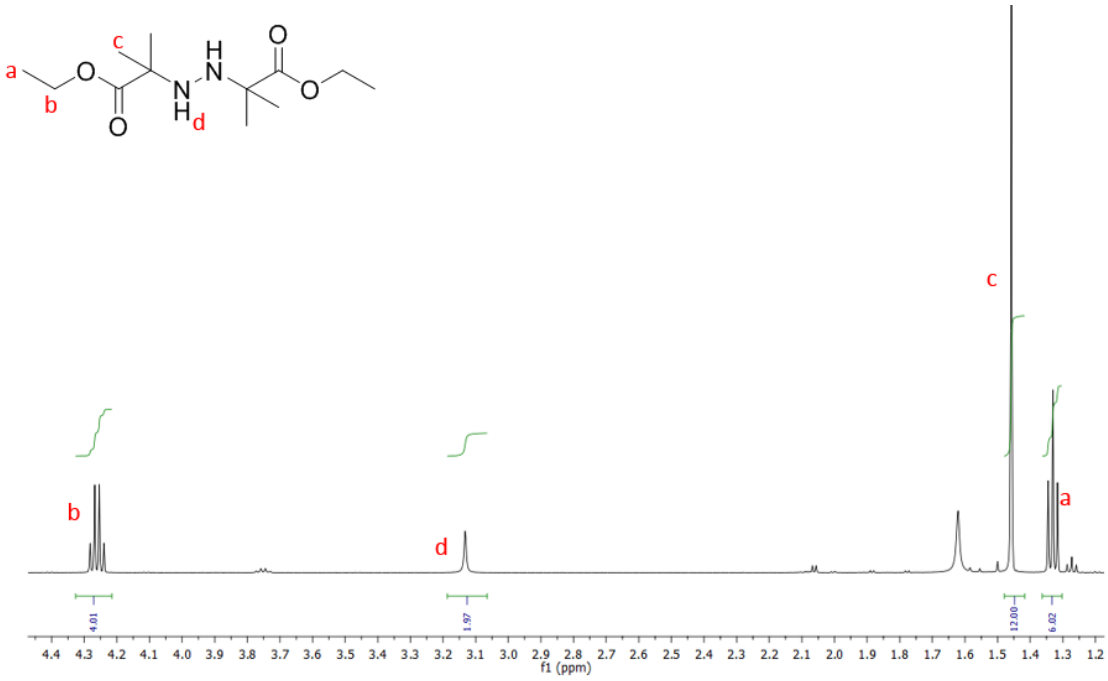

7.13.3 ^{13}C{^{1}H} NMR Spectrum of Compound 52

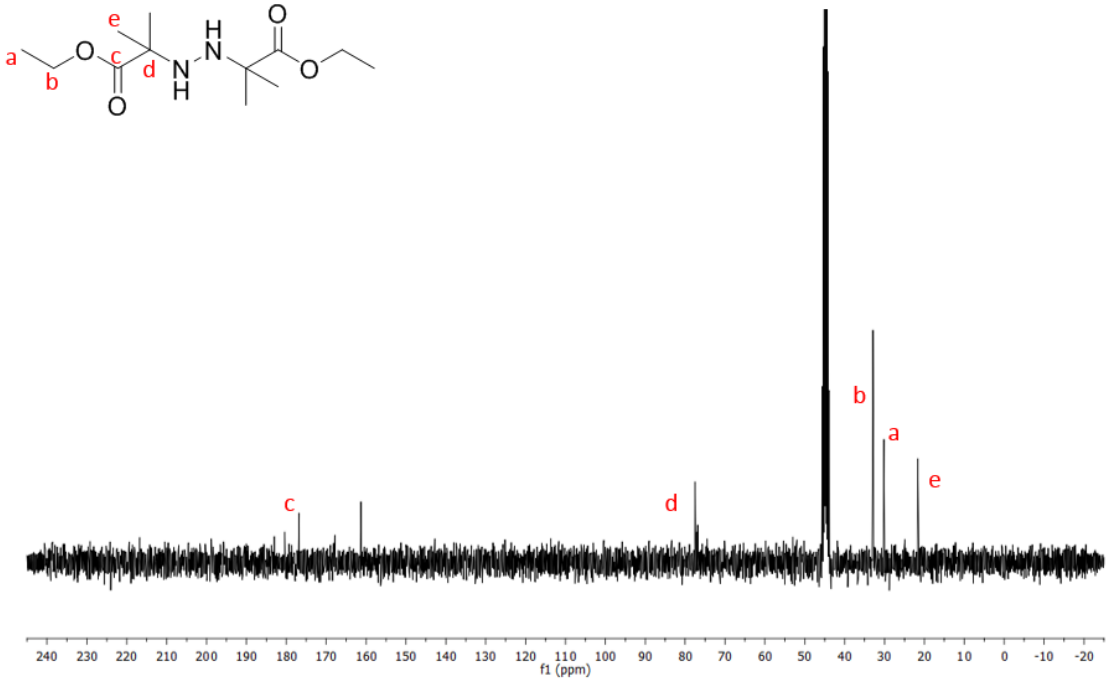

7.14 Compound 53

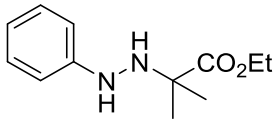

7.14.1 IR Spectrum of Compound 53

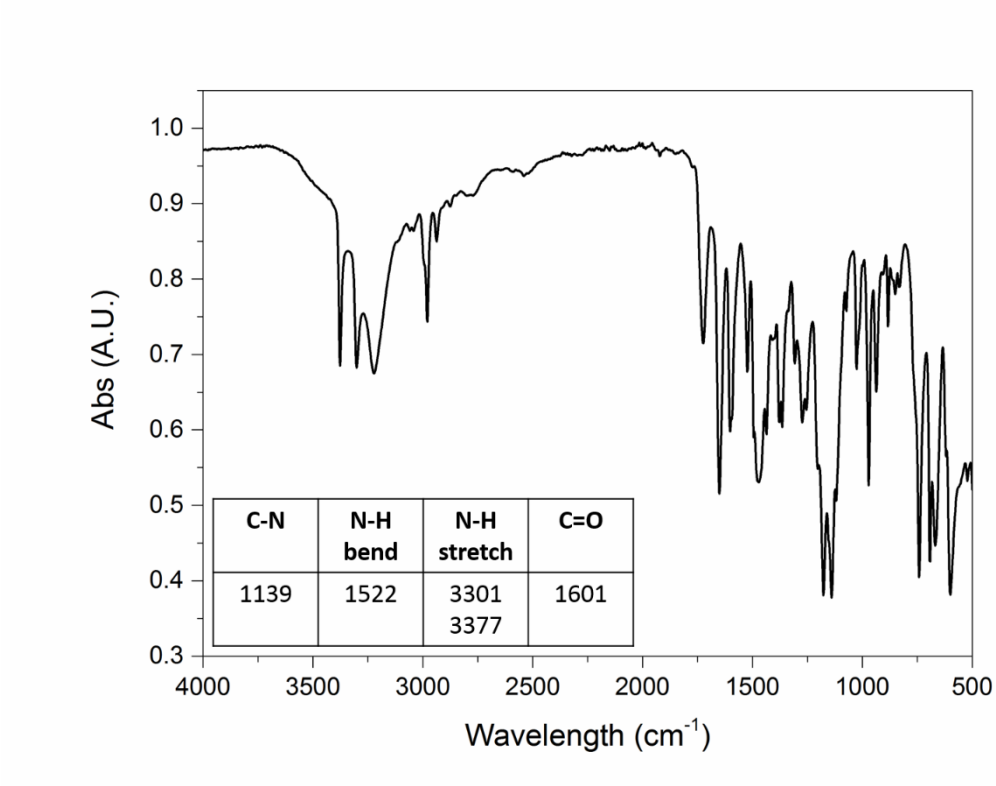

7.14.2 ^{1}H NMR Spectrum of Compound 53

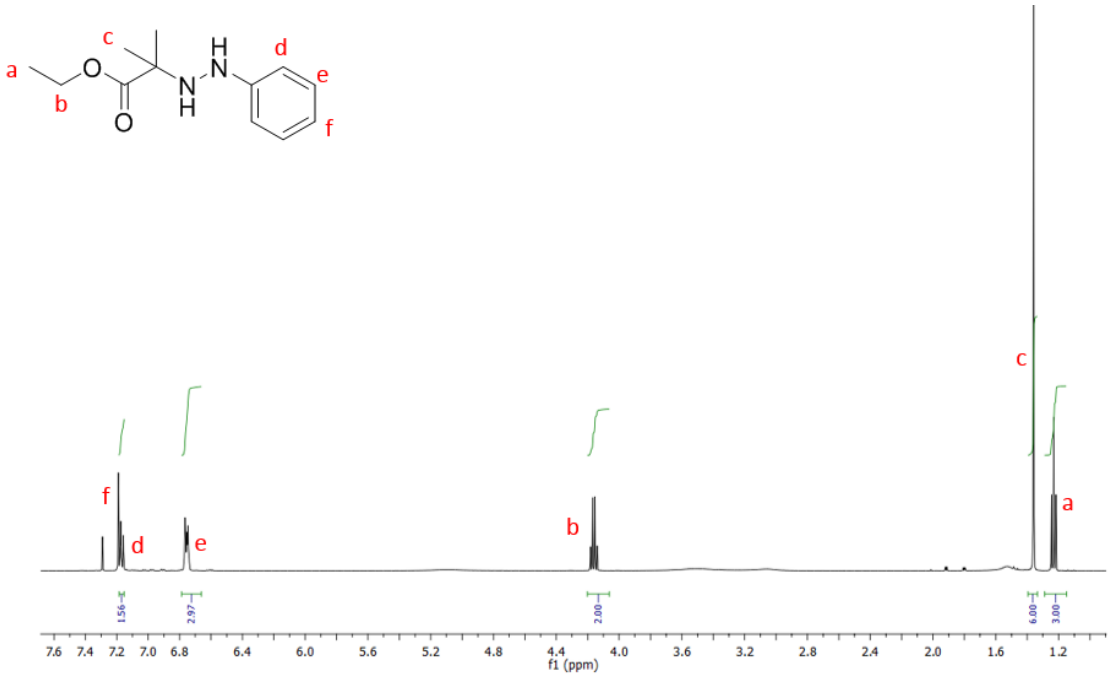

7.14.3 ^{13}C{^{1}H} NMR Spectrum of Compound 53